THE UNIVERSITY OF ALBERTA

Investigation of Some Rock Avalanches in the Mackenzie Mountains

by

©

Patrick John Alexander McLellan

A THESIS
SUBMITTED TO THE FACULTY OF GRADUATE STUDIES AND RESEARCH
IN PARTIAL FULFILMENT OF THE REQUIREMENTS FOR THE DEGREE
OF MASTER OF SCIENCE
IN
CIVIL ENGINEERING

EDMONTON, ALBERTA
Spring, 1983

Canadian Geotechnical Journal

Published by
THE NATIONAL RESEARCH COUNCIL OF CANADA

Revue canadienne de géotechnique

Publiée par
LE CONSEIL NATIONAL DE RECHERCHES DU CANADA

Editor R. M. QUIGLEY **Directeur scientifique**

Assistant to the Editor E. MILLIKEN **Adjointe au directeur scientifique**

Associate Editors/Directeurs scientifiques associés

M. BOZOZUK
J. I. CLARK
Z. EISENSTEIN
M. GARNEAU
J. GRAHAM
G. LEFEBVRE
D. R. McCREATH
R. J. MITCHELL
J. F. NIXON
D. READES
W. D. ROGGENSACK
P. G. SLY
R. N. YONG

PUBLISHING DEPARTMENT
at the National Research Council of Canada

SERVICE DE PUBLICATION
du Conseil national de recherches du Canada

Editor-in-chief C. T. BISHOP **Directeur général**

Assistant Editor-in-chief P. A. REDHEAD **Directeur général adjoint**

Manager B. E. DREW **Directrice administrative**

Publishing Supervisor S. E. JENNESS **Préposé de la publication**

Senior Publication Officer F. M. KAVCIC **Agent supérieur à la publication**

Publication Officer E. ROLFE **Agent à la publication**

THE CANADIAN GEOTECHNICAL JOURNAL (Can. Geotech. J.) publishes papers in English or French covering the general field of soil engineering, together with papers in the related disciplines such as Geology, Soil Science, Snow and Ice Mechanics, and Rock Mechanics as they relate to civil engineering.

Manuscripts for publication should be submitted to **Dr. R. M. Quigley, Faculty of Engineering Science, The University of Western Ontario, London, Ont., Canada N6A 5B9.**

Correspondence concerning accepted manuscripts and corrected proofs should be sent to Research Journals, National Research Council of Canada, Ottawa, Canada K1A 0R6. **Telephone enquiries** should be directed to Dr. S. E. Jenness (613-993-0428).

Reprints may be purchased at the time of publication (an order form is sent out with the galley proof). All orders should be sent to the Printing Department, University of Toronto Press, 5201 Dufferin Street, Downsview, Ont., Canada M3H 5T8. Invoices relating to the reprints will be sent out by the Printer.

Instructions to Authors are published once a year, in the first issue of each volume. Copies may be obtained from the Publishing Department.

The publisher grants permission to individuals who wish to quote short excerpts and reproduce figures, tables, or photographs from articles in this journal, provided that the source of such material is fully acknowledged. As a courtesy the consent of authors of such material should be obtained.

©National Research Council of Canada 1983. World rights reserved.

Copies of articles in this journal may be made for personal or internal use, or for the personal or internal use of specific clients, in research, study, or teaching. Permission for copying beyond that permitted by Section 107 or 108 of the U.S. Copyright Law is granted by the publisher on the condition that the person or institution making the copy or copies pays a copyright fee of $1.00 (U.S.) for each copy of each article to the Copyright Clearance Center, Inc., 21 Congress Street, Salem, MA, U.S.A. 01970. The appropriate remittance should be forwarded to the Clearance Center with a copy of the first page of the article(s) that has been copied. Copies of articles published in this journal prior to 1979 may be made under similar conditions.

The above permission does not extend to other kinds of copying, such as copying for general distribution, for advertising, or promotional purposes, for creating new collective works, or for resale. For such copying, arrangements must be made with the publisher.

LA REVUE CANADIENNE DE GÉOTECHNIQUE (Can. Geotech. J.) publie des articles en français ou en anglais touchant au domaine général de la mécanique des sols ou des disciplines connexes, telles que la géologie et les sciences du sol, de la neige et des glaces, et la mécanique des roches, traitées en fonction du génie civil.

Manuscrits–Les auteurs doivent adresser leurs manuscrits à **Dr. R. M. Quigley, Faculty of Engineering Science, The University of Western Ontario, London, Ont., Canada N6A 5B9.**

La correspondance ayant trait aux manuscrits acceptés et les épreuves corrigées doivent être envoyées aux Journaux de la recherche scientifique, Conseil national de recherches du Canada, Ottawa, Canada K1A 0R6. **On peut obtenir des renseignements en téléphonant** à M. S. E. Jenness (613-993-0428).

Tirages à part–Les tirés à part peuvent être achetés au moment de la publication. Un bon de commande à cet effet accompagne les épreuves: il doit être retourné au Printing Department, University of Toronto Press, 5201 Dufferin Street, Downsview (Ont.), Canada M3H 5T8, qui se chargera de la facturation.

Recommandations aux auteurs sont publiées une fois par année dans le premier numéro de chaque volume. On peut s'en procurer une copie, sur demande, au Service de publication.

L'éditeur accorde aux particuliers la permission de citer de brefs extraits et de reproduire des figures, des tableaux ou des photos dans les articles de la revue, à la condition que la source soit indiquée explicitement. Dans ce cas, il convient, par courtoisie, d'obtenir le consentement des auteurs.

© Conseil national de recherches du Canada 1983. Tous droits réservés.

Les articles de cette revue peuvent être reproduits pour usage personnel ou interne, ou pour l'usage personnel ou interne de clients bien précis dans les domaines de la recherche ou de l'enseignement. L'éditeur accorde la permission de reproduire ces articles malgré les dispositions de la section 107 ou 108 de la Copyright Law des États-Unis à la condition que le copieur, la personne ou l'organisme, paie une redevance de 1,00 $ U.S. pour chaque copie de chaque article au Copyright Clearance Center, Inc., 21 Congress Street, Salem, MA, U.S.A. 01970. Les versements appropriés sont envoyés au Clearance Center avec une photocopie de la première page de l'article (ou des articles) reproduit. Les reproductions d'articles publiés dans cette revue avant 1979 sont soumises à des conditions semblables.

La présente permission ne s'applique pas à d'autres genres de reproduction, notamment la reproduction en vue d'une distribution générale, à des fins de publicité ou de promotion, pour la création de nouveaux travaux collectifs, ou pour la revente. Dans ces cas, il faut prendre les dispositions qui s'imposent en communiquant avec l'éditeur.

POOR COPY
COPIE DE QUALITEE INFERIEURE

Canad
Geote
Journa

Published by th
National Resea
of Canada

Micro

THE UNIVERSITY OF ALBERTA

RELEASE FORM

NAME OF AUTHOR Patrick John Alexander McLellan

TITLE OF THESIS Investigation of Some Rock Avalanches in the Mackenzie Mountains

DEGREE FOR WHICH THESIS WAS PRESENTED MASTER OF SCIENCE

YEAR THIS DEGREE GRANTED Spring, 1983

Permission is hereby granted to THE UNIVERSITY OF ALBERTA LIBRARY to reproduce single copies of this thesis and to lend or sell such copies for private, scholarly or scientific research purposes only.

The author reserves other publication rights, and neither the thesis nor extensive extracts from it may be printed or otherwise reproduced without the author's written permission.

(SIGNED) Pat McLellan

PERMANENT ADDRESS:

2820 Brentwood Blvd. N.W.

Calgary, Alberta, T2L 1J5

DATED December 20 1982

Rockslide Pass rupture surface

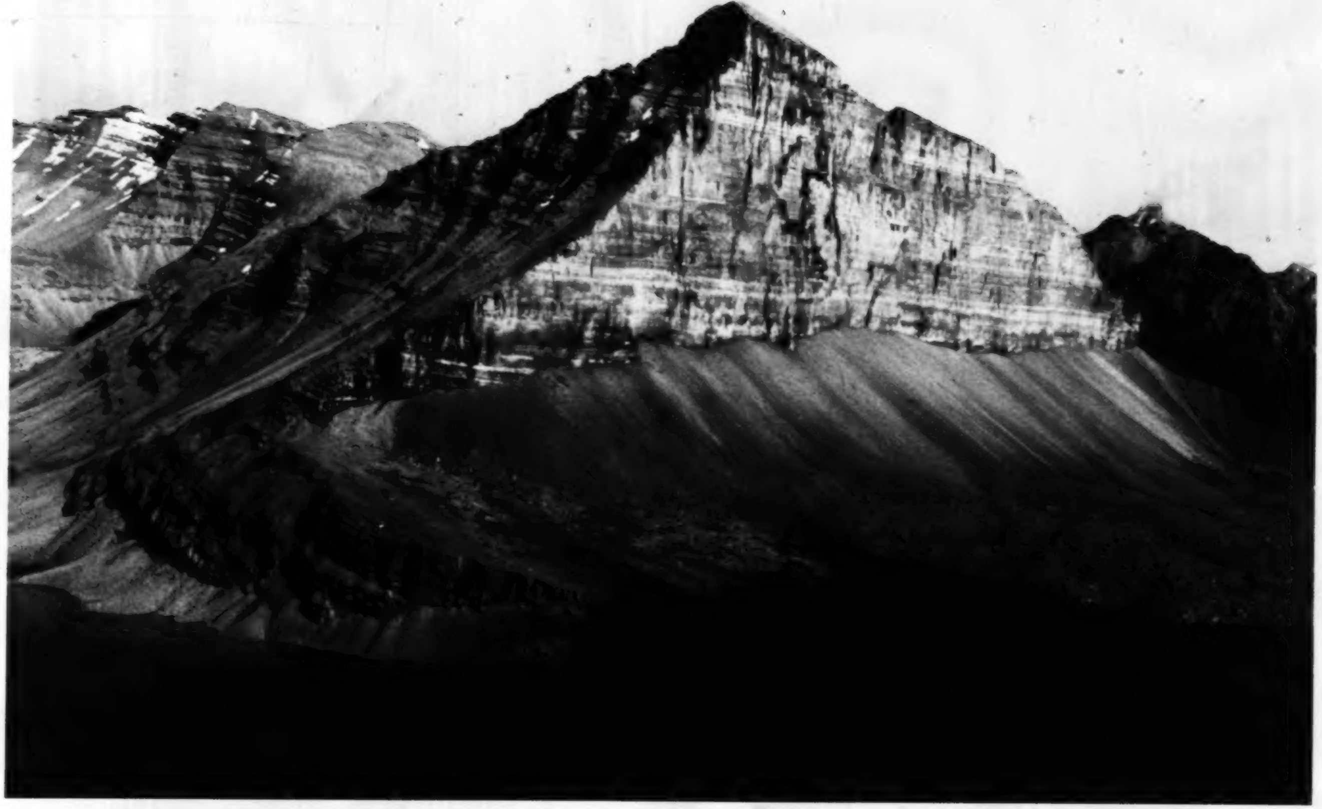

THE UNIVERSITY OF ALBERTA

FACULTY OF GRADUATE STUDIES AND RESEARCH

The undersigned certify that they have read, and recommend to the Faculty of Graduate Studies and Research, for acceptance, a thesis entitled Investigation of Some Rock Avalanches in the Mackenzie Mountains submitted by Patrick John Alexander McLellan in partial fulfilment of the requirements for the degree of MASTER OF SCIENCE in CIVIL ENGINEERING.

....

Supervisor

....

H.A.K. Charlesworth

Date March 28, 1983

ABSTRACT

The dynamic behavior of a suite of rock avalanches from the Mackenzie Mountains is the subject of this research. The two objectives of this thesis are: firstly, to document field observations from the Nozzle and Rockslide Pass rock avalanches; and secondly, to evaluate, modify and calibrate a two-parameter hydraulics model for the purpose of rock avalanche runout and velocity prediction.

Field evidence suggests that the initial movement and subsequent failure mechanism for many of these rock avalanches is a complex combination of sliding, rolling and toppling, with progressive disintegration en route.

An analysis of the morphology of the rock debris at the Twin avalanches indicates local velocities ranged between 12 and 50 m/s based on superelevation and run-up calculations. Projectile velocities of between 95 and 118 m/s are also suggested at the Nozzle rock avalanche.

Koerner's model for snow and rock avalanches has been modified to incorporate uplift pressures and initial velocity assumptions. The frictional and dynamic resistance terms (μ,D) in the equation of motion have been related in a function termed the *characteristic resistance relationship*. An initial evaluation of this relationship for the Mackenzie Mountains rock avalanches does not reveal a significant common trend. Model predictions at the Twin avalanches match the superelevation data over a wide range of (μ,D) pairs.

Predictive capability with the proposed model was evaluated using a number of empirically evaluated parameters. Refinements to these parameters give a reasonably good match of the model simulations with the observed runout distances (within a 4% accuracy) for five of the major rock avalanches in the Mackenzie Mountains. This would suggest that a judicious choice of resistance parameters for mass movements of this type provides a more consistent predictive capability than other more empirical volume/runout type relationships.

ACKNOWLEDGEMENTS

This research was conducted with the support and guidance of Dr. P. Kaiser. I am most grateful to him for his continued encouragement through all stages of the programme. Dr. J. Simmons originally suggested the topic and provided most useful information in the initial stages. I would also like to extend my appreciation to Drs. D. Cruden, N. Morgenstern, and S. Thomson who have always found time for discussing various aspects of the rock avalanche topic. Special thanks go to Dr. O. Hungr and Mr. S. Evans for their helpful advice and infectious enthusiasm for mass movements.

The financial and logistical support of the Boreal Institute for Northern Studies and the Geological Survey of Canada (Terrain Sciences Division) for the field portion of the study are gratefully acknowledged. I was most capably assisted in the field by Peter Barlow whose unfailing interest and companionship made the Mackenzie Mountains a little less remote. Pilot Bob Groats of Northern Mountain Helicopters made up for his questionable coffee with some superb flying in somewhat less than desirable weather conditions, even if we didn't know where we were going. Dr. L. Jackson of the GSC loaned some field equipment to the project and provided most useful commentary on the glacial geology of the Mackenzie Mountains.

I have also appreciated discussions with numerous other individuals whose experience have been invaluable in forming

my own views on the mechanical aspects of the phenomena. Drs. G. Eisbacher, J. Shaw, B. Stimpson, W. Savigny, P. Kershaw, and J. Sobkowicz have been most helpful in this regard. My fellow graduate students, in particular B. Heald, C. MacKay, and J. Agar, who have reviewed parts of this thesis, are also to be thanked for their critical commentary.

Appreciation is extended to J. Kennedy who very aptly typed this thesis and Mr. B. Hayes of Energy, Mines and Resources Canada who provided unpublished topographic maps of some parts of the Mackenzie Mountains.

Financial support from Dr. S. Thomson, the National Research Council of Canada, a Province of Alberta Scholarship, and a number of graduate teaching assistantships are gratefully acknowledged. A special thanks is extended to my employer, M. J. O'Connor and Associates Ltd., who has been most flexible in allowing me time to complete this thesis.

Graduate studies in geotechnical engineering at the University of Alberta are conducted in an invigorating and challenging atmosphere and my appreciation is extended to my educators here and previous instructors who have instilled in me a fasination for applied earth science.

Finally a very special thanks must go to my family and close friends from outside the academic community who have managed to maintain my perspective and have made my stay in Edmonton most enjoyable.

...There's a land where the mountains are nameless,
    And the rivers all run God knows where;
There are lives that are erring and aimless,
    And deaths that just hang by a hair;
There are hardships that nobody recons;
    There are valleys unpeopled and still;
There's a land - oh it beckons and beckons,
    And I want to go back and I will...

The Spell of the Yukon
Robert Service, 1907.

List of Symbols

A	total area of rupture surface
A	area of rupture suface excluding rock bridges
a	acceleration
B	width of channel
b	original width of failure mass
c	rock cohesion of a discontinuity
c_i	rock cohesion of a rock bridge
$\bar{c}$	turbulent resistance coefficient
D	dynamic resistance parameter
D	depth of flow
$\mathbb{F}$	Froude number
F	fahrboeschung
FMAX	maximum frictional resistance parameter
FMIN	tangent of shallowest slope angle or minimum frictional resistance parameter
f	friction coefficient
g	gravitational acceleration
H	height
k	seismic coefficient
k	dynamic resistance parameter/g
L	total horizontal travel distance
l	final average width of debris
m	mass
P	prediction capability index

R_1	basal frictional resistance
R_2	dynamic resistance
R	radius of curvature
r	pore pressure factor
Δs	runout distance
s	distance
U	uplift force
W	weight of block
w	weight of cylinder
v_1	velocity
v	critical velocity
x	horizontal distance
y	vertical distance
α	slope angle
β	slope angle
μ	dynamic friction coefficient or frictional resistance parameter
η	viscosity
ϕ	friction angle
ψ	travel angle
ρ	density
σ	normal stress
τ	shear stress
θ	superelevation tilt angle
ξ	turbulence coefficient

Table of Contents

Chapter   Page

1. INTRODUCTION 1

   1.1 General 1

   1.2 Aims of this Research 2

   1.3 Scope of this Thesis 4

   1.4 Nomenclature and Definitions 6

2. ROCK AVALANCHES IN THE MACKENZIE MOUNTAINS 8

   2.1 Introduction 8

   2.2 Physical Environment 12

      2.2.1 Physiography 12

      2.2.2 Regional Geology 13

      2.2.3 Climate and Hydrology 16

      2.2.4 Seismicity 17

   2.3 Summary of Rock Avalanche Characteristics 18

3. INITIAL MOVEMENT MECHANISMS 23

   3.1 Introduction 23

   3.2 Low Friction Surfaces 24

   3.3 Pore Pressures 29

   3.4 Roller Bearing Friction 31

   3.5 Cliff Collapse, Toppling Mechanisms 35

   3.6 Seismic Accelerations 40

   3.7 A Simple Dynamic Analysis 43

   3.8 Conclusions 52

4. SOME MECHANICAL ASPECTS OF ROCK AVALANCHE MOTION 54

   4.1 Introduction 54

   4.2 Literature Review 56

4.3 Velocity Estimation 71

4.4 Volume and Runout Distance Relationships 90

4.5 Flow Characterization 96

4.6 Summary and Conclusions 103

5. A MODEL FOR ROCK AVALANCHES 106

5.1 Introduction 106

5.2 Theory 106

5.3 Limitations of the Model 112

5.4 Computer Program RADA 116

5.5 Parametric Study 122

5.6 An Appropriate Travel Path - The Frank Slide Example 132

5.7 Discussion and Conclusions 139

6. APPLICATION OF THE MODEL 144

6.1 Introduction 144

6.2 Rock Avalanches from the Mackenzie Mountains ...145

6.3 Velocity Profiles 152

6.4 Applications to Other Mass Movements 163

6.5 Predictive Capability of Model 177

6.6 Summary and Conclusions 190

7. CONCLUSIONS AND RECOMMENDATIONS 195

7.1 Introduction 195

7.2 Conclusions 196

7.3 Recommendations for Further Research 201

REFERENCES 204

APPENDIX A NOZZLE ROCK AVALANCHE 216

A.1 General 216

A.2 Stratigraphy 218
A.3 Structural Geology 220
A.4 Surficial Geology 221
A.5 Detachment Zone 225
A.6 Rock Debris Description 230
APPENDIX B ROCKSLIDE PASS ROCK AVALANCHE 247
B.1 General 247
B.2 Stratigraphy 249
B.3 Structural Geology 251
B.4 Surficial Geology 251
B.5 Detachment Zone 254
B.6 Rock Debris Description 260
APPENDIX C VELOCITY PROFILES 275

List of Tables

Table Page

2.1 Summary of physical characteristics of six rock avalanches from the Mackenzie Mountains....20

2.2 Summary of the travel characteristics of six rock avalanches from the Mackenzie Mountains....21

3.1 Calculation of initial velocities for six rock avalanches from the Mackenzie Mountains. Cases 1 to 6 as described in the text...48

4.1 Some examples of rockslide and rock avalanche velocities.................................73

4.2 Calculation of velocity range predicted from superelevation heights at Twin slides. Location of cross-profiles on Figure 4.1.......................................80

4.3 Projectile velocities for various launch angles, θ_0, which would give the required travel range as shown in Figure 4.6.................89

5.1 Sample input and output data for program RADA, Option 1 for $\mu = 0.0653$ and $D = 40{,}000\ m^2/s^2$.....................................119

6.1 Prediction Capability Test 1 for $\mu = \tan(ANG(N) + 1.0°)$.................................182

6.2 Summary of P-values (percent) for Prediction Capability Tests 1, 2 and 3.............183

List of Figures

Figure Page

2.1 Distribution of rock avalanches in the Mackenzie Mountains (from Eisbacher,1979). Inset map of northwestern Canada showing location of earthquake epicentres for the period 1962-1974 (after Basham *et al*.,1977)................10

3.1 Seepage along the rupture surface (dip = 28°) at Lower U-Turn slide. Note the steped failure surface in the backscarp area........30

3.2 Two different modes of failure above inclined bedding planes. (a)sliding block model (μ = tan 30°) (b) seismically induced condition of basal "roller bearings"(dynamic friction) (after Eisbacher,1979)..30

3.3 Rolling cylinder model of a rockslide. (a) Initial shearing (b) Large rotation with continued shearing (c) Continued motion with front erosion (d) Cylinder and riding block model (Pariseau and Voight, 1978)..33

3.4 View of the failed rock mass at the small slide south of the main failure at Rockslide Pass. Note the fragmented nature of the failure block and the prescence of several smaller blocks on the 17° rupture surface.............................38

3.5 Progressively disintegrated failed mass on the rupture surface at Rockslide Pass. Note the degree of dilation in the block increases to the right where meter size blocks appear to have been shaken from their position.....................................38

3.6 Reconstruction of the initial rupture surfaces for six rock avalanches from the Mackenzie Mountains with approximate centres of mass for the initial and moving rock masses, prior to and at the point of disintegration............................44

3.7 Simple sliding block model with additional horizontal seismic loading...............46

Figure Page

4.1 Plan of North and South Twin avalanches showing locations of measured cross-sections........77

4.2 Cross-sections used for calculation of velocities from superelevation and run-up heights from North and South Twin avalanches........78

4.3 Plot of the calculated avalanche velocity versus horizontal travel distance for North Twin rock avalanche using superelevation, run-up analysis and initial velocity predictions (see Section 3.7)......83

4.4 "Spray" feature at Nozzle avalanche probably originating from the impact and disintegration of large boulders with high energy trajectories.............................85

4.5 Large boulder in the "spray" area located well above the valley floor and the main debris stream......................................85

4.6 Pile of rubble left from the impact of a boulder moving at high velocity.......................87

4.7 Range of possible minimum velocity trajectories for boulders which disintegrated in the "spray" area at the Nozzle rock avalanche.................................87

4.8 Hsu-type (1975) plot of the excessive travel distance versus the volume of the failed mass for several Mackenzie Mountains rock avalanches. The length of the bar indicates the degree of uncertainty in the estimate.........................92

4.9 Plot of the equivilant coefficient of friction (fahrboeshung) versus the estimated volume of the failed mass for several Mackenzie Mountains rock avalanches.........94

5.1 Simple model for frictional and dynamic resistances in a rock avalanche...................109

5.2 Flowchart of Program RADA, Option 1................118

5.3 Test profile geometries for parametric study.......123

Figure Page

5.4 Characteristic resistance relationship for Test A - an assessment of the effects of travel distance on the last slope...............125

5.5 Characteristic resistance relationship for Test B - an assessment of the effects of travel distance on the initial slope............125

5.6 Characteristic resistance relationship for Test C - an assessment of the effects of the length and inclination of the initial slope for the same fahrboeshung............127

5.7 Characteristic resistance relationship for Test D - an assessment of the effects of the length and inclination of the runout slope for the same fahrboeshung.............127

5.8 Characteristic resistance relationship for Test E - assessment of the effects of uplift pressures..................................130

5.9 Characteristic resistance relationship for Test F - an assessment of the effects of initial velocity...............................130

5.10 Reconstruction of original topography before the Frank Slide showing location of travel paths used in this analysis (after Daly *et al.*,1912 and Cruden, 1980)..........135

5.11 Characteristic resistance relationship for the Frank Slide for three travel paths.........137

6.1 Characteristic resistance relationships for six rock avalanches from the Mackenzie Mountains...............................147

6.2 Characteristic resistance relationship for six rock avalanches from the Mackenzie Mountains assuming an r value capable of allowing FMAX = tan 30° (a normal coeffienct of friction).....................151

6.3 Travel path and predicted velocity profiles for the North Twin rock avalanche. Symbol F corresponds to the frictional parameter μ...........................154

Figure Page

6.4 Predicted velocity profile for North Twin rock avalanche with v_o = 15 m/s after 436 m........157

6.5 Predicted velocity profile for North Twin rock avalanche using the entire travel path with velocities from initial sliding and superelevation analysis. Refer to Figure 4.2. 160

6.6 Characteristic resistance relationships for a selection of rapid mass movements............165

6.7 Characteristic resistance relationships for selected rock avalanhes onto glaciers..........171

6.8 Plot of P-value versus Dynamic Parameter D for Test 3.....................................186

6.9 Bar graph of P-values for various prediction capability tests........................188

A.1 Map of Nozzle rock avalanche.......................217

A.2 Longitudinal profile, Nozzle rock avalanche........226

A.3 Equal area projection of joint fabric near Nozzle rupture surface. Frequency contours in percent per 1% area...................228

A.4 (a) Rupture surface at Nozzle, dipping at about 27° (b) Nozzle "ramp" and "rarefaction" zones (c) Nozzle fan area............232

A.5 (a) Exposed section through debris along river(b) Bubbles within sandy debris from above section..239

A.6 Stratigraphic section exposed at undercut bank on river..241

A.7 Plot of percent by area versus mean boulder diameter in a sample area of 7678 m^2.......243

A.8 Plot of percent by volume versus the mean boulder diameter in a sample area of 7678 m^2.......243

B.1 Map of the Rockslide Pass rock avalanche...........248

B.2 Longitudinal profile, Rockslide Pass rock avalanche255

Figure Page

B.3 Equal area projection of joint fabric near Rockslide Pass rupture surface. Frequency contours in percent per 1% area..........259

B.4 (a) Breakaway scar, rupture surface, and part of the "ramp" (b) Alluvial sediments in the "void" area (c) Connectable portions of a dilated slab of carbonate rock from the distal end of the debris (d) Large boulder in wave area....................264

B.5 Equal area plot of poles to bedding for scattered large boulders within the debris with numbered locations from Figure B.1......................................274

C.1 Velocity profile, Damocles rock avalanche..........276

C.2 Velocity profile, North Twin rock avalanche........277

C.3 Velocity profile, South Twin rock avalanche........278

C.4 Velocity profile, U-Turn rock avalanche............279

C.5 Velocity profile, Nozzle rock avalanche............280

C.6 Velocity profile, Rockslide Pass rock avalanche....281

1. INTRODUCTION

1.1 General

Certain types of rapid slope movements such as rock avalanches and debris flows are some of the most destructive natural geomorphic agents known. Historical accounts from Europe, South America, and parts of Asia have recorded great loss of life and property due to massive rockslides that disintegrated into flowing avalanches burying entire towns and valleys. In the Canadian Cordillera, with more people living and working in the mountain environment, the risk posed to the inhabitants by rapid mass movements will increase. Consequently the planning process for land development in mountainous areas must take due consideration of the potential for such disasters. More frequently the question of *mobility* rather than *stability* is being addressed - how far and how fast would a certain rock mass, known to be unstable, travel once failure has occurred?

A recent study by Hungr(1981) has dealt with the dynamic aspects of all types of slope movements, and in particular, the rock avalanche phenomena. In a thorough review of the literature and extensive laboratory flume experiments with granular materials Hungr could not account for the apparent reduced frictional behavior exhibited in rock avalanches. While a deterministic solution for the runout prediction problem would not seem to be easily formulated, other semi-empirical approaches do offer some alternatives. It is this aspect of the rock avalanche problem which will be addressed in this research.

Eisbacher (1977,1978,1979) has described a unique collection of rock avalanches (*sturzstroms*) in the Mackenzie Mountains of the Yukon and Northwest Territories. These apparently dry, very mobile landslides which travelled as much as 7 km from their source, on average slopes of as low as 7.5°, display no obvious features to explain their apparent reduced internal and/or basal resistances. To further investigate these avalanches Kaiser and Simmons (1980) conducted a short field investigation at the Twin, Avalanche and Damocles avalanches. To carry out more detailed examinations of the local geology and to investigate the mechanical aspects of the phenomena for the purpose of calibrating a proposed model, a six week field program was undertaken in 1981 by the writer and an assistant at the Nozzle, Rockslide Pass and U-Turn rock avalanches.

1.2 Aims of this Research

Hungr(1981) outlined a method for analysing the dynamics of a given type of slope movement. The three steps he proposed were:

1. Define the phenomenon by collecting information about its mode of movement, the type and condition of the material, characteristic dimensions and other special

attributes (a phenomenological approach).

2. Formulate a boundary and an initial value problem based on analytical or physical models to describe the motion (a kinematic approach).
3. Determine the constitutive relationship for the material to be used in the equations of motion (a rheological approach).

This inquiry has dealt with the first and second steps (the phenomenological and kinematic approaches) to a large extent, while no attempt has been made to define a unique constitutive relationship for rock avalanche debris.

Specifically the two main aims of this research are:

1. To document field evidence from the Nozzle and Rockslide Pass rock avalanches describing the initial boundary conditions, the dimensions, type and structure of the pre-movement rock masses and rock debris, the mechanical aspects of the avalanche motion, and the suggested velocity spectrum as deduced from morphological evidence. In addition supplementary details from other Mackenzie Mountains rock avalanches are compiled and summarized.
2. To evaluate, modify and calibrate Koerner's model (1976,1980a) for the purpose of rock avalanche runout and velocity prediction, with special reference to a suite of rock avalanches from the Mackenzie Mountains.

At this point it is worthwhile stating that this study was not intended as a regional landslide synthesis or a comprehensive evaluation of rock slope dynamics. However, for the purpose of thouroughness and to provide the proper perspectve a description of the physical environment and the host of factors which influence rock stability in the Mackenzie Mountains are outlined. The initial failure mechanisms which started the masses in motion similarly were not a major direction of inquiry, but one chapter has been devoted to providing an overview of possible mechanisms. Finally, the evaluation of the predictive capablility is limited to Koerner's (1976) model and variations thereof, although other semi-empirical techniques are possible.

1.3 Scope of this Thesis

In Chapter 2 the physical environment in the Mackenzie Mountains and a summary of characteristics of rock avalanches from this range are outlined.

Chapter 3, an overview of the initial failure mechanisms, examines the evidence for low-friction surfaces, pore pressures, roller bearing friction, cliff collapse and toppling mechanisms, and failure induced by seismic accelerations. A primitive dynamic analysis is performed to estimate the initial velocities for six Mackenzie Mountains avalanches.

Specific mechanical aspects of rock avalanche motion are addressed in Chapter 4. A brief literature review of physical hypotheses, semi-empirical models and scale modelling is followed by an evaluation of the velocity spectrum observed or calculated for a group of documented avalanches and rockslides. Volume/runout distance relationships for the Mackenzie Mountains failures are examined and finally a brief overview of morphological evidence testifying to the complex rheology of the flowing debris is presented.

In Chapter 5 Koerner's (1976) model for flowing rock avalanches is examined and its limitations assessed. A computer program, RADA - Rock Avalanche Dynamic Analysis, is described and a parametric study is conducted to evaluate the effects of geometric variations, pore pressures and initial velocity assumptions. To assess travel path variation the Frank Slide was analysed.

A suite of rock avalanches from the Mackenzie Mountains and elsewhere is analysed in Chapter 6. Characteristic resistance relationships and velocity profiles for these movements,assuming single events, are derived and analysed and an assessment of the model for predictive purposes is conducted.

Since summaries and conclusions follow each chapter the last section, Chapter 7 serves as a review of the highlights of the preceding five chapters.

Appendices A and B describe the physiography, stratigraphy, structural geology, detachment zone and the rock debris for the Nozzle and Rockslide Pass rock avalanches, respectively. Appendix C contains the velocity profiles for the six Mackenzie Mountains rock avalanches.

1.4 Nomenclature and Definitions

The names of specific landslides and topographic features described in this thesis follow the nomenclature used by Eisbacher (1977, 1978, 1979), although many of these features have not been given approval by the Canadian Permanent Committee on Geographic Names. Numerous rivers and mountain groups in some of the scarcely explored parts of the Mackenzie Mountains have yet to be named.

A *rock avalanche* is defined in the AGI Glossary of Geology (Bates and Jackson, 1980) as "a very rapid downslope flowage of rock fragments during which fragments may become broken or pulverized... Characteristic features include a chaotic distribution of large blocks, flow morphology and internal structure, relative thinness in comparison to large aerial extent, high porosity, angularity of fragments and lobate form." Varnes (1978) used the term *rockfall-avalanche* or *rockfall-debris flow* for the above phenomena, while Hsu (1975) proposes the German term *sturzstrom*. Mudge (1965) suggested the terms *rockfall-avalanche* and *rockslide-avalanche* to delineate origin; however this distinction is not always readily apparent. For the purposes of this thesis this particular form of landslide will be referred to as a *rock avalanche*, but for reasons of clarity certain parts of the avalanche may be referred to as a slide, a fall or a flow. Otherwise the nomenclature for describing the avalanche debris and the initial failed slope will follow Varnes' (1978) terminology where possible. Snow avalanches will be specifically referred to as such to avoid confusion.

It is readily apparent that some of the terms used in this system are inadequate for describing some of the features and the flow morphology of certain rock avalanches, thus convenient terms will be employed where necessary.

Some measures of rock avalanche mobility and their English equivilents may also be defined. The *fahrboeschung* will refer to the tangent of the *travel angle* defined by the line which joins the most distal tip of the avalanche debris and the top of the crown of the pre-failed mass. The *pauschalgefalle* refers to the tangent of the *mean travel angle* defined by the line which joins the centres of mass of the pre-failed and the rock avalanche debris deposit.

The *area ratio* is an empirical measure of mobility potential defined as the area beneath the line joining the crown and the tip of the debris but above the rock avalanche travel path profile, divided by the area beneath the line joining the crown and the tip of the debris, but above a horizontal line intersecting the lowest point on the travel profile.

2. ROCK AVALANCHES IN THE MACKENZIE MOUNTAINS

2.1 Introduction

Mass movements in the Mackenzie and adjacent Selwyn Mountains have not received a great deal of attention in the past. Douglas (1953) first noted the existence of a number of rockslides in the Wernecke Mountains, which lie east of the northern edge of the Mackenzies, while conducting a regional mapping program. Hughes (1969) has located several rockslides in the same region on the northern fringe of the Mackenzies near the Snake River, however, they have not yet been described. The presence of two enormous rockfall- and rockslide-avalanche deposits in the central Mackenzies were initially noted by Gabrielse *et al.*(1973). These landslides, at Rockslide Pass and Avalanche Lake, are two of the best examples of this type of phenomenon in the Canadian cordillera. These events and several others were examined by Eisbacher (1977, 1978) and later in his regional synthesis of all rock avalanches throughout the Mackenzies with volumes greater than 2×10^6 m^3 (Eisbacher, 1979).

All of Eisbacher's so-called "cliff collapses" and resulting rock avalanches or *sturzstroms* are confined to carbonate formations, most commonly in rocks of lower Paleozoic age. Most of these failures have taken place since the last glacial episode on inclined bedding plane surfaces ranging in dip from 13° to 40°. Eisbacher (1979) makes a convincing case for the contributing role of past earthquake activity for one subset of these avalanches. However, this postulate has not been much advanced beyond the conceptual stage for the other events. Some of the avalanches he studied are curiously located in rather close proximity to each other, forming distinct clusters. For example, the Nozzle and U-Turn avalanches, studied as part of this investigation, are part of a group of some seven large and several small avalanches referred to as the Arctic Red Cluster. The key avalanches studied by Eisbacher (1979) and in this research are shown on Figure 2.1. The inset map shows the location of earthquake epicentres for the period 1962-1974 (from Basham *et al.* 1977, see section 2.2.4)

The frequency of this type of slope movement has not been examined in detail, although Eisbacher (1979) does suggest that some of the avalanches may have occurred at the same time. A chronologic dating of rock avalanche deposits was not attempted in this research. However, such an investigation could be of considerable value in establishing some of the conditions which were critical to the initial failure.

The only other investigation to date of mass wasting processes in this region was a study by Gray (1973) of the geomorphic effects of snow avalanches and rockfalls on steep mountain slopes in the adjacent Wernecke Mountains. A variety of other large mass movements including rockslides, rock topples, slides in frozen soil, rock glaciers, solifluction, debris flows, soil creep, gravitational ridge

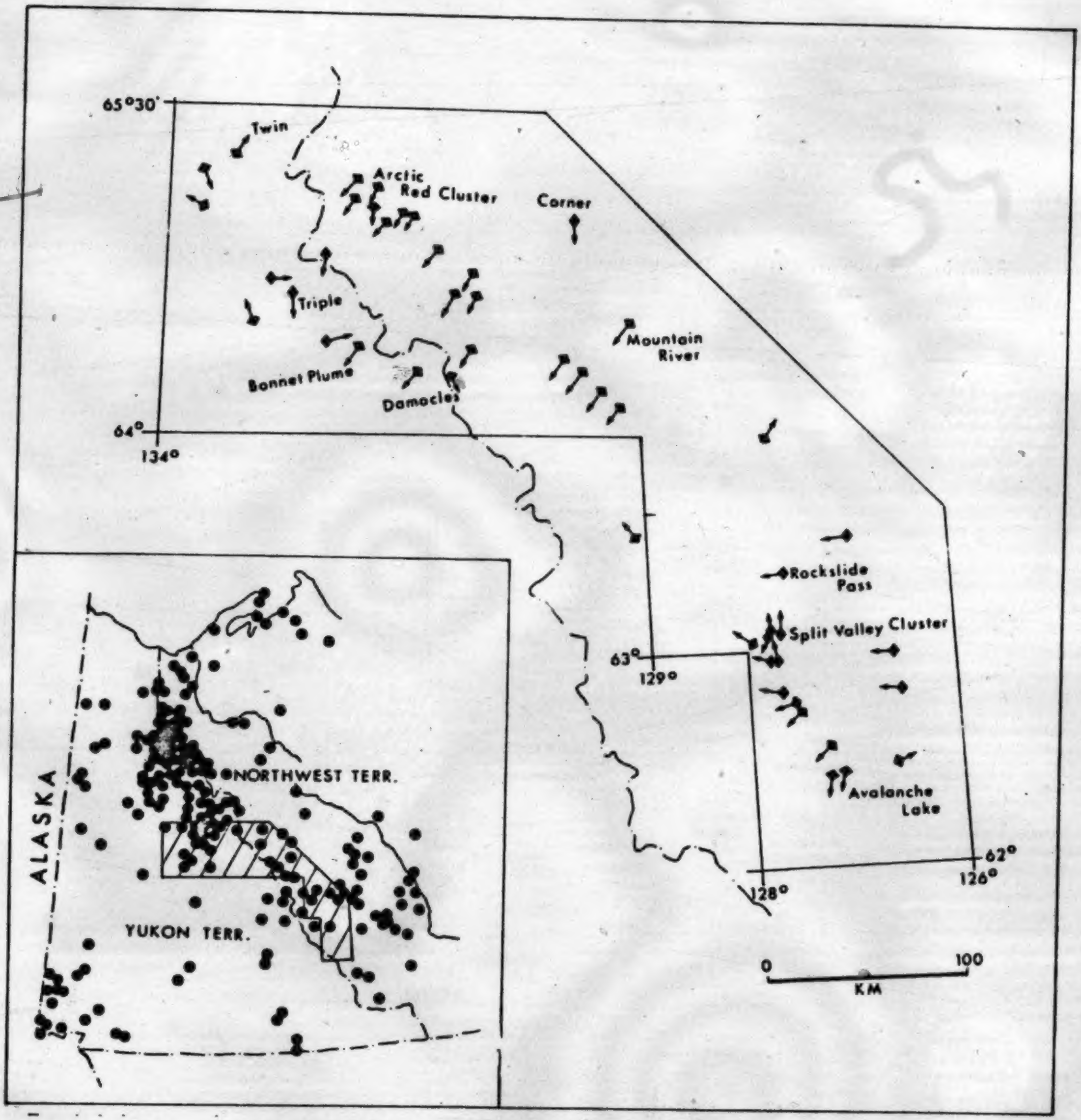
65°30'
Twin
Arctic
Red Cluster
Corner
Triple
Mountain
River
Bonnet Plume
Damocles
64°
134°
Rockslide
Pass
Split Valley Cluster
63°
129°
Avalanche
Lake
62°
128°
126°
0
100
KM
ALASKA
NORTHWEST TERR.
YUKON TERR.

Figure 2.1 Distribution of rock avalanches in the Mackenzie Mountains (from Eisbacher, 1979). Inset map of northwestern Canada showing location of earthquake epicentres for the period 1962-1974 (after Basham *et al.*, 1977).

spreading (*sackung*) and other hitherto undescribed movements have been observed in the Mackenzies by this writer and some of the investigators previously mentioned. Few of these features have been documented to date.

This chapter serves two basic purposes: first, to briefly describe the physical environment in the Mackenzies; and second, to summarize some of the pertinent data from the six rock avalanches which will be referred to in this study. Within the overview of the physical environment, the factors which are relevant to slope movements are described under the subtitles of physiography, regional geology, climate and hydrology, and seismicity. While this study is not intended to be a regional evaluation of rock slope stability, this information is deemed necessary for a proper framework to introduce the two case examples and to develop a suitable model for rock avalanche behaviour. Descriptions of two rock avalanche deposits - Nozzle and Rockslide Pass - are contained in Appendices A and B, respectively.

Additional field investigations were conducted at U-Turn and Concentric landslides by the writer and at Twin, Damocles and Avalanche Lake landslides by Kaiser and Simmons (1980). Because it is felt that the features relevant to a dynamic analysis are apparent at both the Nozzle and Rockslide Pass avalanches, no attempt will be made to identify and describe in detail features from these other landslides. Readers are referred to Eisbacher (1977, 1978, 1979) and McLellan and Kaiser (1983).

2.2 Physical Environment

2.2.1 Physiography

The Mackenzie Mountains lie directly to the east of the Yukon-Northwest Territories border and are bounded by the Selwyn Mountains to the west, the Mackenzie Plain to the east, the Peel Plateau to the north and the Liard Plateau to the south. This large mountainous area is subdivided into two main divisions - the Backbone and the Canyon Ranges - which are further subdivided into several subordinate ranges (Bostock, 1970).

The terrain in the Mackenzie Mountains is typified by uplands with steep, often cliff-forming slopes in the valleys, and plateau areas with slightly subdued mountains, flat drainages and gentle ridges. The sharply sculptured mountains in the highland areas reflect an extensive period of alpine glaciation. A number of scattered small glaciers and rock glaciers still remain in the more rugged Backbone Ranges which rise to heights of up to 2590 m. Local relief within the mountain valleys dealt with in this study is typically between 800 and 1000 m.

There are seven major rivers which drain this area to the Mackenzie River and eventually the Arctic Ocean: the Keele, Redstone, Nahanni, Mountain, Gayna, Arctic Red and the Snake.

2.2.2 Regional Geology

The bedrock geology of the Mackenzie Mountains is only known at a reconnaissance map scale of 1:250,000. The areas which have been covered by this study have been mapped by Gabrielse *et al.*(1973, 1980), Aitken and Cook (1974), Blusson (1974), Norris (1975) and Aiken *et al.*(1982). Three stratigraphic sequences have been distinguished: quartzites and carbonates of Helikian age; sandstones, shale and conglomerate of Hadrynian age; and the youngest sequence of platformal carbonates grading westward into thinly bedded carbonates and basinal shales of Lower Paleozoic Age. The platform facies is characterized by limestone and dolomite occasionally with cherty or slightly arenaceous interbeds. Most of the rock avalanches cited in previous studies occur in Paleozoic age formations: the Cambro-Ordovician Broken Skull Formation (or Franklin Mountain Formation) and the Ordovician-Silurian Whittaker Formation (or Mount Kindle Formation) (Eisbacher, 1979). Quartzites, thinly bedded carbonates, shales and sandstones tend to fail as slumps or form talus blankets (Gabrielse *et al.*, 1973).

Numerous thrust faults and associated imbricates of Laramide age characterize the overthrust Paleozoic strata which have been broadly folded. The regional trend of thrust faults and folds is predominately northwest-southeast with fault and fold axial planes dipping southwest. In the southern Mackenzies the strata are folded into a number of narrow, sharp crested, double plunging, faulted anticlines and broad, flat bottomed synclines (Aitken, 1972). The development of this regional structure was facilitated by a kinematic detachment at three separate levels in the sedimentary succession (Aitken *et al*., 1982).

The surficial geology of the Mackenzie Mountains has not yet been mapped at the reconnaissance map scale. Air photo interpretation and scattered observations by Wheeler (1954) and others were the basis for Prest *et al*.(1968) labelling almost the entirety of the Mackenzies as a region of "limited glacial activity". Surficial geology maps at the 1:250,000 scale have not been produced for either of the two rock avalanche areas studied in this research. However, some comments on the recent glacial history in the Rockslide Pass area are made by Gabrielse *et al*.(1973). Ford (1976) has shown evidence for multiple glaciation in South Nahanni National Park in the southern Mackenzie Mountains, as well as a central region between the maximum extent of Cordilleran and Laurentide ice, which was apparently unglaciated. Hughes (1969, 1972), Hughes *et al*.(1969) and Monroe (1973) have made important contributions to the mapping of complex glacial sediments which lie immediately to the north and west of the northern extremity of the Mackenzies. In a large mapping project associated with the Mackenzie Valley pipeline investigation, several 1:250,000 scale map sheets lying north and east of the Mackenzies were compiled by Hughes *et al*.(1973) and Rutter *et al*.(1973).

In the northern part of the Mackenzies there have been at least three advances of Cordilleran ice, the latest culminating in late Wisconsin time (Hughes, 1972). In this latest advance ice moved northward from confined valleys towards the Peel Plateau. Strong and recurrent alpine glaciation is suggested by the extensive cirque development at higher elevations in this area. The exact margins of the Cordilleran and Laurentide ice masses during the late Wisconsin in this vicinity are in some dispute at present. However, it is likely that some areas were only slightly affected by glaciaton, if at all (Rutter, 1982). The maximum extent of late Wisconsin valley glaciation in the Mackenzie Mountains probably occurred in the interval between 10,000 and 12,000 years ago.

There are several glacial deposits of various ages throughout the interior of the Mackenzies. Subdued terminal and lateral moraines occupy many valleys, although thick moraine deposits are not found at higher elevations, at least in areas reconnoitered in this study. Glaciofluvial deposits, alluvial fans and active floodplains characterize the wide valleys of the major rivers. Mass wasting, mechanical weathering and cryoturbation have masked large upland areas with a mantle of colluvium. As the Mackenzies lie in the zone of discontinuous permafrost such features as solifluction lobes, stone circles and stripes, mud boils and peat palsas are also common. More details on these deposits and related features may be found in works by Hughes *et* *al.*(1973) and Rutter *et al.*(1973).

2.2.3 Climate and Hydrology

Precipitation in the Mackenzies averages around 300 mm/yr (Eisbacher, 1979) , although greater levels up to 750 mm/yr, occur in central Backbone Ranges closer to the Yukon-Northwest Territories border (Burns, 1973). This probably does not have a severe effect on the stability of the well-drained jointed carbonate rock masses in the area, although peculiar drainage circumstances are possible. Very intense rain storms of short duration (10-15 minutes) infrequently occur in the highland areas.

The author has had the opportunity of inspecting the effects of such a very local cloudburst near the U-Turn rock avalanche. During a severe thunderstorm an intense local rainfall in a drainage basin of less than two square kilometres in area, gave rise to a muddy debris torrent which moved rapidly down a narrow stream bed, splashing muddy sediments to several metres height on either side of the channel. The possibility of such intense storms creating high cleft water pressures, if but only momentarily, cannot be ruled out.

Most preciptation is confined to either subsurface or surface drainage courses, although extensive bog and fenland areas are developed in some localities. Colluvial and morainal deposits along the mountain sides are mainly free-draining.

The mean annual temperature in the northern part of the Mackenzies ranges from about -7°C to -9°C in the valleys (Oswald and Senyk, 1977). Permafrost is prevalant throughout large parts of this area.

2.2.4 Seismicity

Knowledge of the seismicity of northern Canada, and the Mackenzie Valley in particular, has been greatly advanced with the installation of a number of new seismograph stations in the late 1960's and early 1970's. Relevant seismic data for the Yukon Territory and the Mackenzie valley have been compiled by Stevens and Milne (1973), and Leblanc and Hasegawa (1974) in association with investigations related to the proposed Mackenzie valley pipeline. Basham *et al.* (1977) present a concise review of seismicity in northern Canada with several more years of records. Most of the following comments have been drawn from the latter publication.

As shown on Figure 2.1 (after Basham *et al.*, 1977) there is a significant cluster of earthquake epicentres located near the Yukon-Northwest Territories border, roughly corresponding to the Richardson and Mackenzie Mountains. The most significant concentrations are located north and south of the Peel River, with a more diffuse scatter of points to the southeast along the length of the Mackenzies. Several of the earthquakes within the Mackenzies registered between 5 and 6 on the Richter magnitude scale.

Based on the conspicuous matching of this epicentre concentration and those areas with the heaviest fault incidence, Basham *et al.* (1977) have reasoned that these events are associated with reactivation of movements along structures of Paleozoic or later age.

Eisbacher (1979) presents a remarkable report of a fault scarp within surficial sediments from the Split Valley area in the central Mackenzies and the high rock avalanche incidence in the immediate vicinity. It is probable that similar features exist at scattered locations throughout the Backbone and Canyon Ranges.

It is difficult to speculate on the frequency of movements since the last glacial episode, but it is reasonable to suggest that this high level of seismicity has been present for some time, and that earthquake events of even greater magnitude (M>6) have occurred in this area.

2.3 Summary of Rock Avalanche Characteristics

Eisbacher (1977,1978,1979) has reported observations from 10 major and several smaller rock avalanches found throughout the Mackenzie Mountains. For the purposes of this research three of these avalanches - Rockslide Pass, U-Turn, and Nozzle - were examined in the field by the writer. At U-Turn there were actually two separate events in different rock types but only the upper larger avalanche will be examined. North and South Twin, and Damocles avalanches were visited by Kaiser and Simmons (1980). In this section pertinent information from these six events, which will be later analysed, are summarized in table form.

Table 2.1 lists the geographic coordinates, the volume, the rock formation which hosts the failure, its lithology, and some special features of the six rock avalanches. The volume estimates were calculated using the best available airphotos, 1:50,000 scale topographic maps and field measurements except at Damocles where field survey measurements alone were used. Details of the stratigraphy were obtained by the writer in field investigations and from previous work as described in section 2.2.2 on regional geology. The brief list of special features was compiled from Eisbacher(1979) and field work by the writer (see also Appendices A and B for more details on the Rockslide Pass and Nozzle rock avalanches).

In Table 2.2 pertinent measurements of mobility and other geometric indicators are summarized. The mean bedding plane inclinations, as found in field investigations by the writer, Kaiser and Simmons (1980), and Eisbacher (1979), do not necessarily represent the mean inclinations of the rupture surfaces. Rather, these measurements have been obtained only from those parts of the failure surfaces which were exposed and accessible. Departures from these values are possible depending upon the degree of stepping or roughness, which remain largely uncertain because of talus cover. The *fahrboeschung*, the travel angle, the total horizontal travel distance, the total elevation loss, and

TABLE 2.1 Summary of Physical Characteristics of Six Rock Avalanches from the Mackenzie Mountains

AVALANCHE	COORDINATES	VOLUME m^3 (approx.)	FORMATION(s)	LITHOLOGY	SPECIAL FEATURES
Damocles	131°08'N 64°17'N	10×10^6	? Lower Cambrian	Limestone, dolomite (1)	lateral spray; adjacent "Jumbled Castle", sharp terminus.
North Twin	133°14'W 65°16'N	8×10^6	Franklin Mountain Fm. (ЄOf)	Dolomite, limestone-grey, crystalline, platy (1)	pile-up at base of rupture surface; superelevation and run-up of debris.
South Twin	133°19'W 65°16'N	10×10^6	as above	as above (1)	as above
U-Turn	131°30'W 65°00'N	65×10^6	Keele Fm. (Hk)	Dolomite-orange, grey crystalline, blocky, some sandy interbeds (2)	ramp; rarefaction zones; changes direction by 120°; tortuous course; nearby associated failures, fault trace.
Nozzle	131°58'W 65°02'N	75×10^6	Sekwi Fm. (Єsk) ?Road River Fm. (ЄDrc)	Limestone-grey, nodular calcilutite, some silty to sandy, fossiliferous, dolomite-orange weathering, dk. grey, crystalline (2)	lateral spray; 1 km rarefaction zone; waves; ramp with about 75% volume; distal fan and "spatter" zone; bubble structures in debris.
Rockslide Pass	127°45'W 63°20'N	370×10^6	Broken Skull Fan (ЄOBs^2)	Limestone-grey, crystaline, some silty beds, rarely sandy; dolomite-orange weathering, grey silty, platy; minor siltstone-orange brown weathering, brown grey	>600 m cliff in backscarp ramp; waves; void area; boulder clusters; largest boulders 22,000 m^3; crevasse pattern; longitudinal, transverse ridges, distal "red rim"; dilation features.

Notes: (1) Kaiser and Simmons, 1980
(2) McLellan, this thesis

TABLE 2.2 Summary of the Travel Characteristics of Six Rock Avalanches from the Mackenzie Mountains

Avalanche	Bedding Plane Inclination (degrees)	Fahrboeschung	Travel Angle (1) (degrees)	Total Horz. Travel (m)	Excessive Travel Distance (m)	Total Elevation Loss (m)	Area Ratio
Damocles	17° (2)	0.131	7.5	4430	3490	580	0.348
North Twin	26° (3)	0.225	12.7	4490	2880	1010	0.200
South Twin	26° (3)	0.200	11.3	4300	2910	860	0.248
U-Turn	24-27°	0.197	11.1	3910	2700	770	0.242
Nozzle	28°	0.133	7.8	7140	5640	950	0.377
Rockslide Pass	14°	0.151	8.6	6560	4980	990	0.749

Notes: (1) Travel Angle = arctan (Fahrboeschung)
(2) Elsbacher (1979)
(3) Kaiser and Simmons (1980)

the area ratio for these events were determined from field and topographic map measurements. The estimated vertical and horizontal error margins for these measurements are 20 m and 150 m, respectively. Their significance is discussed in sections 4.2 and 4.4. As a point of note, an optical rangefinder was used for survey measurements and was found to provide sufficient accuracy for later analysis. The device was most useful in the rough, undulating rock debris terrain where normal measurements with a tape were impractical.

No systematic effort was made to date these avalanches, mainly due to the difficulty in procuring samples for radiocarbon analysis. At no location where the rock debris was exposed in cross-section was organic material observed. Some indication of the age of the avalanche deposits can be obtained from measuring the maximum diameter of certain lichen species. Only at the U-Turn avalanche, where a bed of sandstone was part of the original failure block, could this technique be used. An extrapolation of a growth curve developed in Southern Alaska (Calkin and Ellis, 1980) would suggest that the lichens growing on these strata were between 2,000 and 5,000 years old. This must be treated as largely uncertain since the growth curve may not be appropriate for the conditions at U-Turn and the exact lichen species could not be easily determined. Further work to sort out the chronology of rock avalanche activity in the Mackenzies would be most useful.

3. INITIAL MOVEMENT MECHANISMS

3.1 Introduction

Since the purpose of this research is to examine some dynamic aspects of a select group of rock avalanches from the Mackenzie Mountains, there must be some consideration given to the mechanics of the initial movements. This is important for two main reasons: first, the insights into how these masses initially began to move on such shallow bedding planes are crucial to understanding the mechanics of the subsequent flow; and second, reasonable estimates of the initial velocities of these rock masses are critical for the calibration of a model for predicting the velocity of an avalanche at points along its travel path. These aspects will be explored in greater detail in the succeeding chapters. The purpose of this section, however, is not to present an in-depth examination of the initial movement mechanism at each slide, but rather, to review a range of possible factors which, individually or collectively, may have been responsible for the onset of movements.

The essential question one must ask for a number of the rock slope failures in the Mackenzies is: How can a thick, presumably dry, jointed, blocky, rock mass move down a bedding plane at inclinations less than the reported ultimate friction angle for these materials? Without firm evidence for the existence of low friction surfaces such as shaly or pelitic interbeds, or for uplift pressures, some alternative mode of failure might be dominant. Perhaps a more elaborate mechanism including elements of sliding, toppling and rotation, with disintegration enroute, would be more appropriate. Analytical techniques for simulating this kind of behaviour are not particularly advanced, although Romero and Molina (1974) and Hammett(1974) do offer simplified models for a continuously deforming rock mass. More complicated geometries may be modelled by the Distinct Element Method (Cundall, 1976) which can simulate the interaction of a large number of rigid blocks.

Rather than develop such a model for initial boundary conditions which are largely uncertain, evidence for the existence of low friction surfaces and the presence of pore pressures will be examined. Alternative failure modes such as Eisbacher's (1979) roller-bearing friction, cliff collapse, or toppling-sliding mechanisms, and lastly, the effects of intense seismic shaking are discussed. A simplified dynamic analysis of the initial failure for several geometries from the Mackenzie Mountains, using some of the aforementioned models, is presented for comparison purposes.

3.2 Low Friction Surfaces

Low friction surfaces have not been observed in limited field observations by the writer, Kaiser and Simmons (1980), or by Eisbacher (1977, 1978, 1979). The absence of interbeds of shale, gypsum or similar lower friction materials is largely conjectural, since the basal portion of the failed mass cannot usually be observed and the flanks adjacent to the failure surface are often well covered by talus. For the most part, in the limited exposure of the bedding on the rupture surface there is a lack of striations or gouge marks often associated with the movement of large rock slide masses. This may not be all that surprising, given the apparent rapid rates of weathering characteristic to the carbonate rocks of the area. Because of the very restricted exposure at Nozzle, U-Turn and Rockslide Pass it was not possible to evaluate the local roughness of the rupture surface, hence it is not possible to estimate a relevant i angle. From geometric considerations, however, it is most likely that the failure surfaces at Rockslide Pass, Damocles and probably Lower U-Turn contain stepped surfaces in the vicinity of the back failure scarp (e.g., see cross-section, Figure B.3).

The existence of cohesion c along the bedding planes within the failure zone cannot be ruled out. Terzaghi (1962) has suggested:

$$c = c_i A_g / A \qquad \text{(Eqn. 3.1)}$$

where c_i is the cohesion of the rock substance, and A_g/A is the proportion of the potential rupture surface over which the discontinuity is not present, and the rock substance remains intact. While the cohesion of the rock c_i could be approximated as the tensile strength, there is considerable difficulty in evaluating the A_g/A ratio. Other problems exist in evaluating a relevant cohesion value for analysis (Krahn, 1974; Cruden, 1975), hence the usual procedure in slope stability is to assume it to be a negligible resisting force. Pariseau and Voight (1978) have also shown there is a scale effect on cohesion; a relatively thin slide mass will exhibit a lower total cohesive resistance to sliding than a thick rock mass. Progressive failure - essentially a displacement dependent cohesion - could also be introduced (Pariseau and Voight, 1978).

Since a rational basis for evaluating the role of cohesion in slope failures in blocky carbonates has not been demonstrated, and because of the limited field exposure of the rupture surfaces the conservative procedure used here for a simple dynamic analysis will be to assume zero cohesion.

At Nozzle slide there is some evidence for a thrust fault or possibly flexural slippage along bedding planes as discussed in the previous chapter. While this must be construed as somewhat speculative, it has been demonstrated by Cruden and Krahn (1978) that this style of deformation, commonly associated with the Rocky Mountains (Dahlstrom, 1970), is responsible for the reduction of the peak to the ultimate friction angle and the loss of some cohesion along bedding and fault surfaces. The presence of the reddish brown mineralized karstic dolomite breccia along the east flank of the dip slope at Nozzle may be significant as well. If this unit was continuous beneath the failed slope, as part of, or associated with a fault surface, then the failure may have taken place along a structurally weakened shear zone with, or without, pore pressures. The presence and subsequent effects on stability of water bearing karstic strata in several large landslides outside of this study area may have been overlooked by previous investigators (D. Cruden, personal communication).

Mapping near the rupture surface of the U-Turn slide did not reveal a ubiquitous low friction surface, although a similar, brecciated dolomite as found at the Nozzle slide was noted on the west flank of the rupture surface. In limited field observations at the Lower U-Turn, Rockslide Pass, and Damocles slides no evidence was found for a porous karstified unit nor for reduced friction surfaces to facilitate sliding on shallow slope angles.

The reduction of the peak friction angle to the ultimate friction angle in shearing along discontinuities in rock occurs when the deformation can continue essentially with no change in shearing resistance, at least on a scale of displacement larger than the asperities or the resulting discontinuity (Krahn and Morgenstern, 1979). Values of the ultimate friction angles for various discontinuities in carbonate rocks have been compiled by Krahn (1974) and Coulson (1970). Krahn presents shear test results from bedding, joint and flexural slip surfaces from the Frank slide. The ultimate friction angle tested on bedding planes was 32° while much lower values of 14° and 15° with cohesion intercepts were reported for the joint and flexural slip surfaces, respectively. These lower values may reflect the test procedure to some extent and are not likely to be representative of an operative frictional resistance for bedding plane movements because of the existence of cohesion and surface roughness. Theoretically, one would expect to observe rock slides on rupture surfaces dipping at angles slightly greater than peak angles of friction - 30 to 45 degrees - as has been noted by Cruden (1976) for major rock slides in the Canadian Rockies. This is not the case for several of the rock slides from the Mackenzie Mountains.

The case for a change in the nature of frictional shearing at high velocities or high normal loads has been advanced by several writers (see Literature Review, Section 4.2). In the context of carbonate rocks, Erismann's (1979) lubrication by CO_2 gas is perhaps a more plausible mechanism than his frictional heating postulate. Crawford and Curran (1981) have verified the rate-dependent behaviour of rock joints for certain lithologies, although tests on dolomite from the Lockport Formation, Ontario showed different behavior. Shearing was initially proportional to the shear velocity, which was followed by shearing with a constant, velocity-independent resistance. Additional experimental evidence at higher shear rates (greater than 1 m/s as used by Crawford and Curran, 1981) would be needed to assess the hypothesis for friction reduction on rupture surfaces in the Mackenzie Mountains.

3.3 Pore Pressures

Limited field evidence suggests that pore pressures could have been present at the Upper and Lower U-Turn slides and possibly at the Nozzle and Rockslide Pass slides (see Figure 3.1). Significant amounts of seepage were noted on their rupture surfaces. The observed seepage locations and the exposure of the mountains on several sides implies that the pore pressure distributions may have been quite variable across the rupture surfaces at the onset of movements. In fact, the rupture surfaces at U-Turn, Nozzle, Damocles and Twin slides are located on truncated, bedding plane controlled ridges with at least two exposed flanks. This might suggest a reduction in pore pressures in the vicinity of the initial failure, although the magnitude of this effect is highly uncertain.

It might also have been possible for pore pressures to build up at the toe of a potentially unstable rock mass in a periglacial environment. This could be accomplished, for instance, by the decay of high-level permafrost in the slope or by impeded drainage due to permafrost in the lower portion of the slope (D.Cruden, personal communication). Even if climatic conditions at the time of these avalanches were found to correspond to this type of environment, it would still be most difficult to confirm such a hypothesis.

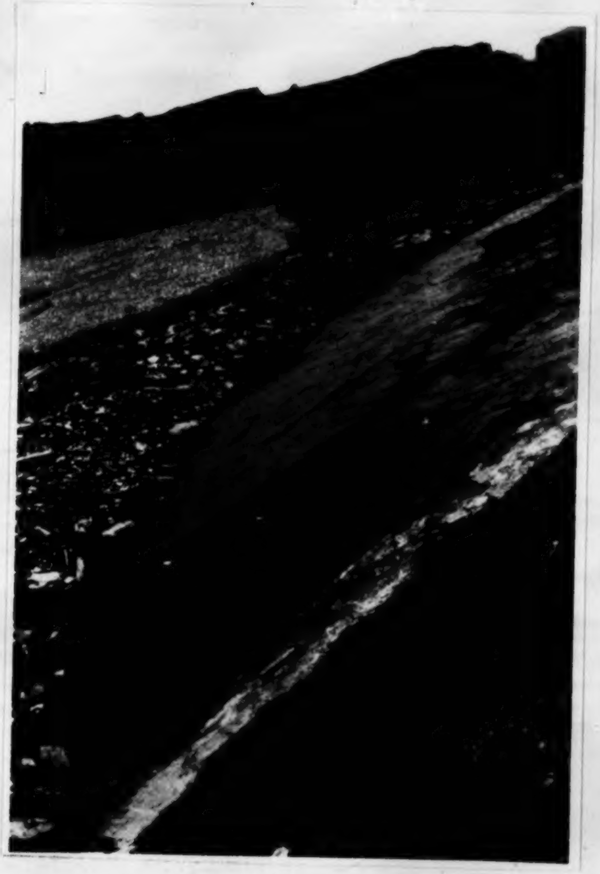

Figure 3.1 Seepage along the rupture surface (dip = 28°) at Lower U-Turn slide. Note the stepped failure surface in the backscarp area.

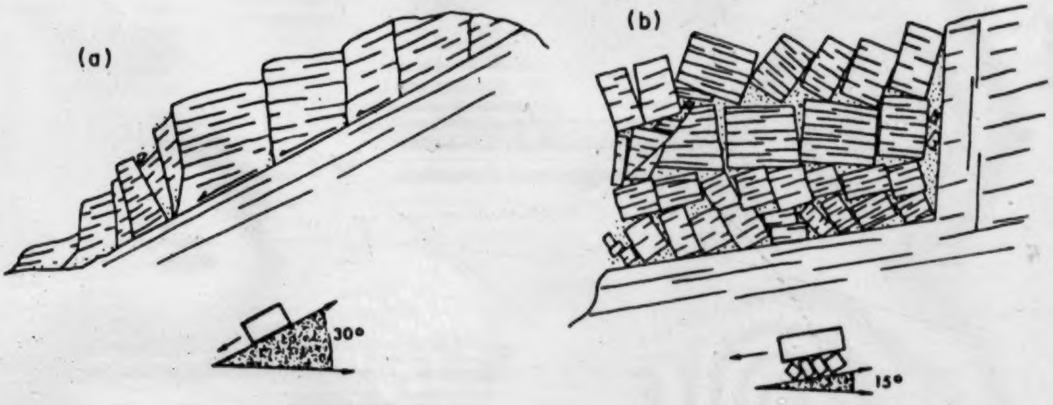

Figure 3.2 Two different modes of failure above inclined bedding planes. (a)sliding block model (μ = tan 30°) (b) seismically induced condition of basal "roller bearings"(dynamic friction) (after Eisbacher,1979).

A fluctuating water pressure due to seasonal runoff variations could also have the effect of inducing progressive failure in a similar manner as would periodic blasting. After a sufficient number of brief displacements due to quick pore pressure buildup and release, the cumulative effect makes the mass vulnerable to catastrophic failure (Pariseau and Voight, 1978). This hypothesis would also be most difficult to confirm or deny without a record of movements for a rock slope in similar surroundings.

Finally, it should also be noted that pore pressures need not be solely due to water. As will be discussed in the review of possible rock avalanche mobility mechanisms (Section 4.2), pore pressures due to steam or other gases are theoretically feasible under certain conditions.

3.4 Roller Bearing Friction

Roller bearing friction has been advocated by Eisbacher (1979) to explain the anomalously low failure slope angles. He has claimed that in the collapse of a mountainside on a gently inclined bedding plane, the disintegrated rock mass is carried forward by the rotation of joint bounded blocks in the basal rupture zone (see Figure 3.2). Furthermore, the rotational movements in the basal zone coincide with crushing and comminution of the constituent blocks. Hence the coefficient of internal friction is reduced from a static value of about tan 32° to a rolling friction of between tan 13° and tan 20°. Eisbacher (1979) further postulates that this basal zone of initial breakage and grinding may be several tens of metres thick.

From the mechanics point of view the analysis of this form of motion could be approximated by the rolling cylinder model as described by Pariseau and Voight (1978). Initial shearing is followed by rotation of small blocks in the basal zone while the bulk of the mass remains intact. The lead block must topple forward so that the nose is eroded (see Figure 3.3). The acceleration a of a block riding on a rolling cylinders is simply:

$$a = f\ g\ \sin\beta \qquad \text{(Eqn. 3.2)}$$

where $f = (1 + w/2W)(1 + 3w/8W)$, w is the cylinder weight and W is the weight of the block supported by the cylinder. Thus the block's acceleration may exceed gravitational acceleration since f ranges from 1.0 (small cylinder) to 1.33 (large cylinder). In fact, providing the cylinders remain independent, the body accelerates regardless of the value of f or the slope angle β.

Clearly this simplistic approach is inappropriate to analyse the onset of movement in some of the rock masses examined in this study. While the high acceleration and velocity predicted by the model may offer some insight into the apparently rapid movement of the rock mass after displacements have occurred, the central problem of the initial limiting static equilibrium of the mass on low slope

Permission to use this diagram was not obtained from the publisher. Readers are referred to the original publication.

Figure 3.3 Rolling cylinder model of a rockslide. (a) Initial shearing (b) Large rotation with continued shearing (c) Continued motion with front erosion (d) Cylinder and riding block model (Pariseau and Voight, 1978).

angles remains unresolved.

There is field evidence in a few cases to substantiate the apparent rotation and comminution of the blocks in the basal portion of the failed rock mass. Eisbacher (1979) reports the forward rotation of blocks above the bedding planes at Triple slides and the writer has noted some loss of material from the base of blocks left on the failure surface of the small failure adjacent to the Rockslide Pass slide. Similarly, it would appear that a large portion of the "ramp" area at Rockslide Pass consists of the upper portion of the mountainside which collapsed, consequently suggesting the removal of much of the stratigraphic succession from the original lower slope. This hypothesis cannot be conclusively verified without recourse to detailed stratigraphic evidence from within the debris. Eisbacher's (1979) observation of the "red rim" at the distal portion of the debris does not necessarily represent the basal portion of the initial rock mass (see Appendix B) and there is other evidence (see Chapter 4) of more complex motion in the debris which is incompatible with a roller bearing or cylinder friction model for a large part of the entire avalanche.

A further difficulty with the model is the actual physics of how a thick, disintegrating, blocky, shear zone may exhibit a reduced coefficient of friction for a short time period, if even that, because of the seizing of the blocks within the zone. Without a means for removing the comminuted material within the shear zone, rolling motion as depicted in Figure 3.3 is not possible because of the close contact maintained between adjacent blocks. The motion would become simply equivalent to the sliding of a block upon a frictional granular material with a normal friction coefficient of about tan 32°.

The above problems with the roller bearing friction concept might be resolved by experimental modelling and/or a theoretical study of the mechanics of shearing in a blocky, progressively comminuted rock mass.

3.5 Cliff Collapse, Toppling Mechanisms

Eisbacher (1979) used the term "cliff collapse" to refer to a slope movement where the mass above the rupture surface has undergone extensive internal disintegration prior to failure. He cites the Dammocles avalanche as an example of such a process. However, an extension of this mechanism to the other avalanches detailed in this study would be presumptuous. The mechanics of the motion of the rock mass has been previously described under the "roller bearing friction" concept, but it might be more appropriate to link this style of movement with the toppling mechanism as initially elucidated by De Freitas and Walters (1973), and later by Goodman and Bray (1976), and Hoek and Bray (1977).

Alternatively, it was initially suggested by Mueller (1968) and furthered by Hammett (1974) that a favourable geometric configuration and block size is conducive to producing a progressive collapse-type mechanism. For the right conditions it is possible for a large blocky rock mass to create the required stresses which can lead to accelerated movemnts. Further pursuit of this topic and its applicability to the initial movement stages for these avalanches would seem to be a promising direction of inquiry.

The first movements in these slopes probably began in weakened rock created during oversteepening of the slopes in the last glacial episode. Mollard (1977) presents a convincing case for the formation of rock avalanches due to glacial erosion which deepens and oversteepens the mountain valley, followed by retreat and stress rebound in the mountain sides. Gerber and Scheidegger (1969) predicted states of tension or compression in the summit areas of mountain masses. The result of these endogenetic stresses in the vicinity of mountain scarps is to reduce strength along discontinuities in the rock mass and consequently displacements may begin. Progressive deformation of the mass further reduces the shearing resistance along discontinuities and may change the geometric configuration of the slope. A catastrophic failure may result when resisting forces become less than the driving forces within one or more parts of the mass.

Of course it is impossible to examine the configuration of the pre-failed slope at any of the examples described here, but some valuable insights may be gained from observations of the proximal parts of the avalanche deposits and from adjacent slopes. Of particular interest is the small slide on the flank of the large failure at Rockslide Pass. This rather unique feature occurred on a slope dipping at 16° to 17°, or at an inclination very similar to the 14° slope on which the major failure took place (see Figure 3.4). No evidence exists for the presence of a low friction material in the basal portion of the mass. Apparently the block initially moved down the slope on a discrete shear zone undergoing progressive disintegration enroute. Several large blocks were left on the upper part of the rupture surface, some of which have lost a portion of their base. Further downslope, where the bulk of the mass has come to rest, there is an interesting pattern of disintegration. The upper end of the mass displays a network of cracks which become progressively larger and more frequent towards the end of the block until the entire mass becomes disintegrated. Metre size blocks seem to have shaken from their position and spread in an arcuate pattern about the end of the block (Figure 3.5). Some blocks have travelled up to 400 metres at right angles to this point, on surfaces sloping at inclinations less than 10°.

It would therefore appear that this disintegrated rock mass may represent a small scale version of the dynamics involved in the adjacent larger avalanche. It appears as if the frozen-in-motion look could reflect the inability of the

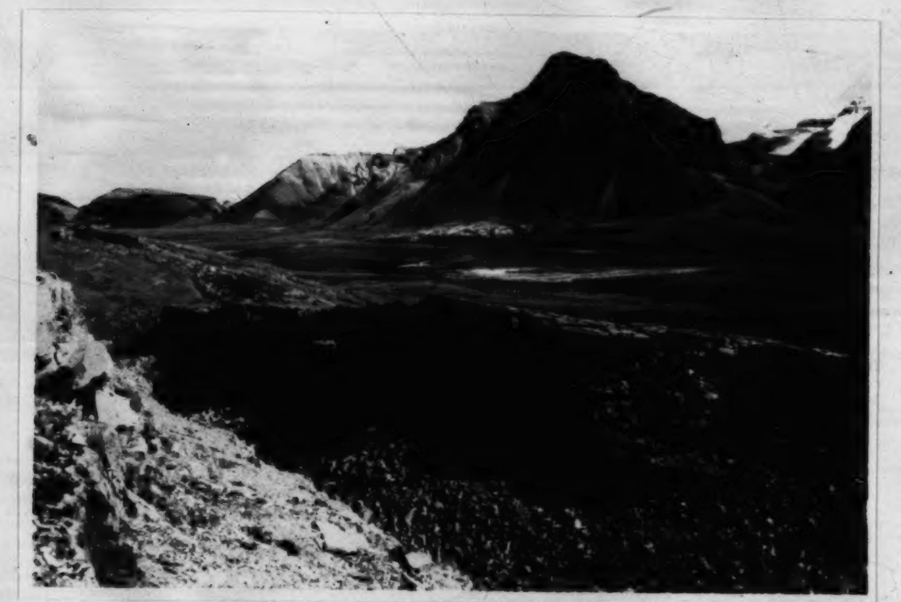

Figure 3.4 View of the failed rock mass at the small slide south of the main failure at Rockslide Pass. Note the fragmented nature of the failure block and the presence of several smaller blocks on the 17° rupture surface.

Figure 3.5 Progressively disintegrated failed mass on the rupture surface at Rockslide Pass. Note the degree of dilation in the block increases to the right where meter size blocks appear to have been shaken from their position.

block to attain a certain threshold energy whereby it would disintegrate completely. Obviously a combination of different modes of movement is relevant here: shearing and rotation within a discrete zone, proceeded by gradual dilation involving rotation, toppling and sliding motions, ending with a total disintegration of the mass into a blocky debris stream.

Very few cases of this type of slope movement can be found in the literature. De Freitas and Walters (1973) report an example of toppling from Nant Gareg-Iwyd in the United Kingdom which does bear some resemblance to the dip slope movements in the Mackenzie Mountains in that it displays dilation features and suggests a rapid downslope movement without developing into a debris stream. Basal shearing would not appear to be present, however.

From an analysis point of view the initial motion of a rock mass undergoing simultaneous fragmentation would be a difficult problem to model. Cundall (1974, 1976) has developed an interactive graphics package to simulate the motion of a fragmented rock slope where two assumptions are made. Firstly, each fragment of the mass is a rigid body of known geometry and, secondly, the nature of the forces between blocks is known. While these two criteria would be hard to satisfy for the given geometries in the Mackenzie Mountains avalanches, the technique does offer an analytical tool for predicting velocities and accelerations in the initial phase of a rock avalanche. Refinements could also allow for additional effects such as pore pressures or seismic accelerations. The application of this method to the cases presented here is beyond the scope of this research.

3.6 Seismic Accelerations

Seismicity has most certainly affected slope stability in this part of the Yukon and Northwest Territories. Basham *et al.*(1977) have shown the Mackenzie Mountains to lie within a zone of moderate earthquake activity. Not surprisingly, the concentration of northwest trending and southwest dipping thrust faults in the area south of the Peel River, as mapped by Norris (1972), roughly correspond to that area encompassing the Twin, Triple and Arctic Red cluster of rock avalanches. Leblanc and Haseqawa (1974) have superimposed on Norris's map the location of epicentres from seismic events recorded in 1972 experiments associated with the Mackenzie Valley Pipeline investigation. The matching of earthquake epicentres and the known fault network within the area is remarkable, although the exact nature of this correlation has yet to be explored. Even more interesting is the close proximity of many of the rock avalanches, e.g. Twin slides, to these epicentres.

Further south in the central portion of the Mackenzies, Eisbacher (1979) reported the existence of a Holocene age fault scarp in the same proximity as the Split Valley cluster of rock avalanches. If this observation is a genuine earthquake induced fault rather than a slump or settlement feature, and the nearby failures can be dated from the same time interval, then a good case can be made for linking the two events. While similar offsets in surficial materials were not observed by the writer in field work of 1981, a unique feature of possibly analagous origin was noted in a few localities near the U-Turn rock avalanche. On two adjacent mountain crests the structure of the bedrock would suggest an intense shaking has occurred; wide gaping cracks separate most of the blocky mass. This feature was not noted everywhere in the area and seems to be limited to exposed pinnacle or horn-like mountain crests which would receive intense shaking in a seismic event. Eisbacher (1979) also reports similar precariously perched blocks above a dilated rock mass at Damocles slide.

The role of earthquakes as a trigger mechanism for rock slides has not been given a lot of attention in the literature. Obvious examples where seismic shaking precipitated catastrophic avalanches have been reported (Hadley 1964; Griggs, 1922; Plafker *et al.*, 1971, Cluff, 1971) but the large uncertainties lie in the area of predicting the effects of seismic accelerations on rock slopes. Solonenko (1977) has reviewed the topic of seismogenic landslides and concludes there are three main reasons for the change in the stability of rock masses within earthquake zones. Firstly, seismic accelerations and the resultant strength decrease due to incremental displacements in the mass create landslides. A simple mechanical model for rock motion is difficult to formulate since movement is vertical, horizontal and rotational. Furthermore, other factors, some of which are difficult to evaluate, must be considered: the depth of the earthquake epicenter, the weight of the active and passive parts of the slide, the time-dependent strength, the angle and direction of approaching seismic waves, shock attenuation, stress relief, the degree of displacement from previous earthquakes, the epicenter distance and the dynamic response of the rock and/or overlying soil. Secondly, he suggests that large scale fault adjustments result in changes in the gradient of unstable slopes causing movements. Thirdly, thixotropic effects on rock, and on soil in particular, create additional hazards such as landslides, subsidence, and liquefaction.

Solonenko (1977) also distinguishes several surface features indigenous to seismogenic landslide zones: gravitational seismotectonic wedges, collapse along faults, toppling of mountain peaks, slippage along discontinuities in landslides, seismovibrational landslides and collapse, seismogravitational collapse on an air cushion, and seismogenic ground avalanches and flows. Many of these phenomena, as described in this thesis, are common in the Mackenzie Mountains as well.

It is apparent that a hindsight determination of the precise effects of seismic accelerations on the stability of rock slopes in the Mackenzies would be a difficult task. Because of the unknown factors of the frequency of earthquake occurrence and their magnitude, the back calculation of stability in these masses must be construed as largely speculative. While a detailed examination of a seismically vibrated rock mass is beyond the scope of this research, a simple dynamic analysis is now presented as a initial inquiry into the problem.

3.7 A Simple Dynamic Analysis

In order to gain some appreciation of the velocities attained in the various proposed models, a simple calculation of the motion of the centres of mass of a number of failures is presented. While the actual physics of the driving and resisting forces is uncertain, it is nevertheless worthwhile to simplify the realities of the situation with approximations. The following procedure should be viewed therefore as a preliminary attempt to model the initial slope movements, but the calculated velocity values are only relevant in a comparative sense.

Figure 3.6 shows the simplified reconstruction of the initial geometries for six rock avalanches from the Mackenzies: Damocles, North and South Twin, Nozzle, U-Turn and Rockslide Pass. The paths over which the centres of mass of the initial blocks moved before encountering an abrupt change in slope are indicated. It will be arbitrarily assumed here that the rock mass begins to

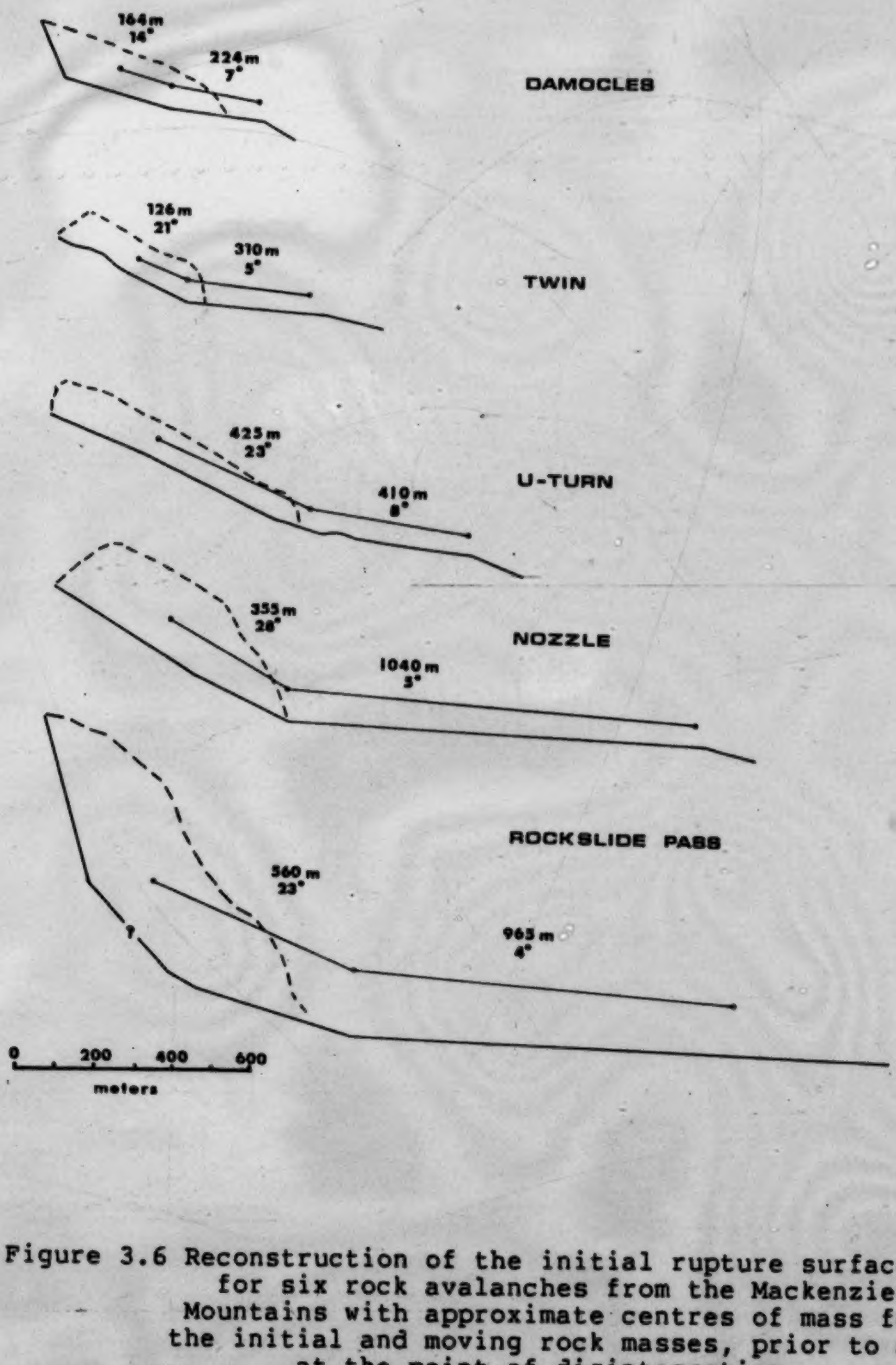
164m
14°
224m
7°
DAMOCLES
126m
21°
310m
5°
TWIN
425m
23°
410m
8°
U-TURN
355m
28°
NOZZLE
1040m
5°
ROCKSLIDE PASS
560m
23°
?
965m
4°
0
200
400
600
meters

Figure 3.6 Reconstruction of the initial rupture surfaces for six rock avalanches from the Mackenzie Mountains with approximate centres of mass for the initial and moving rock masses, prior to and at the point of disintegration.

disintegrate at this point, and until there moved essentially as a sliding block (Cases 1-4) or as a block with rolling cylinder type friction (Cases 5 and 6). For simplicity, the path has been shown as two linear segments, although in reality it is made up of many more segments.

As is commonly the practice in stability evaluation, the effects of seismic loading are equated with an equivalent horizontal force equal to a seismic factor, k, times the weight of the mass, W. Figure 3.7 is an illustration of the statics of the situation, more familiar as the simple sliding block problem. Using Newton's Second Law, the acceleration a of the body can be found as:

$$a = g[(1+k\mu)\sin\beta + (k-\mu(1-r_u))\cos\beta] \qquad \text{(Eqn. 3.3)}$$

where g is gravitational acceleration, μ is the dynamic coefficient of friction, β is the slope angle and r_u is a pore pressure factor equal to the ratio of the uplift force to the normal component of the weight. The velocity of the sliding block v is calculated from the equation of motion:

$$v^2 = v_0^2 + 2\ a\ s \qquad \text{(Eqn. 3.4)}$$

where v_0 is the initial velocity of the block and s is the distance over which the acceleration acts. The velocity can thus be solved at different increments of a slope for a body moving over a variable geometry. No account is taken of

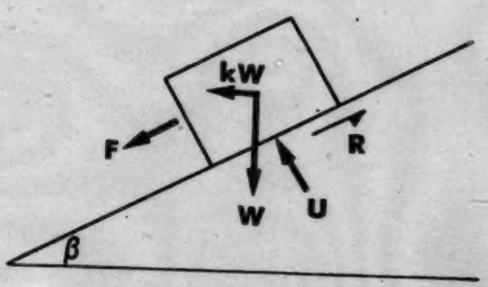

DRIVING FORCE $F = W \sin\beta + kW \cos\beta$

RESISTING FORCE $R = \mu(W \cos\beta - U - kW \sin\beta)$

Figure 3.7 Simple sliding block model with additional horizontal seismic loading.

additional energy losses such as impact at changes in slope, centripetal acceleration, fragmentation or more complicated velocity dependent resistances.

In order to have some basis for comparison, it was arbitrarily decided that the minimum velocity necessary for fragmentation was 15 m/s. Initial calculations showed that in order for the mass centre of each block to be moving at 15 m/s or greater at the end of the indicated slope certain resistance reductions were necessary. Four different cases of sliding resistance were analyzed with Twin slides as the limiting geometry.

In Case 1 the lowest seismic coefficient, k, which would allow the centre of mass of a block to attain 15 m/s without pore pressures or a low frictional coefficient after moving over the indicated geometry at Twin slides was 0.40. This was found by solving the equation of motion (Eqn. 3.4) formulated for the two segment geometry:

$$k = \frac{v^2{}_2/2g - [s_1(\sin a_1 - \mu\cos a_1) + s_2(\sin a_2 \pm \mu\cos a_2)]}{[s_1(\mu\sin a_1 + \cos a_2) + s_2(\mu\sin a_2 + \cos a_2)]} \quad \text{(Eqn. 3.5)}$$

where subscripts 1 and 2 refer to segments 1 and 2 and v_2 is the velocity at the end of the second segment. The coefficient of friction assumed here was 0.58, equivalent to tan 30°. Cohesion was assumed to be zero. Velocity values at the end of each segment, for Twin slides and the other avalanches from the Mackenzie Mountains for the same parameters, are tabulated in Table 3.1.

TABLE 3.1 Calculation of Initial Velocities for Six Rock Avalanches from the Mackenzie Mountains. Cases 1 to 6 as described in the text.

AVALANCHE VELOCITIES (m/s)

Case	Parameters	Segment	Damocles	North & South Twin	Nozzle	U-Turn	Rockslide Pass
1	μ= tan 30°						
	K_1=K_2=0.40	1	20	26	55	52	59
	r_u=0.0	2	17	15	38	51	41
2	μ= tan 30°						
	K_1=13 K_2=0.0	1	61	57	101	106	122
	r_u=0.0	2	41	15	12	49	72
3	μ= tan 11°						
	K_1=K_2=0.0	1	18	24	49	47	116
	r_u=0.0	2	16	15	36	46	112
4	μ= tan 30°						
	K_1=K_2=0.0	1	18	24	49	47	118
	r_u=0.755	2	16	15	36	46	112
5	f=1.0	1	28	30	52	57	66
		2	36	38	67	66	75
6	f=1.33	1	32	34	66	66	76
		2	42	44	82	76	86

It is important to note that the equivalent horizontal force kW which represents the dynamic load due to seismic accelerations is assumed to act over the entire travel path with the same magnitude. This is a oversimplification of the actual situation, for not only would the mass experience horizontal motion but more complicated vertical and rotational movements of variable magnitude would affect the system. Furthermore, extending the effects of this pseudo-static loading over the entirety of the travel path has no theoretical basis. Rather, the reason for applying this equivalent loading is, simply, that without recourse to additional pore pressures or low friction resistances, the rock mass under consideration at Twin slides and some others would be incapable of attaining the limiting velocity of 15 m/s by the end of the second travel segment. There would also appear to be substantiated evidence as previously discussed, for seismically vibrated or self-induced seismicity at a number of these movements. An analytical approach which couples the characteristic rock and debris motion involved has yet to be formulated and is probably a long time from fruition (Hungr, 1981).

Case 2 is an analagous situation with a dynamic friction coefficient (μ = tan 30°), no pore pressure and zero cohesion. However, the equivalent horizontal load, kW, only acts over the first travel segment. The required seismic coefficient, k, which would allow the block to move at 15 m/s at the end of the second segment for Twin slide was found by solving the equation of motion in a fashion similar to the formulation in Eqn. 3.5. Note the much higher velocities initially attained as compared to Case 1.

In Case 3 the solution was found for the required dynamic coefficient of friction μ which would give a velocity of 15 m/s at the end of segment 2 for the North Twin event without recourse to pore pressures or seismic accelerations. Similarly in case 4 velocities were calculated for $\mu = \tan 30°$, $k = 0.0$ and $r_u = 0.755$ which also gave a velocity of 15 m/s at the end of the second segment. Because an increase in pore pressure is actually equivalent here to a reduction in the friction coefficient - $\mu = \mu(1-r_u)$, the predicted velocities for both cases 3 and 4 are identical. The values at the end of segments 1 and 2 are also very close.

In Cases 5 and 6 the velocities are predicted by the rolling cylinder model (Eqn. 3.2). The two limiting cases, with rolling friction coefficient f equal to 1.0 for a small cylinder, and equal to 1.33 for a large cylinder were tested. As shown in Table 3.1 this model predicts velocities considerably greater than the sliding friction case. Note also the continued acceleration of the mass on the second shallow slope for each of the examples.

It is difficult to speculate on the actual velocity spectrum for the initial movement stage in these events. There are very few velocity indicators such as run-up or superelevation near the proximal end of the avalanche to use in assessing the above tested models. These preliminary velocity estimates can be best viewed in a comparative sense to illustrate the effects of the initial slope geometry on the various models. For instance the highest velocities (Cases 2, 3, and 4) are predicted for the initial movements at Rockslide Pass. As seen in Figure 3.6 this is a direct consequence of the long steep (23°) initial slope segment. The initial velocities predicted at U-Turn are generally only slightly greater than those at Nozzle with the exception of Case 2 at Nozzle where the lowest second segment velocity (12 m/s) was calculated. This again is a reflection of the geometric influence.

The rolling cylinder friction model predicts the greatest velocities at the end of the second segment for these two and the remainder of the slides. The predicted velocities for the initial segment of the Twin slides are only slightly greater than those of Damocles with the exception of Case 2. On the other hand, geometric effects (a steeper slope) allow a greater final velocity at Damocles than at Twin slides, excepting the rolling cylinder model velocities.

In terms of an initial mobility potential it can be seen that for Cases 3 and 4 the order of potential would be Rockslide Pass, U-Turn, Nozzle, Damocles and then Twin slides. For Case 2, where a seismic acceleration is only assumed over the first segment, Rockslide Pass, U-Turn and Damocles, respectively, show the greatest initial mobility potential. Similarly in Case 1, where a seismic acceleration is assumed over both segments, U-Turn, Rockslide Pass, and Nozzle, respectively, show the highest mobility potential.

3.8 Conclusions

The initial movement mechanisms for these rock masses are still largely unknown and warrants further research. Field evidence for low friction surfaces has not been found and their existence as well as the magnitude of unknown pore pressures must remain in the domain of speculation. While there are field observations to substantiate Eisbacher's (1979) suggestion of rotational movements within the rock mass, the mechanical and theoretical feasibility of a roller bearing type of friction is questionable. Undoubtedly a more complex motion involving sliding, dilation and toppling is closer to reality. Analytical approaches to the problem are limited in scope, although experimental work could prove useful in calibrating a model. In the writer's view, inadequacies in handling the effects of earthquake and self-induced seismicity are the major impediments to meaningful back calculation of stability and initial velocities. There is substantial evidence to suggest a link between seismic activity in the Mackenzies and the incidence of large rock slides and avalanches. Further investigation of this hitherto untouched topic is recommended.

Finally, a simplified dynamic analysis was performed to predict initial velocities for five modified slope geometries from the Mackenzie Mountains. Various assumptions were employed to test hypotheses for pore pressures, dynamic friction resistances and seismic loading. While the velocity values obtained are based on rather arbitrary assumptions, it is useful to compare the various models in a relative sense, particularly with respect to velocity predictions from Koerner's (1976) avalanche model (see Chapter 6).

4. SOME MECHANICAL ASPECTS OF ROCK AVALANCHE MOTION

4.1 Introduction

This chapter has two main purposes: first, to present an overview of the mechanical approaches to the phenomena of rock avalanches; and second, to investigate some observations from a select group of these events in the Mackenzie Mountains with the intention of characterizing the mode of movement.

The various approaches to the rock avalanche problem can be broadly categorized into three streams:

1. Physical hypotheses based on theories with difficult to characterize parameters (eg. air cushion, fluidization postulates),
2. Semi-empirical approaches such as a frictional energy balance or the application of hydraulics principles, and
3. Empirical approaches such as volume runout correlations, multiple regression, or scale modeling.

The literature related to the above topics is quite diverse, hence the intention of the initial part of this chapter will be to present only a broad overview of the various approaches. The interested reader is referred to Hungr (1981) for a more complete review of the subject. Furthermore, Chapter 5 and 6 will examine in greater detail the semi-empirical treatment of the problem in the context of rock avalanches from the Mackenzie Mountains.

In order to make the proper choice of parameters for a numerical model, compatibility between field observations and the proposed physics of the avalanche motion must be obtained. This in itself, would appear to be the principle problem hindering the development of a deterministic solution to the mobility question. A number of questions remain to be answered:

1. What is the range of velocities and how are high velocities achieved by the avalanche debris early in its motion?
2. What evidence exists for the reduction of a basic friction angle for granular materials or are other elements such as "lubrication" or pore pressures responsible for the apparent excessive travel distance?
3. Why does the initial displaced mass, although disintegrated into small fragments, still show a surprising congruence of stratigraphic order?
4. What is the explanation of the void or "rarefaction" zones as noted at Nozzle, Rockslide Pass and U-Turn avalanches?
5. What is the actual rheology of the avalanche debris in its macroscopic sense and what does this tell us about the existence of turbulence, the strength of the debris sheet, and the "sliding or flowing" question?

While it is not the intention of this thesis to examine these aspects in detail, some observations on these problem areas will be made.

4.2 Literature Review

Physical Hypotheses

Physical hypotheses for explaining the motion of rock avalanches are quite numerous and equally as varied in principle. While no single all encompassing model has been established, several attempts have been made for a number of events. A selection of the various hypotheses, as discussed by Hungr (1981) in his review, are now outlined.

"Lubrication" by mud as originally noted by Buss and Heim, 1881 for the Elm catastrophe is an attractive hypothesis for events where a large portion of the mass traversed saturated sediments or bodies of water. Evidence for the important role that these saturated fines play in the mobility of rock avalanches may be found in several examples from the literature, e.g., the Frank Slide (Hungr, 1981); the Huascaran avalanches (Plafker and Erickson, 1978); Hope rockslide (Matthews and McTaggart, 1978). In a few reported caes, such as the Steinsholthlaup from Iceland (Kjartansson, 1967), or the Mt. St. Helens rockslide avalanche (Voight *et al.*, 1981), the dislocated rock mass had acquired large amounts of water either by the melting of glacial ice or the incorporation of bodies of water in its path. The mixing of this water with alluvium and other detritus enroute has given rise to the extreme mobility in these events.

Air layer lubrication, or the air cushion postulate, proposed by Shreve (1966, 1968a, 1968b) and subsequently by some other investigators (Kelly, 1980) is attractive in cases where the avalanche travel surface has a suitable launching ramp. Presumably the debris is catapulted from the ramp at high velocity and there is little time for the compressed air to escape through the debris sheet by upward seepage. The debris layer then spreads and thins on this cushion of air until the air pressure dissipates and the slide "freezes" in position. Shreve (1968b) has shown that the upward seepage of air through the sheet would not be significant for the duration of the event if the mean permeability was less than 1 Darcy (0.001 cm/sec).

For some time Shreve's air cushion theory received wide acceptance. However, many investigators have since questioned the validity of the concept. Hsu (1975) raised three objections: the lack of air escape features, e.g., at Elm, the flow-like rather than slide-like morphology of the deposits and the absence of *sturzstroms* on the air-less surface of the moon. Others, including Bishop (1973), Voight (1978) and Erismann (1979) have expressed doubt concerning the continuity of the air layer beneath the debris sheet and the mechanism of air entrapment.

Air fluidization as described in the powder mechanics sense (Brown and Richards, 1970) would imply fluidized beds characterized by dilation, a high degree of turbulence, channeling and upward flow structures, elutriation of fines to the surface, and the fall of large particles to the base. Kent (1966) used this analogy to explain the extraordinary mobility of such events as the Frank slide and the Saidmarreh landslide. While the concept may be applicable to powder snow avalanches which display great snow dust clouds, obscuring the main body of the avalanche, the extension to rock avalanches may be of dubious validity. Such features as inverse grading in the deposits (Hungr, 1981; Hadley, 1964), the apparent lack of extensive turbulence exemplified by the maintenance of the original stratigraphy in the deposit (Eisbacher, 1979; Erismann, 1979), and the absence of upward flow structures, suggest that the phenomenon, as described for industrial fluidization processes, is not generally applicable to rock avalanches.

The presence of gaseous pore pressures, often in the form of steam, has been advocated by several authors as a means for reducing the effective stress within a basal shear zone. (Pautre *et al.*, 1974; Habib, 1975; Goguel, 1978; in Hardy *et al.*, 1978; Voight and Faust, 1982). While it is difficult to envisage the presence of pore pressures such as water, at least through the dilatant initial portion of most rock avalanches, the concept of gaseous pore pressures developing and being maintained in the basal zone is quite feasible as demonstrated by the above writers, provided there is sufficient water available. Hungr (1981) has shown that to obtain a gaseous pressure of 400 kPa, capable of fully supporting an 18 m column of broken rock the required initial saturated porosity of the source rock need only be

0.06 percent, certainly a feasible condition for even a tight rock mass. Erismann (1979) proposes another source of gaseous pore pressure in the form of carbon dioxide produced by the dissociation of carbonate rock under the heat of friction. This hypothesis, while not easily verifiable, is attractive for a large number of rock avalanches, which in the Canadian Rockies and the Mackenzie Mountains as well as in the Alps, are indigenous to carbonate rocks. Erismann (1979) also proposes a related mechanism for landslides in granitic terrain - the rock mass has slid on a surface lubricated by frictional melting. There is substantial evidence for this type of process as samples of a pumice-like rock glass have been found at the Koefels slide in Austria (Erismann, 1979) and more recently the presence of a continuous sheet of rock glass ("hyalomylonite") has been noted on the exposed gliding planes of the Langtang landslide in Nepal (Masch *et al.*, 1981).

While the pore pressure and frictional melting postulates are attractive mechanisms for avalanche or landslide mobility it is odd that certain characteristics which one would expect to be ubiquitous to most of these events are found or suggested at only a few. No large steam or gas clouds have been reported at any events in the literature and rock heating has only been noted at a scattered few (Romero and Molina, 1974; Cruden, 1982). Neither is there evidence for large scale compressed gas escape which would give rise to normal grading and certain morphological features such as escape structures.

Hungr (1981) used the term "rock dust liquefaction" to name the process Hsu (1975) proposed for the floatation of coarse debris particles in an interstial fluid of fine debris and pulverized rock dust. This mechanism derives from Bagnold's (1954) early work on the flow of concentrated cohesionless grains in a fluid medium. The frictional resistance to flow for such grains is less than that for sliding between rigid bodies because of the presence of a dispersive pressure which serves to reduce the effective normal stress. This concept has been discussed in connection with rock avalanches in the Mackenzie Mountains by Vallejo (1980). He uses the mechanism to explain why the largest boulders are often found at the front of the flow and the presence of such features as inverse grading and the "ramp" phenomenon. Eisbacher (1980) counters this argument by pointing out that the "ramp" feature has a remarkably coherent internal structure reflecting the original stratigraphy in the failed mass, and hence could not result from an internal dispersive pressure. Nor does inverse grading have to be a result of Bagnoldian flow as Eisbacher (1980) points out. Alternatively, he suggests that the remarkably well preserved dilation features in the rock debris (also noted by the writer, Appendix B) lend credence to Middleton's (1970) kinetic sieving of smaller particles through an open coarse framework to produce inverse grading in an initially unsorted granular mass.

"Mechanical fluidization" is a term coined by McSaveney (1978) to denote the change from simple frictional to complex velocity dependent flow behaviour at high shearing rates. The concept is not new to the rock avalanche problem having been suggested in some form by Howard (1973), Hsu (1975), McSaveney (1975) and Koerner (1977, 1980b). Bagnold (1954) in his original experiments on shearing of dispersions initially alluded to the notion. However, since then (1968) he has concluded that even rapidly sheared concentrated dispersions remain rheologically equivalent to ordinary frictional materials. Goodman and Cowan (1971/1972) and Cowan (1978) have advanced the theoretical formulation of granular flow based on the principles of continuum mechanics. Their use of the effect of microstructure through the introduction of the volume fraction of solids (the ratio of the volume of solids to the total volume) as an independent kinematic variable has been similarily extended in experimental and analytical work by Savage (1979) and McTighe (1979).

An extensive laboratory testing program was undertaken by Hungr (1981) to verify a proposed change in rheology at high shearing rates. In flume experiments with sand there was some volumetric dilation observed, but the material appeared essentially frictional. To investigate whether the mobilizing phenomenon might be restricted to the condition of high normal stresses a series of high velocity and ring shear experiments were conducted. For a variety of materials (dry and wet sand, polystyrene beads, and mixtures of sand and rock flour) the mechanical fluidization hypothesis was not validated. Davies (1982), however, presents an argument to the contrary claiming mechanical fluidization is supported by laboratory tests, the grain flow theory of Bagnold, and some characteristic features of *strurzstrom* deposits.

Another working hypothesis for explaining avalanche mobility is the mechanism of liquefaction. N.R. Morgenstern (personal communication) has suggested that the initial dilatant stage of the movement may become contractant thus facilitating the generation of pore pressures which allow the avalanche to continue to travel over shallow slopes until these uplift pressures dissipate. The concept of liquefaction is not new, although applying the mechanism to a discrete shear zone at the base of a blocky flow has not been attempted previously. The rationale for the existance of pore pressures at the base of the flow derives from early work on the "critical void ratio" by Casagrande (1936) and subsequent contributions by his students (Castro, 1969; Poulos, 1981). Poulos (1981) advanced the concept of "steady-state" deformation in particulate media which is the state when the mass is continuously deforming at constant volume, constant normal effective stress, constant shear stress and constant velocity. By defining the steady state line for a particular soil on a void ratio versus the logarithm of the normalized minor principal stress plot, one may evaluate the potential for pore pressure generation by following a particular stress path. Rather than elaborate on the details of the mechanism the reader is referred to the preceding publications. It suffices to say, however, that while liquefaction may be an attractive postulate for the flow of other particulate media, there must be some reservations in advocating its extension to rock avalanches, at least in the Mackenzie Mountains. Firstly, because of uncertainties in past failure geometry and the apparent lack of bodies of water ,or even saturated alluvium in many cases, it is hard to envisage where a contractant phase and the generation of pore pressures would initiate. Secondly, because there is no field evidence for a particular discrete shear zone of a measurable thickness it is impossible to evaluate which steady state line may be applicable.

Acoustic fluidization is a relatively new concept proposed by Melosh (1979). He suggests that granular debris involved in a rock avalanche may be fluidized by acoustic (pressure) waves generated by the movement of the landslide itself. The fact that dry granular material loses strength when vibrated, in some cases as much as 85% (Barker, 1962), has been known for some time. The reduction would appear to be proportional to the amplitude and frequency of vibration and inversely proportional to the grain size. Melosh (1979) derived a relationship between vibroviscosity, frequency and amplitude of acoustic waves and showed that the shear stress may be permanently relieved in the flowing mass each time the normal stress in the debris temporarily drops to zero. Hungr (1981) concurs with this mechanism as a more plausible alternative to mechanical fluidization. He further suggests that the wave amplitude may be greater at the base hence creating the inverse grading in the debris by a process similar to Bagnold's dispersive pressure. Coarse upper layers could thus ride on a fine, fluidized basal material without much distortion, a notion compatible with the observed stratigraphic congruence in many events.

In summary, there have been ten physical hypotheses described in the preceding section, each of which has been reported to be a key mechanism for rock avalanche mobility. While it is likely that one or more combinations of these mechanisms may be responsible for certain cases it is difficult to suggest a particular one which is compatible with observations for all cases. The acoustic fluidization concept, favoured by Hungr (1981) in his extensive review of the literature, may offer new avenues for a more deterministic approach, however, there are analytical obstacles to be overcome. Finally, it must be pointed out that the nature of rock avalanche deposits necessitates an individual approach with continous evaluation of the physics of the motion as deduced from field observations. To this end, a more appealing approach for predictive purposes are the empirical and semi-empirical methods which are more common in snow avalanche runout prediction.

Energy Balance Approach

Heim (1932) first attempted to model the motion of a rock avalanche by using the analogy of the simple sliding block. He equated the potential energy loss over a curved travel path with the kinetic energy gain and the losses to external frictional forces. The "effective coefficient of friction", μ, for the travel of the block is given by:

$$\mu = \tan \phi = H/L \qquad \text{(Eqn. 4.1)}$$

where ϕ is the apparent angle of friction, and H and L are the height of fall and the total horizontal travel distance, respectively. Heim recognized that the line joining the centres of mass of the initial block and the failed debris was the *Schwerpunktsgefable* and was inclined at the ϕ angle. He preferred for simplicity reasons to equate this with the *fahrboeschung*, the slope of the line joining the top of the crown of the failure slope and the distal tip of the debris. As pointed out by Cruden (1975, 1980), the difference between the inclination of these two lines may be significant.

A review of a number of case histories and an examination of a group of rock avalanches from the Mackenzie Mountains shows that the energy balance approach suggests very much smaller friction coefficients than would be expected for stiff competent rocks. Consequently, some other means of reducing the friction coefficient or of permitting additional energy loss is needed. The range of physical hypotheses directed to this end have been examined in the previous section of this chapter and no single conclusive mechanism has been agreed upon. The presence of a pore pressure could be easily handled within the sliding block model by simply reducing the normal component of the weight by the uplift force. Despite some objections as raised previously, this simple analysis has been used in the back analysis of several debris and rock avalanches (eg. Hardy *et al.*, 1978).

Other more elaborate approaches based on an energy balance with velocity dependent viscous-type resistances (Pariseau, 1980) or a more complex velocity squared dependence (Scheller, 1970; Koerner, 1976, 1977, 1980a, 1980b) have been proposed for rock avalanches. These approaches will be discussed in the context of semi-empirical methods under Hydraulic Approaches in the next part of this review.

Finally, an important point noted by Hungr (1981) offers an explanation for some of the differences between the mean travel angles of various landslides. Some account of the energy losses associated with lateral spreading of the deposit should be considered, i.e., the equivalent coefficient of friction of a wide, spread out avalanche would appear to be less than for a narrow channeled one. One semi-empirical method for the prediction of avalanche runout and extent would be to make use of the travel angle modified for the degree of lateral spreading anticipated which could be based on the "area increase ratio", a concept proposed by Hungr (1981).

Hydraulics Approach

Investigators of snow avalanche dynamics have resorted to the use of the equations of flow in open channels to account for resistances other than friction. The semi-empirical approach employed here involves evaluating a polynomial consisting of a constant (frictional) term, a linear (viscous) term, and a squared (turbulent) term:

$$\tau = \mu\sigma + \eta v/H + \gamma v^2/\bar{c}^2 \qquad \text{(Eqn. 4.2)}$$

where τ and σ are the shear and normal stresses at the base of the flow, μ is the effective friction coefficient, η the viscosity, v the velocity, H the height of the flow, and c the turbulent resistance coefficient.

Voellmy (1955) first introduced the relationship without the viscous term. Salm (1966) confirmed that the viscous term is irrelevant in snow avalanches and that the frictional and turbulent terms could be evaluated empirically. The calculation of avalanche velocities was further advanced by Heimgartner (1977). Koerner (1976) also extended this approach to treat the Huascaran, Goldau, and Elm rock avalanches. Further details of mechanics of the theoretical formulation are developed in the next chapter.

Extensions to the application of these two-parameter models were developed by Perla (1980), Perla *et al.*(1980) and Bakkehoi at al.(1981). Numerical calculation difficulties arise because of mathematical instabilities and the non-unique nature of the solution.

It is worthwhile noting that other approaches to snow avalanche dynamics envoke viscous, rather than turbulent type resistances (Mellor, 1975; Lang *et al.*, 1979; Martinelli *et al.*, 1980). The actual mechanics of the motion would therefore appear to be a rather contentious issue in this area of dynamics. Still others have used empirical correlations with certain topographic parameters to predict runout distance (e.g., Lied and Bakkehoi, 1980).

The application of these semi-empirical techniques to the rock avalanche phenomena does present a few problems. The actual physics of the motion may not be adequately accounted for by using either a viscous or turbulent resistance term in the formulation (Erismann, 1979). Furthermore, the solution actually solves for the motion of a centre of mass body which is not appropriate where the avalanche debris has spread over a large area. A more detailed discussion of these and other enigmatic aspects of this approach is given in the next chapter.

Another method suggested by Hungr (1981) is to use existing computer programs for flood routing which are based on the Chezy formula or a variation on the third term of Equation 3.2. The frictional term could be eliminated by simply subtracting it from the geometrical slope.

In summary, the hydraulics approach offers a more deterministic solution for the runout question where variations in slope geometry and flow path are encountered.

Empirical Volume-Runout Relationships

Scheidegger (1973) and subsequently Koerner (1980b) have shown the rough inverse correlation between the volume of the slide and the effective coefficient of friction or *fahrboeschung*, on a log-log plot. Although there is considerable scatter in the data, a general trend of decreasing μ with increased volume is apparent. Hungr (1981) shows a repetition of the plot in terms of the more appropriate "mean travel angle", the inclination of the line joining the centres of mass of the initial and final masses. There is relatively little change in the trend of the line and the scatter remains. A similar relationship between the potential energy of the initial mass and the tangent of the *fahrboeschung* for extra-terrestrial slides was shown by Howard (1973). Hsu (1975) plots the logarithm of the volume of the slide versus the "excessive travel distance", or distance beyond which a mass moving with a normal friction coefficient (μ = tan 32°) would travel. Only a slightly better correlation results for the landslides represented. However, Eisbacher (1979) has produced a similar plot for the Mackenzie Mountains displaying a relatively poor correlation between volume and excessive travel distance (see Section 4.4).

Scale Modelling

Scale modelling has been used in a few cases to reproduce the runout characteristics of some debris flows and rock avalanches. Moore (1976) carried out model studies of the Rubble Creek landslides using bentonite slurries. Although the model was not properly scaled to meet all similitude requirements of the real situation, Moore did manage to gain several insights into the movement and deformation of the prototype slides. Hsu (1975) used a similar bentonite slurry kinematically scaled to represent the Elm sturzstrom. While acknowledging that dynamic differences between the model and the prototype exist (grain-transmitted stress is dominant in the latter whereas fluid-transmitted stress is dominant in the former), he concluded that the mobility of such events can be adequately evaluated with the use of thixotropic liquids. Certainly these techniques hold promise for modelling complex geometries with tortuous courses or abrupt changes in slope. In a more recent treatment, Nasmith and Mercer (1979) have used model studies of the type performed by Moore (1976) to aid in the design of protective dykes for debris flows at Port Alice, British Columbia.

4.3 Velocity Estimation

Very few eyewitness accounts of a rock avalanche have been recorded. Consequently reliable first-hand estimates of the velocities involved are rare and are often somewhat speculative. Furthermore, a complete record of the velocity of a rock avalanche from start to finish does not exist. It is important to realize as well that the few first-hand velocity estimates pertain to local velocities and do not necessarily represent the average velocity of the event which is probably quite different because of the existence of surges or waves of debris. In some cases the total time for the event was recorded, e.g., the Frank slide and at the the Huascaran avalanches. An average velocity can therefore be calculated, but it may differ considerably from local velocities induced along the path because of variable topography and other effects.

In a few documented cases, rock avalanches have created their own seismic disturbance which has been recorded and used to estimate an average velocity, e.g., the Mayummarca avalanche (Kojan and Hutchinson, 1978); the Lyell Glacier slide (Gordon *et al.*, 1978). In the latter example the seismic trace could be used to discern the end of the major failure and start of the subsequent streaming of debris down the glacier. Superelevation or the tilting of the mobile debris around corners has been used by several writers to estimate local velocities (Moore and Mathews, 1978, Hardy *et al.*, 1978). Similarly, energy considerations have been used to calculate minimum velocities from debris run-up. These two techniques have been applied to some of the Mackenzie Mountains events and will be developed in the proceeding section.

More elaborate methods have been used, such as McSaveney's (1978) use of the curved flow lines on the debris to estimate velocities. Hungr (1981) casts doubt on such techniques since the curvature of lineaments on the surface of the debris need not represent the velocity direction in the basal shear zone. The solution of a semi-empirical polynomial such as in Koerner's (1976) analysis, does enable one to predict a velocity-time record for an avalanche, but this is dependent on the proper choice of frictional and dynamic resistance coefficients. Velocity predictions using this method are developed in Chapters 5 and 6.

A remarkable collection of photographs from the Mount St. Helens event (Voight, 1981) has been used to produce a velocity-time plot for the initial stages of this well known recent rockslide avalanche. Despite the fact that transitory forces such as seismic accelerations and stress relief associated with the ensuing eruption were obviously present, the photographic sequence is the best record to date of the actual distance-time relationship for this type of slope movement.

Table 4.1 is a collection of local and average velocity estimates for numerous rockslide and rock avalanche events.

TABLE 4.1 Some Examples of Rockslide and Rock Avalanche Velocities (m/s)

Event	Rock Type	Average	Local	Source
Elm	meta.	50(1)	80(1)	Heim (1932)
		20(1)	--	McSaveney (1978)
Goldau	sed.	40-70(1)	—	Heim (1932)
Frank	sed.	28(1)	--	McConnell & Brock (1904)
Blackhawk	sed.	--	33(4)	Shreve (1968)
Hope	meta.	--	25(4)	Hardy et al (1978)
Valont	sed.	25-30(3)	--	Muller (1964)
Little Tahoma Peak	volc.	--	36(4)	Fahnestock (1978)
Devastation Glacier	volc.	--	42(2)	Hardy et al (1978)
Lyell Glacier	sed.	17(5)	--	Gordon et al (1978)
Triolet Glacier	ign.	—	34-44(4)	Porter & Orombelli (1980)
Sherman Glacier	meta.	26(3)	12(6)	McSaveney (1978)
		—	67(3)(7)	McSaveney (1978)
		—	52(4)	Shreve (1968)
Mount St. Helens	volc.	—	38-80(9)	Voight (1981)
Mayunmarca	sed.	36(5)	--	Kojan & Hutchinson (1978)
Huascaran (1970)	ign.	78(1)	280(7)(10)	Plafker & Ericksen (1978)
		--	47(2)	Plafker & Ericksen (1978)
		—	33(4)	Plafker & Ericksen (1978)
Huascaran (1962)	ign.	47(1)	17(4)	Plafker & Ericksen (1978)
Huascaran (pre-Columbian)	ign.	93(8)	39(4)	Plafker & Ericksen (1978)
Dusty Creek	volc.	--	15-20(2)	Clague & Souther (1982)
Rubble Creek	volc.	—	22-29(2)	Moore & Mathews (1978)

(1) Eyewitness estimate of slide duration
(2) Superelevation in bends
(3) Frictional energy balance
(4) Frictionless run-up analysis
(5) Seismic record
(6) Curvature in flowlines
(7) Projectile estimate
(8) Extrapolation from previous events
(9) Photographic record
(10) Cratering theory

These values have been obtained by some of the preceeding methods with the exception of Koerner's (1976) analysis. A brief examination of these data reveals that there is a considerable variability in both local and average velocities. There would not appear to be a consistent relationship between the estimated velocity and other factors such as rock type or whether the debris travelled across a glacier for some portion of its path. Average velocities range from about 90 m/s for the pre-Columbian event at Huascaran (Plafker and Erickson, 1978), to about 17 m/s for the Lyell Glacier slide (Gordon *et al.*, 1978) with a mean value of about 43 m/s. Local velocities naturally show a greater range; maximum projectile velocities of 280 m/s were calculated at the Huascaran event (Plafker and Ericksen, 1978), while minimum values of 12 m/s were estimated for the Sherman event (McSaveney, 1978).

Given the uncertainties involved in some of these estimates and the apparent discrepancies which arise for the same event, (e.g., Elm) any calculation of velocities, aside from those made from a photographic record, must be treated as indicators and should not be confused with true velocities.

Superelevation of debris in bends has been used by several investigators to predict the local velocity of a rock avalanche (Moore and Matthews, 1978; Plafker and Ericksen, 1978; Clague and Souther, 1982). All that is needed for this calculation is the transverse slope θ and the configuration of the avalanche path for one location. The velocity v of the avalanche is calculated as if the mass were a fluid moving in a subcritical flow regime (Morris, 1963) using the formula:

$$v = \sqrt{Rg \tan\theta} \qquad \text{(Eqn. 4.3)}$$

where R is the mean radius of curvature of the bend in the slide path and g is the acceleration due to gravity. Some question may arise over the correct choice of the angle θ and the deduction of a mean radius of curvature R is often difficult.

The rheological properties of a rock avalanche have not been dealt with by many writers, but if McSaveney's (1978) evaluations of the Reynold's number is correct, it is likely that the Sherman and most other rock avalanches behave within the laminar flow regime. Furthermore, even a conservative estimate of the Froude number,

$$F = v/\sqrt{gh} \qquad \text{(Eqn. 4.4)}$$

where v is the velocity and h is the depth of flow, reveals that F is greater than 1 and consequently the flow is supercritical. As pointed out by Morris (1963), supercritical flow around a circular curve in a channel will produce a maximum superelevation on the outsides of the bend equal to twice that produced by subcritical flow. In fact, a wave pattern oscillating above and beneath the subcritical flow height by $v^2B/2gB$ is produced (where B is the width of the channel). This wave then continues to move down the channel alternately rising on both sides rather than only on the outside bend. Consequently the equation for subcritical flow (Eqn. 4.3) now becomes $v = \sqrt{(1/2)Rg\tan\theta}$ for supercritical flow.

This extension of the principles of water flow in channels may be a rather poor concept for rock avalanches in the first place. The internal strain and velocity relationships within an avalanche are still largely speculative and hence the appropriateness of a Reynolds or Froude number for a non-Newtonian fluid must be questioned. Consideration of these matters is beyond the scope of this research. An attempt will be made, however, to estimate velocities at the Twin slides with superelevation in bends, assuming subcritical and supercritical conditions as the upper and lower limits on the velocity, respectively.

Figure 4.1 is a plan map of the Twin slides showing the locations of surveyed cross-sections. Profiles 1, 2, 3, 4 and 5 are sites where the maximum tilt angle of the superelevated debris could be reconstructed (as illustrated in Figure 4.2). Debris run-up from profile 6 on the South Twin avalanche will be used to calculate a minimum velocity with a simple energy balance. Cross profile geometries and locations are from field measurements (using an optical

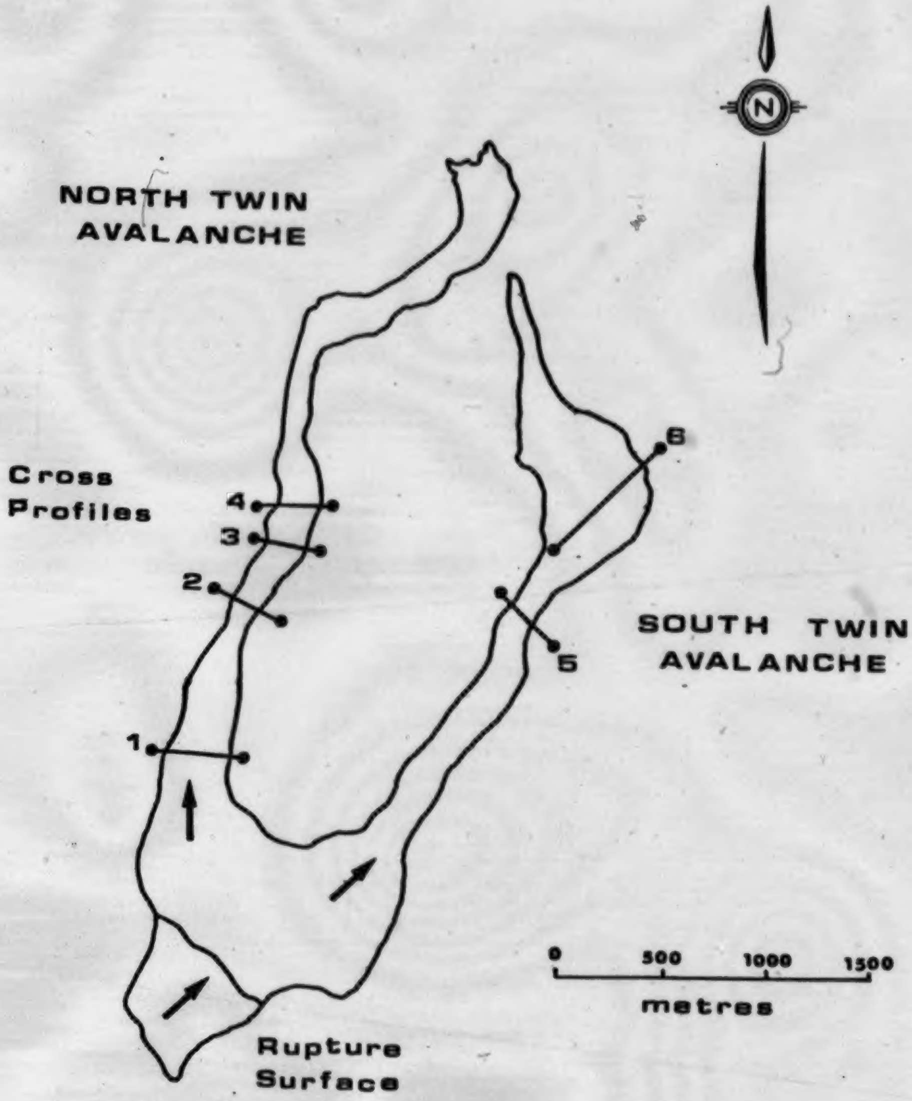
NORTH TWIN
AVALANCHE
Cross
Profiles
4
3
2
1
6
5
SOUTH TWIN
AVALANCHE
N
0
500
1000
1500
metres
Rupture
Surface

Figure 4.1 Plan of North and South Twin avalanches showing locations of measured cross-sections.

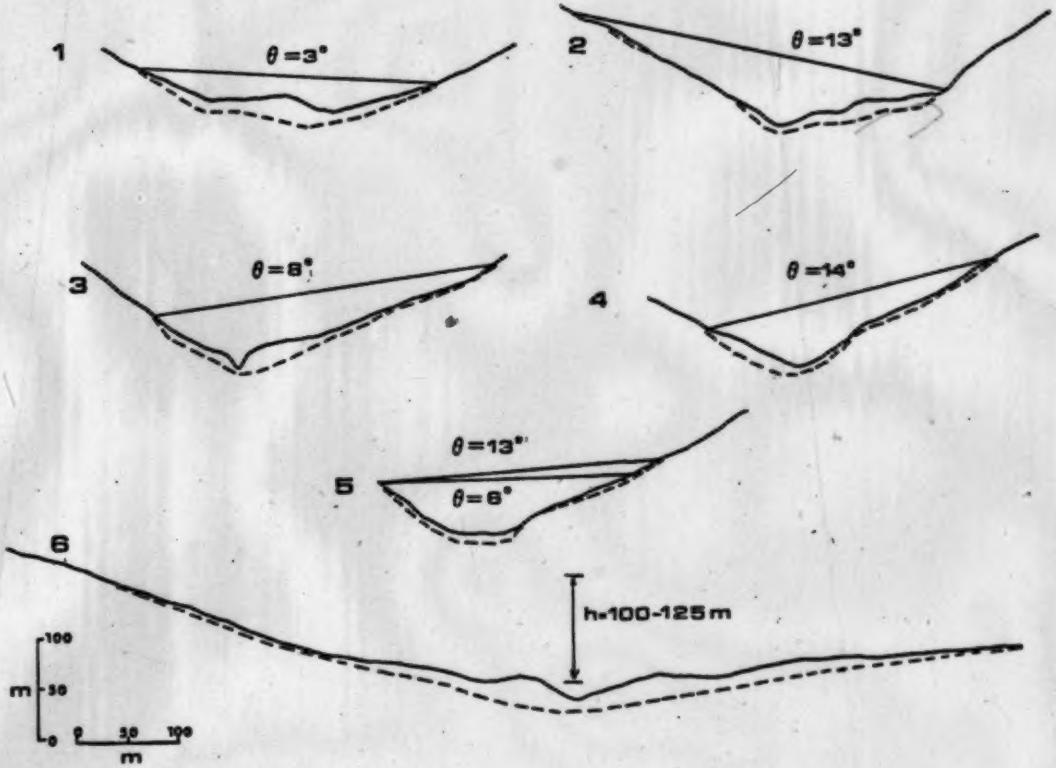
1
θ=3°
2
θ=13°
3
θ=8°
4
θ=14°
5
θ=13°
θ=6°
6
h=100-125m
100
m
50
0
0
50
100
m

Figure 4.2 Cross-sections used for calculation of velocities from superelevation and run-up heights from North and South Twin avalanches.

rangefinder and a clinometer) made by Kaiser and Simmons (1980).

For each superelevation location an approximate arc of curvature through the bend was needed. Because of the difficulty in determining an accurate radius of curvature R, at several of these sites due to talus cover and the apparent lack of curvature in the flow path a reasonable range of between 500 and 1000 m radii will be analysed. While this does allow for considerable velocity variation, the degree of uncertainty in the geometry necessitates this approach.

The calculated velocities for both subcritical and supercritical flow are listed in Table 4.2. Two values of the tilt angle θ are given for cross-section 6 since there is some uncertainty in defining the limit to which debris had risen on the east side of the valley. For R=1000m subcritical velocities (upper bound) range from 23 m/s to 50 m/s while supercritical velocities (lower bound) range from 16 m/s to 35 m/s. For R = 500 m subcritical velocities (upper bound) range from 16to35 m/s while supercritical velocities range from 12 to 25 m/s. Curiously, there is a tendency for velocities to increase down valley. This may reflect the channeling effect and perhaps the incorporation of mobility enhancing, water saturated slope colluvium or stream alluvium. These values would also seem to be in the same range as velocities calculated by similar means for other confined rock avalanches (e.g., Rubble Creek, Dusty

TABLE 4.2: Calculation of Velocity Ranges Predicted from Superelevation Heights at the Twin Avalanches. Profiles located on Figure 4.1.

Cross Profile	Tilt Angle (degrees)	VELOCITY (m/s)			
		Subcritical		Supercritical	
		R = 500 m	R = 1000 m	R = 500 m	R = 1000 m
1	3	16	23	12	16
2	13	33	47	24	33
3	8	26	38	18	27
4	14	35	50	25	35
5	13*	34	48	24	34
	6	23	32	16	23

* two transverse slopes possible

Creek, Devastation Glacier - see Table 4.1).

Run-up Analysis has been used by many investigators to approximate a lower bound estimate of the local velocity in a rock slide or avalanche (see Table 4.1). By assuming that all of the kinetic energy at the front of the flow is converted to potential energy the minimum velocity v at which the flow was moving, neglecting friction, is:

$$v = \sqrt{2gh} \qquad \text{(Eqn. 4.5)}$$

where h is the height to which the debris rises (measured from the top of the flow) up the flank of the obstacle.

No debris run-up was observed at the North Twin avalanche where it entered the main valley (Kaiser and Simmons, 1980). As shown on Figure 4.2 (cross-section 6), near the end of the South Twin avalanche a lower bound velocity could be found using a frictionless energy balance. This prominent run-up feature between 100 and 125 m measured from the estimated surface of the flow at the base of the hill to the top rim of the debris left on hillside. This gives a minimum velocity at this location of between 44 and 49.5 m/s, again, surprisingly high since this area is near the terminus of this flow. Even with a more conservative estimate of an 80 m height difference the minimum velocity would still be 40 m/s. This very rapid drop in velocity suggests, perhaps, that some resistance reduction agent is responsible for the high mobility to this point and that there is a most rapid dissipation of this uplift force at which time the motion ceases abruptly. Alternatively, a thixotropic or rheological change in the debris at some critical point could explain such a rapid loss in velocity.

Also the possibility of there having been snow or ice in the main valley thereby reducing the run-up height (Kaiser and Simmons, 1980) would permit lower velocities at this location.

For comparison purposes a plot of the upper and lower bound velocities versus horizontal travel distance for the North Twin rock avalanche is shown in Figure 4.3. Velocities calculated by superelevation as well as the initial velocities tabulated in Table 3.1 are shown on the graph. This plot might suggest that the velocities in the avalanche oscillate considerably; initially the mass accelerates to high velocities (25-45 m/s) which is followed by a decrease and then a gradual rise to highest values. The dip in the velocity profile between 2,000 and 3,000 m may be attributable to a topographic constriction at this location. Even if the velocity estimate at cross-section 1 was actually greater, because of debris higher in the slope being covered or later removed, the general trend would still be one of increasing velocity with travel distance before the sudden stop. This plot will be most useful in comparison with velocities predicted with the avalanche model discussed in the succeeding chapters.

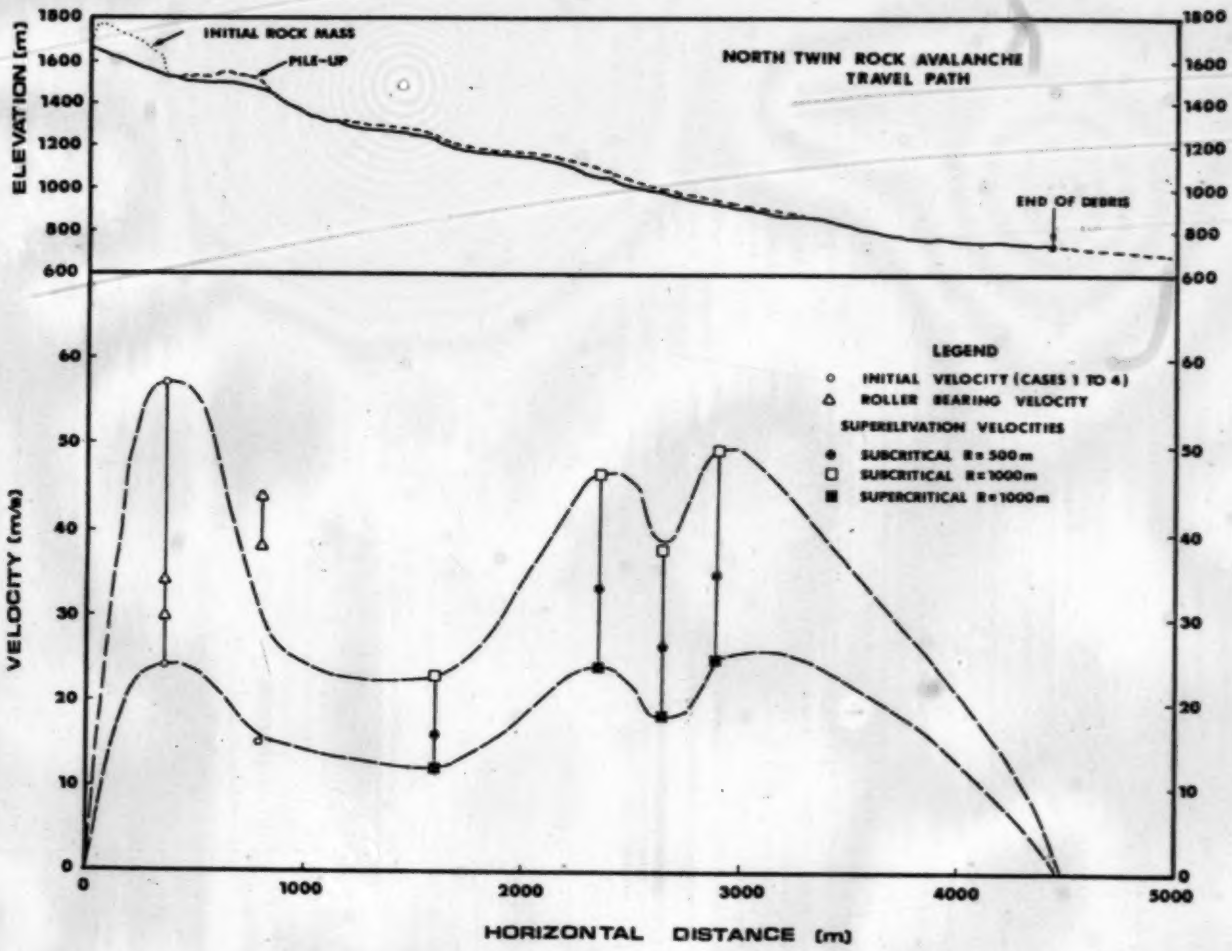

Figure 4.3 Plot of the calculated avalanche velocity versus horizontal travel distance for North Twin rock avalanche using superelevation, run-up analysis and initial velocity predictions (see Section 3.7).

Projectile Velocities have been determined for the rim of rocks which mantle the main debris stream from the 1970 Huascaran avalanche (Plafker *et al*., 1971). Incredibly high velocities, in excess of those achieved from purely gravitational fall, were calculated on the basis of trajectory angles measured from impact scars in the field. While these velocities do not represent the velocity of the avalanche body as a whole, it is puzzling how such extremely high energy trajectories are achieved. Plafker *et al*.(1978) have suggested that the "jetting" action of a topographic constriction may have been responsible for dispersing these rocks with high velocities.

Simple momentum transfer from portions of the rock mass could be used to explain these features; a large boulder moving with a small velocity is capable of imparting a higher velocity to a smaller boulder. Another explanation of how such high velocities are achieved relates to the ongoing disintegration process; when a large block with a high angular velocity impacts and fragments, some of these rocks may be catapulted at close to twice the initial block speed (Hungr, 1981). It is proposed that these "spray" features are in fact rubble left from one or more large boulders when they collided and disintegrated on the slope. Just as in the Huascaran event, these boulders could have originated in the lower part of the "ramp" area. Apparently the large rocks, left in this vicinity and scattered along the adjacent slope, must have been thrown into their present

Figure 4.4 "Spray" feature at Nozzle avalanche probably originating from the impact and disintegration of large boulders with high energy trajectories.

Figure 4.5 Large boulder in the "spray" area located well above the valley floor and the main debris stream.

position since practically no other debris is found in their proximity and most of the area right down to the valley floor (see Figure 4.5). Several circular piles of rubble, suggestive of a large block which shattered on impact, are also found within this area (see Figure 4.6).

A cross-section was surveyed in the field from the top of the ramp area to the start of the zone of "rarefaction" (terminology after Eisbacher, 1979) and over the ridge which separates the spray area from the main body of debris (cross-section B-B' on the map of the Nozzle avalanche, Figure B.2). This profile is shown in Figure 4.6 with a range of possible trajectories which would allow a boulder to impact at the top of the "spray" area. It is postulated that the initial boulders originated in the "ramp" area, most probably closer to the base of this present slope (locations 1 and 2) where collisions would be more apt to occur, rather than near the crest of the slope (location 3).

Using ballistics theory a lower bound estimate on the initial velocity required to give a boulder such a travel range can be calculated. The x coordinate of the block's position at any time is given by $x = v_0 t \cos\theta_0$ and the y coordinate by $y = v_0 t \sin\theta_0 - 1/2gt^2$, where v_0 is the initial launch velocity, t is time, g is gravitational acceleration and θ_0 is the initial angle of trajectory. Combining these equations and eliminating t, we can find the initial velocity v_0 needed for various launch angles θ_0:

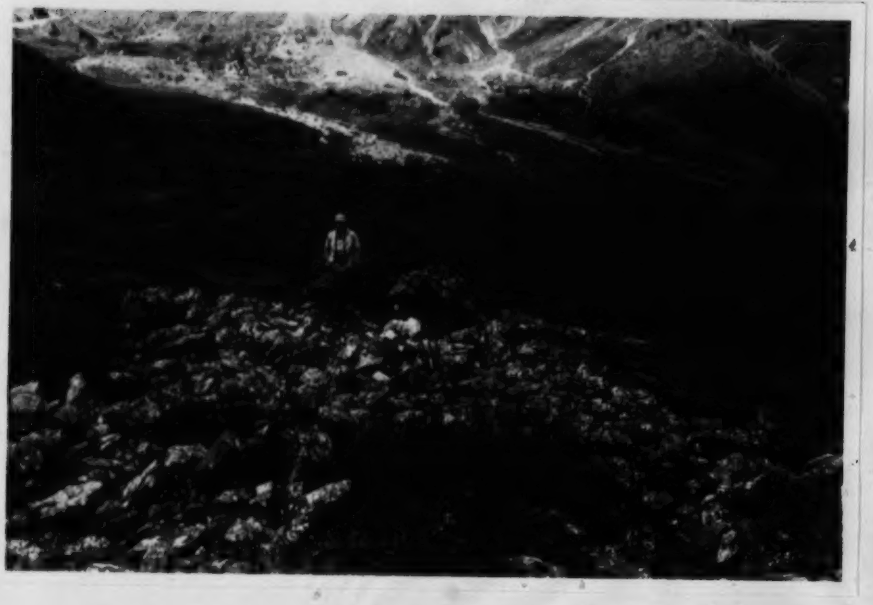

Figure 4.6 Pile of rubble left from the impact of a boulder moving at high velocity.

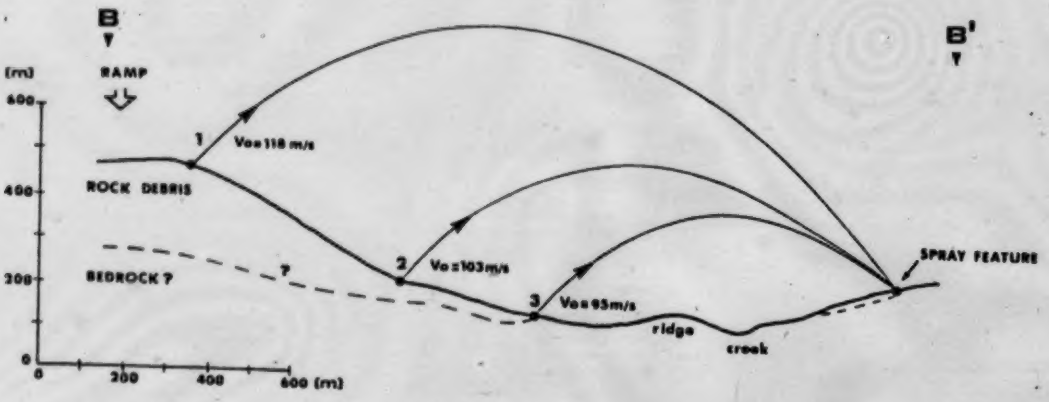
B
B'
(m)
RAMP
600
400
200
0
0
200
400
600 (m)
1
Vo=118 m/s
ROCK DEBRIS
BEDROCK ?
?
2
Vo=103m/s
3
Vo=93m/s
ridge
creek
SPRAY FEATURE

Figure 4.7 Range of possible minimum velocity trajectories for boulders which disintegrated in the "spray" area at the Nozzle rock avalanche.

$$v_0 = \sqrt{g\ x^2/[2(\cos\theta_0)^2(x\ \tan\theta_0 - y)]} \qquad \text{(Eqn. 4.6)}$$

For cases 1, 2 and 3 the launch velocity v_0 has been determined knowing the horizontal travel range x, and the vertical height loss or gain y, needed for a boulder to reach the top of the "spray" area. These values are listed in Table 4.3. It is apparent that a minimum velocity of between 95 m/s and 118 m/s is required for the optimum trajectory angle of 45°. At launch angles greater or less than 45°, an even greater initial velocity is required. The actual launch angle can not be accurately predicted from impact markings, however, it was probably between 10 and 30 degrees since non-elastic energy losses on impact in the "ramp" area, would reduce the rebound angle. If the source area was between locations 1 and 2 as originally suggested, the initial velocity of the projectile would have been roughly between 100 and 200 m/s. Accounting for air drag effects would allow even higher velocities. Note that in Case 1 the minimum launch angle possible due to the impeding ridge would be 4.5° which gives an unreasonable minimum initial velocity of 547 m/s.

Even greater velocities than 100 to 200 m/s are possible if the shattered boulders which are spread even further east along this side of the valley, originated from the ramp area. This would give maximum trajectories in the order of 1.8 km, not an unrealistic figure considering some of the boulders launched from the morainal ramp in the

TABLE 4.3 Projectile Velocities for Various Launch Angles, θ_0, Which Would Give the Required Travel Range as Shown in Figure 4.5

Degrees	Case 1 x = 850 m y = +55 m	Case 2 x = 1170 m y = 0 m	Case 3 x = 1620 m y = -250 m
0	*	**	229
5	434	260	183
10	198	185	159
20	127	128	133
30	105	116	122
40	97	109	118
45	95	103	118
50	96	109	121
60	101	116	131

* Minimum trajectory angle 4.5°
** Not possible

Huascaran event apparently travelled 4 km before impact (Plafker *et al.*, 1971).

4.4 Volume and Runout Distance Relationships

As previously mentioned in the literature review (Section 4.2), Scheidegger (1973) and Hsu (1975) have verified a proportional relationship between the total volume of the mass involved in a rock avalanche and the propensity for the mass to move an excessive distance, beyond which would be expected for normal frictional sliding. Eisbacher (1979) has produced a similar plot of the logarithm of the slide volume versus the excessive travel distance for several of the rock avalanches from the Mackenzie Mountains. His plot, which admittedly is based on rather dubious total volume estimates, does not show a very well defined correlation by any means. In fact, a negative correlation of volume with excessive travel distance could be suggested. He has speculated that the reason for this discrepancy lies in the restrictive topographic control at a number of the Mackenzie slides. While on one hand a tortuous course and obstacles are responsible for the relatively short runout at U-Turn avalanche, the channeling effects at Twin and Nozzle avalanches could be responsible for their greater runout distance. Davies (1982) has shown shown a good correlation between the deposit length and volume, although he purposely neglects the Twin and Nozzle avalanches because of their extreme runout.

After a more detailed examination of the slide geometry and avalanche debris in this study, it was apparent that some discrepancies in volumes and runout distances might alter the character of the above mentioned plot. For the two main avalanches described in this study - Rockslide Pass and Nozzle, and for the North and South Twin, Damocles and U-Turn avalanches, new volumes were calculated from the reconstructed original geometry produced with the aid of better survey control, 1:50,000 topographic maps, and photographs. Since there are no topographic maps or photographs of these sites prior to the failures, these volumes must similarily be considered as the best estimates with the available data. Because of uncertainties in the degree of bulking and the entrainment of alluvium or moraine in the debris, any estimates of pre-failure volume based on the surface exposure of debris would be highly uncertain and consequently were not attempted.

Figure 4.8 is a Hsu-type plot of the re-evaluated volume estimates versus excessive travel distances for several of the rock avalanches presented in this study. Considering that the abscissa of the plot is a logarithmic scale, the correlation is not particularly pronounced. Nevertheless, if U-Turn was excluded because of its numerous direction changes, it would be a fair generalization to suggest that excessive travel distance is vaguely proportional to the volume or mass of the initial failure. Both the Damocles and the Twin avalanches appear to the left

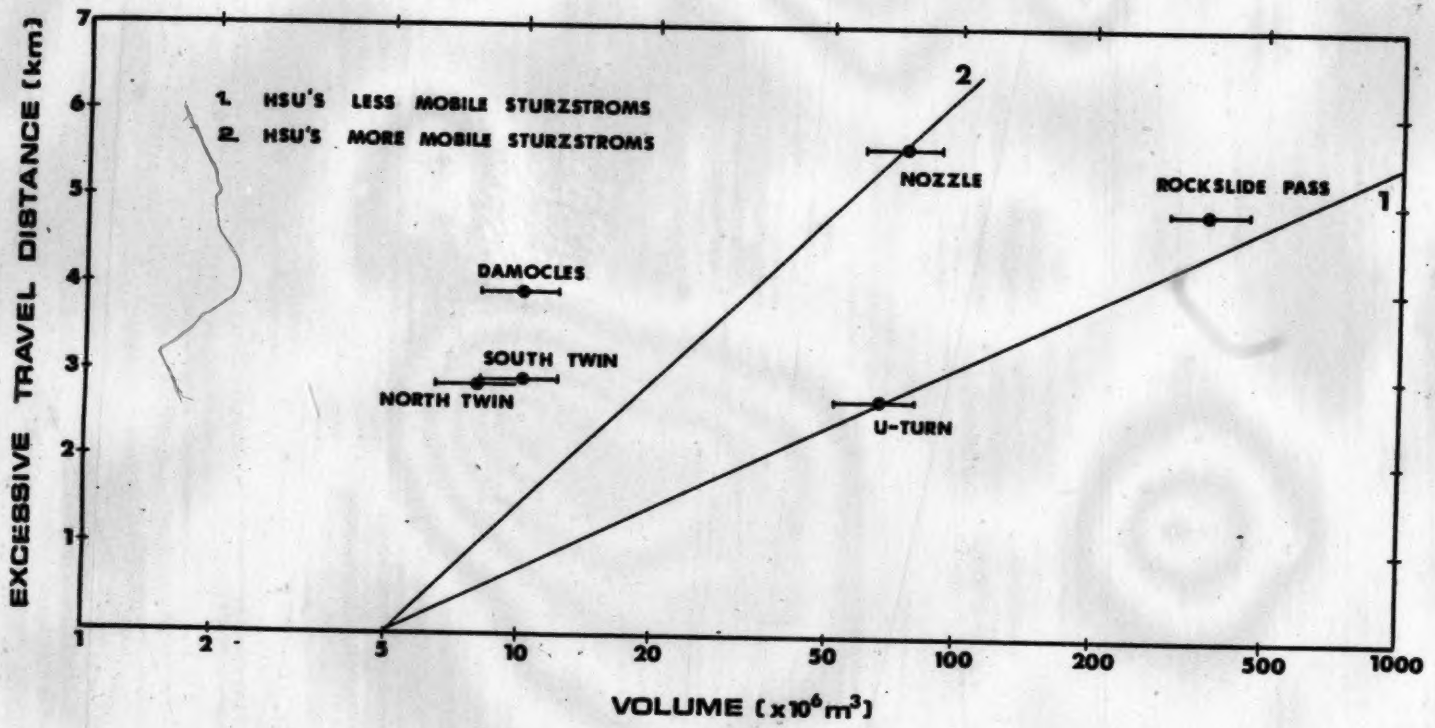

Figure 4.8 Hsu-type (1975) plot of the excessive travel distance versus the volume of the failed mass for several Mackenzie Mountains rock avalanches. The length of the bar indicates the degree of uncertainty in the estimate.

of Hsu's (1975) "mobile *sturzstroms*" line suggesting that smaller volume events are capable of excessive runout distances as well. There also does not appear to be a distinction between the excessive runout distance for confined versus unconfined geometries; for instance, Rockslide Pass and Damocles avalanches are not separated from the other more confined events on this plot.

For comparison, a plot of the logarithm of the equivalent coefficient of friction - the *fahrboeschung* versus the logarithm of the estimated volume (after Scheidegger, 1973) is shown in Figure 4.9. The few select observations from the Mackenzies show a similar scatter on on this plot as on the Hsu-type plot. It is interesting to note the difference between these points and the relationship proposed by Scheidegger (1973). A more detailed examination of other events from the Mackenzies would be necessary to more clearly evaluate this trend.

It should be noted that both the equivalent coefficient of friction, and the excessive travel distance are both based on the travel of the most extreme tip of the rock avalanche. As pointed out by Cruden (1975), Hungr (1981) and others, the more appropriate choice of mobility indicator would be the mean travel angle, or the inclination of the line joining the centres of mass of the pre-failed rock mass and the avalanche debris. In many cases this angle is only one or two degrees different from the *fahrboeschung* angle. However, for a few of the Mackenzie

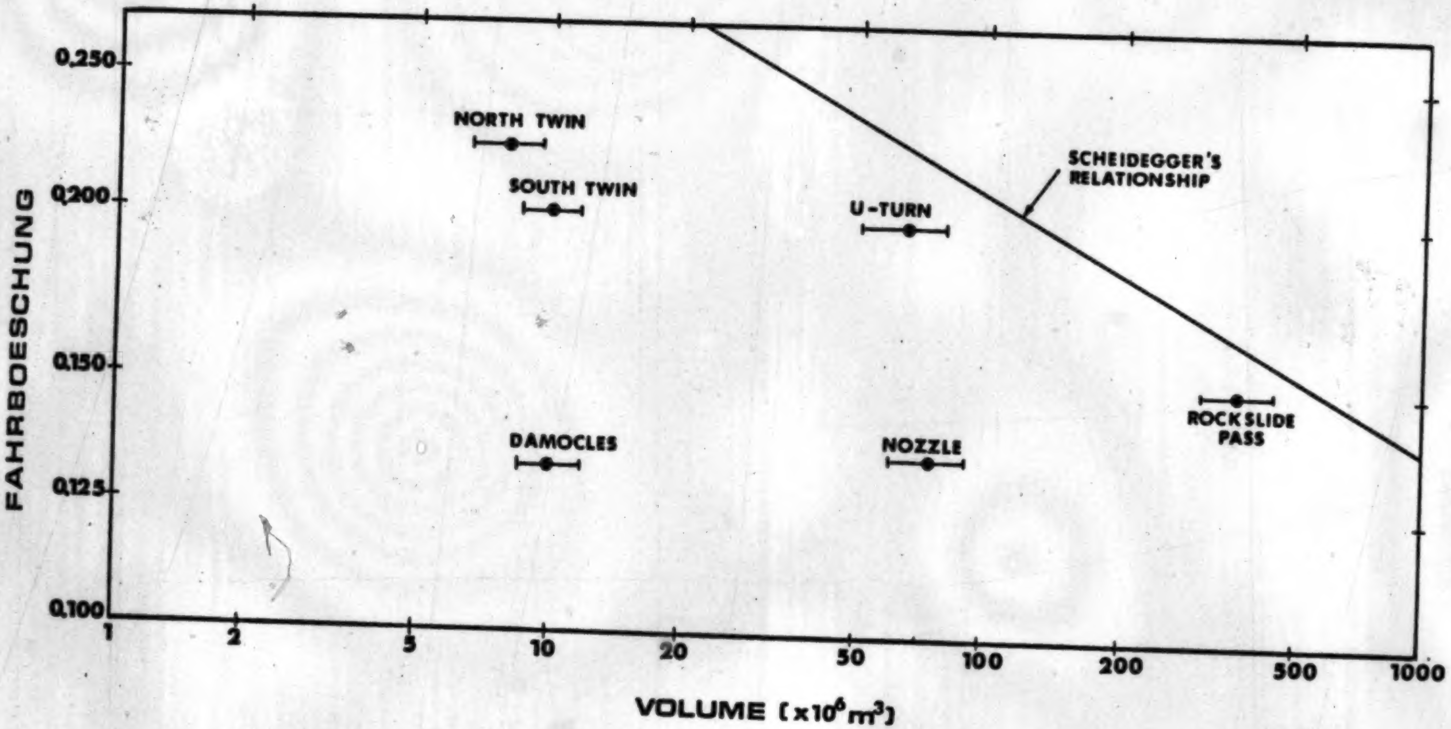

Figure 4.9 Plot of the equivilant coefficient of friction (fahrboeschung) versus the estimated volume of the failed mass for several Mackenzie Mountains rock avalanches.

events from the Mackenzies there would be a greater discrepancy. Because of insufficient data on the thickness of debris at most of these avalanches, no attempt has been made to calculate their respective mass centres. The significant effects this difference would have on the above described correlations should be recognized, however.

Hungr (1981) makes an interesting point concerning the equivalent coefficient of friction for a rock mass undergoing simultaneous longitudinal and lateral spreading. While internal shearing losses do not modify the appropriateness of using Coulumb's Law to calculate the equivalent coefficient of friction (as in Heim, 1932), the motion of a rock mass which is spreading laterally results in an "unproductive" expenditure energy. In other words a landslide, such as the Frank Slide which has spread out considerably from its original width, would appear somewhat less mobile than a narrow channeled one. This modifies Eqn. 4.1 as follows:

$$\mu = H/[L + 0.5(l - b)] \qquad \text{(Eqn. 4.6)}$$

where H and L are the vertical and horizontal displacements of the centre of mass, and b and l are the original and final average width of the debris mass, respectively (Hungr, 1981). In such cases the *fahrboeschung* would be a better estimate of the effective friction coefficient than the tangent of the mean travel angle.

For the six rock avalanches examined in this study, only one - Damocles - shows an increase in width. The remainder also show varying degrees of widening and narrowing but the average final width of the debris is less than the original width. This may offer an explanation for the pronounced channeling effects, for if Eqn. 4.6 was applied, these avalanches would exhibit increased equivalent friction coefficients. Consequently these data points would fall marginally closer to Scheidegger's (1973) regression line for most large landslides (see Figure 4.8). Damocles, however, would have a somewhat smaller *fahrboeschung* value.

Regardless of these variations on the exact nature of this type of volume runout correlation, it can be concluded that there is sufficient evidence for the existence of a relationship of this type, albeit á poorly defined one, for a select group of large, generally confined rock avalanches from the Mackenzie Mountains. More complicating factors such as abrupt topographic obstructions or entrainment of mobility enhancing material (i.e., saturated alluvium) undoubtedly produce some discrepancies in this trend.

4.5 Flow Characterization

Within this section a brief examination is made of the specific features at some of the Mackenzie Mountains rock avalanches which are relevant to a dynamic model. Although the intention of this research is not to conduct an inquiry into the origin or offer an explanation for these features, it is nonetheless imperative to be aware of these complexities when applying a simple model to predict movement rates. To this end, only a qualitative assessment of these phenomena is offered; a more rigorous mechanical approach to the nature of these features is beyond the scope of this thesis.

Morphological evidence from a number of the rock avalanche deposits is suggestive of a degree of complexity not considered by a simple frictional resistance model. The existence of transverse ridges or waves, longitudinal ridges, crevasse-like depressions, and surface folds in the debris (see Appendices A and B) is a fairly convincing indication of a more complex, possibly velocity dependent rheology. Only a few authors have considered these features and their relation to the dynamic behaviour of the avalanche in motion. McSaveney (1978) has evidence from calculated vertical strain rates in the Sherman Glacier avalanche to suggest that the mass moved as flexible sheet with properties of a dilatant Bingham plastic. He offers quantitative explanations for similar features as above by analogy to compressional and tensional stresses within the debris. More complicated motion is suggested by the existence of textural and lithological concentrations within the debris, especially as observed at Rockslide Pass.

A rather common feature of many rock avalanche deposits is the presence of xenolithic cones within the runout portion of the debris accumulation (Cruden, 1982; Hungr, 1981; McSaveney, 1978). Either the processes which create such features are absent or mechanical weathering has obscured their form since only a few faintly cone-shaped features have been noted at the six avalanches examined in this study. Similarly, a distal or lateral ridge feature (e.g., the Blackhawk landslide, Shreve, 1964) was not found. On the other hand a "spray" or "spatter" zone extending well beyond the limit of larger rock debris was noted at the Nozzle, Rockslide Pass, and Damocles avalanches.

As suggested by Eisbacher (1979) it is possible that a few of these avalanches may have actually been two or more separate events. Such features as the "spatter" zone, the boulder shadow effect (Nozzle avalanche, Appendix A), and the superimposed ridges at the U-Turn avalanche are suggestive of more than one stage of movement; an initial failure catapults debris far ahead of the main flow which follows, over-riding and burying some of the debris left previously in the mid-section of the avalanche path. There does not appear to be firm stratigraphic evidence within the debris for this hypothesis. The implications, however, of a multi-stage or perhaps a layered flow are significant; velocity prediction models based on a centre of mass approximation are probably inappropriate for handling such complexities.

Rarefaction zones, a term coined by Eisbacher (1979), refers to those areas at Nozzle and U-Turn avalanches where there are sections along the avalanche path with little or no debris accumulation. These peculiar features are evidence of perhaps a more involved momentum transfer process which manages to catapult debris far ahead of its source. Other explanations, such as the incorporation of fine grained, saturated alluvium, or melted snow or ice, for instance, are not untenable hypotheses for the enhanced mobility. A satisfactory resolution of this problem has not been found. Additional model or analytical approaches to this end would be most useful.

Boulder Texture and Sorting have been examined at the Nozzle and Rockslide Pass avalanches and on airphotos at U-Turn and Damocles avalanches. No systematic spatial distribution of size fractions was obvious from this study; the largest boulders appear to be almost uniformly distributed on the surface of the debris, with the exception of the coherent portion of the ramp feature. In a fashion not uncommon to rockfall deposits (Rapp, 1960), some of the largest, if not the largest boulders are found at the distal tip of the deposit. In one case, at the Nozzle rock avalanche, the largest boulder in the debris was located almost 300 m beyond the rock debris proper in the distal "spray" or "spatter" zone. Whether this peculiarity is a result of the boulder acquiring a high angular velocity and hence a greater rolling velocity or a greater momentum because of its greater mass remains unresolved. Alternatively, if this portion of the debris was actually "floating" along on a shearing surface, why are not more large clasts found in the same vicinity? Along the same lines of approach, McSaveney (1978) has back-calculated the strength of the debris sheet based on the maximum boulder size as initially done by Johnson (1970). He has then used this strength determination as a confirmation of the sliding velocity of the avalanche as determined from a simple frictional sliding model. These options were not explored since the debris thickness and the depth the large boulders were buried could not be determined.

Stratigraphic congruence, or the preservation of the original stratigraphic order, is occasionally noted in the debris of rock avalanches. This phenomenon is most readily apparent at Rockslide Pass as shown by Eisbacher (1979); a distinct orange weathering rim of rock apparently from the basal portion of the failed cliff encircles the periphery of the distal end of the deposit. Furthermore the existence of dilation features within this deposit lends credence to the deformable sheet postulate of McSaveney (1978).

On the other hand the stratigraphic congruence was not noted at the more confined or channeled avalanches, e.g., Nozzle and U-Turn. It is possible that a more turbulent-like character is dominant over certain portions of the latter events. Sample Reynolds and Froude number calculations, despite their approximate nature (e.g., McSaveney, 1978) suggest that the flow is supercritical but within the laminar regime almost all the time. While the rheological treatment of the topic was not pursued in this study it is worthwhile noting that velocity dependent resistances (i.e., resistance, $R = f(v^2,v)$) used in some models for determing avalanche velocities may not be compatible with the physical character of the debris deposits where evidence for a laminar or turbulent flow character is lacking.

Pore Pressures have often been suggested as a means for reducing the frictional resistance of an avalanche. In the few avalanches examined here there is little field evidence to substantiate their presence throughout the entirety of the avalanche. The possibility of there having been saturated alluvium, snow, ice or even small bodies of water lying along the avalanche path cannot be ruled out though. It is possible that the bubbles noted in the distal exposure of the debris at the Nozzle avalanche (see Appendix A) could be entrapped air. However, more work would be needed to confirm the extent of this phenomenon. Until such time as the separation of the debris and the underlying till or alluvium can be observed in cross-section, a means for the generation and maintenance of pore pressures in a flowing and sliding rock avalanches mass will likely remain in the domain of speculation.

In conclusion, the more enigmatic areas of rock avalanche motion (from a selection of such events from the Mackenzie Mountains) have been identified and briefly examined in this section. It is apparent that the internal rheology and energy dissipative mechanisms which are present within a moving avalanche remain largely uncertain and warrant further investigation. From the brief inquiry made at each of six Mackenzie Mountains rock avalanches, some general conclusions may be drawn:

1. The motion of a rock avalanche is more properly dealt with by using three or more separate stages of movement. Firstly, an initial failure stage imparts a preliminary velocity to the coherent rock mass. A disintegration phase soon follows where the mass attenuates and loses further energy due to internal distortion and dilation. This is followed by a third, more complex stage involving both sliding and flow within the almost entirely disintegrated mass of rock fragments. Depending on the rheology many variations on this last mode of movement are possible including: sliding, rolling, laminar, turbulent, or plug flow.
2. There appears to be a morphological and hence a rheological distinction between confined (e.g., Twin, Nozzle) and unconfined (e.g., Rockslide Pass) rock

avalanches. Such features as rarefaction zones and hydraulic jump effects are characteristic of the former and are lacking in the latter. Unconfined debris streams including the fan area of the Nozzle avalanche typically possess such surface morphological features as transverse ridges, longitudinal grooves and ridges, folds, and distal and lateral rims.

3. The "sliding or flowing" question is largely semantic; as evidenced by the observed stratigraphic congruence and the well preserved dilation features at Rockslide Pass, and conversely the lack thereof, over certain segments of some of the channeled rock avalanches, there is reason to believe that both sliding and flowing are occurring simultaneously within the mass, albeit of varying proportions.

4.6 Summary and Conclusions

By way of summary the highlights of the preceding sections are briefly outlined:

1. A review of the literature of rock avalanche mechanics has revealed a wide range of hypotheses directed towards the mobility problem. In a brief examination of some ten postulates it is concluded that probably more than one agent is likely responsible for the apparent dynamic behavior of a given rock avalanche. Definitive deterministic solutions to the travel

distance and velocity spectrum questions are probably a long time from fruition. Semi-empirical or empirical approaches such as the application of equations of hydraulic flow or scale modelling offer more reliable predictive capablities at this time.

2. A review of the velocity spectrum from 18 mobile rockslides and rock avalanches has not shown any degree of consistency; for a variety of events, local and average velocities range over almost an order of magnitude. Furthermore, there is evidence for a large velocity variation over short distances at a single event. Application of superelevation and run-up analysis at the North Twin avalanche shows an upper bound velocity range of between 16 and 50 m/s and a lower bound velocity range of between 12 and 35 m/s for various measured cross-profiles. A simplified inquiry into the "spray" feature at the Nozzle rock avalanche has shown that the minimum projectile velocities necessary to produce the observed feature would be between 95 and 118 m/s.
3. The empirical volume-runout relationships proposed by Hsu (1975) and Scheidegger (1973) were tested with re-evaluated volumes from Damocles, Twin, U-Turn, Nozzle, and Rockslide Pass avalanches. A poor correlation similar to that shown by Eisbacher (1979) was confirmed.
4. Some qualitative aspects of the debris texture and

sorting, surface morphology, internal structure and geometry were examined in an effort to characterize the mode of movement at some of the avalanches. Numerous rheological complexities remain as an impediment to using a simple frictional model to predict avalanche velocities. A separation of rock avalanche motion into three or more distinct parts is seen as physically more appropriate for analysis, but dynamically indeterminant unless a spectrum of local velocities is available for comparison. Furthermore, there is a morphological and most probably a rheological basis for distinguishing confined and unconfined rock avalanches.

5. A MODEL FOR ROCK AVALANCHES

5.1 Introduction

Various semi-empirical models which invoke concepts from open channel hydraulics have been proposed for analysing snow and rock avalanches (see Literature Review, Section 4.2). It is the purpose of this chapter to develop Koerner's (1976) two-parameter model and to examine the underlying assumptions and limitations of the model. The sensitivities of various factors are assessed in a parametric study on a test slope geometry. The Frank slide is then used as an example to evaluate various travel paths applicable for analysis. More details on the formulation of the equations of motion used here are contained in papers by Koerner (1976, 1980a, 1980b), Perla *et al.*(1980), and the user's manual for a computer program entitled RADA - Rock Avalanche Dynamic Analysis - by McLellan (1982). Only the rudiments of the theory will be stated here and the reader is referred to the above papers for more background.

5.2 Theory

In Chapter 3 the dynamics of the simple sliding block analogue were examined with respect to the proposed initial failure mechanism. The only resistance acting to slow the motion of the mass was that of friction, R_1. As shown by Heim (1932), the average coefficient of friction on a sliding block is given by the *fahrboeschung* or the inclination of the line joining the top of the pre-failed block and the distal tip of the debris. Voellmy (1955) proposed that a second resistive force acts to slow the motion of snow avalanches; evidence from powder avalanches suggested that turbulence was a common feature of these slope movements. Hence the analogy to a velocity squared dependent turbulent resistance, such as used in water flow. This resistance, R_2 is given by:

$$R_2 = \rho g \, v^2/\xi \qquad \text{(Eqn. 5.1)}$$

where v is velocity, ξ the turbulence coefficient, ρ is the density, and g is gravitational acceleration. Using a simplified bilinear geometry and an assumption regarding flow depth, a prediction of snow avalanche velocities and pressures in the runout zone could be made.

Salm (1965) suggested that the sum of resistances R, acting to slow a snow avalanche, could be represented by a polynomial with three terms accounting for frictional (velocity independent), viscous (velocity dependent), and turbulent (velocity squared dependent) resistances (see equation 4.2). He found the velocity dependent term to be inconsequential in comparison with the velocity squared term. Because of evidence suggesting that rock avalanches attained high velocities over much of their path, it was similarly felt that the viscous resistance term would be insignificant (Koerner, 1976). This assumption may be incorrect and a discussion of evidence to the contrary is presented later in this chapter. The solution to the differential equation of motion is now presented in a similar fashion as done by Koerner (1976).

From Newton's Second Law:

$$m\, dv/dt = F_1 - (R_1+R_2) \qquad \text{(Eqn. 5.2)}$$

where m is the mass of a body in motion and dv/dt is the time rate of change of velocity. As shown in Figure 5.1, the basal resistance R_1, acting against a sliding disintegrating element is given by:

$$R_1 = \mu(D_f \rho g \cos\beta - U) \qquad \text{(Eqn. 5.3)}$$

where μ is the dynamic coefficient of friction, D_f is the depth of flow measured perpendicular to the slope, β is the slope angle and U is an uplift force (due to pore pressures) along the base of the element. Similarly, the driving force F_1, may be expressed as mg $\sin\beta$, where m is the mass of the element. Substituting F_1, R_1, and R_2 into Eqn. 5.2 one obtains:

$$m\, dv/dt = mg \sin\beta - \mu(D_f \rho g \cos\beta - U) - \rho g v^2/\xi \qquad \text{(Eqn. 5.4)}$$

After simplification and the substitution of r_u, equal to the ratio of the uplift force to the normal component of

DRIVING FORCE $F_1 = mg \sin\beta$

FRICTIONAL RESISTANCE $R_1 = \mu(D_f \rho g \cos\beta - U)$

DYNAMIC RESISTANCE $R_2 = \rho g \frac{v^2}{\xi}$

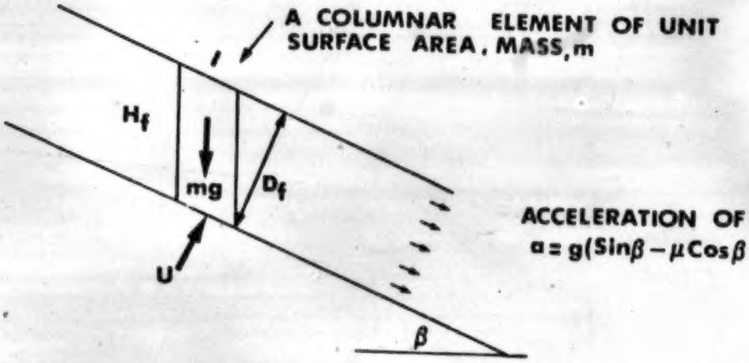
A COLUMNAR ELEMENT OF UNIT SURFACE AREA, MASS, m
H_f
mg
D_f
U
β

ACCELERATION OF ELEMENT

$$a = g(\sin\beta - \mu\cos\beta\,(1-RU)) + \frac{v^2}{K}$$

$$RU = \frac{\text{UPLIFT FORCE}}{\text{NORMAL COMPONENT OF WEIGHT}}$$

$$K = \frac{D_f\,\xi}{g}$$

NOTE: LATERAL FORCES ON ELEMENT NOT CONSIDERED
(SEE TEXT FOR EXPLAINATION OF SYMBOLS)

Figure 5.1 Simple model for frictional and dynamic resistances in a rock avalanche.

weight, the acceleration a of the element can be given by:

$$a = g(\sin\beta - \mu(1-r_u)\cos\beta) + v^2/k \qquad \text{(Eqn. 5.5)}$$

where $k = D_f\xi/g$.

When the acceleration of the body is zero, the mass is in equilibrium with the resisting forces and the velocity is given by v_c, the "critical velocity":

$$v_c = [D_f\xi(\sin\beta - \mu(1-r_u)\cos\beta)] \qquad \text{(Eqn. 5.6)}$$

The differential equation of motion of the form shown in Eqn. 5.6 was solved by Koerner (1976), for the movement of an avalanche over a variable slope. The velocity of the avalanche v_i, at the end of segment i, for a small travel distance Δs_i, is given by:

$$v_i = \sqrt{\frac{(v_{c_i}^2(\exp(2\Delta s_i/k) - 1) + v_{i-1}^2)}{\exp(2\Delta s_i/k)}} \qquad \text{(Eqn. 5.7)}$$

The $D_f\xi$ term will henceforth be referred to as the "dynamic" resistance parameter and will be denoted by D. Note that the dynamic resistance is inversely proportional to the dynamic resistance parameter (Eqn. 5.1). Furthermore the lowest resistance and consequently the highest velocities are produced for the highest D values. While it is recognized that the depth of flow and the "turbulence" coefficient undoubtedly vary over the length of the avalanche path, it is assumed here, as was done in a similar manner by Koerner (1980a, 1980b), Perla *et al.*(1980), and Bakkehoi *et al.*(1981), that the product of the two is a constant. Note that as D approaches infinity, Eqn. 5.8 yields the velocity of a sliding block. The critical velocity v_c is largely the determinant of the real velocity, i.e., when the critical velocity is greater than the real velocity the mass is accelerating and it is decelerating when the the critical velocity is less than the real velocity.

The final reach or runout distance, Δs_i on the last segment of a profile for an avalanche is given by:

$$\Delta s_i = (D/2g)\ \ln(1 - v_{i-1}^2 / v_{c_i}^2\ ) \qquad \text{(Eqn. 5.8)}$$

With equations 5.7 to 5.9 inclusive, the velocity and reach of an avalanche can be predicted knowing only the slope geometry and the proper choice of frictional and dynamic resistance parameters μ and D. Similarly, the range of (μ, D) pairs which will predict a given runout distance may be back calculated in an iterative process from just the geometry. It is also possible to assess the effects of an uplift force which reduces the normal component of weight.

5.3 Limitations of the Model

This numerical solution of a two-parameter avalanche model must be construed as a simple attempt to describe a complex physical process. The method is semi-empirical in the sense that, although it is based on certain physical principles, the exact nature of the frictional and dynamic resistances is probably grossly simplified. Several assumptions have been made in the model without due consideration of their effects. Basically, the limitations of the model fall into two categories: firstly, analytical and computational problems, and secondly, the physical characterization of the avalanche process.

A "uniqueness" problem arises in the step-by-step solution of Eqn. 5.8 to find the optimal (μ,D) pair. There is an infinite number of (μ,D) pairs and corresponding velocities for each profile segment for a given set of boundary conditions. These are the profile geometry and the initial and final velocities equal to zero. On a plot of the frictional parameter versus the logarithm of the dynamic parameter this function is bounded by the two limiting slope angles. The function will henceforth be referred to as the "characteristic resistance relationship". Even if the velocities were known at several points along the avalanche path the uniqueness problem would still exist, albeit somewhat more restricted. In addition, the analysis shows that for rather wide variations in μ and D, velocities produced are quite reasonable based on the limited field evidence available and suggested velocity ranges from similar events (see Section 4.3). Consequently an exact solution to the problem is not possible with a two or three parameter model.

The more serious limitations of the proposed model stem from inconsistencies in matching the model to the actual physics of rock avalanche motion. As pointed out in the previous chapter the physical characterization of the motion is an enigmatic area, still largely unresolved. While the two model parameters here do account for many of the uncertainties, there is, nevertheless, some question about their appropriateness.

Whether the movement of a rock avalanche is within the turbulent or laminar flow regime depends upon a number of factors. Simple Reynolds number calculations and observations by Eisbacher (1979), Erismann (1979), McSaveney (1978), and Johnson (1978) as well as the writer, would suggest that turbulent flow, taken in its classical sense, is seldom achieved. The maintenance of stratigraphic order and the jigsaw puzzle effect within rock avalanche deposits lend credence to plug-flow or deforming flexible sheet analogies. The physics of these phenomena are largely speculative as well. There is, however, justification for using a velocity squared dependent resistance aside from strictly empirical reasons. Koerner (1977, 1980b) relates his so-called "scattering" and "rolling" motion within an avalanche to Bagnold's (1954) dispersive pressure model.

Consideration of the boundary shear stress results in a dynamic resistance formulation analogous to the Chezy flow formula with a velocity squared dependence. Consequently it is deemed preferable to denote the velocity dependent term here as a "dynamic" rather than a "turbulent" resistance, since the latter implies a random motion of particles in a classical fluids sense.

The equations developed in the previous section arise from the application of Newton's Second Law; consequently the motion of the avalanche refers to the centre of mass of a body, be that a group of particles or a continuum. Difficulties which arise in the choosing of an appropriate travel angle have already been mentioned in Section 4.2, but the choice of the best travel profile for this analysis is yet another difficulty. To know the approximate travel path of the body's centre of mass would be ideal. However, this is nearly impossible to define prior to a failure. Furthermore the extent of the attenuation of the disintegrating debris mass would be most difficult to estimate. To this end, the entire travel path from the top of the failed block to the distal end has been used because it may be obtained most easily. Alternatively the approximate motion of the centre of mass could be analysed or perhaps the motion of an element of mass near the front of the initial failed mass could be used. The effects of using these different motion paths are considered in Section 5.4.

The well documented avalanche mobility dependence on volume or mass is not accounted for in this particular model. Similarly, there is no capability for altering the density of the flow along its path. The entrainment of surficial material and subsequent enhanced mobility or inertial effects are not considered. Losses of debris along the travel path are, likewise, neglected. The slight loss in downslope velocity from the centripetal acceleration effect on a curved slope is not considered in the analysis as was done by Perla *et al.*(1980). However, because of the similar derivation of the equation of motion, the mass to drag ratio (M/D) in Perla's model is identical to the dynamic resistance parameter D of this model divided by gravitational acceleration (D/g).

Another element not considered in this formulation was a means of accounting for impact losses at abrupt changes in slope. Perla *et al.*(1980) have proposed a correction for momentum lost at a slope transition, but the effect is relatively minor where a smooth concave profile is approximated by a large number of straight line segments.

The effects of poorly defined processes such as "lubrication" by mud or frictional heating are not dealt with explicitly; rather these mechanisms can be thought of as being concealed in the frictional resistance term μ. Similarly other proposed mechanisms such as fluidization, liquefaction or dispersive pressures are not handled directly in the model. They may however, also be thought of as reducing the dynamic friction μ by the factor $(1-r_u)$. The r_u ratio, as previously defined, accounts for uplift pressures within the basal portion of the mass. Other energy dissipation schemes such as air resistance or sound which have been suggested in the snow avalanche realm are deemed to be relatively minor considerations for rock avalanches.

Finally, no account is taken of the confinement or lateral spreading effects, although, these could also be handled by altering the dynamic frictional coefficient, μ.

In summary, the proposed model presents an almost "black box" approach to the determination of relevant velocities and runout distances. A number of physical processes, which are as yet only vaguely understood, are accounted for by a simple frictional and dynamic resistance pair. While much of the uncertain physics can be conveniently concealed within these parameters, the selection of the appropriate travel path for analysis is perhaps a more limiting factor in the extensive application of the model.

5.4 Computer Program RADA

A computer program entitled RADA - Rock Avalanche Dynamic Analyis - was developed to solve the differential equations of motion for a variety of geometric configurations and program options. Only the rudiments of the program are described here and the reader is referred to the Users Manual for RADA (McLellan ,1982) for additional details.

The simplified flowchart shown on Figure 5.2 illustrates the logic route followed in Option 1 of program RADA. The sequence begins by reading the name of the particular avalanche, the number of profile segments, the program option number, the estimated volume, and a pore pressure factor. Next, the number of resistance pairs to be evaluated and the increment to be added to the dynamic resistance parameter is read. This is followed by the profile data which consist of a slope angle and a distance for each profile segment. An example of input is shown in Table 5.1.

The program begins by computing the *fahrboeschung* or slope of the line joining the crown and the tip of the avalanche debris. Next, the area ratio is calculated. This parameter was devised in order to investigate the hypothesis that profiles with a steep initial drop, hence a higher area ratio, are more apt to display an excessive travel distance.

The initial value of the dynamic resistance parameter D is then set. The procedure followed for finding a (μ,D) pair is to search for the value of the frictional resistance parameter μ which forces the avalanche to stop at a given end position. This is accomplished by setting an initial guess for μ as:

$$\mu(1) = 1/2\ (\mathrm{FMAX} + \mathrm{FMIN}) \qquad \text{(Eqn. 5.9)}$$

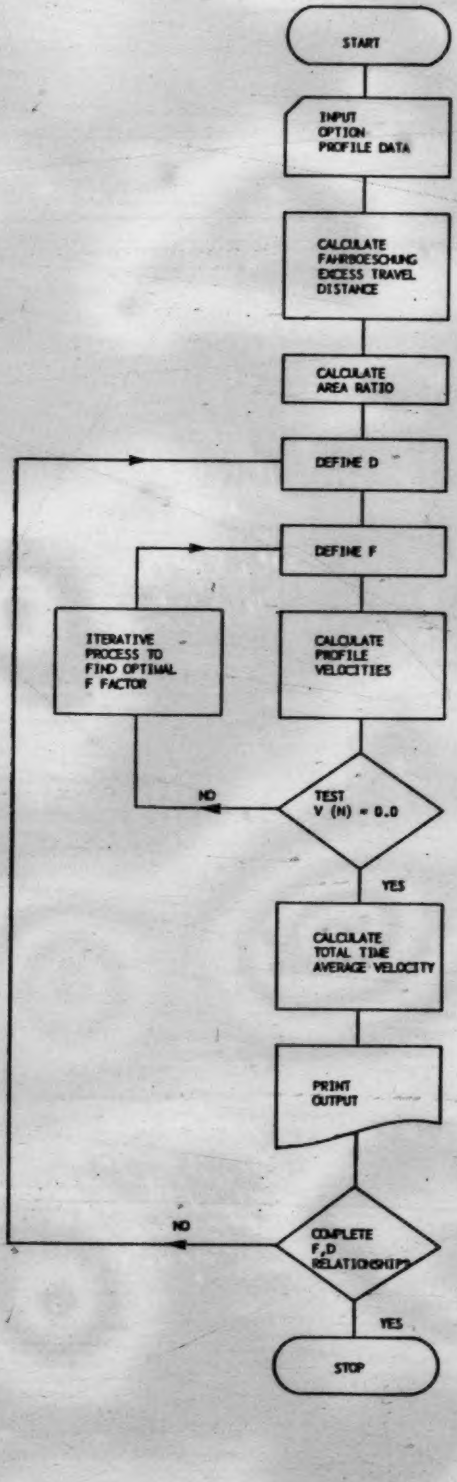
START
INPUT
OPTION
PROFILE DATA
CALCULATE
FAHRBOESCHUNG
EXCESS TRAVEL
DISTANCE
CALCULATE
AREA RATIO
DEFINE D
DEFINE F
ITERATIVE
PROCESS TO
FIND OPTIMAL
F FACTOR
CALCULATE
PROFILE
VELOCITIES
NO
TEST
V (N) = 0.0
YES
CALCULATE
TOTAL TIME
AVERAGE VELOCITY
PRINT
OUTPUT
NO
COMPLETE
F,D
RELATIONSHIPS?
YES
STOP

Figure 5.2 Flowchart of Program RADA, Option 1.
$F = \mu$

TABLE 5.1: Sample Input data for Program RADA, Option 1

No. of D Increments	Dynamic Parameter - Increment	No. Profile Segments	Option No.	Volume x $10^6 m^3$	r_u
20	10000	17	1	75	0.00

Nozzle Slide, NWT.

Profile Data
-segment slope angle
and distance

30.0	400
25.0	280
4.0	1050
14.0	115
17.9	295
8.5	677
7.6	303
2.0	570
8.7	263
9.2	623
4.8	482
4.2	827
3.8	150
3.8	150
3.8	301
0.9	625
-3.3	175

Sample output from program RADA, Option 1 for
$\mu = 0.0653$ $D = 40,000\ m^2/s^2$

```
NOZZLE SLIDE,NWT.                          FRICTIONAL PARAMETER =   0.0653
VOLUME =  75.0 MILLION  CU. M.                DYNAMIC  PARAMETER =   40000  M/S**2
                                                      RU VALUE =   0.0

                                                 FAHRBOSCH UNG  =   0.133
                                       EXCESSIVE TRAVEL DISTANCE =   5536  METERS
                                           TOTAL TRAVEL DISTANCE =   7286  METERS
                                          TOTAL ELEVATION LOSS =    949  METERS
                                                      AREA RATIO =   0.377

  SECTION    ANGLE    DISTANCE  INITIAL  CRITICAL VELOCITY       REAL VELOCITY
                         (M)    VELOCITY       (M/S)                 (M/S)
                                 (M/S)

     1        30.0       400       0.0         133.3                  58.2
     2        25.0       280      58.2         120.8                  66.0
     3         4.0      1050      66.0          13.6                  53.2
     4        14.0       115      53.2          84.5                  55.4
     5        17.9       295      55.4          99.0                  63.1
     6         8.5       677      63.1          57.7                  61.6
     7         7.6       303      61.6          52.0                  60.4
     8         2.0       570      60.4         *****                  49.6
     9         8.7       263      49.6          56.9                  50.6
    10         9.2       623      50.6          61.6                  53.9
    11         4.8       482      53.9          27.3                  49.5
    12         4.2       827      49.5          18.0                  41.7
    13         3.8       150      41.7           5.7                  40.3



    14         3.8       150      40.3           5.7                  38.9
    15         3.8       301      38.9           5.7                  38.2
    16         0.9       625      38.2         *****                  21.0
    17        -3.3       175      21.0         *****                   0.0

           TOTAL TRAVEL TIME =  167.9  SECONDS
           AVERAGE VELOCITY  =   43.4  M/S
```

where FMAX and FMIN are the *fahrboeschung* and the tangent of the shallowest segment slope, respectively. The velocities at the end of each segment are then computed and if the avalanche stops short or goes past the end position a new estimate for μ is used. If it stops short, i.e., the final segment velocity is less than 0.0 m/s, $\mu(2)$ is found by substituting $\mu(1)$ for FMAX in Eqn. 5.10. If it goes past, i.e., the final segment velocity is greater than 0.10 m/s, the next guess for $\mu(2)$ is found by substituting $\mu(1)$ for FMIN. The procedure is repeated up to 25 times if necessary, until a μ value is found with at least a three figure accuracy and the final segment velocity drops into the range 0.0 to 0.1 m/s. Usually this is accomplished with less than 5 iterations. A similar algorithm for finding a resistance pair to satisfy the start and end positions, but using a predefined frictional resistance was found to be unsuitable because of numerical instabilities generated while trying to isolate an optimal D parameter. A series of tests is used in the program to circumvent other numerical problems which arise when velocities drop to zero before the final travel segment.

When an optimal resistance pair is found that forces the avalanche to stop at a given end position, the total time and average velocity over the travel path are computed. Unless the complete dynamic and frictional resistance relationship has been determined, the program returns to define a new D and the above algorithm is solved for a new μ

value. Normally twenty resistance pairs are adequate to define the relationship which becomes asymptotic to the maximum μ value (see Figures 5.4 to 5.9 later in this chapter). The program then prints a table which gives the avalanche name and volume, the frictional and dynamic resistance coefficients, various geometric indicators and a listing of the initial, critical and real velocities for each profile segment (see Table 5.1).

There are 3 major options available with the program. Option 1, as outlined previously, is used to define the unique frictional and dynamic resistance relationship for a given avalanche profile. A pore pressure assumption may be used in this, and the other options. Option 2 is used in a predictive fashion to determine the runout distance and velocity spectrum for an avalanche given only a slope geometry and a predetermined (μ,D) pair. Option 3 is similar to Option 1 for it calculates the frictional and dynamic resistance relationship for a given slope profile where the starting and end positions are known. This option allows for the input of an initial velocity at some position in the travel path. This could be used, for example, to determine avalanche mobility after an initial portion of the path where sliding motion predominated over a flowing or velocity squared dependent motion.

Other program options are available which generate plots of the avalanche path, the frictional and dynamic resistance relationship, and the velocity profiles for various (μ,D) pairs.

5.5 Parametric Study

To better evaluate the effects of varying geometries, uplift pressures or initial velocities on the characteristic resistance relationship a limited parametric study was conducted on a representative test profile. The sensitivity of the relationship to these influences is of considerable importance; for instance, the function is greatly influenced by uplift pressures but only minutely affected by certain changes in slope geometry. Evaluation of these effects for a given profile will be of value later, when rock avalanches of varying geometry and material constituents are examined (see Chapter 6).

It is worthwhile noting that the characteristic resistance relationship, is not a unique solution to the equations of motion. There is actually only one (μ,D) pair which satisfies the boundary conditions and consequently produces a velocity profile matching the real velocity. But because this particular pair cannot be uniquely defined and velocities from a wide range of (μ,D) pairs are reasonable, no attempt to isolate a particular resistance pair has been made. The effects of these factors on the relationship are usually apparent without the need to determine an optimal resistance pair.

The test profile geometries used in this parametric study are illustrated in Figure 5.3. The basic profile

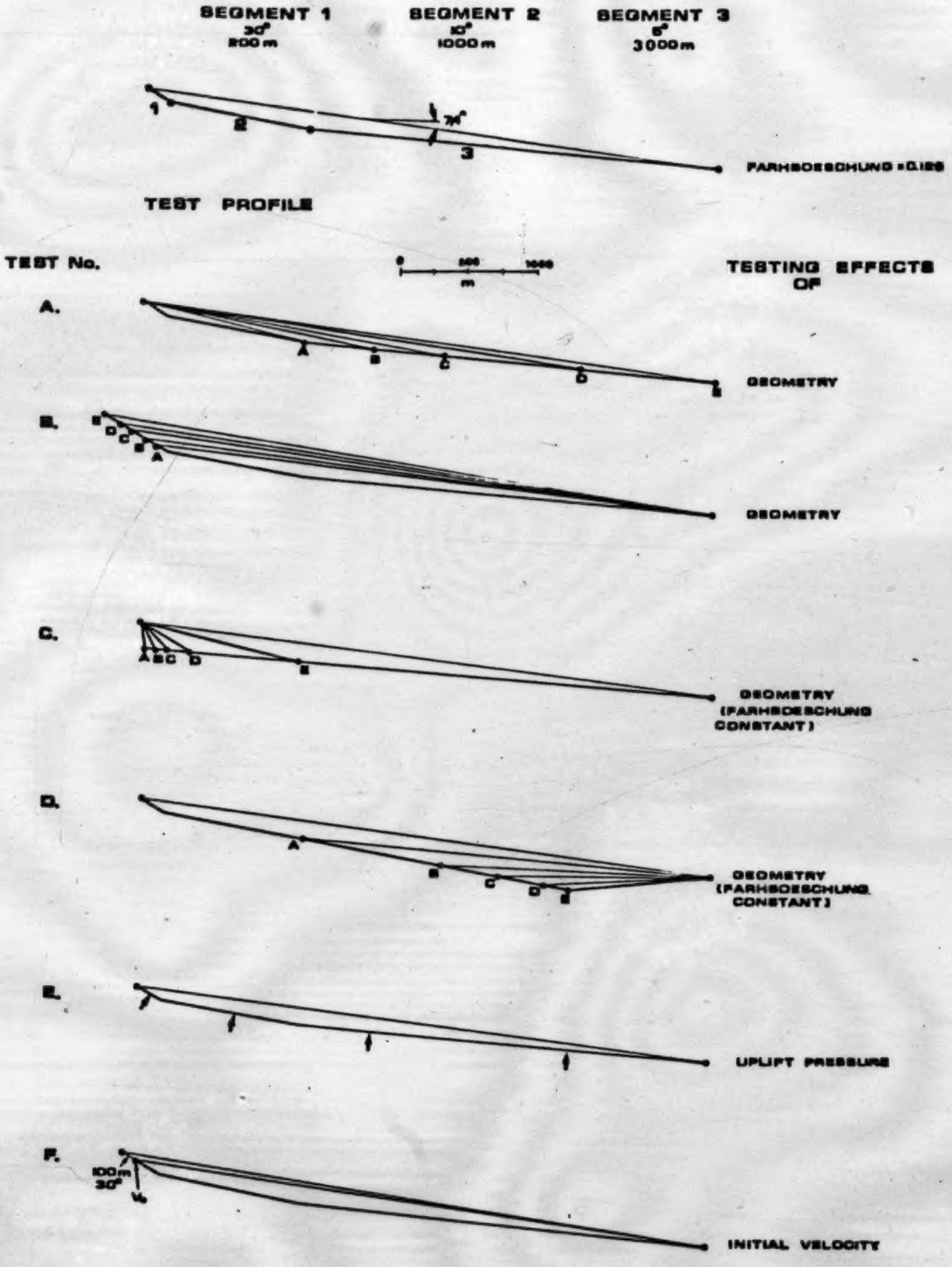
SEGMENT 1
30°
200 m
SEGMENT 2
10°
1000 m
SEGMENT 3
5°
3000 m
1
2
3
7.2°
FARHBOESCHUNG =0.126
TEST PROFILE
TEST No.
0
500
1000
m
TESTING EFFECTS OF
A.
A
B
C
D
E
GEOMETRY
B.
E
D
C
B
A
GEOMETRY
C.
A
B
C
D
E
GEOMETRY (FARHBOESCHUNG CONSTANT)
D.
A
B
C
D
E
GEOMETRY (FARHBOESCHUNG CONSTANT)
E.
UPLIFT PRESSURE
F.
100m
30°
V_0
INITIAL VELOCITY

Figure 5.3 Test profile geometries for parametric study.

consists of 3 linear segments of variable inclination and length: Segment 1, 30°, 200m; Segment 2, 10°, 1000m; and Segment 3, 5°, 3000m. The *fahrboeschung* for this profile is 0.129. This particular geometry was chosen because it represents a typical rock avalanche profile from the Mackenzie Mountains; a 200 m shallow dipping initial slope is proceeded by a relatively flat runout slope of 4 km length. Six test analyses were performed on the profiles shown in Figure 5.3 to assess the effects of geometry, uplift pressures and initial velocity.

In the first two tests the effects of different geometries and a varying travel angle are examined. In Test A the characteristic resistance relationships for the basic test profile and several profiles modified by shortening the length of the final runout slope were evaluated. These are shown on Figure 5.4. Note that μ is plotted against the logarithm of D in order to accentuate the changes in the function. A lower bound limit for D is arbitrarily set at 100 m^2/s^2. Below this value numerical instabilities arise which render the μ solving algorithm incapable of finding an optimal resistance pair. In Test B the *fahrboeschung* is similarly altered for a series of profiles with varying travel distance on the initial slope (Figure 5.5).

Both these plots indicate the significance of geometrical factors on the characteristic resistance relationship. Changes in the final runout segment distance or the initial slope length alter the *fahrboeschung* which

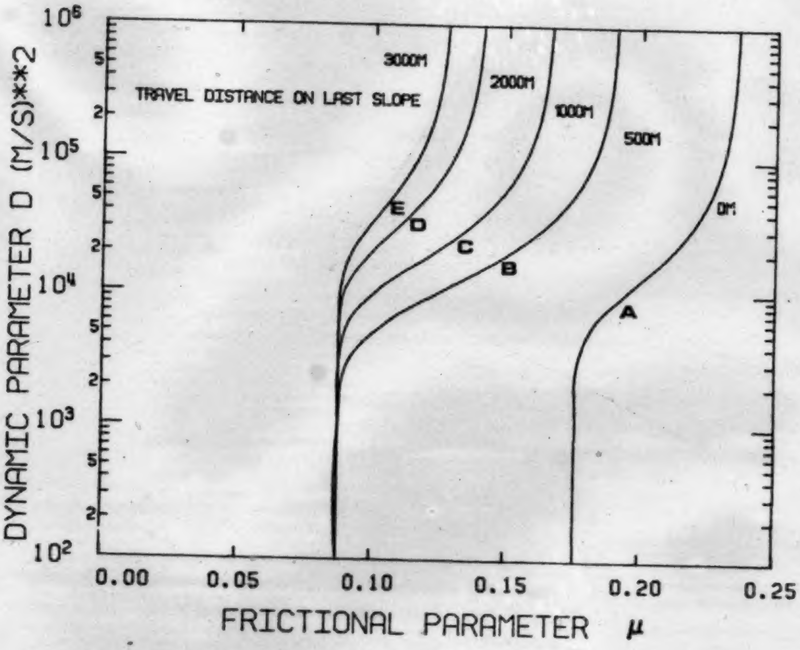

Figure 5.4 Characteristic resistance relationship for Test A - an assessment of the effects of travel distance on the last slope.

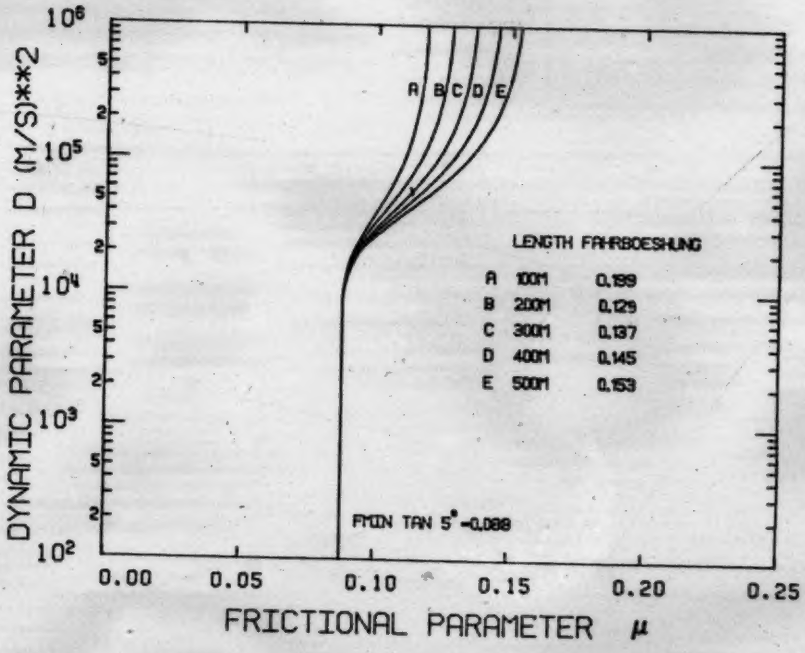

Figure 5.5 Characteristic resistance relationship for Test B - an assessment of the effects of travel distance on the initial slope.

defines the maximum resistance attained for entirely frictional energy losses. The effect is more pronounced for large changes in the final runout segment length. Also of importance is the fact that these geometrical changes did not affect the lower bound frictional resistance attainable here - that value being equivalant to the slope of the shallowest profile segment. Note also that the change in the final runout slope length also induces a translation of the first inflection point in the characteristic resistance curve at a point just greater than the minimum frictional parameter. From these two tests, we may therefore conclude that the upper and lower bound limits to the frictional parameter μ are the *fahrboeschung* and the slope of the shallowest segment, respectively.

Tests C and D (see Figure 5.3) were conducted for a series of profiles each with an identical *fahrboeschung* of 0.129. In Test C the influence of the length and inclination of the initial slope segment was assessed. As previously discussed, the area ratio for a profile with a steep initial fall is higher than the area ratio for a profile with a shallow dipping initial slope. Consequently high velocities are possible earlier in the case of the steep slope, and it might be expected that a different (μ,D) pair would be needed to produce the same runout as the example with a shallow initial slope. As seen in Figure 5.6, this is not the case. The characteristic resistance relationship is relatively insensitive to the

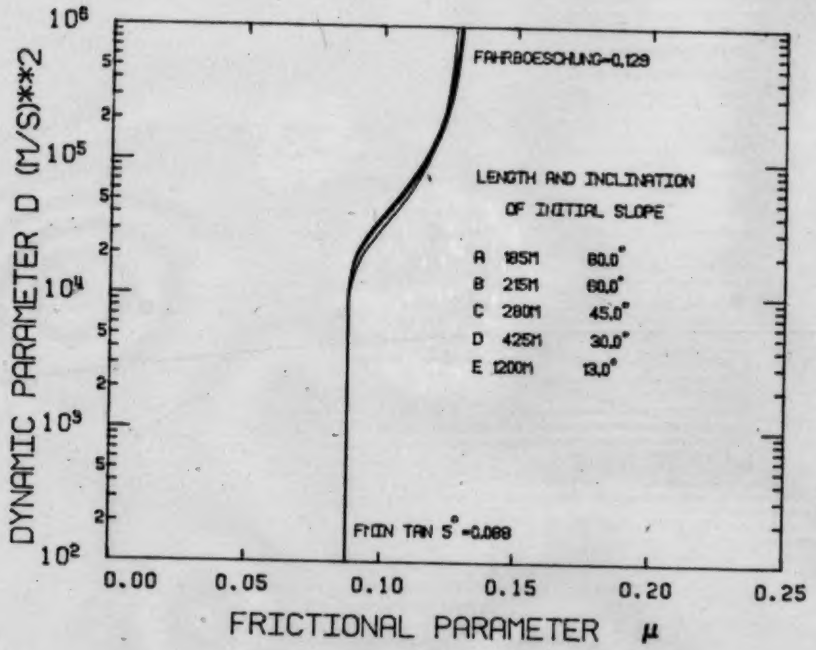

Figure 5.6 Characteristic resistance relationship for Test C - an assessment of the effects of the length and inclination of the initial slope for the same fahrboeschung.

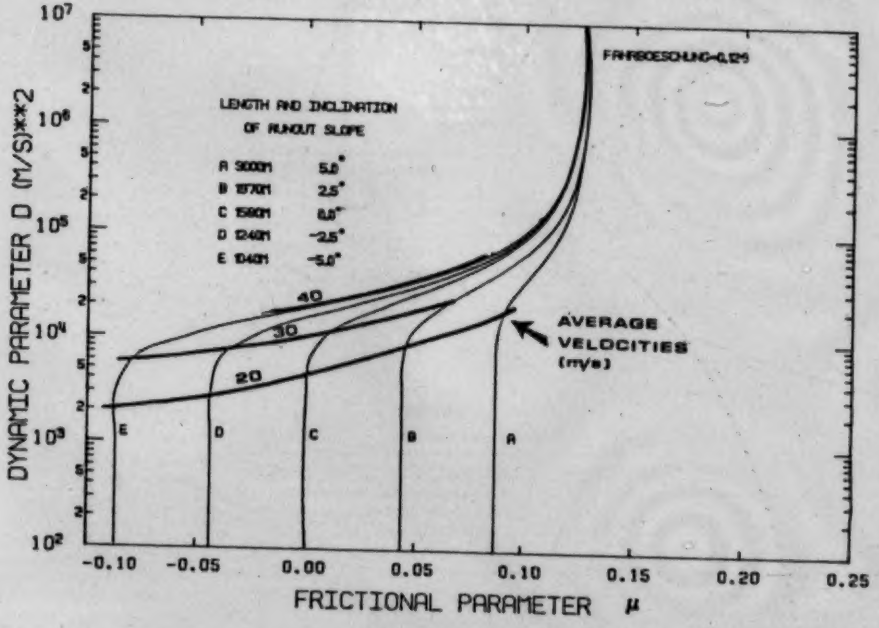

Figure 5.7 Characteristic resistance relationship for Test D - an assessment of the effects of the length and inclination of the runout slope for the same fahrboeschung.

initial slope, at least for the range of inclinations and lengths analysed with the test profile. The velocities attained at the end of the initial slopes in these tests (for $D = 10{,}000\ m^2/s^2$) are also quite similar: 54 to 49 m/s for Cases A to D. Only in Case E is the initial velocity (35 m/s) appreciably lower than these values.

The effects of the length and inclination of the final runout slope on the resistance relationship are quite pronounced as demonstrated in Figure 5.7. In fact, the frictional parameter may have quite a range, depending upon the inclination of the last profile segment. No matter what the profile is before the last segment, the lower bound value of the frictional parameter will be the tangent of the last segment's slope angle. Consequently for a slight run-up of the debris at the terminus of an avalanche, the solution yields a negative friction parameter as the dynamic resistance increases (D value decreases). This anomalous result would appear to be physically impossible, although it does satisfy the boundary conditions of the problem. Nevertheless, other applications of the model to similar geometries (see Section 6.2) suggest that the negative frictional parameter is usually inadmissible since the predicted average velocity range is often below the normal range of average velocities based on eyewitness accounts. There are exceptions to this generalization, however (see Section 5.5).

Also shown on this plot are lines connecting the average velocities of 20, 30, and 40 m/s for each of the test geometries. These lines span a wide range of frictional and dynamic parameters. Consequently, even if one could reasonably limit the range of the average velocities possible, a judicious choice of the most appropriate (μ,D) pair remains as an impediment to using the model for prediction purposes.

In Test E the influence of uplift pressure was assessed. Four examples with r_u factors of 0.2, 0.4, 0.6 and 0.8 were analysed using the test slope profile. As seen in Figure 5.8, the assumption of an uplift pressure equal to some factor times the normal component of the overlying weight results in a translation of the characteristic resistance relationship to the right. The upper limit on the frictional parameter is given by the *fahrboeschung* divided by $(1-r_u)$. Similarly the lower limit on the frictional parameter is given by the tangent of the minimum slope angle divided by $(1-r_u)$. It is interesting to note that an r_u value of 0.8 allows for a frictional parameter μ within the range of values normally expected for peak sliding friction coefficients for hard rocks ($0.7 > \mu > 0.5$). Certainly it appears that uplift pressures, be they air, gases or water, have a significant effect on the characteristic resistance relationship, when applied in this form. Notwithstanding the fact that the generation and maintenance of this phenomenon is a poorly

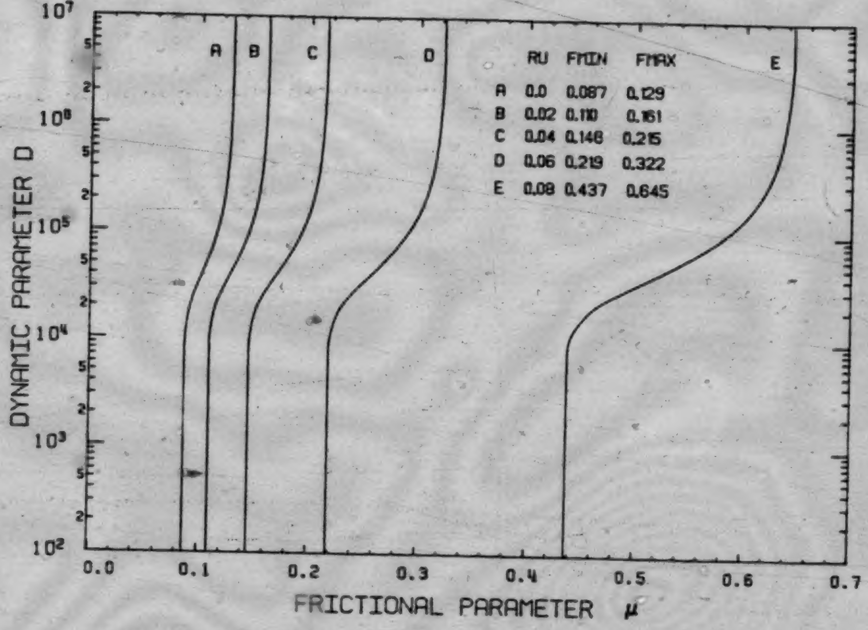

Figure 5.8 Characteristic resistance relationship for Test E - assessment of the effects of uplift pressures.

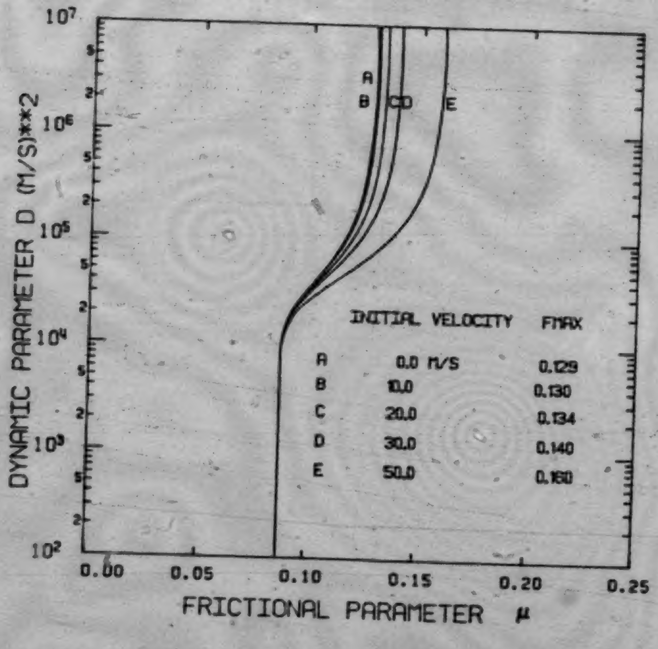

Figure 5.9 Characteristic resistance relationship for Test F - an assessment of the effects of initial velocity.

definable feature at most rock avalanches, it is clearly demonstrated that the application of this simple theory, can produce dramatic changes in the resistance function. More elaborate schemes with the initiation of uplift pressures at the end of a disintegration phase, followed by dissipation analagous to a consolidation type process, are also possible but extend beyond the scope of this treatment.

Option 3 of Program RADA allows for the input of a pre-determined velocity at some point in the profile. To assess the affect that this may have on the characteristic resistance relationship a series of initial velocities was used with the test profile shown in Figure 5.3 (Test F). Initial velocities of 0, 10, 20, 30 and 50 m/s were used as the input for segment 1 of the profile and the (μ,D) resistance relationships were subsequently determined for each case. As shown in Figure 5.9, the use of an initial velocity has the general effect of altering the frictional resistance parameter μ, while still allowing the avalanche to stop at a given location. If this initial velocity is in excess of that velocity which would be calculated with the maximum frictional resistance parameter - the *fahrboeschung* - then the maximum allowable μ value shifts to the right of the *fahrboeschung*. For instance, assume that the initial velocities tested in Figure 5.9 (except Case A) were acquired after sliding along 100 m of the initial slope inclined at 30° (above the start of Segment 1). This modified profile would correspond to a new *fahrboeschung* of 0.138. Consequently all initial velocities in excess of 27 m/s, which is the velocity found with μ = FMAX = 0.138, will shift the maximum frictional parameter to the right of 0.138. Similarly for initial velocities less than 27 m/s, the maximum frictional parameter shifts to the left of 0.138.

While this translation of the upper bound frictional parameter for input velocities may produce a significant alternation of the characteristic resistance relationship, it should be noted that the change produces only minimal differences in the (μ,D) pairs from the range of the dynamic resistance parameters deemed to be relevant for the Mackenzie Mountains rock avalanches.

The significance of the results from this parametric study will be apparent in the application of the model to more complex geometries (see Chapter 6).

5.6 An Appropriate Travel Path - The Frank Slide Example

One of the assumptions used in the derivation of the equation of motion is that the driving and resisting forces act on a body as though its weight is concentrated at its centre of mass. Regardless of whether the body is rigid or disintegrated the motion of its centre of mass along a centre line is described by Newton's Second Law. In the case of most snow avalanches and some rock avalanches the centre of mass of the initial failure block follows a path similar to the profile taken from the top of the highest block to the most distant tip of the debris. Negligible differences arise in the solution when the more concise centre of mass approach is used. Furthermore, the entire profile is much simpler to reconstruct for analysis than a centre of mass travel path.

This approach is adequate for many rock avalanches where the attenuation of the debris is inhibited. However, several examples from the Mackenzie Mountains may not be amenable to this simple treatment - particularly those events where the "ramp" feature may contain upwards of two thirds of the displaced mass. A sufficient number of debris thickness measurements was not available to construct an isopach map of the debris at the avalanches examined in this study, but preliminary estimates suggest that significant differences between the crown to distal tip measured travel angle and the mean travel angle (joining the centres of masses) exist at the Nozzle and Rockslide Pass events. Further clarification of the appropriate travel path to use at these and other events is required if the physics of the motion equation are to be rigorously satisfied. An even more difficult task would be to evaluate the expected degree of attenuation in the debris prior to a failure.

Irrespective of the above reservations concerning the appropriate travel path, the previously described model has been used for such landslides as Elm, Huascaran, Goldau (Koerner, 1976) and Rubble Creek (Hardy *et al.*, 1978). For analysis purposes directed towards the prediction of runout distance and not necessarily the appropriate velocities, the entire profile approach would appear to be adequate in these examples.

On the other hand, the Frank Slide in Alberta exhibits a marked difference between the centre of mass travel path and the entire, top to end, travel path. A cross-section showing the two travel paths is shown in Figure 5.10. A third possible travel path, which may be more appropriate than the above two, is also shown (c-e). By analogy to a fluid, the motion of a particular element of mass at the base of the initial failed mass can be examined. Assuming a plausible initial velocity at some distance beyond the base of the failure block, the characteristic resistance relationship for its travel path to the end of the debris can be found. This approach is attractive because it is compatible with the observed stratigraphic congruence noted at many such events. In contrast, the entire travel path from a to e on Figure 5.10 would suggest that material at the top of the mass finds its way to the very end of the avalanche - a supposition contrary to field observations. It may also be that the "fluid element" travel path approach requires an altered equation of motion which will satisfy the lateral force imbalance at the front of the flow. This deficiency was not examined since the intention here is to assess, in a general fashion, the consequences of a variable travel path.

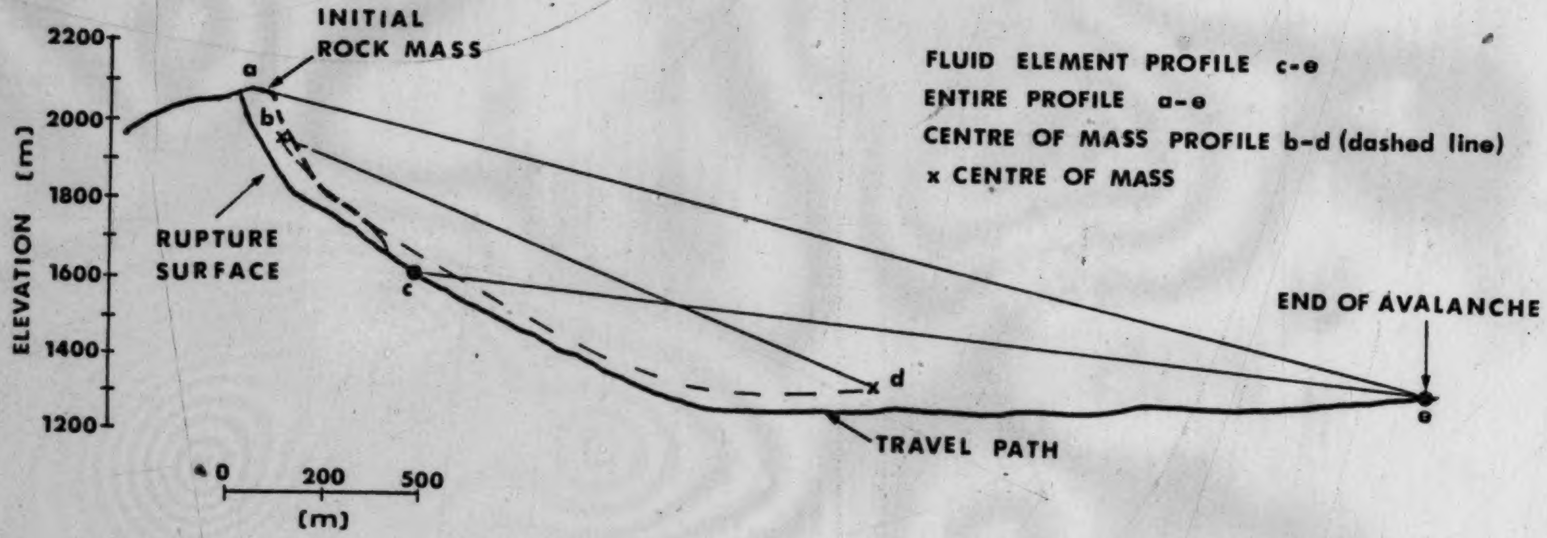
INITIAL
ROCK MASS
FLUID ELEMENT PROFILE c-e
ENTIRE PROFILE a-e
CENTRE OF MASS PROFILE b-d (dashed line)
x CENTRE OF MASS
ELEVATION (m)
2200
2000
1800
1600
1400
1200
a
b
c
d
e
RUPTURE
SURFACE
END OF AVALANCHE
TRAVEL PATH
0
200
500
(m)

Figure 5.10 Reconstruction of original topography before the Frank Slide showing location of travel paths used in this analysis (after Daly *et al.*, 1912 and Cruden, 1980).

For the above described travel paths the characteristic resistance relationships were found (Figure 5.11). As expected, the upper and lower bound frictional parameters for the entire profile and the centre of mass profile are given by the *fahrboeschung* and the minimum slope angle, respectively. Because the fluid element profile has a path identical to the entire profile below point c, the two curves converge on the same minimum frictional parameter of 0.080. Upon initial inspection it appears that the range of resistance pairs which will satisfy the various travel paths is rather large - the frictional parameter ranges from about 0.1 to 0.4 while the dynamic parameter varies over 3 orders of magnitude. Using the best eyewitness estimate of the total time for the event (Anderson, 1979) an average velocity of 35 m/s is calculated for the total travel path. This is probably high because all the debris did not travel the entire length as shown on Figure 5.10. Using a centre of mass travel path an average velocity of 18 m/s is estimated. As shown on Figure 5.11, the (μ,D) pairs matching these best estimates of the average velocity, are located very close to minimum frictional resistance, while the dynamic parameter ranges between 1,000 and 10,000 m^2/s^2.

From the above exercises it must be concluded that the use of a centre of mass analysis can produce a radically different characteristic resistance relationship from that obtained from using the entire profile or a "fluid element" profile. In the case of the Frank slide this variability is

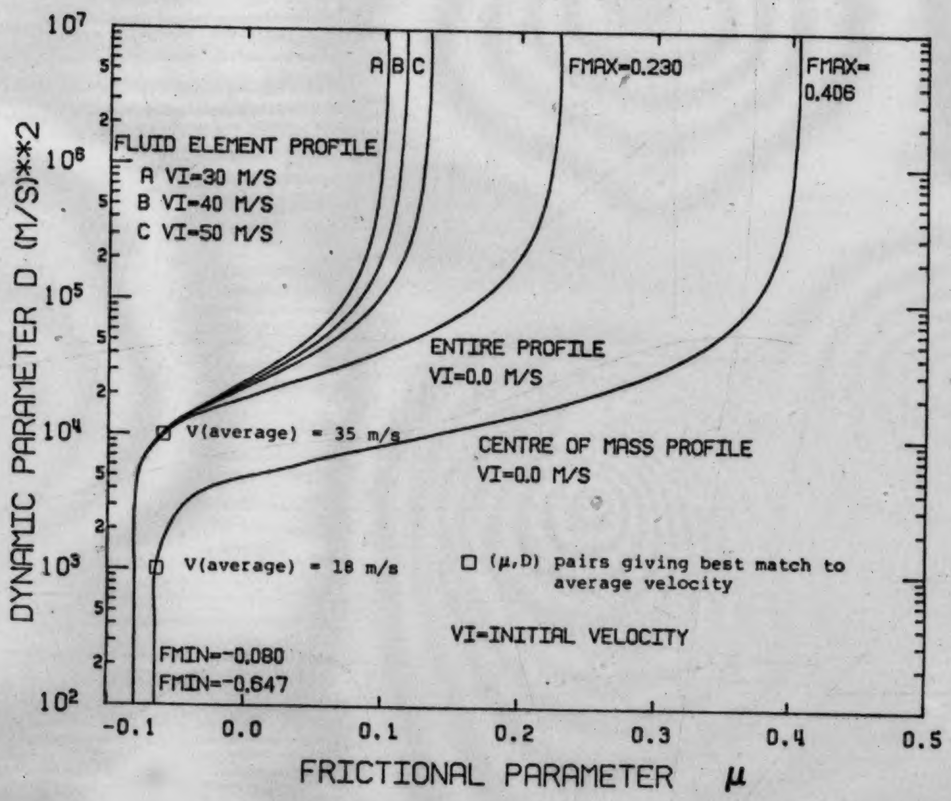

Figure 5.11 Characteristic resistance relationship for the Frank Slide for three travel paths.

found to be largely insignificant for velocity determination since only a small range of (μ,D) pairs will reproduce the same average velocity as that calculated from eyewitness accounts of the total travel time. Runout prediction, however, is quite sensitive to small (μ,D) variations. Had the relevant dynamic parameter ranged between 10,000 and 100,000 m^2/s^2 the range of the frictional parameter would be much greater, and consequently the choice of an appropriate travel path would be most important.

Resolving the travel path question is further complicated by lateral spreading or confinement which should alter the frictional resistance term in the equation of motion. Therefore, because of this problem and the difficulties in ascertaining the degree of longitudinal spreading beyond the centre of mass of the avalanche debris, the procedure followed for future analyses will be to use the entire travel path where available. Although this may be inconsistent, in some cases, with the actual physics used in the velocity derivation, it does offer a somewhat more reliable and proven method for a semi-empirical prediction of runout. Further exploration of the validity of this assumption can only be undertaken once the location of the centres of mass from the landslides cited in this study are determined.

5.7 Discussion and Conclusions

A model for rock avalanches, based on analogous theories of motion for snow avalanches has been examined, modified and applied in this chapter. While considerable differences exist between the density and strength properties of snow and rock it is proposed that the same physical laws can be used to model the motion of these phenomena. Many uncertainties arise in the choice of appropriate parameters in this model, although some problem areas are circumvented by combining the effects of a few poorly defined influences into one single frictional resistance parameter. The equations of motion as originally derived by Koerner (1976) have been slightly modified to become more compatible with the physics of the situation - the velocities of the flow can be found after an initial movement phase which is not consistent with the avalanche model, and uplift pressures, be they due to water, air or gas, may be applied to the travel path.

These adaptations render the model slightly more conformable with the real situation, but several significant reservations still remain. The first problem area is the characterization of the mode of movement; inconsistencies with the observed rheological behaviour of this type of material suggest that a viscous resistance term and some account of the plug-like flow motion over portions of the avalanche may be more appropriate. This complex area has not been addressed and a general assumption of a uniform motion with one frictional parameter and one dynamic resistance parameter is used.

A second major reservation concerns the choice of an appropriate travel path for analysis. The physics of the velocity formulation apply to a centre of mass path, although such a travel profile is often difficult to obtain. Furthermore the accurate prediction of an extreme runout is not obtainable with the evaluation of only the centre of mass travel path. To this end, the entire travel path, a much more easily measured profile, will be used for analysis purposes.

Thirdly, there are many other aspects of the physical characterization, such as lubrication, dispersive pressures, volume dependence, and material entrainment, which remain unresolved. However, for the purposes of the succeeding applications it will be tacitly assumed that these factors are concealed implicitly in the model parameters or they have negligible influences.

Finally, the fourth difficulty with the model is the numerically unstable nature of the solution algorithm. The isolation of the optimal (μ,D) pair that allows the avalanche to stop at a predetermined position is quite sensitive to small variations in the resistance parameters. Consequently quite different runout predictions are often possible with only slight variances in the (μ,D) pair, even though velocities are reasonable over a wide range of resistance parameters. Similarly, the "uniqueness" problem limits the velocity prediction capability of the model. Even with better velocity records at known events the indeterminate nature of the solution would remain.

The parametric study conducted in this chapter draws attention to a few of the more significant factors which determine the complete characteristic resistance relationship. The *fahrboeschung* and the slope of the shallowest profile segment are the maximum and minimum frictional resistance parameters, respectively. Only small alterations in the minimum slope angle produce large changes in the relationship while less pronounced effects occur when the *fahrboeschung* is altered. The effect of assuming an uplift pressure along the travel path has been shown to produce remarkable changes in the characteristic resistance relationship. This may offer an explanation for the quite low frictional parameters (negative in some cases) which arise when an uplift pressure is not used. Because of the already indeterminant nature of the two-parameter model, the inclusion of this third variable would not make the choice of appropriate resistance parameters any simpler. The topic of pore pressure generation and dissipation, while obviously meriting more investigation, is deemed to be beyond the scope of this investigation because of the absence of information to describe the basal parts of these avalanches.

The effect of using an input velocity, derived from an alternative dynamic model for the first portion of a failure, has also been assessed. Only for input velocities substantially different from those predicted by the model over the same slope, will the characteristic resistance relationship be significantly altered. This also suggests that for other model formulations using a viscous or a plug-like flow - which are probably more appropriate over portions of the avalanche - the relevant (μ,D) relationship is not significantly affected as long as the velocities predicted by the alternate models are similar to those predicted by this model.

Finally it must be remembered, that in theory, there is only one point on the characteristic resistance relationship curve which will produce an exact match to the real velocities of the avalanche under consideration. The extremes of the function would not appear too important in this regard. As shown in the parametric study there is a range of (μ,D) pairs capable of giving a reasonable average velocity for a given aval anche. An attempt to bound the relevant (μ,D) pairs from an assorted group of avalanches is conducted in the next chapter.

In summary, Koerner's model as presented here, with a number of alterations, still remains a semi-empirical approach to the rock avalanche dynamics problem. Nevertheless, the convenient yet simplistic masking of certain difficult to quantify physical attributes, makes this model attractive for predictive purposes. Only a limited number of avalanches have been analysed by this method (e.g., Koerner, 1976, 1977, 1980a, Hardy *et al.*, 1978) hence the model must be calibrated with more field evidence before its predictive reliability can be assessed in a comprehensive manner.

6. APPLICATION OF THE MODEL

6.1 Introduction

The primary purpose of this chapter is to present the results of the application of the proposed model to a selection of rock avalanche paths from the Mackenzie Mountains. For each of the six travel paths examined the characteristic resistance relationship and the velocity profiles were determined. In order to assess the influence of a pre-determined initial velocity and uplift pressures, the North Twin rock avalanche was chosen for a detailed study. Subsequent model predictions were compared with other velocity estimates from superelevation and run-up analyses. Consequently the range of relevant (μ,D) pairs applicable for analysis for similar terrain was found.

It is apparent that a number of competing factors influence the solution to the equation of motion for an avalanche moving over a variable profile. By comparison with a selection of documented rock avalanches and other rapid mass movements, various mobility hypotheses may be tested with the model. Such aspects as fluid content, rock lithology, whether or not the mass moved over snow or ice for a portion of its travel path, and the effects of confinement are evaluated using details from documented cases in the literature.

Finally, the predictive capability of the model for the rock avalanches from the Mackenzie Mountains is assessed.

6.2 Rock Avalanches from the Mackenzie Mountains

Topographic profiles for the rock avalanches discussed in Chapter 2 were obtained from 1:50,000 NTS maps modified by more detailed field survey measurements. The travel paths for the avalanches, assumed to run from the tops of the rupture surfaces and along approximate centre lines, were determined from thickness measurements and projected cross-sections at each of the events. These longitudinal profiles are shown in Appendix C with their respective predicted velocity profiles.

North and South Twin avalanches profiles were similarly obtained from topographic maps and modified by debris thickness measurements taken by Kaiser and Simmons (1980). The North Twin profile used in the analysis was shown in Chapter 4 (Figure 4.2) in conjunction with velocity estimates made with run-up and superelevation observations. The South Twin avalanche profile is shown in Figure C.3 with the predicted velocities. The Damocles avalanche profile (Figure C.1) was constructed from field measurements taken by Kaiser and Simmons (1980). The U-Turn, Nozzle, and Rockslide Pass avalanche profiles (Figures C.4, C.5 and C.6, respectively) were similarly constructed with 1:50,000 NTS topographic maps and field measurements made by the writer. For reasons discussed previously the entire travel paths were used for analysis in each of the above cases. for reasons discussed previously (see Chapter 5).

Morphologically and mechanically it would appear that many of the confined rock avalanches from the Mackenzies display striking similarities (see Appendices A and B and Eisbacher, 1979). Consequently one might expect to see a particular resistance reduction phenomenon such as uplift pressures or other agents (e.g., snow, ice or saturated alluvium). This hypothesis may be tested with the proposed model.

Examination of the characteristic resistance relationships for these avalanches (Figure 6.1) does not reveal such a common entity. The range of the frictional parameter μ is between -0.058 and 0.225 and the six characteristic curves span a large range between the widest limits of the dynamic parameter relevant for an average velocity match. As previously noted in the parametric study, the maximum frictional parameter is defined by the *fahrboeschung* which varies from 0.225 for North Twin to 0.131 for Damocles. Similarly the value of the minimum friction parameter is defined by the tangent of the minimum slope angle on the profile. Note that for all of the profiles analysed here, except for the North Twin avalanche, the (μ,D) relationship could not be defined below a certain frictional parameter. The iterative procedure to solve for the frictional parameter μ, giving a velocity of zero at the end of the travel path, becomes numerically unstable when there are travel segment slope angles less than the final slope angle on the path. Only for frictional parameters

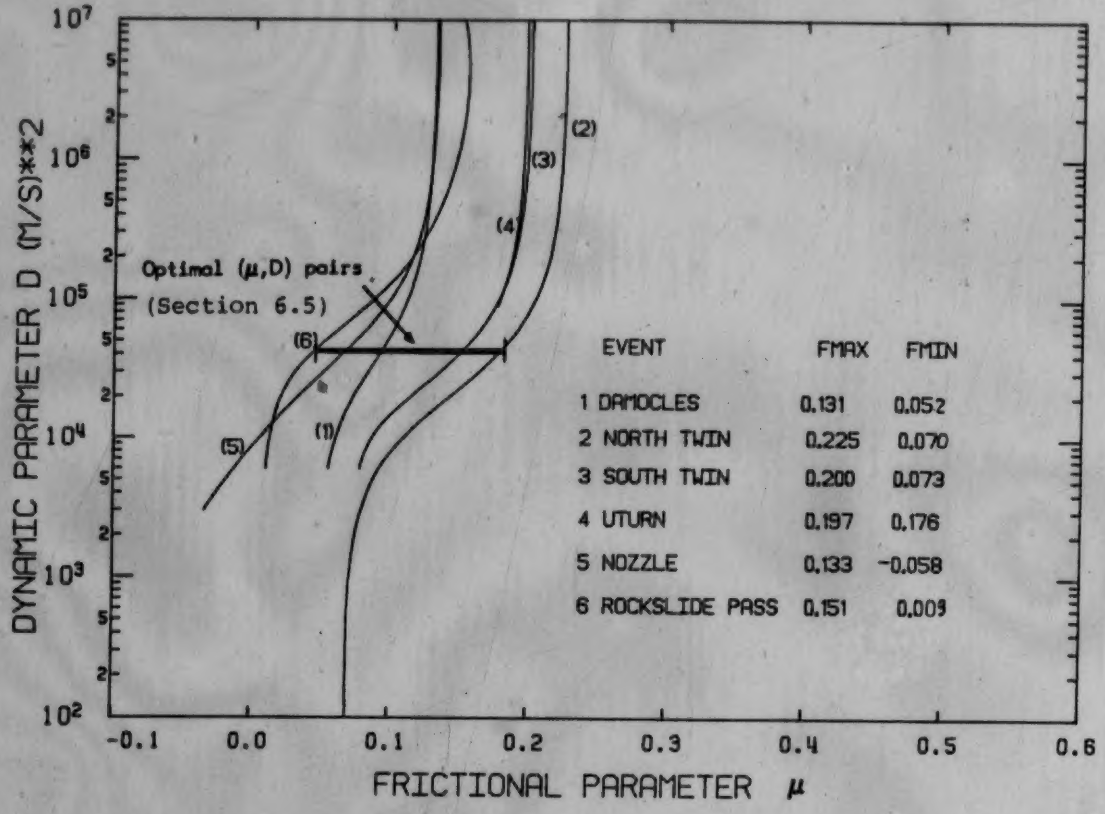

Figure 6.1 Characteristic resistance relationships for six rock avalanches from the Mackenzie Mountains.

greater than the tangent of the final slope angle will the solution converge. In the case of the U-Turn avalanche this was particularly acute since the final travel segment slopes at nearly 10°. This is further sugggestion that the model is inadequate for certain portions of the avalanche.

It is apparent that the *fahrboeschung* is a large determinant of the resistance function, although the relevant velocity matching (μ,D) pairs are usually found closer to the minimum frictional parameter limit, i.e., in close proximity to the first inflection point for each curve. This was initially apparent from the few analyses which have been performed to date for the Huascaran and Rubble Creek events (Koerner, 1976, Hardy *et al.*, 1978) and from the best estimates of the optimal (μ,D) pair for the North Twin rock avalanche (to be developed in the next section of this chapter).

One particular oddity which throws the postulate of a common resistance pair into jeopardy is the difference between the North and South Twin characteristic resistance curves. For the same rock type, travelling down parallel paths from identical starting positions, one would expect almost identical (μ,D) pairs capable of accommodating the slight differences in runout. Such is not the case. For the same frictional resistance parameter, within a relevant dynamic parameter range (say $10{,}000 \ m^2/s^2 < D < 100{,}000 \ m^2/s^2$), the difference between the dynamic parameters for the Twin avalanches ranges between 3,500 and 45,000 m^2/s^2.

An interesting observation can be made regarding the separation of the more confined avalanches which follow a more tortuous course - North and South Twin, and U-Turn - as opposed to the less confined, spreading avalanches - Damocles, Rockslide Pass and Nozzle. For the same frictional resistance less dynamic resistance is required for the less confined avalanches, or alternatively, for the same dynamic resistance less frictional resistance is required by the less confined avalanches. This would seem to be verification of the notion that the more confined, channeled course is bound to produce greater internal disruption in the flow, and consequently mobility would be reduced. These presuppositions will be examined later in applications to other events (see Section 6.4).

In the parametric study (Section 5.5) the characteristic resistance relationship was seen to be radically altered by the inclusion of an average uplift pressure. The effect of assuming a constant r value was to shift the resistance curve to the right (refer to Figure 5.8). For the purposes of evaluating this effect in a general fashion for the Mackenzie Mountains rock avalanches an initial assumption was necessary; given the premise that the maximum attainable ϕ angle for the rock involved is equal to 30°, what average uplift pressure, in the form of an r_u value, will allow FMAX = tan 30°, thus uniquely defining the upper limit of the characteristic resistance relationship? In other words, for normal frictional behaviour assuming a granular material, what uplift pressures are needed to reproduce the observed runout distances for each of the events? This limiting value of r is easily found for each case as:

$$r_u = 1 - (1/\mu)\tan\psi \qquad \text{(Eqn. 6.1)}$$

where μ is the maximum allowable frictional parameter (equal to tan 30°) and ψ is the *fahrboeschung* angle.

A table of the r_u values necessary to increase the maximum frictional resistance parameter from the *fahrboeschung* to tan 30° is shown on Figure 6.2. This plot displays the characteristic resistance relationships for the six avalanches where an uplift pressure allows for normal frictional behaviour with $\mu = 0.577$ (tan 30°) as an upper limit. The similarity in r_u factors (0.61 to 0.77) simply reflects the closeness of the *fahrboeschung* angles for these avalanches. Below this value the dynamic and frictional resistances compete with each other, thus defining the (μ,D) relationship. As in Figure 6.1, numerical instabilities preclude a solution to the $v_n = 0$ algorithm for certain profile geometries.

The plot shows a slightly more defined grouping of the resistance relationships for North and South Twin, U-Turn and the Damocles avalanches than was noted on Figure 6.1. Nevertheless the range of the frictional parameter for all six events is much larger, from -0.16 to 0.57. The curves

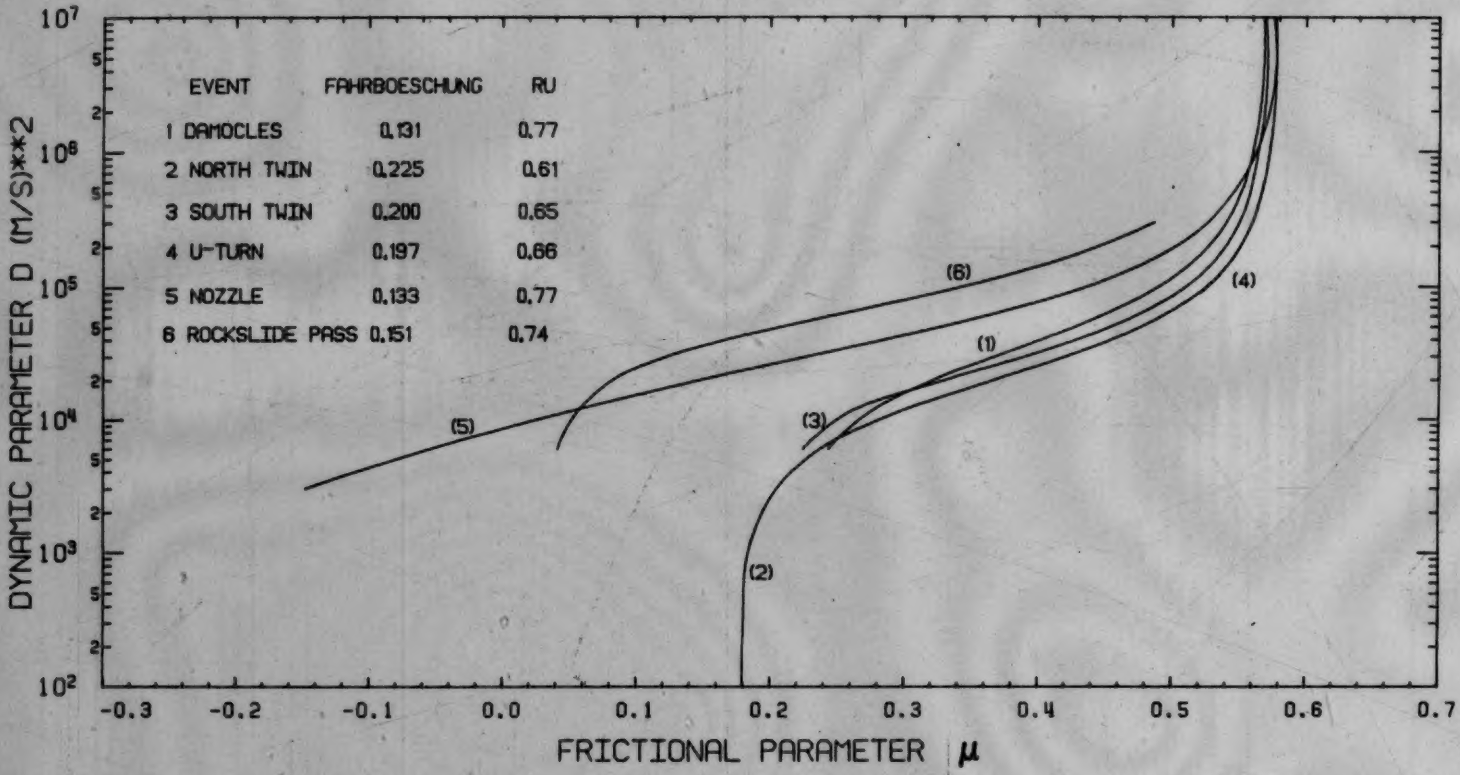

Figure 6.2 Characteristic resistance relationship for six rock avalanches from the Mackenzie Mountains assuming an r_u value capable of allowing FMAX = tan 30°.

for Nozzle and Rockslide Pass are distinctly separated from the others. This would again suggest that less dynamic resistance is required for these events with the same frictional resistance as the other four. There is almost an order of magnitude difference, on the dynamic resistance scale, between the Rockslide Pass and the North Twin curves - a further suggestion that the two avalanches may have had distinctly different behavior.

6.3 Velocity Profiles

For each point on a characteristic resistance curve, as shown in Figure 6.1, there is a unique velocity profile defined for the given travel path. At one extreme, with μ = FMAX and D $=\infty$, the *fahrboeschung* defines the frictional parameter for the sliding block model. This analogue will produce the highest velocities, while at the other extreme, with μ equal to the tangent of the last slope segment, the lowest velocities are produced. Between these two limits is an optimal resistance pair which will best simulate the actual velocity profile.

In this section the velocity profiles from one of the six avalanches under study is examined in detail. Because the North Twin avalanche path offers the best available velocity indicators, as determined from superelevation and run-up analyses, it will be tested for a variety of assumptions. Predicted model velocities are then compared to the range of velocities obtained by other means.

Velocity and travel path profiles for the other five avalanches - South Twin, Nozzle, Damocles, U-Turn and Rockslide Pass - are contained in Appendix C. For comparison purposes these analyses were performed on the entire travel paths with no uplift pressure or initial velocity assumptions.

North Twin Rock Avalanche

Figure 6.3 shows the predicted real velocities at the North Twin avalanche for a group of (μ,D) pairs from the characteristic resistance relationship curve. The critical velocity (from Eqn. 5.7) for μ = 0.143 and D = 50,000 m^2/s^2 is shown on the same plot for illustrative purposes. Note the match between the increasing and decreasing portions of the critical and real velocities, respectively. Where the critical velocity is greater than the real velocity the mass is accelerating, and where the critical velocity is equal to the real velocity the mass is decelerating. The general trend of the velocity is to increase initially on the short steep slope. This is followed by a drop in velocity as the mass moves over a flatter slope. The velocity then rises abruptly and remains relatively high (50-60 m/s for the sliding block model) over most of the length of its travel path. The velocity then drops quickly to zero on the final runout slope.

For greater frictional resistance the predicted model velocities show less sensitivity to variations in the

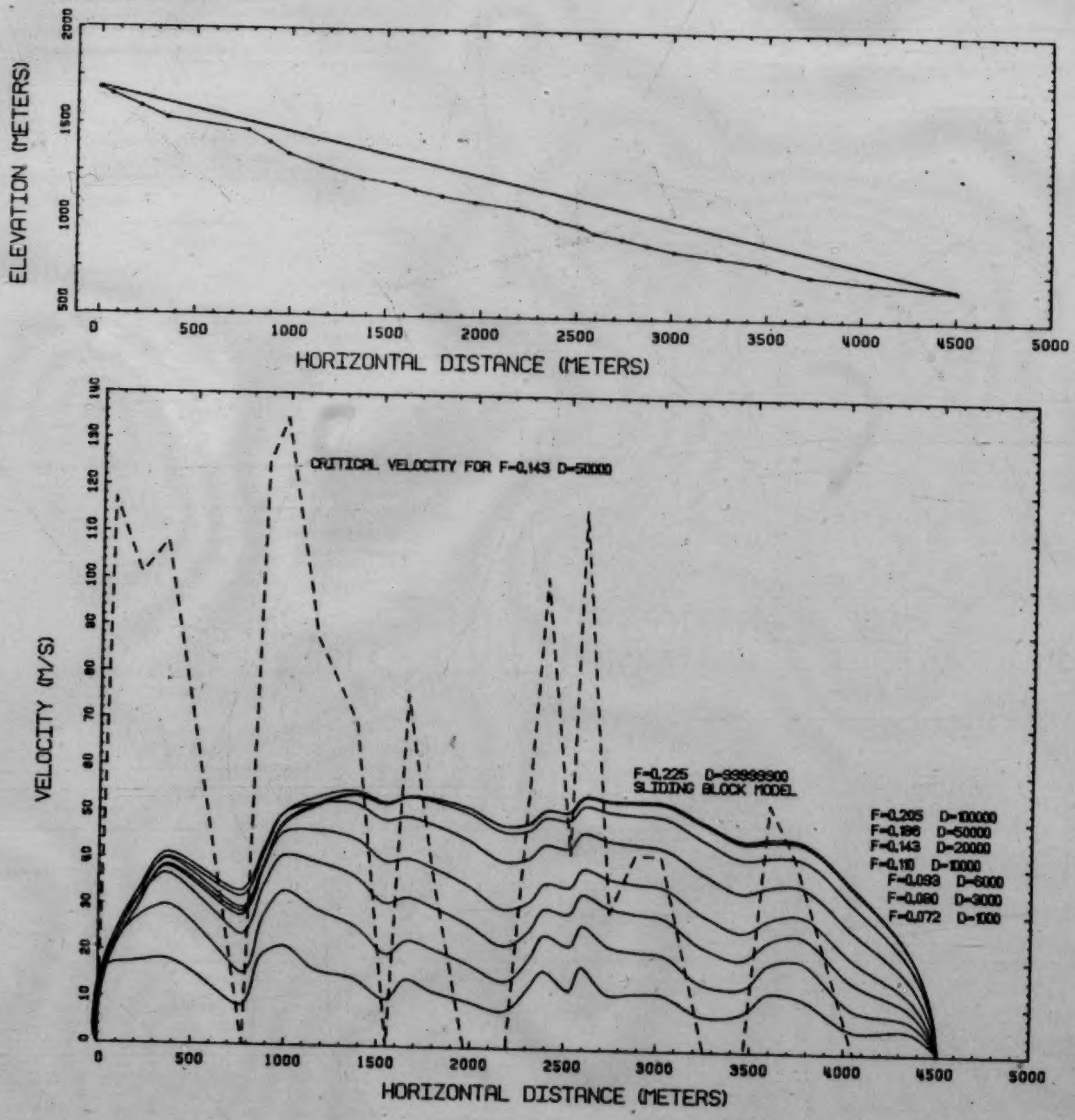

Figure 6.3 Travel path and predicted velocity profiles for the North Twin rock avalanche. Symbol F corresponds to the frictional parameter μ.

topography. As an example, at about a horizontal travel distance of 2500 m a change in the slope inclination from 22° to 12.5° and back to 26° produces a well-defined undulation in the velocity profile for $\mu = 0.072$ and $D = 1000\ m^2/s^2$. However, for the higher frictional resistance of $\mu = 0.205$ and for $D = 100{,}000\ m^2/s^2$. this effect is much less pronounced. Similarly a drop in velocity after 1000 m for velocity profiles with μ less than 0.110 becomes an increase in velocity for μ greater than 0.110. This change reflects the competing action of the two resistances and tendency of the frictional block model to maintain high velocities once initially attained.

Interestingly, as the predicted velocities increase for increasing frictional resistances, the dynamic parameter D increases in an exponential fashion from 10^3 to ∞. This reflects the marginal effects of the velocity squared dependence at higher velocities.

Another feature of the velocity profiles for high frictional resistance parameters is the tendency to attain high velocities - 30 to 60 m/s - followed by very abrupt deceleration as the avalanche comes to a halt. This characteristic is consistent with the few eyewitness observations which claim that the rapidly moving mass seemed to almost "freeze" in place before stopping. Also of note is the fact that the frictional block model ($\mu = 0.225$, $D = \infty$) attains a slightly lower velocity, until about 1500 m, than the model predictions with $\mu \geq 0.186$ and

$D \geq 50{,}000\ m^2/s^2$. This is a consequence of the attainment of very high initial velocities and the nature of the solution process.

Effect of Initial Velocity Assumption

Figure 6.4 is a similar plot of the velocity profiles for North Twin with the assumption of an initial velocity. Using the centre of mass profile as shown in Figure 3.7 the velocity of the failure block after 136 m of movement was calculated. A value of 15 m/s was found with the assumption of $\mu = 0.141$ - a dynamic frictional coefficient deemed reasonable, yet by no means verifiable (see Section 3.7). From this point onwards the velocity profiles were determined in a similar fashion as done above. Note that the total horizontal travel distance is about 350 m short of the length shown on Figure 6.3. This is due to the difference between the centre of mass of the pre-failed block and the top of entire profile used in the original analysis. Similarly the change in the profile length reduced the *fahrboeschung* from 0.225 to 0.218. Strictly speaking, the end of the profile should rightly be the centre of mass of the debris, however, this could not be easily determined with the known information. Consequently for illustrative purposes and consistency the travel path to the tip of the debris was used here.

The predicted velocity found with $\mu = 0.141$ after 435 m would have been calculated with the original centre-line

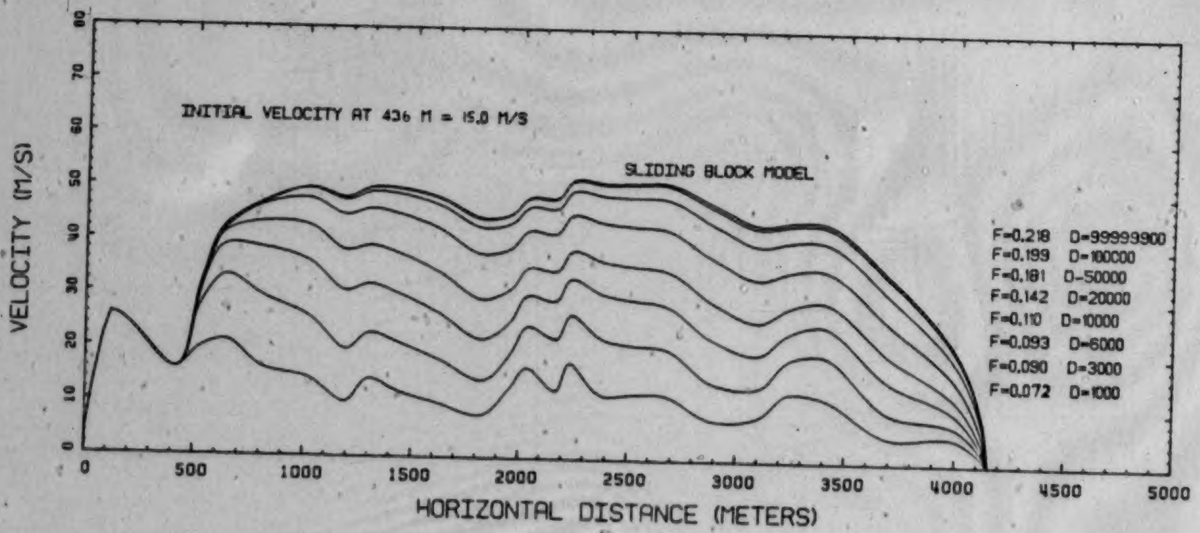

Figure 6.4 Predicted velocity profile for North Twin rock avalanche with v_o = 15 m/s after 436 m.

profile using μ = 0.080 and D = 3000 m^2/s^2. Velocities up to twice this value would be predicted with characteristic resistance pairs closer to the sliding block model. Nevertheless, the rest of the velocity profile for the initial velocity assumption case is remarkably similar in form and magnitude to that shown in Figure 6.3. Only for μ greater than 0.142 do the characteristic resistance pairs differ from the original profile calculation. Predicted peak velocities are a maximum 2 or 3 m/s lower with the initial velocity assumption.

Effect of an Uplift Pressure Assumption

Applying the uplift pressure assumption of r_u = 0.61, which reduces a normal FMAX = tan 30° to the *fahrboeschung* 0.225, does not produce any notable changes in the model velocity predictions. The velocity profiles are identical with those produced by using the entire profile without an uplift pressure assumption (Figure 6.3). This result would be expected since the "effective" maximum frictional parameter for the initial assumption made is simply $(1-r_u)$ tan 30°, which is equal to the *fahrboeschung* 0.225. Because the uplift pressure has no effect on the dynamic parameter, the frictional parameters in the (μ,D) pairs in Figure 6.3 are simply reduced by the factor $(1-r_u)$. Consequently, while a significantly different characteristic curve is produced for an uplift pressure assumption, this additional apparent reduction to the frictional parameter has no effect on the predicted model velocities.

Comparison with Superelevation and Run-up Analysis

A more revealing test of the predicted velocities from the model would be to compare them with the limited velocity ranges suggested by superelevation and run-up analyses. While these indicators may not be all too precise for reasons cited previously, they do offer a reasonable alternative model for comparison.

Ideally one would like to delineate the appropriate (μ,D) pair suitable for prediction purposes. However, as Figure 6.5 shows, the various models do not exhibit a great deal of compatibility. The initial velocity range for both the Koerner's model and the various models proposed in Chapter 3 are in reasonable agreement to about 750 m. The rolling friction models are certainly less realistic since they provide for continuous acceleration. In a rather odd fashion, the first superelevation velocity range is substantially below the dynamic model's predicted velocities for μ greater than 0.090. Rather than displaying a gradual slowing of velocity as the avalanche moved over progressively less steep terrain, the superelevation predicted velocities show a marked increasing tendency until about 3000 m with the exception of a slight dip at 2650 m.

Obviously, the two-parameter dynamic model presented in Chapter 5 does not offer a particularly concise simulation

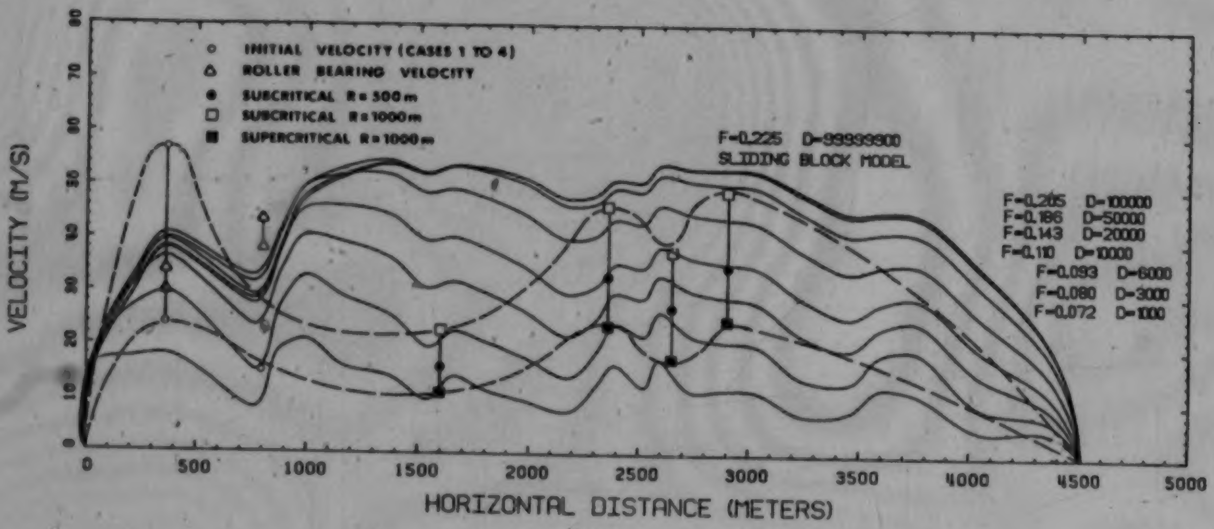

Figure 6.5 Predicted velocity profile for North Twin rock avalanche using the entire travel path with velocities from initial sliding and superelevation analysis. Refer to Figure 4.2.

of the velocity spectrum attained by the North Twin rock avalanches, that is, if the superelevation analysis is correct. As seen in Figure 6.5, the range of suitable (μ,D) pairs which bound the velocity profile beyond 800 m, extend over the entire range from $\mu = 0.143$, D = 50,000 m^2/s^2 to $\mu = 0.072$, D = 1000 m^2/s^2. Even with the elimination of the spurious superelevation velocity at 1600 m and the final run-up velocity prediction, the (μ,D) range is 0.080 to 0.143, and 3000 to 20,000 m^2/s^2, for μ and D respectively. Unquestionably some of the variability here is attributable to the choice of the radius R used in the calculation of velocity. Uncertainties is this regard preclude a more definitive bound to the relevant (μ, D) pairs in Koerner's model for this example.

There are several other possible explanations for the apparent inconsistency in the models. Firstly, the two-parameter model predicts velocities for a single (μ,D) pair without consideration of possible variances in either of these two parameters over the course of the avalanche. As previously discussed in Section 5.3, this inadequacy, along with several others to account for supposed changes in the rheology of the avalanche debris or the frictional resistance of the travel path, may be a severe impediment to an accurate velocity determination. Even when a reasonable sliding velocity for the initial part of the failure is applied (Figure 6.3), a velocity profile almost identical to Figure 6.5 is produced. As previously discussed, an uplift pressure assumption will not change the velocity profiles significantly provided the maximum frictional parameter, $(1-r_u)\tan 30°$, is equivalent to the *fahrboeschung*. Values greater than the *fahrboeschung* will not converge to a solution and values less than *fahrboeschung* will predict lower velocities because of greater dynamic resistance losses.

Secondly, the travel path used in the analysis was the entire profile from the crown of the slide to the distal tip of the debris. To rigorously satisfy the physics of the velocity formulation, the centre of mass travel path should have been used. Lower velocities would have been predicted, although the anomalous increase along the travel path would still not be accounted for.

Another major uncertainty lies in the accuracy of the velocities derived from superelevation. It is most difficult to envisage the suggested gradual increase in velocity over the middle portion of the avalanche. Even if the debris at the first superelevation cross-profile were treated as run-up rather than superelevation a minimum velocity of about 20 m/s would be suggested. In addition to some of the previously mentioned limitations to this analysis (Section 4.4) there is some question as to the precision of the field measurements used to determine the tilt angle θ. Active colluvial and alluvial processes have obscured the avalanche debris in places, raising some doubt as to the exact limits to which it has risen along the valley walls (Kaiser and Simmons, 1980). Perhaps more disconcerting, however, is the presence of apparent superelevation along the valley walls of both North and South Twin avalanches where there is no obvious directional change. This in itself is suggestive of a more complex mode of movement, perhaps with wave-like oscillations capable of "splashing" debris along valley sides in a more random fashion. Kaiser and Simmons (1980) have also speculated that the travel path may have been altered by the presence of snow or ice . However, this hypothesis could not be firmly proven with field evidence.

In conclusion, this application of Koerner's model to the North Twin rock avalanche has proven to be somewhat less than successful with the available data. In order to accurately delineate relevant model parameters there is a need for a more comprehensive spectra of velocity indicators, a body of information not likely available at any of the Mackenzie Mountains rock avalanches.

6.4 Applications to Other Mass Movements

In Figures 6.1 and 6.2 the characteristic resistance relationships for a number of rock avalanches from the Mackenzie Mountains were shown. It might have been expected that similar frictional and dynamic resistances were operating along the travel paths of these events. However, as these plots have shown, there would appear to be other significant factors determining the function. It is possible that a particular unifying characteristic may be capable of explaining this inconsistency; perhaps it reflects variances in material constituents, water contents, sliding surface conditions or geometric constraints. It is the purpose of this section to examine a selection of such hypotheses directed towards isolating a unique, unifying characteristic. To this end, a group of rock avalanches chosen from around the world and from a variety of terrain, will be analyzed by the model.

It should be borne in mind that these variances are not mutually exclusive. The observed (μ,D) relationship could reflect the combined effects from one or more such influences, in which case the isolation of one would be nearly impossible. Furthermore, it must be remembered that there is only a restricted range of the frictional and dynamic parameters relevant to discussion, since in theory, only one (μ,D) pair is capable of modelling the actual velocity profile.

Hypothesis 1

In Hypothesis 1 it is postulated that the $(\mu,\log D)$ relationship, as shown on Figure 6.6 for a selection of rapid mass movements, reflects the influence of material entrainment - be that alluvium, till, snow, ice, water or vegetation.

Four of the profiles used in this analysis were obtained from well documented rock avalanche examples in the

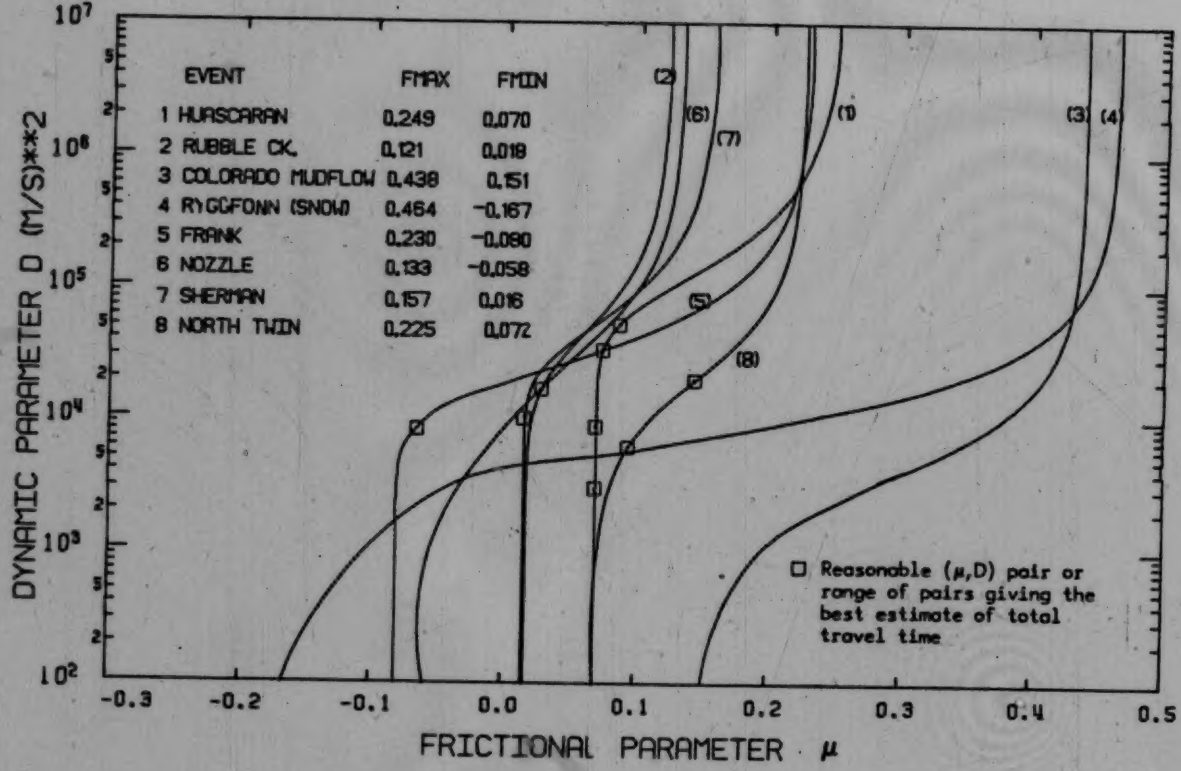

Figure 6.6 Characteristic resistance relationships for a selection of rapid mass movements.

literature. Nozzle and North Twin avalanches were examined previously in this research and by Eisbacher (1979). Two other rapid mass movements, a mudflow and a snow avalanche, were also analyzed with the model for illustrative purposes. While the applicability of the same physics to a reportedly laminar flow is questionable in the former, the model is well suited to the latter; it was used as an example by Bakkehoi *et al.*(1981) in their application of an analagous two-parameter model. Relevant details from these six examples are now briefly examined. The reader is referred to the appropriate references for more detailed information.

The Huascaran avalanches in 1962 and 1970 originated on Nevados Huascaran, the highest peak in the Peruvian Andes. A combined total of some 22,000 casualties resulted from these highly mobile flows which initially started as large cliff failures involving both ice and rock. The long horizontal runout and high velocities reported at these events are associated with the steep travel path and the extreme fluidity acquired when the moving mass extrained large volumes of snow, water, saturated alluvium, and moraine along its route. Eventually the avalanches turned into debris flows which continued to wreck havoc down the Rio Santa. Detailed description of the avalanches and their deposits may be found in papers by Plafker and Ericksen (1978), Plafker *et al.*(1971), and Cluff (1971).

The Rubble Creek avalanche of southwestern British Columbia involved an estimated 25 x 10^6 m^3 of dacitic lava which travelled up to 4.6 km, entraining valley alluvium enroute, on an average slope of 8° (Moore and Matthews, 1978). A state-of-the-art treatment of this type of landslide was compiled by Hardy *et al.* (1978).

The Frank landslide in southwestern Alberta has been one of the most intensely studied rockslides in the western hemisphere (McConnell and Brock, 1904; Daly *et al.*, 1912; Krahn, 1974; Cruden and Krahn, 1978; Hungr, 1981). The movement of the large wedge of Paleozoic limestone initially began as a rock slide along bedding planes and soon disintegrated into a fragmented avalanche which spread debris in a fan shaped lobe across the valley bottom incorporating river alluvium and possibly some glacial till in the process.

The Sherman Glacier rock avalanche, which took place during the Alaskan earthquake of 1964, has attracted the attention of many investigators, notably Shreve (1966), Marangunic (1972), and McSaveney (1978). A slightly metamorphosed, well fractured block of sandstone and siltstone was shaken loose from Shattered Peak and subsequently travelled across the Andres Glacier, over a bedrock ridge and down the Sherman Glacier to cover a total area of 8.25 km². The incorporation and melting of large amounts of soft snow was felt to be partially responsible for the apparent high mobility.

The alpine mudflow from the Tenmile Range of central Colorado was documented by Curry (1966). After a long period of intense rainfall, a series of mudflows was observed moving over and through saturated talus on slopes as steep as 41 degrees. These flows were seen to move as pulses at peak observed velocities of about 16 m/s.

The Ryggfonn snow avalanche from near Stryn, Western Norway was mapped by Lied and Bakkehoi (1980) and was used by Bakkehoi *et al.*(1981) in the application of a slightly modified version of Koerner's (1976) model.

For each of the above mass movements a longitudinal profile of the presumed travel path was obtained or constructed from information contained in the pertinent references cited. Where possible, the best match of the estimated total travel time or average velocity with the value predicted by the model was found. The relevant (μ,D) pair or range of pairs for these events and for the North Twin rock avalanches are shown on Figure 6.6.

Examination of this figure reveals a wide variation in characteristic resistance curves. The maximum frictional parameters range from 0.121 for Rubble Creek to 0.464 for the Ryggfonn snow avalanche. The minimum values range from -0.167 to 0.151 for the Colorado mudflow and the Ryggfonn snow avalanche, respectively. The more relevant range of (μ,D) pairs as deduced from matches to the average velocity for selected events is smaller - from -0.12 to 0.145 and from 3000 to 60,000 m^2/s^2, for μ and D respectively.

It is therefore apparent that a common trend is not revealed on this plot. The Huascaran event, which represents an extreme example of the influences of entrained material, and the other known events which are known to have had a significant proportion of entrained moraine and alluvium - Rubble Creek and the Frank slide - do not show any particular resemblances. The two events which contained some amount of snow and ice in their mass for at least a part of their travel - the Sherman Glacier and the Huascaran avalanche - do not show a marked similitude, and certainly do not bear any likeness to the Ryggfonn snow avalanche. Nor does the (μ, log D) relationship for the Colorado mudflow show any agreement with any of the other events. Nozzle and North Twin rock avalanches from the Mackenzies, are equally as varied and do not exhibit a discernible parallelism with each other, nor with any particular event. Hypothesis 1, as tested for this selection of rapid mass movements, is therefore rejected.

Hypothesis 2

In Hypothesis 2 it is postulated that the (μ,log D) relationship reflects the slide or travel path surface's frictional characteristics. Specifically, it is proposed that the rock avalanches, which have taken place onto snow or glacial ice, exhibit a reduced frictional resistance and are apt to travel further.

This working hypothesis may be relevant to the suite of rock avalanches from the Mackenzie Mountains.
Circumstantial evidence from Damocles, Rockslide Pass,North

and South Twin (Kaiser and Simmons, 1980), and possibly Nozzle is suggestive of the possibility of there having been ablating glacial ice, or perhaps isolated seasonal ice or snow fields along their respective travel paths at the time of the event. Additional field evidence such as contact relationships between moraine or alluvium and the avalanche debris, surface morphology, glacier trim lines and a reliable chronological dating of the features would be required before such a postulate could be adequately evaluated.

For the purposes of testing Hypothesis 2, the characteristic resistance relationships for a suite of rock avalanches which took place onto glaciers have been determined. By comparison of this group with relationships found for the selection of rapid mass movements (Figure 6.6) and the Mackenzie Mountains rock avalanches (Figure 6.1), a reasonable evaluation of the hypothesis can be made.

Figure 6.7 is a plot of the (μ,log D) relationships for six rock avalanches which moved onto and along glacier ice for some portion of their travel paths. Only two estimates of the average velocity were available for the events and are shown on the plot as the (μ,D) pairs which best match these values.

The Sherman Glacier slide (McSaveney, 1978), perhaps the best known of this type of phenomena, was briefly described for Hypothesis 1.

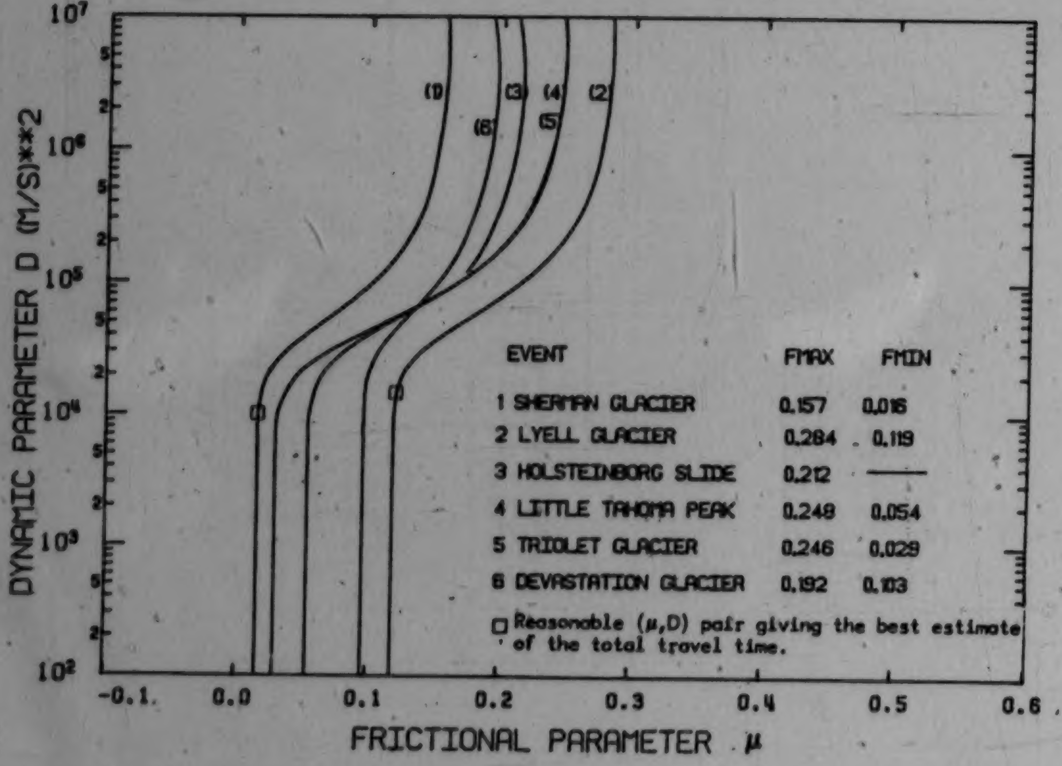

Figure 6.7 Characteristic resistance relationships for selected rock avalanches onto glaciers.

The Lyell Glacier slide on South Georgia Island was described by Gordon *et al.* (1978). The profile used in the analysis is admittedly rather approximate because of the large contour interval on his location map. Nevertheless, the general trend of the relationship is adequately determined. The initial rockfall, from a steep buttress of slates and greywacke, and the subsequent travel of the rock, firn, and ice debris down the glacier were detected on a seismic record, from which an average velocity could be calculated.

The failure of a steep gneissic cliff onto and down a glacier near Holsteinborg in Greenland was described by Kelly (1980). An initial mass of some 3×10^6 m^3 was transported up to 7 km over glacial ice and moraine.

The Little Tahoma Peak rockfalls and avalanches, on the east side of Mount Rainer, Washington, travelled some 7 km down the Emmons Glacier and the White River Valley. It is believed that up to seven separate rockfalls, totaling 11×10^6 m^3 in volume, with only short time separation, were initiated by a small steam explosion on the mountain (Fahnestock, 1978).

The Triolet Glacier avalanche of 1917 was believed to have originated as a rockfall from the Italian flank of the granitic Mount Blanc massif. Descending onto the glacier and fragmenting, it moved rapidly down valley for 7.2 km at estimated speeds up to 35 m/s (Porter and Orombelli, 1980).

The Devastation Glacier avalanche from southern British Columbia is described by Mokievsky-Zubok (1977), Patton (1976), and Hardy *et al.*(1978). A 13.7 x 10^6 m^3 mass of tuff, volcanic breccia and ice broke away from a fissured cliff and travelled down the glacier into a narrow creek bed and eventually emerged into the Meager Creek valley giving an average slope of 9° to 10°.

6.7 does not reveal a particular common entity aside from parallelism among the characteric resistance relationships for the six avalanches. Nor is there any marked distinction between this group and the previous group of rapid mass movements or the Mackenzie Mountains avalanches, of Figures 6.6 and 6.1, respectively. While the envelopes of the characteristic resistance relationships for these three plots overlap considerably, there is some suggestion of a slight translation of the curves on Figure 6.7 to the right. The opposite of this might be expected, however, for a surface with a reduced frictional resistance. Maximum and minimum frictional parameters are defined by the *fahrboeschung* and slope of the final segment slope angle, respectively.

Possibly one or several reasons could be responsible for the lack of a well defined characteristic curve for this particular type of avalanche: the proportion of the travel path actually on the glacier; the type of snow or ice, the thickness of the snow cover; the rock type; the degree of lateral spreading; or the magnitude and distribution of pore pressures generated by the inevitable melting of some of the surface cover. Regardless, the hypothesis must be rejected as unsubstantiated. No significant trend in the characteristic resistance relationships emerges from the application of the model to this group of avalanches. The reduction in frictional resistance, whether significant or not, is probably masked by one or several influences.

Hypothesis 3

In Hypothesis 3 it is postulated that differences in the (μ,log D) relationships may reflect differences in rock lithologies. It might be reasonable to believe that certain rocks, possessing unique elastic, structural, or frictional properties, are capable of longer runout distances. As mentioned previously, the propensity for carbonate terrains to host the majority of rock avalanches in the northern Canadian cordillera could possibly reflect a particular material property. This hypothesis will be tested by re-examination of the resistance relationships shown in Figures 6.1, 6.6 and 6.7.

Consideration of those avalanches which involved carbonate rocks - the six from the Mackenzies and the Frank slide - reveals that there is no apparent unifying characteristic in their (μ,log D) resistance relationships. Frictional parameters from the relevant velocity range span the width of the envelope - from -0.97 for the Frank to 0.145 for North Twin. Those avalanches involving volcanic rocks - Rubble Creek, Devastation Glacier, Little Tahoma Peak - have a slightly more defined envelope of curves, but still do not display a unique relationship which distinguishes the three from the other events. The two avalanches involving argillaceous or clastic rocks - the Sherman Glacier and Lyell Glacier events - are distinctly separated on Figure 6.7, and show little hint of similarity. The Holsteinborg and Triolet Glacier avalanches, both from granitic terrains, are much closer together on this plot, although the trend would need to be assessed for more events of this type before the resemblance could be deemed significant.

In conclusion, for the select group of avalanches examined here, Hypothesis 3 must be rejected. The influence of rock lithology may again be masked by one or more other factors. It might also be noted that the sample of avalanches is obviously biased, for there are few suitable events reported in the literature involving shale, sandstone or metamorphic rocks.

Hypothesis 4

In Hypothesis 4 it is postulated that confined and unconfined debris runout geometries are distinguishable on the basis of their respective resistance relationship curves. Both the Frank and the Sherman Glacier slides are excellent examples of unconfined spreading avalanches while most of the events from the Mackenzies described in this study, with the possible exception of Rockslide Pass and Damocles, are confined to narrow valleys.

Examination of Figures 6.1, 6.6 and 6.7 reveals that, within the range of relevant velocities, the Frank, Sherman Glacier, and Rockslide Pass avalanches show some of the lowest frictional parameters, as opposed to the more confined avalanches. This observation would appear to be contrary to Hungr's (1981) suggestion that a less productive expenditure of energy takes place in a spreading avalanche and that consequently one would expect a greater equivalent coefficient of friction or *fahrboeschung* than for a more confined geometry. Competing mechanisms may be responsible for this disrepancy. Furthermore, the Lyell Glacier slide was relatively unconfined, but displays a much greater optimal frictional parameter, -0.120, than the other three unconfined events. Nor would there appear to be any resemblance of a common trend in the remaining group of confined or channeled avalanches in this respect.

In conclusion, Hypothesis 4, must be tentatively rejected since there is not sufficient data to confirm the existence of a discernible difference in the characteristic resistance relationship for confined and unconfined rock avalanches.

Within this section four hypotheses have been tested on a varied selection of rock avalanches, using Koerner's two-parameter model. It may now generally be concluded that there is no easily recognizable characteristic which may explain the variances in the relevant (μ,D) pairs for this group of mass movements. It appears that a number of competing factors, and or other influences mask the specific elements which define the unique characteristic resistance relationships for each of these mass movements. Alternatively, there may be sufficient grounds for questioning the proposed model, simply because of its inability to match the actual behaviour of a number of these events.

6.5 Predictive Capability of Model

To this point in the chapter the model presented has been applied to a number of rock avalanche profiles from both the Mackenzie Mountains and other examples from around the world. Only limited success has been attained in an attempt to isolate an optimal (μ,D) resistance pair capable of characterizing a particular type of avalanche. While it appears that the competing efforts of several influences may preclude a solution to this problem, there are more empirical approaches which may be satisfactory for predictive purposes.

Empirical models that are based on a relationship between the original volume and the excessive travel distance of the rock mass (Scheidegger, 1973; Hsu, 1975) are probably of marginal value for runout prediction purposes simply because the volume of the initial rock mass can not easily be predicted before the event. While it is possible that several of the failures in the Mackenzie Mountains were sufficiently pre-defined by an elaborate tension crack and fissure network prior to collapse, it is more likely that immediate pre-failure volume controls are less conspicuous. Consequently, a Hsu-type relationship, which admittedly is rather poorly defined for this area anyway, would probably be rather unreliable for runout prediction.

Simple application of an averaged *fahrboeschung* or equivalent coefficient of friction to predict runout in a particular type of terrain of a limited geographic extent may prove successful in some cases. In the Mackenzie Mountains, however, there are more complicating factors, such as avalanche paths with abrupt direction changes, which give rise to a range of equivalent coefficients of friction. As a result, the use of an average value could prove rather unreliable, at least for the group of rock avalanches examined here.

As an alternative approach, it is proposed that Koerner's (1976) two-parameter model can be used with a suite of empirically derived frictional and dynamic parameters. Several prediction capability tests using the travel path profiles from six Mackenzie Mountains rock avalanches will be conducted in this section with this method.

Examination of Figure 6.6 reveals a rather wide variation in (μ,D) resistance pairs capable of predicting the accurate runout distance at each of the five avalanches for which a range of likely velocities is known. By excluding the upper and lower ranges of the dynamic parameter D for the Huascaran event (due to its incorporation of a large ammount of alluvium, ice, snow, and water) the most reasonable range of velocities falls in a band between about 5,000 and 30,000 m^2/s^2. The frictional parameter ranges from -0.70 to 0.145 on this plot. This is a revealing feature which should facilitate the choice of an appropriate μ value; when the abscissa of the characteristic resistance relationship is plotted on a logarithmic scale the most appropriate (μ,D) pairs will have a tendency to be located very close to the inflection point of the characteristic resistance relationship curve. This suggests that on average the tangent of the last runout slope angle is only slightly less than the optimal frictional resistance parameter. While this hypothesis has yet to be proven valid for the selection of Mackenzie Mountains avalanches, it is deemed to be acceptable enough for this application on the basis of the evidence presented in Figure 6.6.

Prediction Capability Tests

In prediction capability Test 1, the ability of the model to match the observed runout distance for the six rock avalanches is assessed. Option 2 of Program RADA is used to determine the final stopping position of a hypothetical avalanche with predefined resistance parameters; μ being given by the tangent of the average slope angle in the distal portion of an initially assumed runout distance plus one degree, and D being given by values of 7,000, 14,000 and 20,000 m^2/s^2. The choice of a one degree addition to the FMIN value was not an arbitrary value; the relevant velocity matches for most of the events on Figure 6.6 lie between the equivalents of 0.5° and 1.5° from the FMIN value.

For each of the six avalanches the most likely travel path of runout beyond the observed stopping position was determined from topographic maps and field surveying. A series of simulations was performed with the model using the above described (μ,D) pairs. Where the predicted runout was beyond the Nth segment of the observed travel path, the additional distance, ΔR, was noted. Similarly if the avalanche did not reach the limit of the observed runout, the difference, ΔR, was calculated. A prediction capability index (in percent), referred to as the P-value, was found by dividing the difference, ΔR, by the total measured runout (actual distance on the ground surface). Table 6.1 is a compilation of the pertinent model parameters used in Test 1. Note that the final runout segment slope angle for the Nozzle avalanche was -3.3° but a value of 1.0° was used in defining the frictional parameter μ. This alteration is justified considering that the distal portion of the avalanche only climbed a short distance on the opposite side of the river and a much greater portion of debris had spread laterally upon entering the valley.

Most of the predictions of runout distance presented in Table 6.1 for Damocles, U-Turn, Nozzle and Rockslide Pass were less than the observed distances. North and South Twin showed rather conservative predictions; P-values were greater than zero. The best choice of the dynamic parameter D was 14,000 m^2/s^2, for which the absolute mean P-value for the six events was 14.7%. The absolute mean P-value of 17.1% was only slightly worse for D = 20,000 m^2/s^2, while for D = 7,000 m^2/s^2 the mean P-value was 26.7%. Further refinement of the choice of the D parameter produces only a marginal improvement in the predictive capability of this test.

In Test 2, the sliding block model was evaluated, using entirely frictional energy losses (μ = FMAX, D = ∞). In this case the average value of the equivalent coefficients of friction (0.173) from each of the six avalanches was used as the test μ parameter. The results of the test are listed in Table 6.2. Very conservative estimates of runout are predicted for the U-Turn, and the North and the South Twin avalanches - P-values of 29.4%, 48.7% and 25.8%, respectively. On the other hand, runout estimations at the Damocles and Nozzle avalanches are greatly underestimated; calculated P-values were -45.9% and -27.2%, respectively. Only at the Rockslide Pass avalanche does the mean *fahrboeschung* yield a reasonable prediction - the simulation gives a runout distance less than one percent in error. The absolute mean P-value for Test 2 is 29.6%, which is

TABLE 6.1 Prediction Capability Test 1 for $\mu = \tan(\text{ANG(N)} + 1.0°)$

Event	N	S(N) (m)	ANG(N) (degrees)	μ	D (m^2/s^2)	R (m)	P-value (percent)
Damocles	19	681	3.0	0.0699	20000	+209	+4.6
				0.0699	14000	-157	-3.5
				0.0699	7000	-452	-10.0
North Twin	27	138	4.0	0.0875	20000	+1431	+30.7
				0.0875	14000	+802	+20.5
				0.0875	7000	+145	+3.7
South Twin	23	375	4.2	0.0910	20000	+884	+20.0
				0.0910	14000	+266	+6.8
				0.0910	7000	-335	-8.6
U-Turn	19	110	10.0	0.1940	20000	-1718	-42.5
				0.1940	14000	-1850	-47.4
				0.1940	7000	-2616	-67.0
Nozzle	17	175	1.0*	0.0349	20000	-11	-0.2
				0.0349	14000	-135	-1.9
				0.0349	7000	-441	-6.1
Rockslide Pass	15	550	0.5	0.0262	20000	-327	-4.6
				0.0262	14000	-684	-9.6
				0.0262	7000	-4602	-64.6

* Substituted for actual ANG(N) = -3.3°

TABLE 6.2 Summary of P-values (percent) for Prediction Capability Tests 1, 2 and 3

			TEST 1			TEST 2	TEST 3							
			$\mu = \tan(\beta_N + 1.0°)$			$\mu = (FMAX)_{aver}$	$\mu = \tan(\alpha)$							
			a	b	c		a	b	c	d	e	f	g	h
Event	α	D (m^2/s^2)	7000	14000	20000	∞	7000	14000	20000	30000	40000	45000	50000	60000
Damocles	5.0°		-10.0	-3.5	+4.6	-45.9	-14.9	-14.2	-10.5	-2.3	+5.9	+9.5	+13.4	+20.0
North Twin	10.0°		+3.7	+20.5	+30.7	+48.7	-26.8	-12.5	-9.4	-3.9	+0.2	-2.0	+3.8	+7.0
South Twin	9.0°		-8.6	+6.8	+20.00	+25.8	-26.5	-21.3	-17.5	-9.7	-4.0	-1.8	+0.5	+4.3
U-turn	8.0°		-47.4	-92.5	+29.4	-38.6	-21.3	-8.0	+14.6	+19.2	+19.2	+20.4	+23.2	+23.8
Nozzle	4.5°		-6.1	-0.2	-0.15	-27.2	-57.2	-15.1	-10.5	-7.6	-3.8	-2.2	-0.9	+1.0
Rockslide Pass	3.0°		-64.6	-9.6	-4.6	-0.7	-68.0	-28.2	-24.5	-15.9	-6.3	-2.6	+1.6	+10.7
Absolute Mean			26.7	14.7	17.1	29.6	38.7	18.8	13.4	9.0	6.6	6.4	7.2	11.1

certainly less favourable than the prediction capability of the best (μ,D) pair of Test 1.

Since more reasonable predictions were achieved with use of a frictional parameter only slightly greater than the tangent of the final slope angle and an almost arbitrarily chosen D value, it was felt that perhaps an improved, less empirical method for choosing μ could give a better predictive capability. What characteristic slope angle from the initial slide surface or potential avalanche profile might be a better choice for the determination of a frictional parameter?

A new slope measurement, to be referred to as the α angle, was defined for this purpose. The α angle is the inclination of the line joining the most distal tip of the avalanche and the point on the travel path at which total disintegration is deemed to have occurred. In the case of Nozzle and Rockslide Pass this point would be at the outer boundary of the ramp feature, while at the Twin slides for instance, this point would be at the base of the bedrock ridge which split the original mass into separate avalanches. Obviously some discretion is required in the choice of these two points. However, for most examples, a reasonable estimate of the most distant point from a primative prediction of runout using a mean *fahrboeschung* will produce adequate results. This is because the distal portions of most of the rock avalanches from the Mackenzies often occupy glaciated valleys sloping at shallow angles (1°

to 5°) for relatively long distances. Consequently an error in the initial runout prediction is not of great concern, since the model predicted runout will commonly give the same α angle as used previously. Alternatively an iterative procedure could be used to converge on the optimal α angle, although, this was not found to be necessary for the six examples examined in this study. The measured α angles for these avalanches are found in Table 6.2.

In Test 3, the predictive capability of the model for a frictional parameter equal to the tangent of the α angle and a range of dynamic parameters from 7,000 to 60,000 m^2/s^2, was assessed. The calculated P-values for these simulations are contained in Table 6.2. The tabulated absolute mean P-values show the best choice of a dynamic parameter is between 40,000 and 50,000 m^2/s^2, where the predicted runout is only 6.6% and 7.2% in error, respectively. For illustrative purposes the P-values are plotted versus the dynamic parameter in Figure 6.8.

In order to optimize the choice of the dynamic parameter, the D axis intercepts from this plot were averaged. The mean value of 41,400 m^2/s^2 was obtained using all six events. However, because the U-Turn avalanche was felt to be a rather exceptional case with several abrupt directional changes, it might be more reasonable not to include this event in the calculation of the optimal D value. When this was done, a mean value of almost 45,000 m^2/s^2 was obtained.

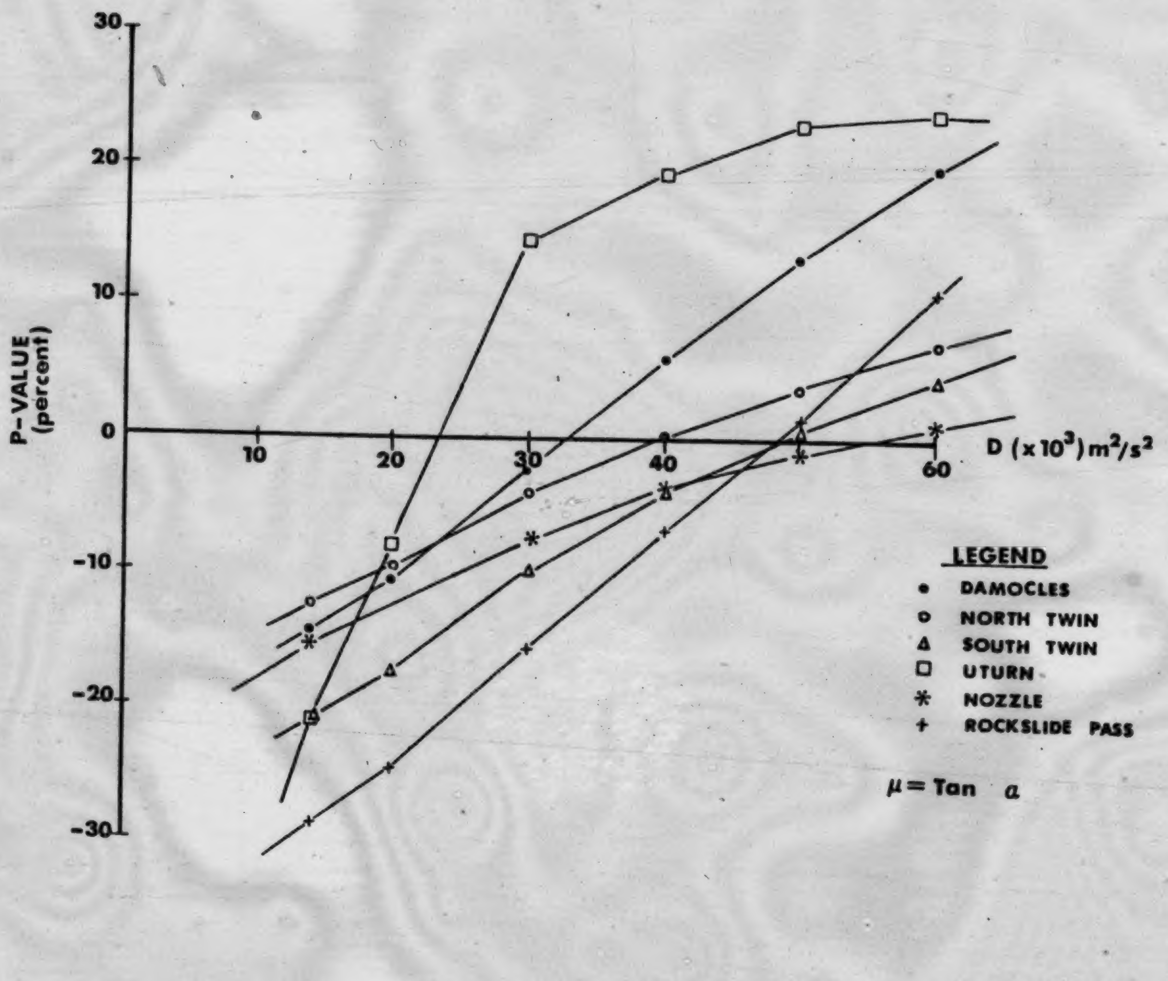

Figure 6.8 Plot of P-value versus Dynamic Parameter D for Test 3.

When this resistance pair ($\mu = \tan \alpha$, $D = 45{,}000\ m^2/s^2$) was tested on the six avalanches, including U-Turn, an absolute mean P-value of 6.4% was obtained (Test 3f). Both the Damocles and U-Turn runouts were over-estimated at +9.5% and +20.4%, respectively, while the other predictions were all less than 3% in error. The absolute mean P-value, not including the exceptional U-Turn avalanche, was 3.6%. This represents a substantial improvement over the previous model predictions of Tests 1 and 2.

By way of comparison, the predictive capabilities of several resistance pairs from the three tests are shown in bar graph form on Figure 6.9. This diagram distinguishes the more random nature of the runout predictions based on the assumptions used in Tests 1 and 2. A plot of the absolute mean P-values for the six avalanches clearly shows the best resistance pairs suitable for prediction purposes in the Mackenzie Mountains.

The velocities predicted with the optimal (μ,D) pair are usually closer to the upper limit of velocities as predicted with the *fahrboeschung*. While it may be doubtful that the sliding block model is the best choice for velocity prediction, it may nonetheless, offer the best runout prediction tool. For comparison purposes the range of the optimal (μ,D) pairs is shown on Figure 6.1.

It is worthwhile pointing out at this point, that using the model in a predictive fashion with a simple uplift pressure assumption, as done in Figure 6.2 for instance,

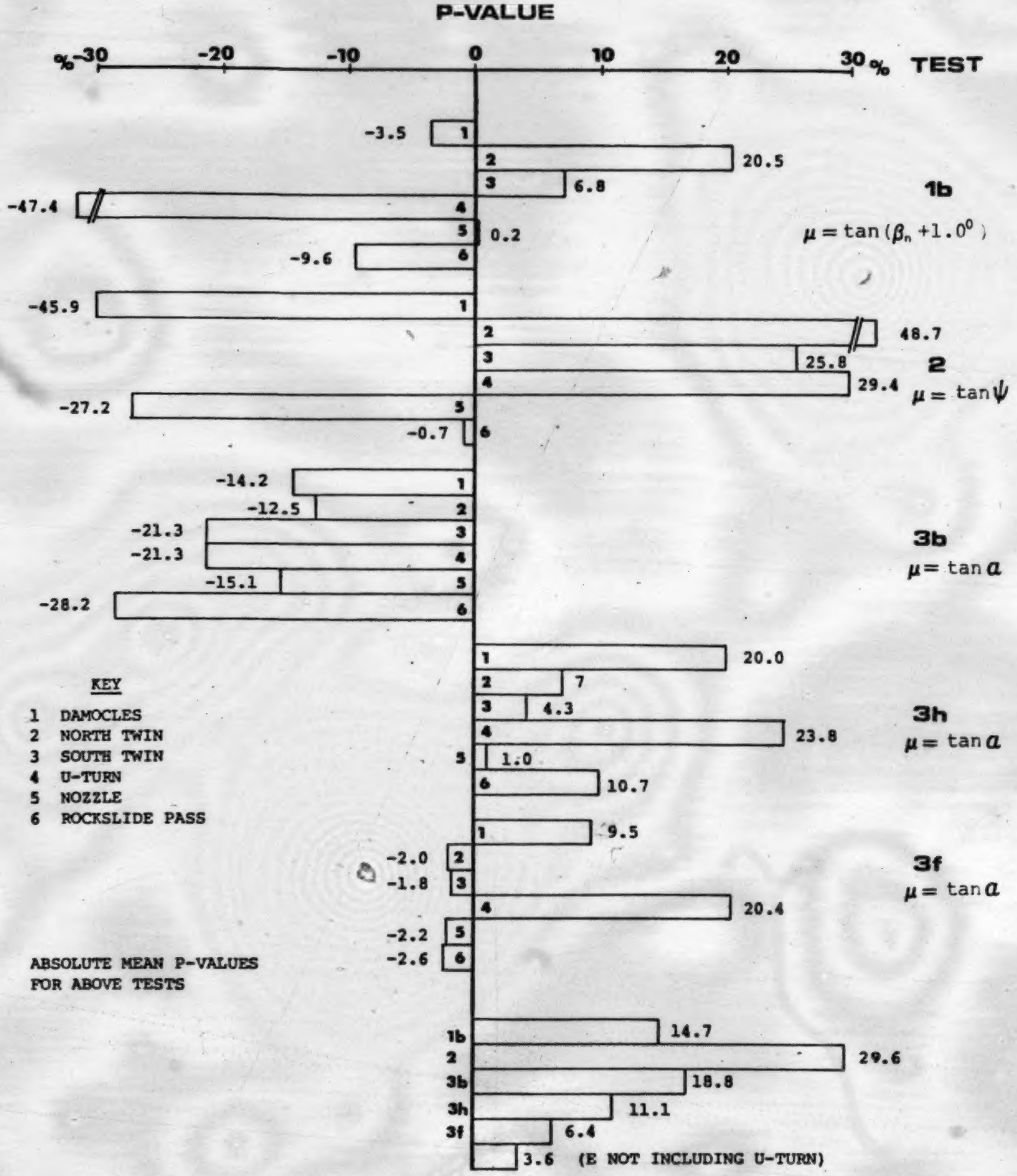

Figure 6.9 Bar graph of P-values for various prediction capability tests.

would yield almost identical results. Alternatively, the model could be used with r values in excess or less than the value needed to reduce a normal coefficient of friction (e.g., tan 32°) to the observed maximum frictional coefficient (FMAX). The input of a third parameter without a basis for predicting its value, would unnecessarily complicate an already indeterminate system of equations. Consequently, development of the uplift or pore pressure postulate was not pursued.

In conclusion, the aforementioned procedure has been used to satisfactorily refine the choice of resistance parameters for prediction purposes in the Mackenzie Mountains. While previous efforts to match a limited number of superelevation and run-up derived velocities to the model predictions have not proved very successful, the semi-empirical basis suggested here for choosing μ and D, does offer the most reasonable method to date for predicting rock avalanche runout distance. Nevertheless, the method should not be construed as the best manner for modelling actual, more complex avalanche motion. Velocity predictions with these parameters are probably in excess of the real velocities over most of an avalanche travel path.

Extension of this type of treatment to rock avalanches and other mass movements from around world should be done in a cautious manner. The optimization of the prediction capabilities for this suite of movements in the Mackenzie Mountains does not imply that the method is directly applicable elsewhere, although the hypothesis does merit examination.

6.6 Summary and Conclusions

The highlights from each section in this chapter are summarized as follows:

1. The characteristic resistance relationships for six Mackenzie Mountains rock avalanches (assuming single events) were determined with Program RADA. There was not a unique relationship, even over a limited range of (μ,D) resistance pairs, which would adequately model the avalanche runout for the entire group. Even the North and South Twin avalanches display different characteristic resistance relationships, despite having a common origin and nearly identical travel paths. The application of a common uplift pressure assumption produces a great change in the (μ, D) relationships for the six avalanches, although there is little or no difference in their respective predicted velocity profiles. There is some indication that the less confined rock avalanches may have a separatable range of relevant (μ, D) pairs capable of matching the avalanche runout. Even if a common characteristic resistance relationship was found the choice of the best velocity-matching (μ, D) pair would be most difficult; an infinite number of pairs will reproduce

the given runout distance.

2. Velocity profiles for the Mackenzie Mountains rock avalanches were predicted using a range of (μ, D) pairs from their respective characteristic resistance relationships. The velocities predicted by superelevation and run-up analyses at the North Twin avalanche were compared with the predictions from Koerner's two-parameter model. Generally, the model simulation was not in very good agreement with the velocity range indicated by simple energy considerations; a range of frictional and dynamic resistance parameters is capable of matching these velocities over various parts of the avalanche travel path. These inconsistencies stem mainly from the inability of the model to precisely match the actual movement of the mobile rock mass. Invoking an initial velocity assumption, or the use of a simple average uplift pressure assumption do not produce any more enlightening results; a very similar range of velocities is predicted by the model. Until a more complete record of the velocity spectrum in a rock avalanche is obtained, the choice of the appropriate resistance parameters to use in such a model, will remain difficult.

3. In order to assess whether the proposed model is

capable of separating rock avalanche behavior on the basis of unique material character or geometric configuration, a series of hypotheses was tested. Entire travel path profiles for a group of rock avalanches and other mass movements, largely from outside the Mackenzies, were analysed with the model.

It was postulated that the characteristic resistance relationships for these rapid mass movements might reflect one or more of the following effects: (1) material and or fluid entrainment;(2) reduced frictional resistance for rock avalanches on to snow or ice;(3) differences in rock lithology and respective mechanical properties;(4) geometric confinement.

For all cases, with the possible exception of the last effect, the hypotheses were rejected. Delineation of the best estimate of the (μ, D) pair capable of matching the observed average travel velocity for these events, similarly does not reveal a consistent relationship for the above hypotheses. It is not impossible, however, that further exploration of this topic with a larger sample of rock avalanches might reveal less obvious trends.

4. To assess the predictive capability of the proposed model a series of tests was performed on the entire travel path profiles from six Mackenzie Mountains rock avalanches. Evaluation of the characteristic

resistance relationships for these events (section 6.2) and comparison with other rock avalanches, has shown that the most reasonable frictional and dynamic parameters may range from -0.70 to 0.145 and from 5,000 to 30,000 m^2/s^2, respectively. To more narrowly define the optimal resistance pairs relevant for a dynamic analysis a series of tests was conducted using three variations on the choice of the frictional resistance parameter. The best velocity matching μ parameter typically was found to be slightly greater than the tangent of the minimum and very often the final runout slope inclination (β_n). Consequently for Test 1 $\mu = \tan(\beta_n + 1.0°)$. In Test 2 the maximum allowable frictional parameter without uplift pressures was used, μ(max) = *fahrboeschung*. For Test 3, an empirical angle measurement equal to the inclination of the average runout slope (or slope of streaming) was defined and termed the α angle. The frictional parameter used was $\mu = \tan \alpha$.

A parametric study of the runout prediction capablity of the model using these resistance parameters has shown that the best prediction for the group of six avalanches is found using $\mu = \tan \alpha$, and D = 41,400 m^2/s^2. On average there is a 6.4% error in the prediction of actual runout distance for this choice of parameters. Eliminating the extraordinary U-Turn avalanche because of its numerous changes in travel path and high run-up energy losses, increases D to 45,000 m^2/s^2 and results in an average prediction error of 3.6%. This compares most favourably with the Test 1 hypothesis prediction error of 14.7%, or Test 2 - using the *fahrboeschung* - which gives an average prediction error of 29.6%. While the method used in Test 3 is preferable for runout prediction it should be noted that it normally overpredicts velocities.

7. CONCLUSIONS AND RECOMMENDATIONS

7.1 Introduction

The topic of rock avalanche dynamics has been the subject of numerous inquiries, both observational and analytical, by geologists, geomorphologists, physicists and engineers. Recently, a number of papers (Davies, 1982; Hungr, 1981; Koerner, 1980b; Erismann, 1979, Hardy *et al.*, 1978) have reviewed parts of the literature on the mechanical treatment of the phenomena and have attempted to resolve the most enigmatic aspect of the topic - the explanation for the observed mobility enhancement which enables large, blocky rock to travel great distances beyond that expected for a normal frictional material. The above authors do not appear to agree on any one particular agent to explain this phenomenon. While this study is not intended as a critical review of these hypotheses some review and evaluation is a prerequisite for an investigation of this nature. Accordingly therefore, a portion of this thesis has attempted to assimilate previous field and analytical experience into a rational yet simplistic model for rock avalanches.

In summary this study has:

1. Examined the physical environment, the geology, and various morphological and mechanical aspects of a group of rock avalanches from the Mackenzie Mountains.
2. Assessed possible failure mechanisms for some of these

events,

3. Briefly reviewed the literature of rock avalanche dynamics,
4. Evaluated velocity information and analysed the North Twin rock avalanche with superelevation, projectile, and run-up data,
5. Summarized the morphological character of the avalanche debris from field evidence,
6. Evaluated, modified and applied Koerner's (1976) model in a parametric study,
7. Analysed a suite of Mackenzie Mountains rock avalanches and other mass movements with the model in an effort to explain the apparent mobility enhancement, and
8. Devised an empirical technique to predict runout distance with the model.

Summaries and specific conclusions may be found at the end of each chapter and only the major findings and original contributions that have resulted from this study are recapitulated in the following section.

7.2 Conclusions

1. Six rock avalanches from the Mackenzie Mountains of the Yukon and Northwest Territories display excessive runout distances beyond which would be expected for normal frictional materials. These large mass movements with volumes ranging from 8 to 370 x 10^6 m^3 have travelled from 3.9 to 7.1 km on average slopes

ranging from 7.5° to 12.3°. The host rock type for these major movements is typically a very competent dolomite or limestone, although the movements are not confined to any one particular formation. Unique features such as lateral spray areas, boulder sorting, superelevation and run-up of debris, rarefaction zones, proximal ramps, transverse, longitudinal and en-echelon ridges, and stratigraphic congruence were observed in the rock avalanche debris. A satisfactory explanation for the initial failure mechanism at a number of these landslides is deemed to be an insoluable problem at this time given that the initial boundary conditions and the geometry of the failure masses are unknown. Field evidence suggests that the initial motion probably consisted of elements of sliding, rolling and toppling. The roller bearing friction concept is deemed to be an inadequate model for predicting initial velocities.

2. From a review of the literature it is concluded that, while there is a plethora of proposed models for rock avalanche motion, the empirical or semi-empirical approaches offer the best techniques for velocity and or runout prediction at this time.

3. Superelevation data from the Twin rock avalanches were analysed and suggest an upper bound (subcritical)

velocity range of between 16 and 50 m/s and a lower bound (supercritical) range of between 12 and 35 m/s for various measured cross-profiles. Run-up data would suggest a minimum velocities between 44 and 50 m/s for the distal portion of the South Twin avalanche. A simplified inquiry into the spray feature at the Nozzle rock avalanche has shown that the minimum projectile velocities necessary to produce the observed feature would be between 95 and 118 m/s.

4. A re-evaluation of the volumes of the pre-movement masses from the six rock avalanches has been shown not to alter significantly the volume-runout type relationship as proposed by Eisbacher (1979).

5. On the basis of field observations and air-photo interpretation there appears to be a morphological and a mechanical basis for separating confined and unconfined rock avalanches.

6. Koerner's (1976) model for rock avalanches has been modified to handle uplift pressures and initial velocity assumptions. These two variations have been shown to produce significant changes in the relevant resistance parameters capable of matching a given runout distance.

7. The dynamic (velocity squared dependence) and frictional (velocity independent) resistance terms in the equation of motion have been related in a function termed the "characteristic resistance relationship". Consideration of the range of relevant average velocities for a given avalanche may reduce the choice of resistance pairs for analysis.

8. An evaluation of the characteristic resistance relationships for six Mackenzie Mountains rock avalanches, assuming single events, does not reveal a significantly similar choice of resistance parameters with or without uplift pressure assumptions. There does appear to be some basis for the separation of confined and unconfined rock avalanches on this plot.

9. A model predicted velocity profile for various resistance pairs for the North Twin rock avalanche does not match the superelevation and run-up predicted velocities particularily well. This is thought to be primarily due to the changing frictional and dynamic reistances throughout the avalanche as a consequence of variations of the mode of motion, i.e., sliding, rolling, laminar or turbulent flow regimes are possible over certain portions of the travel path.

10. An application of the model to other mass movements has

not revealed a ubiquitous link to explain the observed enhanced mobility. Material or fluid entrainment, travel over snow or ice, rock lithology and properties, and geometric configuration were examined with cases from the literature. However, there does not appear to be a systematic order to the model parameters derived for these rock avalanches.

11. To assess the predictive capability of the proposed model a series of tests was performed on the travel profiles from six Mackenzie Mountains rock avalanches. Evaluation of the characteristic resistance relationships for these events has shown that the most reasonable frictional and dynamic parameters (for predicting velocities) range from -0.70 to 0.145 and from 5,000 to 30,000 m^2/s^2, respectively. A number of empirically derived variations on the frictional parameter were used to evaluate an optimum resistance pair for these avalanches. Velocity prediction is best done by using $D = 14,000\ m^2/s^2$ and $\mu = \tan(\mathrm{FMIN} + 1.0°)$. By assuming that the frictional parameter μ is equal to the tangent of an easily derived angle, called the a angle, it was found that the best runout prediction for the six events (average error of 6.4%) could be acheived with $D = 41,400\ m^2/s^2$. Elimination of the U-Turn avalanche because of its frequent changes in travel path results in an average prediction error

of only 3.6%. This compares most favourably with other methods such as using an average *fahrboeschung* which would give an prediction error of 24.6%.

7.3 Recommendations for Further Research

Several relatively unexplored facets of the rock avalanche phenomenon have been briefly addressed in this study. These areas of possible future research merit may be broadly classified into three groups: geological studies, inquiries into the initial movement mechanisms, and the modelling of rock avalanche dynamics. Recommendations for future research from each of these groups are now discussed.

Geological Studies Detailed mapping of the surficial and bedrock geology and the rock avalanche debris at each of the landslides described by Eisbacher (1979) would greatly enhance our understanding of the avalanche process and perhaps shed further light on the elusive answer to the mobility problem. A systematic attempt to date these landslides would be of considerable value in assessing the present threat from rock avalanches in the Mackenzie Mountains. This could be done by palynology, lichenometry or radiocarbon dating methods for instance. A more thorough mapping of the fabric and boulder orientations, particularily in relation to the original stratigraphy, could prove most useful in characterizing the mode of movement in a rock avalanche. Finally, a concerted effort could be made to locate and analyse the basal portion of one of these rock avalanches.

It also became apparent during the course of this study that an orderly classification of rock slope movements, with rockslides and rock avalanches as end members of a continuum would be most useful as a basis for future studies. In particular, a standardized nomenclature for the morphological features associated with these movements would be of value.

Initial Movement Mechanisms Circumstantial evidence from a number of movements described here would suggest that seismic accelerations could have played a major role in initiating the first movements of these slopes. Further work to simulate the mechanics of these movements, such as physical or analytical modelling, would go a long way towards quantifying the effects of earthquakes on rock slopes. Furthermore, better estimates of the initial velocities of these dry, blocky rock debris masses could be attained.

Rock Avalanche Dynamics Hungr (1981) favoured the acoustic fluidization process as a possible explanation for mobility enhancement. Analytical or physical model studies to more fully explore this concept and their application to seismically vibrated rock debris masses are recommended. Model studies of such poorly defined effects as lateral spreading, channeling and momentum transfer would also be of value. Similarly further reearch on the potential for pore pressure generation and maintenance is suggested.

In terms of Koerner's (1976) model, some initial attempts to scale the resistance parameters (e.g., Bakkehoi *et al.*,1981) by other variables such as volume have shown to be promising. Further exploration of this approach to refine the (μ,D) parameter choice is recommended. The determination of the proper travel path for analysis and a comparison of different methods as done for the Frank Slide in Chapter 5, would determine whether the centre of mass or the entire travel path is more appropriate for prediction purposes. Finally, further work in defining the relevant resistance parameters for rock avalanches from different surroundings might reveal common trends not identified in this research.

REFERENCES

Aitken, J.D., Cook, D.G., and Yorath, C.J. 1982. Upper Ramparts River (106G) and San Sault Rapids (106H) map areas, District of Mackenzie. Geol. Surv. Canada. Memoir 338.

Aitken, J.D. 1972. Mackenzie Arc - The cordilleran structural province, *In* Variations in Tectonic Styles in Canada, editors R.A. Price and R.J.W. Douglas, Geological Association of Canada, Special Paper No. 11, pp. 37-41.

Aitken, J.D.and Cook, D.G. 1974. Geological maps, northern parts of Mt. Eduni and Bonnet Plume Lake map areas, District of Mackenzie. Geol. Surv. Canada, Open File 221.

Anderson, F.W. 1979. The Frank Slide Story. Frontier Publishing Ltd., Calgary, 58 p.

Bagnold, R.A. 1954. Experiments on a gravity-free dispersion of large solid spheres in a Newtonian fluid under shear. Royal Soc. London Proc., Ser. A, Vol. 225, pp. 49-63.

Bagnold, R.A. 1968. Deposition in the process of hydraulic transport. Sedimentology, Vol. 10, pp. 45-56.

Bakkehoi, T., Cheng, T., Domaas, U., Lied, K., Perla, R., and Schieldrop, B. 1981. On the computation of parameters that model snow avalanche motion, Can. Geot. J., Vol. 18, pp. 121-130.

Barkan, D.D., 1962. Dynamics of Bases and Foundations. McGraw Hill, New York, 434 p.

Basham, P.W., Forsyth, D.A. and Wetmiller, R.J. 1977. The seismicity of northern Canada. Can. J. Earth Sci., Vol. 14, pp. 1646-1667.

Bates, R.L. and Jackson, J.A. 1980. Glossary of Geology, 2nd edition, American Geological Institute. Virginia, 751 p.

Bishop, A.W., 1973. Stability of tips and spoil heaps. Quart. Journ. Eng. Geol., Vol. 6, pp. 335-376.

Blusson, S.L. 1974. Five geological maps, northern Selwyn Basin, Yukon Territory and District of Mackenzie. Geol. Surv. Canada, Open File 205.

Bostock, H.S. 1970. Physiographic subdivisions of Canada.

In Geology and Economic Mineral of Canada, R.J.W. Douglas ed., Geol. Surv. Can., Economic Geology Report. 9-30, with Map 1254A.

Brown, R.L. and Richards, J.C. 1970. Principles of Powder Mechanics. Permagon Press, Oxford, 223 p.

Bull, W.B. 1964b. Geomorphology of segmented alluvial fans in western Fresno County, California, U.S. Geol. Surv. Profess. Paper 352E, pp. 89-129.

Burns, B.M. 1973. The climate of the Mackenzie Valley - Beaufort Sea, Vol. 1, Environment Canada, Atmosph. Environ. Climatological Studies, No. 24.

Buss, E. and Heim, A. 1881. Der Bergsturz von Elm. Worster, Zurich, 133p.

Calkin, P.E. and Ellis, J.M. 1980. A lichenometric dating curve and its application to Holocene glacier studies in the Central Brooks Range, Alaska. Arctic and Alpine Research, Vol. 12, pp. 245-264.

Casagrande, A. 1936. Characteristics of cohesionless soils affecting the stability of slopes and earth fills. Contributions to Soil Mechanics, 1925-1940. Boston Soc. of Civil Engineers.

Castro, G. 1969. Liquefaction of Sands. Harvard Soil Mechanics Series, No. 81, Cambridge, Mass., 26 p.

Clague, J.J. and Souther, J.G. 1982. The Dusty Creek landslide on Mount Cayley, British Columbia. Can. J. Earth Sci., Vol. 19, pp. 524-539.

Cluff, L.S. 1971. Peru Earthquake of May 31, 1970, Engineering geology observations. Bulletin of the Seismological Society of America, Vol. 61, No. 3, pp. 511-533.

Cowan, S.C. 1978. Micro structural continuum models for granular materials. Proceedings of the U.S.-Japan Seminar on Continuum Mechanical and Statistical Approaches in the Mechanics of Granular Materials, (Cowan, S.C. and Satake, M., eds.), Gakujutsu Bunken Fukyu-kai, Tokyo. 1978, pp. 162-170.

Crawford, A.M. and Curran, J.H. 1981. The influence of shear velocity on the frictional resistance of rock discontinuities. Int. J. Rock Mech. Min. Sci. & Geomech. Abstr., Vol. 18, pp. 505-515.

Cruden, D.M. 1975. The influence of discontinuities on the stability of rock slopes. Proc. 4th Guelph Symposium on Geomorphology on Mass Wasting, pp. 107-117.

Cruden, D.M. 1976. Major rockslides in the Rockies. Can. Geot. J., Vol. 13, pp. 8-20.

Cruden, D.M. and Krahn, J. 1978. Frank Rockslide, Alberta, Canada. *In* Rockslides and Avalanches, Vol. 1, (ed. Voight, B.) Elsevier, New York, pp. 97-112.

Cruden, D.M. 1980. The anatomy of landslides. Can. Geot. J., Vol. 17, pp. 295-300.

Cruden, D.M. 1982. The Brazeau Lake Slide, Jasper National Park, Alberta. Can. J. Earth Sci., Vol. 19, pp. 1011-1024.

Cundall, P. 1974. Rational design of tunnel supports, a computer model for rock mass behaviour using interactive graphics for input and output of data. U.S. Army Corps of Engineers, Tech. Rep., MRD-2-74.

Cundall, P.A. 1976. Computer interactive graphics and the Distinct Element Method. *In* Rock Engineering for Foundations and Slopes, ASCE Conf., Boulder, Colo., Vol. 2, pp. 193-199.

Curry, R.R. 1966. Observation of Alpine mudflows in the Tenmile Range, central Colorado. Geol. Soc. America Bull., Vol. 77, pp. 771-776.

Daly, R.A., Miller, W.G., and Rice, E.S. 1912. Report of the commission appointed to investigate Turtle Mountain, Frank, Alberta. Geol. Surv. Can. Memoir 27, 34 p.

Dahlstrom, C.D.A. 1970. Structural geology in the eastern margin of the Canadian Rocky Mountains. Bull. Can. Pet. Geol., Vol. 18, pp. 332-406.

Davies, T.R.H. 1982. Spreading of rock avalanche debris by mechanical fluidization. Rock Mechanics, Vol. 15, pp. 9-24.

De Freitas, M.H. and Watters, R.J. 1973. Some field examples of toppling failure. Geotechnique, Vol. 23, No. 4, pp. 495-514.

Erismann, T.H. 1979. Mechanisms of large landslides. Rock Mechanics, Vol. 12, pp. 15-46.

Eisbacher, G.H. 1977. Rockslides in the Mackenzie Mountains, District of Mackenzie. Report of Activities, Part A, Geol. Surv. Can., Paper 77-1A, pp. 235-241.

Eisbacher, G.H. 1978. Observations on the streaming mechanism of large rock slides, northern cordillera. Current Research, Part A, Geol. Surv. Can., Paper 78-1A, pp. 49-52.

Eisbacher, G.H. 1979. Cliff collapse and rock avalanches (*sturzstroms*) in the Mackenzie Mountains, northwestern Canada. Can. Geot. J., Vol. 16, pp. 309-334.

Eisbacher, G.H. 1980. Cliff collapse and rock avalanches (*sturzstroms*) in the Mackenzie Mountains, northwestern Canada: Reply. Can. Geotech. J., Vol. 17, pp. 151-152.

Fahnestock, R.K. 1978. Little Tahoma Peak rockfalls and avalanches, Mount Rainer, Washington, U.S.A. *In* Rockslides and Avalanches, Voight, B., editor, Elsevier, Vol. 1, pp. 181-196.

Ford, D.C. 1976. Evidences of multiple glaciation in South Nahanni National Park, Mackenzie Mountains, Northwest Territories. Can. J. Earth Sci., Vol. 13, pp. 1433-1445.

Gabrielse, H., Blusson, S.L. and Roddick, J.A. 1973. Geology of Flat River, Glacier Lake and Wrigley Lake Map Areas, District of Mackenzie and Yukon Territory. Geol. Surv. Canada Memoir 366, 153 p.

Gabrielse, H., Tempelman-Kluit, D.J. Blusson, S.L. and Campbell, R. 1980. MacMillan River - Sheets 105 and 115, Map 1398A, Geol. Surv. Canada.

Gerber, E. and Scheidegger, A.E. 1969. Stress-induced weathering of rock masses. Ecolgae Geol. Helv., pp. 401-416.

Goguel, J. 1978. Scale-dependent rockslide mechanisms, with emphasis on the role of pore fluid vaporization, *In* Rockslides and Avalanches, Voight, B., editor, Elsevier, Vol. 1, pp. 693-706.

Goodman, M.A. and Cowin, S.C. 1971/1972. A continuum theory for granular materials. Arch. Rat. Mech. Anal., Vol. 44, pp. 249-266.

Goodman, R.E. and Bray, J.W. 1976. Toppling of rock slopes. Proc. Speciality Conference on Rock Engineering for Foundations and Slopes. Boulder, Colorado, ASCE, Vol. 2, pp. 201-234.

Gordon, J.E., Birnie, R.V. and Timmis, R. 1978. A major rockfall and debris slide on the Lyell Glacier, South

Georgia. Arctic and Alpine Research, Vol. 10, No. 1, pp. 49-60.

Gray, J.T. 1973. Geomorphic effects of avalanches and rock-falls on steep mountain slopes in the central Yukon Territory.*In* Research in Polar and Alpine Geomorphology, 3rd Guelph Symposium on Geomorphology , pp. 107-117.

Griggs, R.F. 1922. The Mageik Landslide. *In* The Valley of Ten Thousand Smokes. National Geographic Society, pp. 135-147.

Habib, P. 1975. Production of gaseous pore pressure during rock slides. Rock Mechanics, Vol. 7, pp. 193-197.

Hadley, J.B. 1964. Landslides and related phenomena accompanying the Hebgen Lake earthquake of August 17, 1959. U.S.G.S. Professional Paper 435, pp. 107-135.

Hammett, R.D., 1974. A study of the deformation of a discontinuous rock mass. Ph.D. thesis, James Cook Univ. of North Queensland, Australia, 237 p.

Heim, A. 1932. Bergsturz und Menchenleben. Zurich, Vierteljahrsschrift 77, No. 20, Beiblatt, 218 p.

Heimgartner, M. 1977. On the flow of avalanching snow. J. Glaciology, Vol. 19, pp. 357-363.

Hardy, R.M., Morgenstern, N.R. and Patton, F.D. 1978. The Garibaldi Advisory Panel Report. Dept. of Highways, Prov. Government of British Columbia, Vol. 1, 2 and 3.

Hoek, E. and Bray, J. 1977. Rock Slope Engineering. (2nd ed.), Institute of Mining and Metallurgy, London, 402 p.

Howard, K. 1973. Avalanche mode of motion: implications from lunar examples. Science, Vol. 180, pp. 1052-1055.

Hsu, K.J. 1975. Catastropic debris streams. (Sturzstroms) generated by rockfalls. Geol. Soc. America Bull., Vol. 86, pp. 129-140.

Hughes, O.L., Campbell, R.B., Muller, J.E. and Wheeler, J.O. 1969. Glacial limits and flow patterns, Yukon Territory, south of 65 degrees North Latitude. Geol. Surv. Canada, Paper 68-34.

Hughes, O.L. 1972. Surficial geology of northern Yukon Territory and northwestern district of Mackenzie, Northwest Territories, Geol. Surv. Canada, Paper 69-36, 11 p.

Hughes, O.L., Veillette, J.J., Pilion, J. and Hanley, P.T. 1973. Terrain evaluation with respect to pipeline construction, Mackenzie transportation corridor, central part, Lat. 64° to 68°N. Task Force on Northern Oil Development, Report No. 73-37, Information Canada.

Hungr, O. 1981. Dynamics of Rock Avalanches and other types of Slope Movements. Ph.D. thesis, Dept. of Civil Engineering, University of Alberta, 506 p.

Johnson, A.M. 1970. Physical Processes in Geology. Freeman-Cooper, San Francisco, 577 p.

Johnson, B. 1978. Blackhawk landslide, California, U.S.A. *In* Rockslides and Avalanches,Vol. 1, editor Voight, B., Elsevier, New York, pp. 481-504.

Kaiser, P. and Simmons, J. 1980. Unpublished field observations from Twin, Avalanche Lake and Damocles rock avalanches, Mackenzie Mountains, Yukon and Northwest Territories.

Kellerhals, R. and Bray, D.I. 1971. Sampling procedures for coarse fluvial sediments. ASCE Journ. Hydraulics Div., Vol. 97, pp. 1165-1180.

Kelly, M. 1980. A prehistoric catastrophic rock avalanche at Holsteinsborg, West Greenland. Bull. Geol. Soc. Denmark, Vol. 28, pp. 73-79.

Kent, P.E. 1966. The transport mechanism in catastrophic rock falls. Journal of Geology, Vol. 74, pp. 79-83.

Kjartansson, G. 1967. The Steinsholtshlaup, Central-South Iceland on January 15th, 1967. Jokull 17 Ar., pp. 249-262.

Kojan, E. and Hutchinson, J.N. 1978. Mayunmarca rockslide and debris flow, Perv. *In* Rockslides and Avalanches, Voight, B., editor, Elsevier, New York, pp. 315-364.

Koerner, H.J. 1976. Reichweite und Geschwindigkeit von Bergstuerzen und Fliesschneelawinen. Rock Mechanics, Vol. 8, pp. 225-256.

Koerner, H.J. 1977. Flow mechanisms and resistances in the debris streams of rock slides. Bulletin of the International Association of Engineering Geology, No. 16, pp. 101-104.

Koerner, H.J. 1980a. The energy-line method in the mechanics of avalanches. Journal of Glaciology, Vol. 26, No. 94, pp. 501-505.

Koerner, H.J. 1980b. Modelle zur Berechnung der Bergsturz - und lawinenbewegung (Model conceptions for rock slide and avalanche movement) . Proceedings International Symposium Interpraevent 1980. Bad Ischf, Austria. Sept. 8-12,1980, Vol. 2, pp. 15-55.

Krahn, J. 1974. Rock Slope Stability with Emphasis on the Frank Slide. Ph.D. thesis, Dept. Civil Engineering, University of Alberta, 244 p.

Krahn, J. and Morgenstern, N.R. 1979. The ultimate frictional resistance of rock discontinuities. Int. J. Rock Mech. Min Sci. and Geomech. Abstr., Vol. 16, pp. 127-133.

Lang, T.E., Dawson, K.L., and Martinelli, M. 1979. Application of numerical transient fluid dynamics to snow avalanche flow. Part I. Development of computer program AVALNCH. Journal of Glaciology, Vol. 22, No. 86, pp. 107-115.

Leblanc, G. and Hasegawa, H.S. 1974. Earthquake data and design ground motions for the Yukon Territory and the Mackenzie Valley. Environmental-Social Committee, Northern Pipelines, Report No. 74-15, Information Canada.

Lied, K. and Bakkehoi, S. 1980. Empirical calculations of snow avalanche runout distance based on topographic parameters. Journal of Glaciology, Vol. 26, pp. 165-177.

Marangunic, C., 1972. Effects of a landslide on Sherman Glacier, Alaska. Ohio State Univ. Res. Found., Inst. Polar Studies Rep., No. 30.

Martinelli, M., Lang, T.E. and Mears, A.I. 1980. Calculations of avalanche friction coefficients from field data. Journal of Glaciology, Vol. 26, No. 94, pp. 109-119.

Marsh, L., Erismann, T., Heuberger, H., Preuss, E., and Schoecker, A. 1981. Frictional fusion on the gliding planes of two large landslides. Geological Hazards, Earth Movements, Section 17, Proc. 26th International Geological Congress, Paris. pp. 11-15.

McConnell, R.G. and Brock, R.W. 1904. Report on the great landslide at Frank, Alberta, Canada. Can. Dep. Inter., Annu. Rep., 1902-1903, Part B, 17 p.

McLellan, P.J. 1982. User's Manual - Program RADA, Rock Avalanche Dynamic Analysis. Dept. of Civil

Engineering, University of Alberta.

McLellan, P.J. and Kaiser, P.K. 1983. Two rock avalanches from the Mackenzie Mountains, N.W.T.. Abstract, Geological Association of Canada Annual Meeting, Victoria, B.C..

McSaveney, M.J. 1975. Sherman Glacier rock avalanche of 1964: its emplacement and subsequent effects. Ph.D. thesis, Ohio State University.

McSaveney, M.J., 1978. Sherman Glacier rock avalanche, Alaska, U.S.A. *In* Rockslides and Avalanches, Voight, B., Ed., Elsevier, Vol. 1, pp. 197-258.

McTigue, D.F. 1979. A non-linear continuum model for flowing granular materials, Ph.D. thesis, Stanford University, 176 p.

Melosh, J.H. 1979. Acoustic fluidization: A new geologic process? Journal of Geophysical Research, Vol. 84, pp. 7513-7520.

Middleton, G.V. 1970. Experimental studies related to problems of flysch sedimentation. *In* Flysch sedimentology in North America., Lajoie, J:,editor, Geological Association of Canada, Special Paper 7, pp. 253-272.

Mokievsky-Zubok, O., 1977. Glacier-caused slide near Pylon Peak, British Columbia. Can. J. Earth Sci., Vol. 14, pp. 2657-2662.

Mollard, J.D. 1977. Regional Landslide types in Canada. *In* Reviews in Engineering Geology, Vol. III, Coates, D.R., editor, Geol. Soc. America, pp. 29-56.

Monroe, R.L., 1973. Terrain maps, Mackenzie Valley, Upper Ramparts River 106G, San Sault Rapids 106H, Carajou Canyon 96D, Geol. Sur. Canada, Open File 132.

Moore, D.P. and Matthews, W.H. 1978. The Rubble Creek landslide, southwestern British Columbia. Can. J. Earth Sci., Vol. 15, pp. 1039-1052.

Moore, D.P. 1976. The Rubble Creek landslide, Garibaldi, British Columbia, M.A.Sc. thesis, Dept. of Geological Sciences, University of British Columbia, 84 p.

Morris, H.M. 1963. Applied Hydraulics in Engineering. Ronald Press, New York, 455 p.

Mueller, L. 1964. The Rock slide in the Vaiont Valley. Felsmechanik und Eng. Geol., Vol. 2, pp. 1489-2120.

Mueller, L., 1968. New considerations on the Vaiont slide. Rock Mech. & Eng. Geol., Vol. 6, No. 1-2, pp. 1-107.

Mudge, M.R. 1965. Rockfall-avalanche and rockslide-avalanche deposits at Sawtooth Ridge, Montana. Geol. Soc. Am. Bull., Vol. 76, pp. 1003-1014.

Nasmith, H.W. and Mercer, A.G. 1979. Design of dykes to protect against debris flows at Port Alice, British Columbia. Can Geotech. J., Vol. 16, pp. 748-757.

Norris, D.K. 1972. Geological map of the western part of the excursion area; Intern. Geol. Cong. 24th Sess., Field Excursion A/4 - Lower and Middle Paleozoic Sediments and Paleontology of Royal Creek and Peel River, Yukon, and Powell Creek, N.W.T., Lenz. A.C. and Pedder, A.E.H., editors, p. 39.

Norris, D.K. 1975. Geological maps, Hart River, Wind River and Snake River, Yukon and Northwest Territories. Geol. Surv. Canada, Open File 279.

Nye, J.F. 1952. The mechanics of glacier flow. J. Glaciology., Vol. 2, No. 12, pp. 82-93.

Oswald, E.T. and Senyk, J.P. 1977. Ecoregions of Yukon Territory. Fisheries and Environment Canada. 115 p.

Pariseau, W.G. and Voight, B. 1978. Rockslides and Avalanches: Basic principles, and perspectives in the realm of civil and mining operations. *In* Rockslides and Avalanches, Voight, B., editor, Vol. 2, pp. 1-92.

Pariseau, W.G. 1980. A simple mechanical model for rockslides and avalanches. Engineering Geology, Vol. 16, pp. 111-123.

Patton, F.D. 1976. The Devastation Glacier Slide, Pemberton, B.C., Abstract,Symp. on Geomorphology of the Canadian cordillera and its bearings on mineral deposits, Geol. Soc. Canada, Cordillera Sect., p. 26.

Pautre, A.F., Sabarly, F. and Schneider, B. 1974. L'effet d'echelle dans les ecroulements de falaise. Proc., 3rd Congress. ISRM, Denver, Vol. II-B, pp. 859-864.

Perla, R., Cheng, T.T. and McClung, D.M. 1980. A two-paramter model of snow-avalanche motion. Journal of Glaciology, Vol. 26, No. 94, pp. 197-207.

Plafker, G., Ericksen, G.E. and Concha, J.F. 1971. Geological aspects of the May 31, 1970, Peru earthquake. Bulletin of the Seismological Society of America, Vol. 61, No. 3, pp. 543-578.

Plafker, G. and Ericksen, G.E. 1978. Nevados Huascaran avalanches, Peru. *In* Rockslides and Avalanches. Voight, B., editor, Elsevier, Vol. 1, pp. 277-314.

Porter, S.C. and Orombelli, G. 1980. Catastrophic rockfall of September 12, 1717 on the Italian flank of the Mount Blanc massif. Z. Geomorph. N.F., Vol. 24, No. 2, pp. 200-218.

Poulos, S.J. 1981. The steady state of deformation. ASCE, Vol. 107, No. GT5, pp. 553-561.

Prest, V.K., Grant, D.R. and Rampton, V.N. 1968. Glacial Map of Canada. Geol. Surv. Canada. Map 1253A.

Rapp, A. 1960. Recent development of mountain slopes in Karkevagge and surroundings, northern Scandinavia. Geol. Ann., Vol. 42(2/3), pp. 71-200.

Romero, S.V. and Molina, R. 1974. Kinematic aspects of Vaiont Slide. Proc. 3rd Congress ISRM, Denver, Vol. II-B, pp. 865-870.

Rutter, N.W., Boydell, A.N., Savigny, K.W. and Van Everdingen, R.O. 1973. Terrain evaluation with respect to pipeline construction, Mackenzie transportation corridor, Southern part, Lat. 60° to 64°N. Task Force on Northern Oil Development, Report No. 73-36, Information Canada.

Rutter, N.W. 1980. Late pleistocene history of the Western Canadian ice-free corridor, Canadian Journal of Anthropology, Vol. 1, No. 1, pp. 1-8.

Salm, B. 1966. Contributions to avalanche dynamics. Scientific aspects of snow and ice avalanches, Davos, IASH. Publ., 69.

Savage, S.B. 1979. Gravity flow of cohesionless granular materials in chutes and channels, J. Fluid. Mech., Vol. 92, pp. 53-96.

Scheidegger, A.E. 1973. On the prediction of the reach and velocity of catastrophic landslides. Rock Mechanics, Vol. 5, pp. 231-236.

Scheller, E., 1970. Geophysikalische Untersuchungen zum. Problem des Taminser Bergsturzes. Diss., E.T.H., Zurich.

Sharpe, C.S. 1938. Landslides and Related Phenomena.

Cooper Square Publishers Inc., New York, 137 p.

Shreve, R.L. 1966. Sherman Landslide, Alaska. Science, Vol. 154, pp. 1639-1643.

Shreve, R.L. 1968a. The Blackhawk Landslide. Geol. Soc. America Special Paper 108, 47 p.

Shreve, R.L. 1968b. Leakage and fluidization in air-layer lubricated avalanches. Geol. Soc. America Bull., Vol. 79, pp. 653-658.

Solonenko, V.P. 1977. Landslides and collapses in seismic zones and their prediction. Bulletin of the International Association of Engineering Geology, Vol. 15, pp. 4-8.

Stauffer, M.R. 1966. An empirical study of three dimensional fabric diagrams used in structural analysis. Can. J. Earth Sci., Vol. 3, pp. 473-498.

Stevens, A.E. and Milne, W.G. 1973. Seismic risk in northern Yukon and adjacent areas. Environmental-Social Committee, Northern Pipeline, Rept. 73-7, Information Canada.

Terzaghi, K. 1962. Stability of slopes on hard, unweathered rock. Geotechnique, Vol. 12, pp. 251-270.

Vallejo, L.E. 1980. Cliff collapse and rock avalanches (sturzstroms) in the Mackenzie Mountains, northwestern Canada: Discussion. Can. Geotech. J., Vol. 17, pp. 149-151.

Varnes, D.J. 1978. Slope movement types and processes. *In* Landslides: Analysis and Control, Transportation Research Board, National; Academy of Sciences, Washington, D.C., Special Report 176, Chapter 2, pp. 12-33.

Voellmy, A. 1955. Ueber die Zerstoerungskraft von Lawinen. (The destructive power of avalanches). Schweizerische Bauzeitung, Zurich, Vol. 73, pp. 159-165; 212-217; 246-249; 280-285. (Translation by Alta Avalanche Study Centre, Wasatch National Forest, U.S. Dept. of Agriculture, Forest Service, Translation No. 2, 1964, 65 p.)

Voight, B. 1981. Time for the first moments of the May 18 eruption. *In* The 1980 Eruptions of Mount St. Helens, Washington. Lipman, P.W. and Mullineaux, D.R., editors, U.S.G.S. Professional Paper 1250, pp. 69-86.

Voight, B., Glicken, H., Janda, R.J. and Douglass, P.M.

1981. Catastrophic rockslide avalanche of May 18. *In* The 1980 Eruptions of Mount St. Helens, Washington. Lipman, P.W. and Mullineaux, D.R., editors, U.S.G.S. Professional Paper 1250, pp. 347-377.

Voight, B. and Faust, C. 1982. Frictional heat and strength loss in some rapid landslides. Geotechnique, Vol. 32, No. 1, pp. 43-54.

Wheeler, J.O. 1953. A Geological Reconnaissance of the Northern Selwyn Mountains Region, Yukon and Northwest Territories. Geological Survey of Canada, Paper 53-7, 42 p.

APPENDIX A

NOZZLE ROCK AVALANCHE

A.1 General

The Nozzle rock avalanche is located at coordinates 131°58'W and 65°02'N within the Arctic Red Cluster of avalanches. The failure originated on a bedding plane slope in a V-shaped valley which extends off an unnamed tributary of the Arctic Red River. Most of the failed mass is found below the rupture surface, although rock debris is spread over a distance of 5 km down the narrow valley and into the major valley where it has fanned out in a distinctive jet or nozzle-like fashion (see Figure A.1).

The local elevation in the vicinity of this avalanche ranges from about 800 m in the valley bottoms to 2100 m for some nearby peaks. Most of the terrain is gently sloping on the well vegetated valley sides, but changes to moderately steep, exposed slopes as one moves out of the wide valley bottom. The regional structural style gives this area a distinctive topographic pattern related to northwest-southeast striking, moderately dipping, carbonate strata.

Drainage in the tributary valley is accomplished by a single stream with two main branches. A deep channel up to 20 m in depth has been incised through the avalanche debris and the stream alluvium. Water flow is quite variable, subject to seasonal variations and the occasional intense

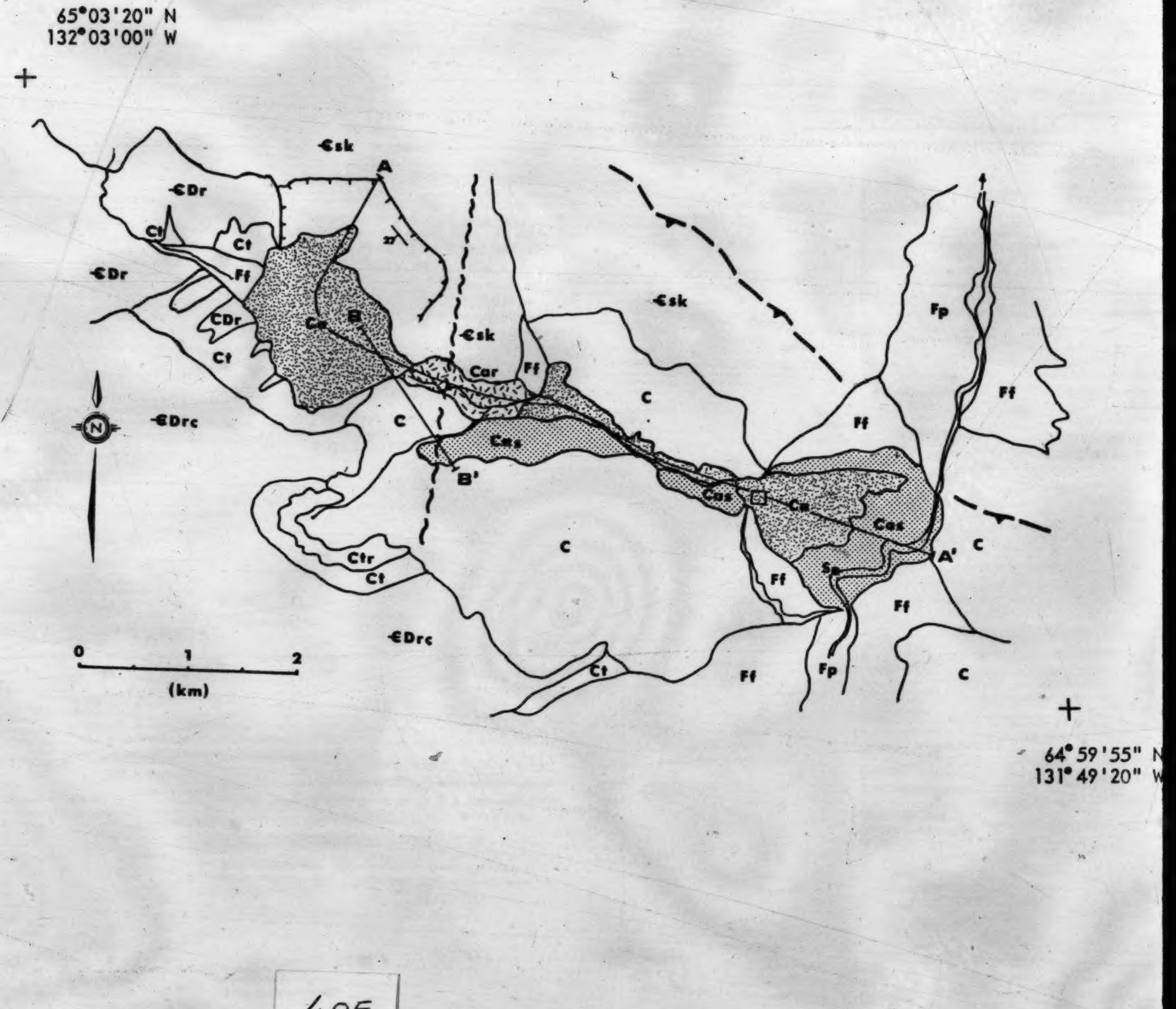
65°03'20" N
132°03'00" W
Ꞓsk
A
ꞒDr
Ct
Ct
Ff
ꞒDr
CDr
Ct
Ca
B
Ꞓsk
Car
Ff
Ꞓsk
C
ꞒDrc
C
Cas
B'
Fp
Ff
Ff
Cas
Ca
Cas
A'
C
Sa
Ff
Ff
C
Ctr
Ct
ꞒDrc
Ct
Ff
Fp
C
N
0
1
2
(km)
27
64° 59'55" N
131° 49'20" W

1 OF

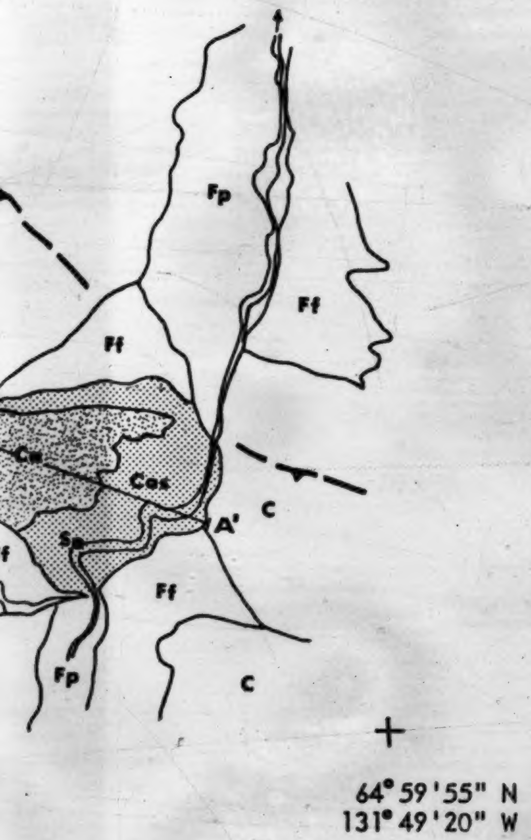

Figure A.1 Map of Nozzle rock avalanche.

LEGEND

Surficial Deposits

C	Colluvium - undifferentiated, over moraine or bedrock
Ca	Rock avalanche debris deposits, (Car) rarefaction zone, (Cas) spray, spatter or thin debris
Ct	Talus, (Ctr) protalus ramparts
F	Fluvial/Alluvial deposits - undifferentiated
Ff	Fluvial fan deposits
Fp	Floodplain deposits

Bedrock

-€sk	Sekwi Fm - limestone, dolomite, marine
-€Dr	Road River Fm - limestone, shale, dolomite, (€Drc) marine debris flow deposits

Symbols

28	Bedding
	Fault (thrust fault, direction unknown)
	Rockslide scar
☐	Boulder survey location
•S	Stratigraphic section location

2 OF 2

rain storms capable of generating minor floods and debris torrents.

A.2 Stratigraphy

The region located south of the Grand Forks of the Arctic Red River is underlain by Helikian to Devonian age rocks thrust over younger Paleozoic rocks by the Neptunist Fault (Aitken *et al.*, 1982). Within the vicinity of the Nozzle avalanche there are two formations which were originally deposited in the Selwyn Basin to the west. The Sekwi Formation (-Єsk) which hosts most of the original rock mass involved in the avalanche, is of Cambrian age, and the Road River Formation (-ЄDr), with a sub-unit of mappable debris flows (-ЄDrc), is of Cambrian to Devonian age. The following description of these rock units and the structural geology was obtained from the recent publication on the Upper Ramparts River (106G) and the San Sault Rapids (106H) map areas by Aitken *et al.* (1982) and from field observations by the writer.

The Sekwi Formation (-Єsk) is a marine platform unit comprised of limestone, dolomite, minor shale and quartzite. It overlies the Backbone Ranges Formation and is unconformably overlain by the Road River Formation. No complete stratigraphic section has been measured although estimates place the total thickness near 1000 m. In this region limestone is more common than dolomite which acquires a more distinctive orange and yellow weathering colour. The limestone varies from thin to thickly bedded, nodular calclutites, commonly argillaceous and silty, to skeletal and non-skeletal calcarenites. Oolite beds are common and mudcracks, ripple marks and fossils were infrequently noted. The grey to orange and yellow weathering dolomite is commonly microcrystalline. In some areas near the rupture surface the dolomite is black, fine-grained, often crystalline with some oncolites. Aitken *et al.* (1982) report the presence of mudrocks, up to 30 m thick, in the section, although these were not revealed in the short reconnaissance of the failure slope area. These grey to brown, and occasionally red to reddish brown weathering calcareous argillites contribute to the well bedded aspect of the formation as observed on air photos. Quartzite, sandstone and chert beds are rare within this sequence but are not unknown.

The Road River Formation (€Dr) of mid-Cambrian to early Devonian age is a thick, dark unit of recessive, shaly rocks overlain by Devonian carbonates. Within this area a major portion of the formation is grey, laminated, fissile shale. The lowermost beds in the section are limestone, very finely crystalline dolomite, and conglomerate, with minor chert and occasional fossils. The conglomerate is a conspicuous unit with coarse rounded dolomite clasts set in a fine-grained dolomitic matrix. Aitken *et al.* (1982) have interpreted these sediments, some of which are up to tens of metres thick, as debris flows or slides. A stratigraphic section for the formation has not been measured in this vicinity, although his estimates place the total thickness between 1370 and 1520 m.

A.3 Structural Geology

The study area comprises a portion of a large thrust block with several splays in the hanging wall of the Plateau Fault. This block becomes increasingly broken by splays parallel to the Plateau Fault as one moves towards the northwestern boundary of the Mackenzie Mountains. Dislocation along thrust faults has taken place typically through Helikian gypsum or shale units. This structural pattern is thought to be of Laramide age and is similar to subthrust imbricate zones in the southern Rocky Mountains as described by Dahlstrom (1970). Flexural slip surfaces associated with folding or thrusting would also be expected within this block of strata.

No major folds occur within the Plateau Sheet,but some flexures and small drag folds associated with splays from faults are present. At least two folds, possibly associated with thrust faults, were noted in the valley side opposite the Nozzle rupture surface (see Figure A.1). They are of little consequence to the structure in the immediate vicinity of the failure. A major fault of unknown displacement, striking in a north-northeasterly direction was shown by Aitken *et al*. (1982) to intersect the valley and traverse the east side of the bedding plane ridge exposed to the west of the rupture surface. Examination of this feature on air photos and in the field reveals a complex set of small displacements offsetting the Road River Fm. and Sewki Fm. strata. It is possible that this fault could be one of the set of rejuvenated older faults of pre-Rapitan age mapped by Aitken *et al.* (1982) approximately 40 km to the northeast. Most of these older faults are oriented in a northwesterly direction.

A preliminary survey of minor structural features in the map area reveals that most of the minor faults are oriented in a northwest to northeast direction and dip steeply at 60° to 80° to the east. Minor fold axes trend predominantly west-northwesterly to east-southeasterly and plunge at less than 5°, although a number of fold axial planes, possibly associated with the above described north-northeasterly trending fault, trend in a southerly direction and have axes that plunge at 10° to 30°.

A.4 Surficial Geology

The surficial geology and glacial history of the northern Mackenzie Mountains have not been investigated in detail by the Geological Survey of Canada. Some comments on the Pleistocene sediments have been made by Aitken *et al.* (1982) and Rutter *et al.* (1973) for map sheets to the north, but the exact extent and date of the last glacial episode in the Arctic Red River area remain largely unknown.

In Figure A.1 the major surficial deposits in the vicinity of the Nozzle rock avalanche are shown. The following description of these materials was derived mainly from air photo interpretation and field observations by the writer. A description of the rock avalanche debris is contained in Section 2.3.5.

Exposures of glacial till are relatively rare within the study area. Only at a few isolated sections where the stream has cut through the rock avalanche debris and at two localities in the main valley were morainal materials observed. Most of the highland areas are sufficiently covered by colluvium or alluvium to mask the presence of till. It is most probable, however, that only a thin cover of till is present within the tributary valley. Air photo interpretation would suggest that thicker accumulations of morainal materials are present in the main valley north and south of the study area.

Alluvial deposits (stream or fan sediments) are most common in this mountainous terrain. Large alluvial fans with intermittent debris flow channels are present both above and below the rupture surface and in the "ramp" area. These sediments are usually coarse, moderately sorted cobbles and gravel with occasional sand or silt lenses. Active fluvial and mass wasting processes have buried a portion of the rock avalanche debris in Eisbacher's "zone of rarefaction" or that part of the valley below the ramp where there appears to be very little avalanche debris.

Similarly, there are alluvial sediments overlying rock debris along the length of the narrow tributary valley before the main valley is reached. It is highly probable that the occasional damming of this stream by trees and other debris carried by high water during spring runoff could have given rise to the complicated stratigraphy observed in the narrow confines of its channel.

The spreading of the avalanche debris across the river valley has altered the drainage course of the main stream where it enters the valley. Alluvial sediments which previously were deposited in a wide fan now accumulate to the south of the fan area. The unnamed river in the main valley, a tributary of the Arctic Red River, is occupied by a maze of branching channels between coarse gravel and cobble bars and islands. This pattern is uncharacteristically broken only where the avalanche debris has blocked the river. Finer grained sediments, possibly incorporated into the debris, partially cover the coarser rock debris at the distal end of the fan. Depressions in this area have had sufficient peat accumulation to maintain an elevated water level, giving the area a boggy aspect.

Most of the sloping terrain in the map area is covered by a thick accumulation of colluvium consisting of cryoturbated soil and weathered rock. Such features as patterned ground, stone stripes, solifluction lobes, and felsenmeere are characteristic of this high alpine, permafrost environment. Active talus cones are present along the north facing slopes of the ridge opposite the rupture surface. Striking examples of protalus ramparts exist at the base of the talus slopes within the distinct cirque feature shown in the lower part of the map (Figure A.1).

No attempt was made to unravel the glacial chronology in this area, although it is reasonable to suggest, based on previous work (Hughes, 1972), that this area has probably experienced several episodes of glacial activity. Abundant evidence, such as the cirques, the nearby steep arete-like ridges and the presence of till confirm this, but other more supporting stratigraphic observations, glacier trimlines or datable material were not observed, nor obtainable during field investigations. Without more detailed mapping and comparison with similar terrains the accurate determination of the conditions prior to the rock avalanche are not likely to be convincingly resolved. It is deemed unlikely, however, that the avalanche could have initially occurred onto a glacier simply because of the incompatability of this postulate with the observed stratigraphic relationships and the lack of certain features which would be expected for such conditions (e.g. kettle-like depressions in the debris or the mixing of avalanche debris and glacial sediments).

A.5 Detachment Zone

The rock mass involved in the failure was a wedge shaped block, somewhat thicker in the west, which moved down a composite bedding plane surface with an approximate average dip of 27°. The inclination of this rupture surface appears to lessen by a few degrees near the base of the slope which lies in a distinct trough separating it from the main accumulation of the debris. This thick pile of debris has a particularly congruent aspect, especially the vicinity immediately adjacent to the rupture surface; large blocks of strata with attitudes only slightly rotated from their original position in the pre-failed slope face the trough area. Most of the debris has remained in this large pile-up feature, and the more mobile portion of the avalanche changed directions by 90° and streamed some 5 km down the narrow valley (see longitudinal profile, Figure A.2).

Bedding in the rupture surface is only exposed in a few localities where streams have incised gullies through a mantle of weathered rock and colluvium. To the west of this dip surface is a vertical cliff of close to 200 m height which forms the flank of the original rock mass (see Figure A.4a). A large accumulation of talus obscures the bottom portion of this wall. Carbonate rocks of both the Sekwi and Road River Formations are exposed in this area (Aiken *et al.*, 1982),but it was not possible to locate either the surface of the unconformity or the rupture surface in this vicinity during field investigations because of poor or

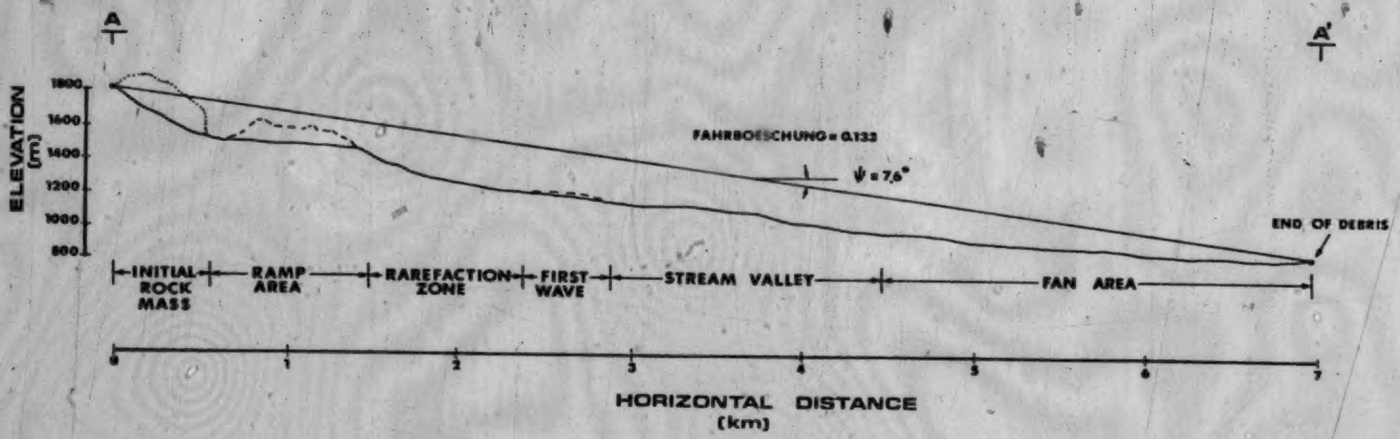

Figure A.2 Longitudinal profile, Nozzle rock avalanche.

inaccessible exposure.

Most of the rupture surface is relatively free of great accumulations of debris except for a small area halfway down the surface below the crown of the slide. Seepage was noted on the surface in a number of localities. However, it was not possible to ascertain whether this was a temporary phenomenon associated with recent rainfall or if it was of a more permanent nature.

To the east of the rupture surface is a steep ridge which drops steeply to the valley below. Orange weathering rocks of the Sekwi Formation with an almost cavernous appearance, possibly due to karst and or intense deformation associated with a nearby fault, give this area a rather unstable looking appearance.

Eisbacher (1979) estimated the volume of the rock mass involved as 50 x 10^6 m^3 , but a reconstruction of the original geometry, based on 1:50,000 scale topographic maps, places the volume at approximately 75 x 10^6 m^3. A rough estimate of the volume of debris, from a number of thickness estimates is 79 x 10^6 m^3 (+15%). Both these estimates must be viewed as speculative given the number of uncertainties in the initial geometry and the degree of material entrainment.

Figure A.3 is an equal area projection of the joint fabric from the base of the steep cliff area adjacent to the rupture surface. Since the fabric appeared uniform no attempt was made to define separate structural domains.

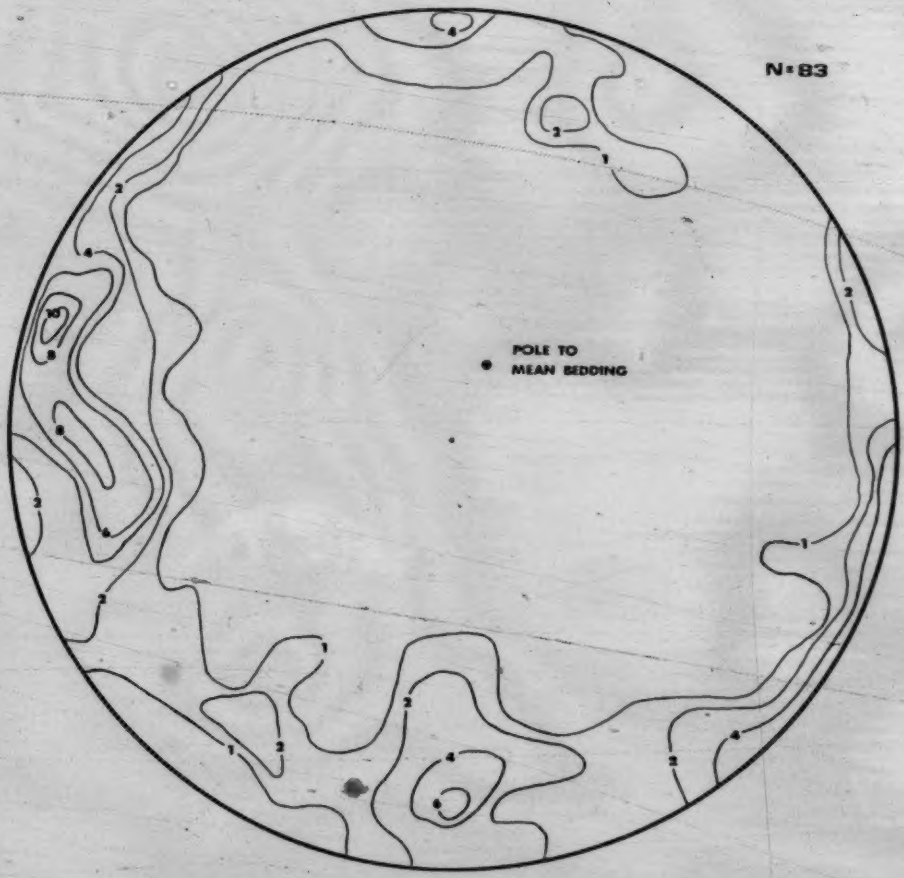

Figure A.3 Equal area projection of joint fabric near Nozzle rupture surface. Frequency contours in percent per 1% area.

While the number of measurements shown on this contoured plot is slightly less than the number of altitudes deemed necessary for statistical purposes (Stauffer, 1966) the plot is useful for displaying the general joint pattern. A mean bedding orientation, as determined for 10 measurements from this area is also shown. Note that the mean dip of the bedding in this area is 22°, some 5° less than the attitude of the rupture surface to the east. This is probably a reflection of a change in the bedding attitudes at depth within the side of the mountain.

There are two well-defined joint sets shown on the diagram. A more dominant set is very steeply dipping (80°-90°) and oriented almost due north, parallel to the steep cliff. The second, less conspicuous set strikes to the west and dips steeply to the north. The two sets are approximately perpendicular to each other and the bedding. A small cluster of poles to joints lies very close to the pole to the mean bedding plane. This could represent a group of joints oriented parallel or subparallel to the bedding which were opened with displacements associated with the main failure. Other variations from the mean trends might represent the influences of nearby folds and faulted strata.

The joint spacing within the area surveyed for the fabric study was found to vary over certain sections. Within the more competent dolomite, the spacing varied from 0.2 m to 0.5 m on average, but there were local areas with more intense (0.05 m to 0.3 m) spacing. Some of the more argillaceous dolomite and limestone had a flaggy aspect with bedding plane partings at 2 to 5 cm intervals. The observations made in this area do not necessarily represent the true in-situ fracture density, however. A secondary set of discontinuities associated with the large displacements which occurred during the main failure have superposed a bias on the sample of measurements.

A.6 Rock Debris Description

Ramp Area

As shown in Figure A.1 a large portion of the initial rock mass has come to rest in the area above the "ramp", feature described by Eisbacher (1979). This accumulation of semi-congruent debris, which varies in estimated thickness from 75 m to 125 m, contains close to two-thirds of the total volume of rock involved in the avalanche. The surface of this feature is quite undulatory with a shallow grass covered depression in the centre surrounded by isolated hills mainly composed of large boulders. The thickest part of the accumulation is in the northwest corner where the bedding plane surface has deflected a greater portion of the rock mass. A shallow lake and a thick accumulation of alluvium has been trapped in front of a steep 25° slope on the west side of the debris pile. On the opposite side of the debris pile, the surface slopes gradually to the east and then drops abruptly on a 30° slope before levelling out in the valley on about a 15° slope. The total elevation loss from the top of the debris pile to the flat alluvium below is slightly over 300 m.

A shallow gully, draining the trough area north of the debris pile, cuts along the east edge of the slope exposing bedrock. Eisbacher (1979) has suggested that the arcuate shaped scarp at the front of the ramp may have resulted from a slope failure, subsequent to the main failure, which catapulted debris in a second phase down the length of the valley. There was no field evidence to substantiate this style of movement.

Rarefaction Zone

At the base of this slope the debris was constricted by the valley sides. Only a few large isolated, partially buried boulders are present in this vicinity; active mass wasting from the steep north slope has covered some portion of the avalanche debris with alluvium and rock fall (see Figure A.4b). For a distance of about 1 km from the base of the "ramp" to the first deep accumulation of debris there is an area which appears almost devoid of debris. Eisbacher (1979) termed this area a "zone of rarefaction", presumably denoting an apparent change in travel character or velocity. While it is likely that some portion of the debris has been buried in this area it is, nonetheless, a distinct region with considerably less debris than portions of the avalanche

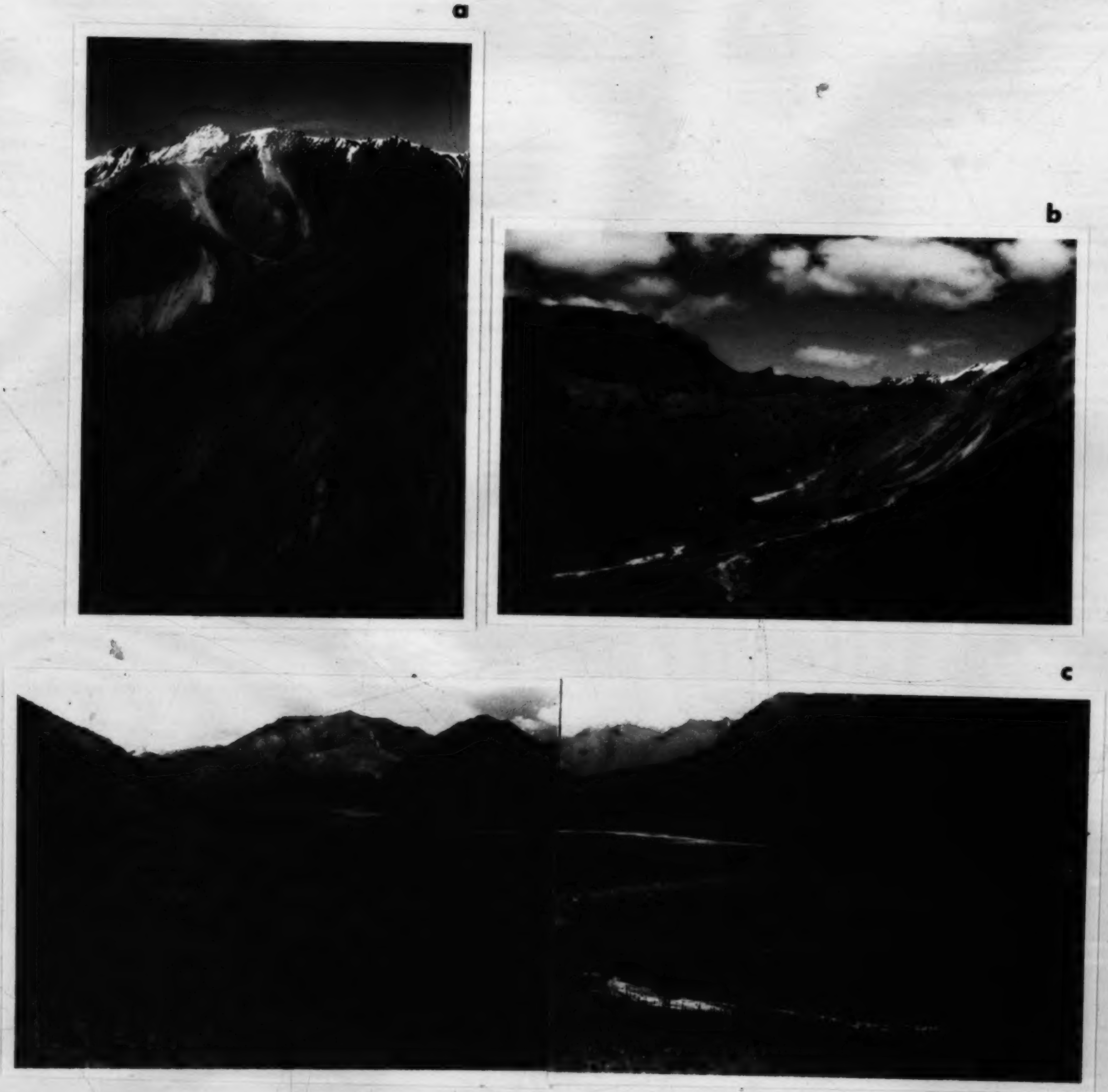

Figure A.4 (a) Rupture surface at Nozzle, dipping at about 27° (b) Nozzle "ramp" and "rarefaction" zones (c) Nozzle fan area.

above or below this point.

Spray Area

Directly south of this "rarefaction zone" is another feature with possibly an analogous origin. A wide swath of debris including boulders with volumes up to 1500 m^3 lie perched at heights up to 100m above the valley bottom along the flanks of the north facing slope for a distance of about 950 m. This "spray" feature has also been reported at the Damocles slide (Eisbacher, 1979) and similar features, referred to as "splash" or "spatter" areas, have been noted elsewhere, e.g., Frank slide (Hungr, 1981). Because of the isolated position of many of these boulders and the scarcity of finer debris below their location, it is more likely that they have acquired their position as high velocity projectiles rather than as part of a wider "spray"-like phenomenon. This distinction is rather arbitrary since such a "spray" would undoubtedly be comprised of a group of projectiles and a finer groundmass.

This hypothesis is further explored in section 4.3 (see also Figures 4.3 to 4.6).

Stream Valley

To the east of the zone of rarefaction and just below the point where an alluvial fan enters the valley from the north is a wave-like accumulation of rubble. The thicker portion of the debris has piled up on the north side of the valley to a maximum thickness estimated from cross-sections at nearly 30 m. A minimum height of debris measured in this area where the creek cuts through the "wave" was 16 m. Directly southeast of this position the surface of the debris tapers off rapidly. Most of the debris accumulation has taken place on the north side of the stream.

Numerous large boulders with volumes greater than 3,000 m^3 are found scattered throughout a scarcely vegetated cover of rubble. Some of these boulders are conspicuously grouped in close proximity to each other suggesting they may have acquired this position as part of a much larger block which disintegrated upon impact. Another interesting feature noted at two locations below the "wave" is a peculiar shadow effect on the lee side of some large boulders; an arc of fragmented rubble of meter size rocks has accumulated immediately down-valley of these boulders.

Between the area below the "wave" and the start of the fan where the main valley is gained, debris has been channeled through a relatively confined valley. In some places stream-cut exposures of the avalanche debris are covered with alluvial sediments. Thickness measurements are further complicated by uncertainties in identifying the contact between avalanche debris and the underlying sediment and/or till. Widening and narrowing of the debris below the wave gives the impression of a pulsating flow of materials down the narrow channel.

Another revealing observation, most noticeable on air photographs, is the presence of a lighter toned margin some 100 to 250 m wide lying mainly to the south of the stream and extending right from the "spray" area to the apex of the fan. On the ground surface this region is conspicuously less prolific in vegetation. While there are a few scattered half-buried boulders with mean dimensions less than 0.5 m to be found in this area there does not appear to have been a thick accumulation of rubble covering these slopes. This area possibly represents a zone of dust accumulation as has been reported elsewhere for rock avalanches, e.g., Lyell Glacier slide, (Gordon *et al.*, 1978) or the Elm rock avalanche (Heim, 1932).

Fan Area

Upon entering the main valley the debris stream has spread out in a fan-shaped form with distinct regions separatable on the basis of morphology (see Figure A.4c) Close to the apex of the fan is an area with two circular shaped accumulations of debris resembling bevelled cones. Most of the debris streamed towards the centre of the fan roughly producing a succession of wave-like ridges of 8 to 15 m height separated by shallow troughs or flat areas, now occupied by small ponds or bogs. These transverse ridges become less prominent to the south of the centre line through the fan and are truncated by a wide ridge oriented in an east-west direction that extends a fair distance towards the river. Viewed from the air the transverse ridges faintly define an open fold on the surface of the debris with an axial plane oriented parallel to the longitudinal ridge.

North of the fold is another more pronounced longitudinal ridge but of shorter length. From this position the debris surface tapers gradually at less than 5° to the lateral margin of the fan. This region is occasionally punctuated by isolated boulders and very faintly defined wide conical mounds (less than 10 m diameter, height 2-4 m) which are arranged in an en echelon fashion. A lightly vegetated margin similar to that observed south of the stream valley, extends for some 100 m or more beyond the north edge of the bouldery rock debris.

Towards the centre of the fan, beyond the wave-like ridges, the surface of the debris tapers towards the wetlands which occupy a large region right up to the river bank's edge. This area of stunted spruce trees and shallow wet depressions has the occasional partially buried boulder on its surface. A very irregular contact of a digitate outline separates this area from the rock debris proper to the west.

The southern part of the fan is in abrupt contact with the alluvial sediments which have been deposited over and adjacent to the debris. This contact is marked by a distinct rim of nearly 5 m height that tapers to become indistinguishable towards the south-east. The better soil and abundant water have given this area a more prolific tree growth. Only a couple of conical shaped mounds of less than 10 m diameter and 3 m height were noted along the border of the rim. A great abundance of large boulders and smaller rubble are found immediately north of the rim and to the east right up to the river edge.

Distal "Spatter" Zone

The distal edge of the debris could not be accurately outlined from air photos nor field observations. While it appears that most of the debris terminates at the river edge, there were a number of isolated boulders, some partially buried, which could be seen on the opposite side of the river valley. It might be possible that some of these have originated as rock falls from the adjacent mountain, but most probably they are part of the distal portion of the avalanche which may have travelled beyond the rock debris proper on or within a layer of saturated alluvium. The degree to which the avalanche "spatter" may have risen on the opposite slope could not be determined, but it is likely that a large volume of material was not involved since a fall-back ridge is not visible at the base of the slope.

Stratigraphic Section

Many excellent sections throughout the debris are exposed where the river has downcut its channel. It was not possible, in examination of the river banks on the west side of the river, to detect a contact, either distinct or gradational, between the avalanche debris and the presumed underlying river alluvium. There was one exposure near the extreme southern tip of the fan on the opposite side of the river, which upon inspection by binoculars, appeared to show a contact between different materials, but this could not be confirmed.

Figure A.5a is a typical exposure of the debris along the river edge. The light coloured, near vertical face is covered with a fine coating of silty sand which washes down from the top of the exposure. Figure A.6 is a detailed stratigraphic section from a nearby location (see map, Figure A.1) showing the variations in texture through this 8.5 m exposure.

The lower portion of the section is 1.5 m of coarse, river alluvium which is overlain by 1.5 m of colluvium composed of mainly silty slope wash. The next 3 m exposure of the section is mainly silty, sandy, grey and brown gravel with the occasional rusty brown sand lense. Only a faint stratification, not traceable for more than a meter, could be discerned.

At the top of this part of the section a pattern of 1 to 2 mm diameter bubbles can be seen in a loose, clayey, silty, sandy gravel (see Figure A.5b). Bubbles are occasionally noted in alluvial deposits and may have one of several origins: intergranular openings between grains held

Figure A.5 (a) Exposed section through debris along river(b) Bubbles within sandy debris from above section.

in place by dry clay; bubble cavities formed by air entrapment at the time of deposition; interlaminar openings in thin laminated sediments; buried but unfilled mud cracks; or voids left by the decay of entrapped vegetation (Bull, 1964). It is possible that these bubble-rich sediments represent the basal part of the debris stream where a high proportion of river alluvium and or slope colluvium had been entrained. This air may have been trapped in bubbles during the rapid movement of the debris over the saturated river alluvium. Clay balls, also characteristic to alluvial fan sediments, were similarly observed in this part of the section.

Overlying this material is 1.5 m of yellow brown to grey brown, clayey to gravelly sand with a more open structure and the occassional silty pod. A dark black band of dense, shaly silt forms a distinct, yet untraceable inclined marker above the sand.

The next 4 m of the section is comprised of sandy to cobbly, subangular boulders which become progressively larger in diameter higher in the section. Similarly the matrix dominated structure becomes an open, loose framework at the top of the section. This inverse grading of the debris is often reported for rock avalanche deposits, e.g., the Frank slide (Hungr, 1981). However, the feature is not necessarily ubiquitous. An examination of the exposed portions of the east river bank revealed that inverse grading is not prevalent throughout the debris, and is only

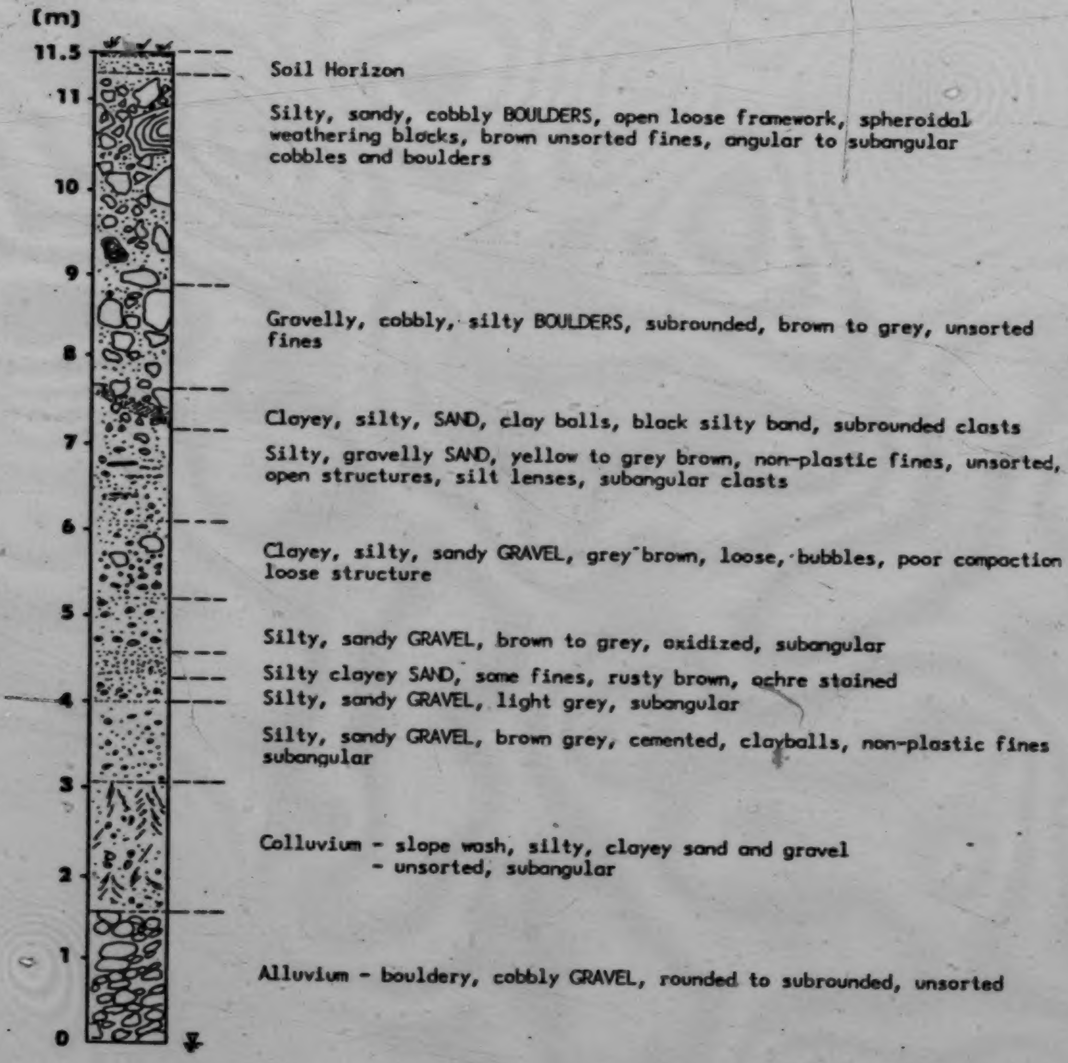

Soil Horizon

Silty, sandy, cobbly BOULDERS, open loose framework, spheroidal weathering blocks, brown unsorted fines, angular to subangular cobbles and boulders

Gravelly, cobbly, silty BOULDERS, subrounded, brown to grey, unsorted fines

Clayey, silty, SAND, clay balls, black silty band, subrounded clasts

Silty, gravelly SAND, yellow to grey brown, non-plastic fines, unsorted, open structures, silt lenses, subangular clasts

Clayey, silty, sandy GRAVEL, grey brown, loose, bubbles, poor compaction loose structure

Silty, sandy GRAVEL, brown to grey, oxidized, subangular

Silty clayey SAND, some fines, rusty brown, ochre stained

Silty, sandy GRAVEL, light grey, subangular

Silty, sandy GRAVEL, brown grey, cemented, clayballs, non-plastic fines subangular

Colluvium - slope wash, silty, clayey sand and gravel
- unsorted, subangular

Alluvium - bouldery, cobbly GRAVEL, rounded to subrounded, unsorted

Figure A.6 Stratigraphic section exposed at undercut bank on river.

restricted to certain areas.

Detailed textural and lithologic analyses were not performed on samples from the debris. Hand lens examination would suggest that most of the clasts in the debris are angular to subangular, and only rarely subrounded. Striated, rounded clasts were not observed. Dolomite, limestone, and rarely quartzite are the dominant lithologies present. A small sample of clast orientations did not show a preferred fabric, but a larger sample might reveal a more characteristic trend. Additional studies of the above nature are recommended.

Debris Texture, Sorting and Fabric

From the few cross-sections through the debris exposed along the stream channel inverse grading was only faintly developed, if at all. Nevertheless, a casual examination of the surface of the debris in this area or across the fan would give one the impression of a much coarser boulder deposit with little or no fines. Such is not the case, as was shown in the exposures through the stream channel.

To ascertain the range of boulder sizes which are present on the debris surface a sample area of 7678 m^2 near where the avalanche entered the main valley was examined (see location on Figure A.1). Boulders with a mean diameter greater than 1 m were measured within this area. Figure A.7 is a plot of percent area coverage against the mean diameter for the 386 measurements. The percentage of area covered by

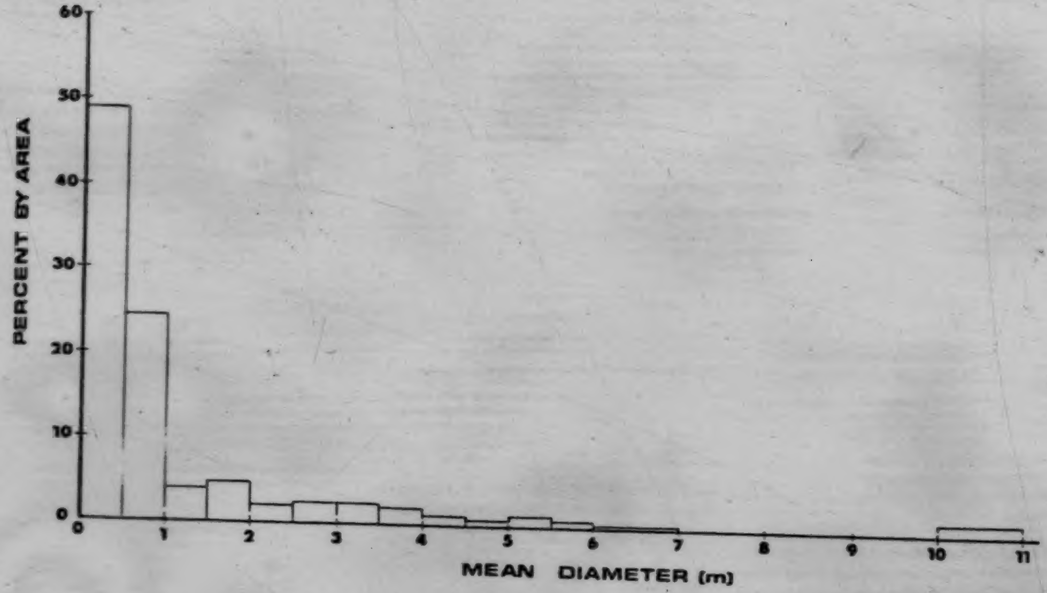

Figure A.7 Plot of percent by area versus mean boulder diameter in a sample area of 7678 m².

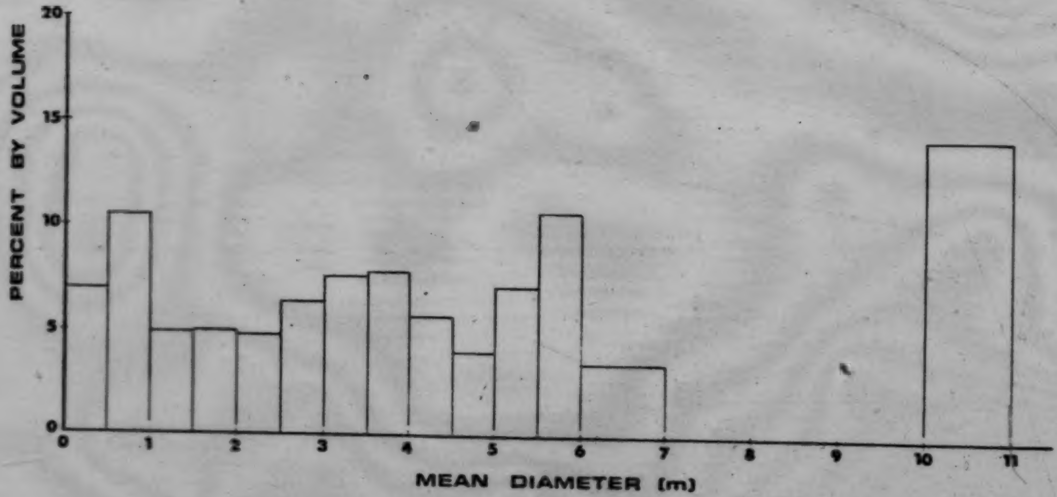

Figure A.8 Plot of percent by volume versus the mean boulder diameter in a sample area of 7678 m².

each clast size was determined by assuming that the area for each boulder was equal to the square of its mean diameter. Discrepancies between the plan area and the area of boulders actually measured due to the undulatory nature of the surface and preferential boulder orientations were deemed to be insignificant for the level of accuracy sought in this exercise. The percent surface area is expressed as a portion of the total area surveyed. The two size fractions less than 1.0 m were visually estimated as percentages of the total area coverage.

Figure A.7 shows in a general fashion, the relatively small area actually covered by the large boulder sizes. The pronounced negative skew is indicative of the much greater surface area coverage by the size fractions with mean diameters less than 1 m. The best visual estimate of the percentage of void area on the surface was 29%.

To further investigate the boulder size distribution the "area-by-number" method, described by Kellerhals and Bray (1971) and later used by Hungr (1981), was applied to estimate the percentage by volume of each size fraction. This technique will yield results consistent with other methods such as conventional sieve analysis for percentage by weight (Hungr, 1981). The method is similar to the procedure used for the percentage-by-area approach described above; size categories are defined and a count of all particles of each category on the surface of the sample area is made. This percentage is then converted into percentage-by-volume when multiplied by the geometric mean size of the particular category.

As seen in Figure A.6 the percent-by-volume histogram shows a much different distribution than the percent-by-area approach. There is not a marked concentration of boulders within any one particular size fraction and the distribution is quite even over the range of mean boulder diameters. Because of the diameter cubed relationship the percent-by-volume method favours the larger size fractions, i.e., the highest percentage-by-volume size fraction was the 10 m to 11 m size which was for one boulder.

This initial inquiry into the boulder size distribution has only dealt with the surface of the avalanche debris in one small study area. The actual size distribution at depth within the debris and its spatial variation are undoubtedly quite different. The technique does merit further application, particularly as applied to the spatial size distribution of the surface debris.

Field and air photo studies have not revealed a systematic pattern of variation in boulder size throughout the length of the deposit; some of the largest boulders, greater than 3000 m^3, are scattered along the travel path in the valley and right to the end of the fan. Curiously, one of the large boulders with a volume in excess of 5000 m^3 is located right at the distal end of the north edge of the fan, well beyond the rock debris proper. Typically such large boulders are cubic in shape, display a well developed fracture network, and in a few cases have broken into two or more separate blocks. Grooves, scratches or other signs of abrasion are not present, but may have been obscured by weathering.

McSaveney (1978) has documented an interesting clast fabric in the debris at the Sherman Glacier rock avalanche; long axes generally parallel flow direction, and occasionally transverse fabric modes are present. An attempt to measure other long axes of boulders on the Nozzle debris surface proved less successful. A small sample of 28 boulder attitudes near the "ramp" area was measured and plotted on an equal area stereonet, but no common orientation was observed. This does not preclude the possibility that a significant orientation of boulders could be present within a different part of the debris.

In summary, a number of morphological features have been described for the Nozzle rock avalanche. Many facets of the debris structure and their explanation remain unmentioned, however. Further work is recommended in more accurately defining the debris fabric and size distribution as they relate to the mode of movement.

APPENDIX B

ROCKSLIDE PASS ROCK AVALANCHE

B.1 General

The Rockslide Pass rock avalanche is located on a tributary of the Natla River in the central Backbone Ranges of the Mackenzie Mountains at geographical coordinates 127°45'W and 63°20'N. This area is part of the Redstone Plateau which is characterized by flat to slightly dipping strata and wide, U-shaped, glaciated valleys. Some mountains within this region rise to 2380 m. The main valley in the study area is at an elevation of nearly 1300 m. The Rockslide Pass avalanche is very close to the drainage divide separating the Natla and North Redstone Rivers.

This little-known rock avalanche involved an estimated volume of 370 x 10^6 m^3, making it probably the largest single event landslide of its type within the Canadian Cordillera. As shown in Figure B.1, an entire mountainside bounded by two well-defined, almost perpendicular joint surfaces, has collapsed and disintegrated, sending rock debris both up and down the wide glaciated valley. Most of the rock mass rests at the base of the rupture surface, but a significant portion has travelled over 3 km beyond the edge of the ramp feature towards the south.

1 OF

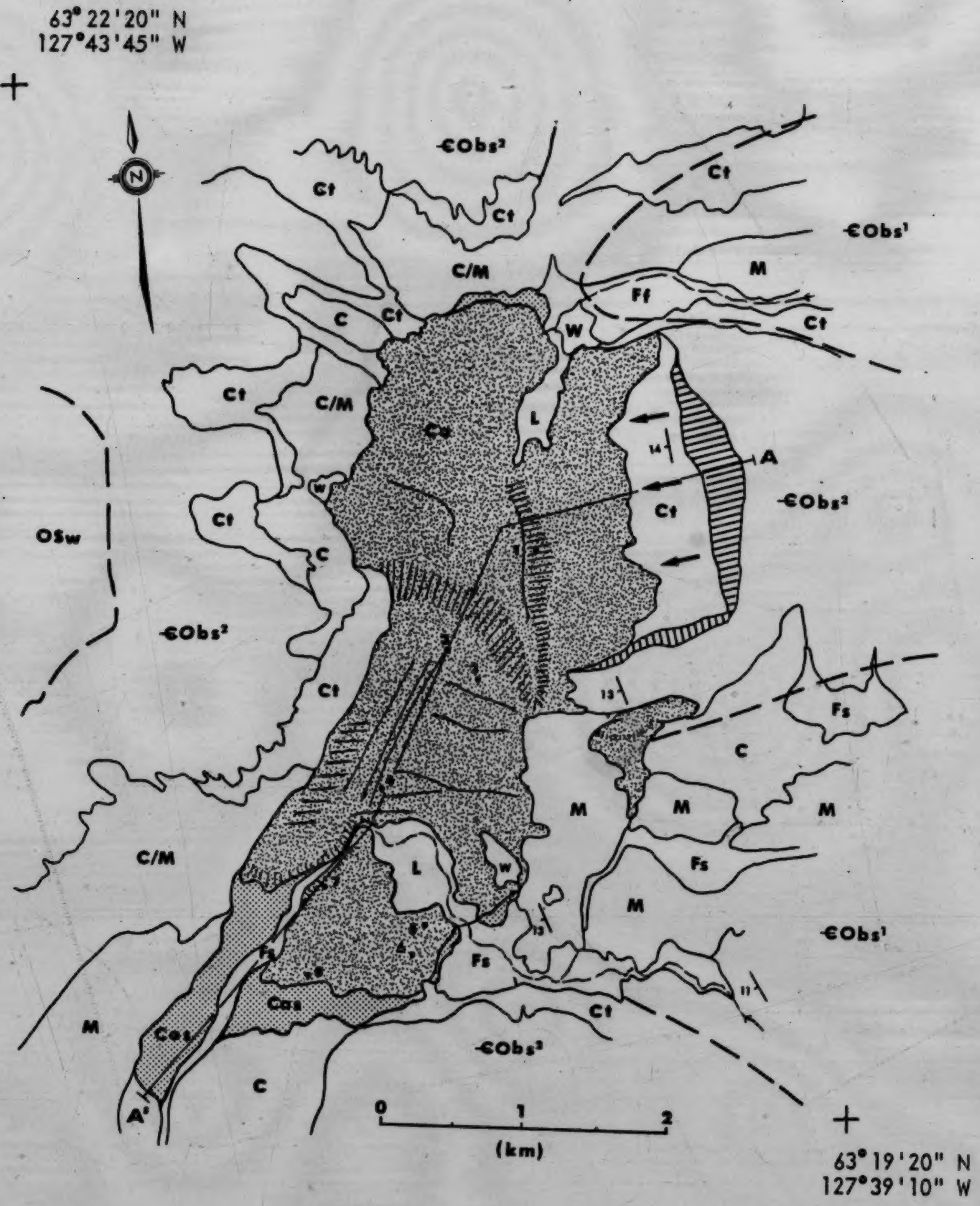
63° 22'20" N
127°43'45" W
N
-€Obs²
Ct
Ct
Ct
-€Obs¹
C/M
M
Ff
C
Ct
Ct
W
Ct
C/M
Ca
L
14
A
-€Obs²
Ct
W
Ct
OSw
C
-€Obs²
Ct
13
Fs
C
M
M
M
C/M
Fs
L
W
M
-€Obs¹
13
Fs
Fs
Cas
11
Ct
M
Cas
-€Obs²
C
A'
0
1
2
(km)
63° 19'20" N
127°39'10" W

LEGEND

Surficial Deposits

C	Colluvium - undifferentiated, thin deposits over till or bedrock
C/M	Colluvium over moraine
Ca	Rock avalanche debris deposits, (Cas) thin debris, "spray" or "red rim" areas
Ct	Talus
F	Fluvial/Alluvial deposits
Ff	Fluvial fan deposits
Fs	Stream alluvium deposits
L	Lacustrine deposits - ponded lake sediments, silt and clay, some stream alluvium at surface
M	Glacial till- thin cover of colluvium

Bedrock

OSw	Whitaker Fm - grey dolomite, light grey basal limestone
-€Obs	Broken Skull Fm - grey, buff and orange weathering dolomite

SYMBOLS

14 ╲	Bedding
— —	Inferred geological boundary (Bedrock)
∼	Stream
═	Topographic ridges in debris
//||\\\\	Steep slopes
|||||||	Breakaway scar
//	Crevasse-like troughs
(w)	Small lakes
•7	Boulder survey points

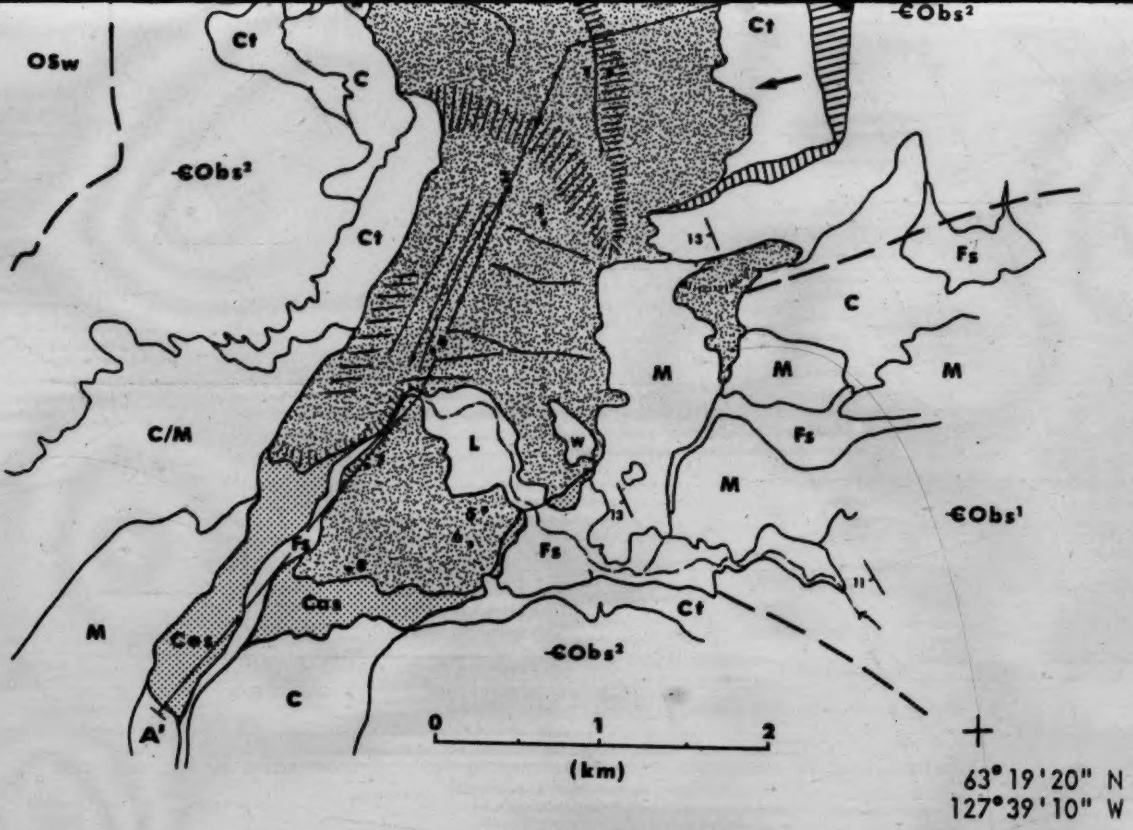

LEGEND

Surficial Deposits

C	Colluvium - undifferentiated, thin deposits over till or bedrock
C/M	Colluvium over moraine
Ca	Rock avalanche debris deposits, (Cas) thin debris, "spray" or "red rim" areas
Ct	Talus
F	Fluvial/Alluvial deposits
Ff	Fluvial fan deposits
Fs	Stream alluvium deposits
L	Lacustrine deposits - ponded lake sediments, silt and clay, some stream alluvium at surface
M	Glacial till- thin cover of colluvium

Bedrock

OSw	Whitaker Fm - grey dolomite, light grey basal limestone
-€Obs	Broken Skull Fm - grey, buff and orange weathering dolomite and limestone; 1. basal silver grey sandstone and sandy dolomite overlain by orange weathering dolomite; 2. grey limestone and dolomite.

SYMBOLS

14 ╲	Bedding
— —	Inferred geological boundary (Bedrock)
∼	Stream
═	Topographic ridges in debris
//||\\\\	Steep slopes
||||||||	Breakaway scar
//	Crevasse-like troughs
(w)	Small lakes
•7	Boulder survey points

2 OF 2

Figure B.1 Map of the Rockslide Pass rock avalanche

B.2 Stratigraphy

The area under study lies on the eastern side of the Redstone Plateau which is underlain by a relatively flat to gently dipping platform of Helikian through Devonian age strata. Within the immediate area near the Rockslide Pass avalanche Gabrielese *et al.* (1973) have distinguished three separate formations of Cambrian through Silurian age: the Rockslide Pass Formation (€r), the Broken Skull Formation (€Obs), which has been subdivided into several members, and the Whittaker Formation (OSw). The entirety of the original failure took place within the Cambrian to Ordovician age Broken Skull Formation. The following description of the stratigraphy has been obtained from field work conducted by the writer and a more detailed stratigraphic section measured by Gabrielse *et al.*(1973) on the same ridge some 2.5 km to the east.

According to the measured section by Gabrielse *et al.*(1973) the entirety of the greater than 600 m thickness of strata exposed in the main cliff face at the back of the rupture surface belongs to the upper member of the Broken Skull Formation. In the adjacent measured section about 150 m of silvery grey weathering sandstones and sandy dolomites of the lower member are distinctly separated from the upper member. The basal part of this member is comprised of a 100 to 150 m sequence of orange-buff weathering dolomites. This distinctive strata is readily apparent in the lower portion of the exposed cliff and throughout the distal portion of the avalanche debris. Overlying this unit is a sequence of carbonate strata, which are considered to be correlative with the upper Broken Skull Formation in the region. This part of the formation is not distinguished from the younger Ordovician Sunblood Formation because the basal beds of the latter, which are usually most distinctive elsewhere, have not been seen within this area (Gabrielse *et al.*, 1973).

More than 400 m of the upper member of the Broken Skull Formation, probably including some of the Sunblood Formation, have been described in detail by Gabrielse *et al.* (1973, Part II, p. 32). The base of this member consists of medium to thinly bedded, dark grey to pale purple, orange weathering, fine grained dolomite occasionally laminated with silty, brown weathering dolomite. Higher within the section the strata are predominantly medium to thickly bedded, grey, crystalline limestone interbedded with silty to sandy, orange weathering dolomite which thins upwards. Sandy lenses, oolitic limestone, conglomerate, mudcracks, silty laminae and bioclastic limestone are occasionally found within this sequence. The strata exposed on the upper portion of the cliff have not been described in any measured section, although visual inspection suggests that it is comprised of similarly alternating limestone and dolomite.

B.3 Structural Geology

The Rockslide Pass avalanche is located on the west side of the Redstone Plateau, a gently dipping homocline. Faulting appears to be of little importance within this immediate area, although a number of minor faults, apparently with vertical displacement, have been mapped in the vicinity. A couple of north-northwesterly trending faults are found some 24 km south of the avalanche on the North Redstone River. The closest fault, oriented in an east-west direction, displaces Broken Skull (ꞒObs^2) and Whittaker (OSw) Formation strata on the ridge located west of the distal tip of the avalanche debris. Folded strata were not observed within the map area.

B.4 Surficial Geology

The surficial geology in the vicinity of the Rockslide Pass rock avalanche has not been mapped to date as part of a regional scale investigation. Pertinent comments on the glacial history of the region east and south of Rockslide Pass may be found in Gabrielse *et al.*(1973). The major surficial geology units observed within the area are shown on the accompanying general map (Figure B.1). A more detailed description of the landslide debris is contained in Section 2.4.5.

Till , presumably derived in more than one glacial episode can be seen within the area surrounding the Rockslide Pass avalanche. Two or possibly three glacial trimlines were observed along the east side of the ridge opposite the main failure. Examination of the lowest of these trimlines revealed a grey, silty, gravel till, quite distinct from the typical brown, grey diamicton of angular to subangular clasts found within the gorge area where the stream has cut through the debris. Morainal ridges were also observed at the front of the three cirque basins opposite the rupture surface and along the flanks of the valley north-east of the avalanche. These features have a rather subdued morphology, and are occasionally covered by talus from adjacent steep slopes. At no location was moraine material observed to overlie or become mixed with the avalanche debris. Immediately south of the rupture surface is a wide valley leading to Rockslide Pass where glacial till has been deposited creating a relatively flat topography with gently sloping hills, and wide alluvial deposits.

These alluvial sediments are typically coarse gravel and cobbles, which were probably deposited as part of a wide outwash plain immediately following the last glacial activity in this area. Within the avalanche debris is a wide "void" area occupied by a succession of finer alluvial sediments. Exposures along the banks of the present stream reveal a stratigraphy of layered sand, silt, and clay, occasionally burying angular boulders. Beneath the steep gorge cut by the stream through the debris is an area of abandoned channels and narrow ridges (less than 2 m height) which are suggestive of there once having been a very rapidly flowing river below the gorge. These features are cut through coarse alluvial sediments, which overlie and are mixed with the avalanche debris, and are situated well above the present water course. The above evidence suggests that a large lake was once partially impounded by the avalanche debris and only after a period long enough to accumulate sufficient sediment, did the water manage to down cut a channel through the debris and underlying moraine.

To the north, above the main debris accumulation, a similar impoundment of drainage has resulted in the creation of a small lake with a comparable thickness of fine alluvial sediments. An amazing vortex-like funnel denotes the opening of the main underground channel through which a portion of the lake water drains to below the "ramp". The recently published 1:50,000 NTS map sheet for this region (95M/5) labels the area in front of the rupture surface adjacent to this feature as a "sinkhole", presumably in explanation of the disappearance of the drainage course within the debris.

Colluvium, mostly talus, is found along most of the steep sloping terrain on the sides of the valley. Active talus cones, occasionally covered with debris flow sediments, mark the limit of the debris along its western edge and occasionally are found to overlie the debris. Colluvial soils, largely till derived, are found along the south-facing slopes in a few localities.

Surficial permafrost features such as mud boils, patterned ground, and rarely solifluction lobes were noted within the map area.

Undoubtedly this area has undergone more than one glaciation as evidenced by the position of various moraine features and the sculptured nature of the cirque basins and aretes above the valley. Permanent ice is still present within a number of isolated cirques south of the detachment area and till to the northeast is remarkably fresh-looking. However, without a more regional scale of investigation and a chronologic inquiry into the age of these features, the particulars of the most recent glaciation and the effects this might have had on inducing the original failure, remain largely speculative.

B.5 Detachment Zone

The detachment of the original rock mass from the front of the mountain face has left a remarkable scar defined by a sharp, near-vertical cliff face trending north-northwesterly. The south flank of the failure surface is marked by a similar 100 to 300 m cliff face. A considerable thickness of talus blankets the lower parts of these cliffs (see Frontispiece and Figure B.2).

The bedding surface which dips at 12° to 14° to the southwest is only exposed in a gully along the north side of the rupture surface area. Talus, rockfall, slide debris, and colluvium cover almost the entirety of the surface. A

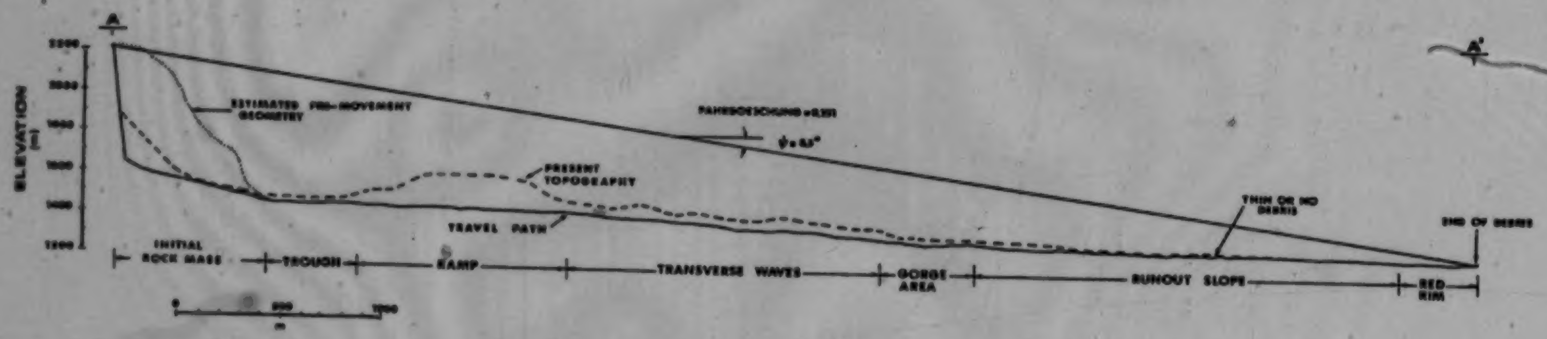
A
A'
ELEVATION (m)
2200
2000
1800
1600
1400
1200
ESTIMATED PRE-MOVEMENT GEOMETRY
FAHRBOESCHUNG = 0.231
ψ = 13°
PRESENT TOPOGRAPHY
TRAVEL PATH
THIN OR NO DEBRIS
END OF DEBRIS
INITIAL ROCK MASS
TROUGH
RAMP
TRANSVERSE WAVES
GORGE AREA
RUNOUT SLOPE
RED RIM
0
500
1000
m

Figure B.2 Longitudinal profile, Rockslide Pass rock avalanche

wide trough feature, similar to that observed at the Nozzle avalanche detachment zone, separates the rupture surface and the "ramp". A deep depression is located in the extreme southern corner of the trough, adjacent to the thickest portion of the "ramp".

The present exposure of the unfailed portion of the mountain and nearby rock slopes suggest that the pre-movement topography was likely as steep as the north side of the mountain and possibly was defined by two slopes giving an approximately concave profile. Probably most of the mass moved as a large coherent block in a westerly direction and only upon the change in slope did the mass begin to disintegrate. No surface exposures of slickensides or gouge marks were found on the rupture surface or on blocks within the debris. However, the presence of shaly interbeds, possibly pre-sheared, at the base of the block would not be impossible.

Some seepage was noted on the northern edge of the rupture surface where the bedding surface is hidden by less than a metre of colluvium. It is highly probable that other sources of seepage are present along the bedding planes obscured by talus further to the south.

Eisbacher (1979) claimed that the basal portion of the failure block was comprised of dolomite with numerous siltstone beds. Upon closer inspection, it was noted that orange weathering strata, largely dolomite, are found both beneath and above the rupture surface. A number of silty and occasionally sandy, purple dolomite beds were noted in the southerly exposure of the prominent east-west ridge to the south of the detachment area, but it could not be determined how close these beds are to the rupture surface. The presence of orange to rusty weathering beds is not limited to the base of the block; numerous such beds were observed in the section exposed on the high cliff at the back of the rupture surface.

Gabrielse *et al.*(1973) initially estimated the total volume of rock involved in the avalanche as some 500 x 10^6 m^3. Eisbacher (1979) reiterated a similar estimate of 450 x 10^6 m^3. It is not known whether these estimates are based on debris thickness measurements or on a reconstructed initial failure geometry. Using a series of cross-sections constructed with the aid of survey measurements and a NTS 1:50,000 scale topographic map (95M/5), a re-evaluated volume of 370 x $10^6 m^3$ was calculated.

A secondary avalanche of a part of the ridge south of the breakaway zone shows an amazing resemblance to the larger primary avalanche (see Figure B.1). A block of less than 1 x 10^6 m^3 moved down a 16° to 17° dip slope and partially disintegrated sending a stream of rubble several hundred meters at right angles to the original direction of movement, on a slope of less than 10°. Photographs of this feature and a discussion of its significance to the dynamics of the larger failure are found in Chapter 3.

Almost the entirety of the original rock mass moved down the rupture surface and came to rest within the wide valley bottom. The mass closest to the breakaway surface has a semi-congruent or jigsaw puzzle aspect with many large disjointed blocks becoming progressively more disintegrated further from the trough area. Eisbacher (1979) has suggested that most of the "ramp" originated from the top of the cliff, but the distinctive orange weathering beds of the basal portion of the upper member of the Broken Skull Formation are found in scattered locations throughout, and within this area, as well as up-valley and towards the distal tip of the avalanche. Further discussion of this "ramp" feature follows in the next section.

Detailed bedding and joint fabric measurements were made on the cliff beneath the north exposure of the rupture surface and on the south facing ridge above the small failure. Figure B.3 is an equal area projection of the joint fabric from these two locations. A mean bedding orientation of 351/13 is also shown. No attempt was made to separate the joint fabric into structural domains nor to evaluate the statistical significance of the concentrations shown.

Inspection of the diagram reveals the presence of two joint sets broadly perpendicular to bedding. The east-west trending, near-vertical set of joints appear to be better developed. However, there also appears to be a slight separation of the concentration into two subgroups. This

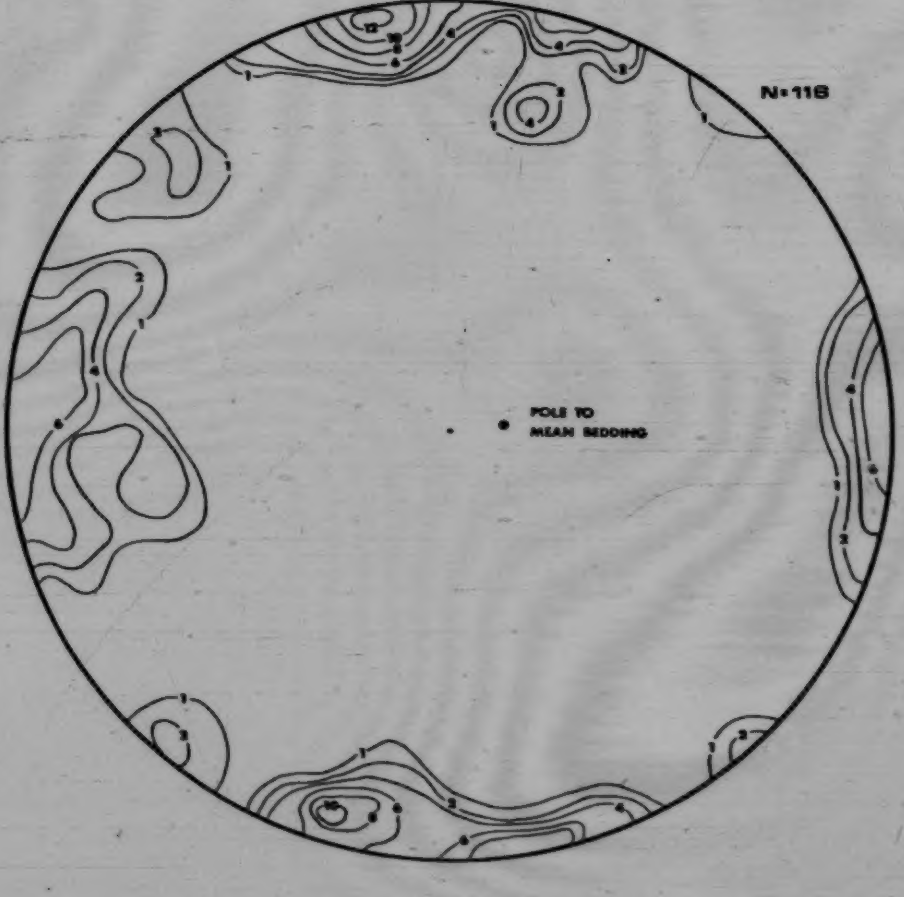

Figure B.3 Equal area projection of joint fabric near Rockslide Pass rupture surface. Frequency contours in percent per 1% area.

separation was not due to variances in the fabric at the two locations where measurement were taken. The second, less well developed joint set roughly parallels the vertical cliff face, although a similar but less significant scatter in the concentration is also present. Additional measurements of discontinuity fabric would be necessary to determine the exact nature of these variances.

Joint spacing was measured in two small, limited surveys within the above areas. In the more dominant grey, crystalline, limestone strata the general spacing of joints was 0.8 to 1.0 m and bedding thicknesses ranged from 0.2 to 1.2 m. The average block exposed in these outcrops was roughly rectangular with a maximum dimension aligned with the down dip direction. The spacing of the more prominent joints with a well developed gape was not evaluated. However, this information would be of considerable more use in a kinematic analysis.

B.6 Rock Debris Description

Ramp Area

More than two-thirds of the failed rock mass has accumulated in a large "ramp" feature with a surface area of about 1.2 km^2 (see also Figure B.4a). The maximum thickness of this semi-congruent pile of debris is about 200 m near the trough area. Best estimates of the pre-failure valley geometry would place the average thickness near 175 m. The front edge of the debris has risen some 250 m from the valley bottom up the slope opposite the breakaway scar, trapping a small lake.

A most striking feature observed in the ramp is the preservation of the stratigraphic sequence. Large blocks, with volumes in excess of 30,000 m^3, may be connected along strike in several localities. This jigsaw puzzle effect is even more pronounced by the presence of orange weathering dolomite beds which are traceable for some distance in a few areas. The largest blocks, although mainly concealed by talus and surface debris, are exposed on the steep slope facing the trough, near the southern edge of the breakaway surface.

The surface topography is marked by a few, small diameter (<50 m) depressions between faintly defined ridges oriented parallel to the trough. A grass covered depression in the south-central part of the ramp contains a number of circular depressions of 10 m depth or less. The largest of these contains an intermittent pond which was seen to fill up to several meters height following a heavy rainfall. Within two days the water had almost completely drained to beneath the debris surface.

In the up-valley portion of the ramp the topography tapers gradually down to the level of the small lake trapped in front of the debris. Some lithologic and textural separation of the debris is visible within this area below the highest part of the ramp. However, the jigsaw puzzle effect is much less pronounced. A distinct rim of orange to orange-brown weathering rocks mask the northern most distal edge of the debris. A noticeable reduction in boulder size is also apparent moving towards the northern extremity of the debris.

The thickest part of the ramp is a wide promontory which extends south of the main accumulation. Steep 35° talus slopes mark the southern, arcuate shaped front of the ramp. The central portion of this frontal part is comprised of smaller sized debris and hence supports a more developed vegetative cover.

Transverse and Longitudinal Ridges

As shown on the map and the longitudinal profile (Figures B.1 and B.2, respectively), one of the most striking features of the Rockslide Pass avalanche is the presence of a conspicuous wave-like pattern of transverse ridges. Immediately below the ramp the first wide-crested "wave" spans the east side of the debris and is truncated by a faint depression in the centre of the debris. The second "wave" is again predominantly on the east side but extends about three-quarters of the way across the debris stream. The amplitudes of these "waves" range between 20 and 30 m. Neither "wave" is perfectly perpendicular to the direction of flow. A third "wave" with a shorter span exists immediately in front of the gorge area and is separated from the second wave by an approximately 25 m deep trough.

Whether these "waves" reflect the original surface topography (e.g., moraines) or are an expression of compressive forces within the debris sheet cannot be easily determined. It is highly unlikely, though, that all three "waves" are actually a buried succession of terminal moraines.

Subtle lithologic and textural differences faintly define a longitudinal ridge and a wide groove to the west of the centre of the debris stream. The more coherent blocky nature of some of the limestone involved in the avalanche gives rise to a rather conspicuous boulder train appearance along these ridges when viewed from the front of the ramp. Similar textural and lithologic variations were noted by McSaveney (1978) for longitudinal and transverse ridges on the Sherman Glacier rock avalanche.

Moving towards the west lateral margin of the debris the thickness of the debris thins and the average boulder size decreases. A pronounced ripple-like effect is produced by a series of east-west aligned, 1-2 m high, elongate hills, before the west lateral margin of the debris is reached.

Void Area

Situated about half-way down the length of the debris stream is an almost square-shaped depression which is nearly encircled by coarse, rock avalanche debris (see Figure B.4b). A number of partially buried boulders are

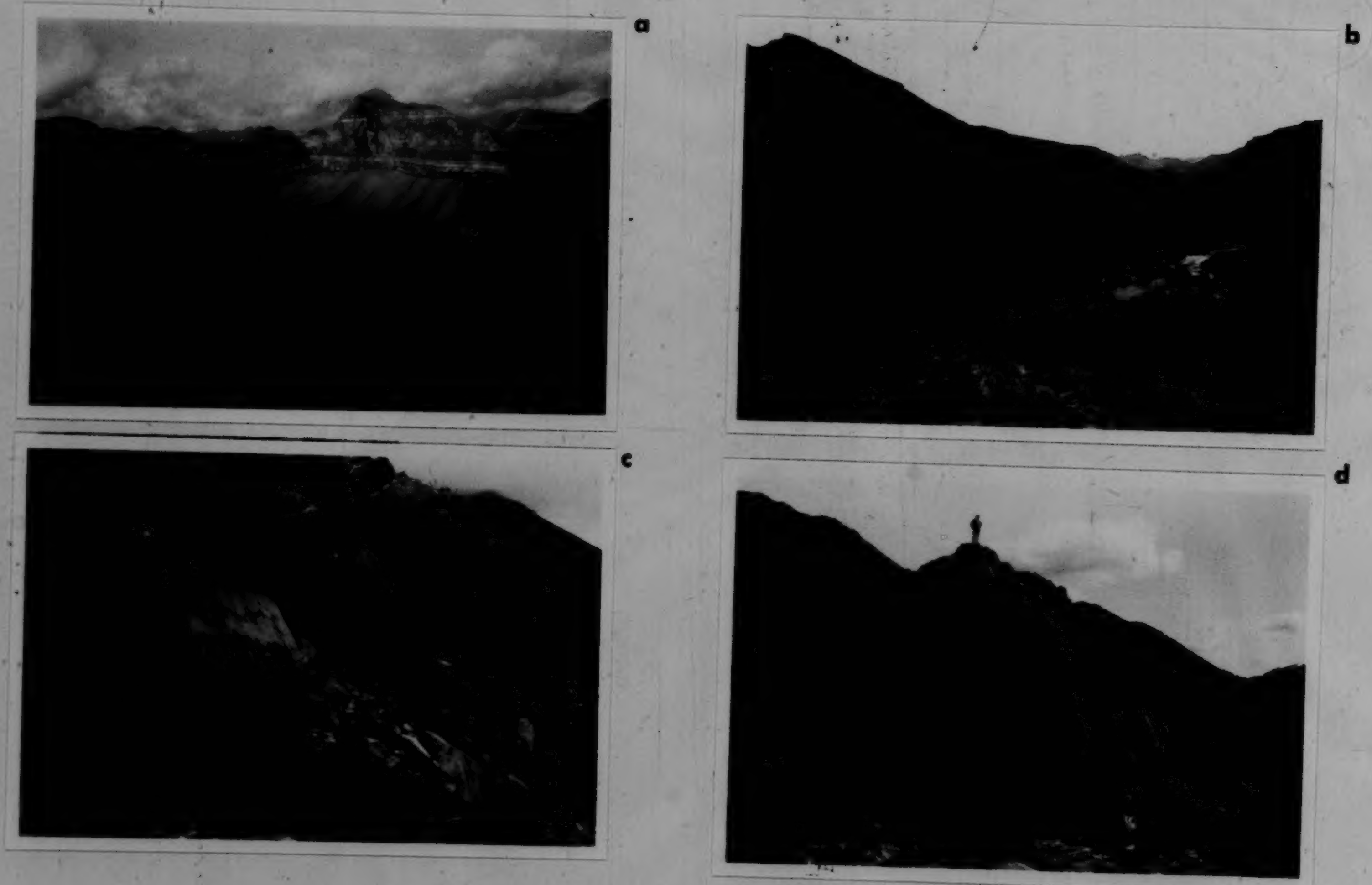

Figure B.4 (a) Breakaway scar, rupture surface, and part of the "ramp" (b) Alluvial sediments in the "void" area (c) Connectable portions of a dilated slab of carbonate rock from the distal end of the debris (d) Large boulder in wave area.

scattered around the periphery of this "void" area which has been infilled with fine alluvium. The present stream, which flows across the debris, cuts a wide arc through this alluvium. However, there is evidence of abandoned, shallow channels on the surface elsewhere on the flat plain. The contact between the debris and the finer sediments is usually quite sharp. A distinct cluster of large boulders is found just inside the debris at the southern extremity of the area.

It would appear that this void area originally was a wide depression, possibly filled with alluvial, glaciofluvial or glaciolacustrine sediments. The distal tip of the rock avalanche, upon encountering such material, perhaps acquired an enhanced mobility and hence the majority of the rock debris was carried across the depression. The few boulders and the finer rubble left behind were subsequently buried by alluvial or lacustrine sediments produced when the natural stream drainage was impeded. Subsequently the stream course has incised its path across the alluvium and has downcut a channel through the gorge area.

Gorge Area

Where the stream has downcut its channel beneath the flat, alluvial sediment accumulation there are excellent exposures of the avalanche debris with an uncertain amount of till and/or alluvium. This deduction was based on the presence of a number of rounded to subrounded, gravel to cobble sized clasts which were located in a few exposures in the lower part of the gorge. Generally the gorge is between 35 and 40 m deep with steeply sloping sides at about a 40° inclination. An obvious slump feature of surface dimensions 220 x 60 m^2 was noted along the lower portion of the west side of the gorge.

A thick armour of coarse stream alluvium and a mantle of washed colluvium fill the bottom of the gorge, obscuring any exposures of the lower part of the debris. For the most part there is a problem distinguishing a distinct contact between the upper, extremely coarse, bouldery debris and the lower, finer, sandy, gravelly materials; the size distribution from the top of the section to the lowest exposure is usually gradational. There is evidence of inverse grading throughout the gorge area,although it was not present in all exposures examined. In one locality on the west side of the gorge there was a peculiar imbricate arrangement of large clasts in the upper part of the section, very much resembling the pattern of overlapping flat cobbles in a rapidly flowing stream. The area was not accessible for more detailed fabric measurements.

On the east side of the gorge a number of large (>1 m^3) boulders about 10 m below the top of the bank display an odd connectibility over a distance of about 3 m. This pattern was not observed elsewhere along the length of the bank exposure which consists mainly of unsorted, angular to subangular, sand, gravel and cobbles.

There were subtle colour differences noted within the exposure. The upper portion of the gorge was typically dark grey and grades into a grey brown with depth. There was not, however, firm textural evidence for separating a more moraine-like material from the overlying rock avalanche debris. In one locality on the west side near the top of the gorge a number of large angular boulders and cobbles were set in a fine-grained matrix of light brown silt, closely resembling rock flour. The abundance of fine material throughout the section is in contrast to the much coarser exposures of the debris in the ramp area. More detailed textural, lithologic and fabric studies would be needed to precisely delineate the degree of material entrainment and or rock debris comminution in this vicinity.

In the area east of the gorge the topography is generally flat with one large (300 x 125 m^2), north-south oriented depression. A faint series of arcuate parallel ridges define the eastern edge of this darker grey and brown, slightly finer area of debris. A roughly semi-circular rim of large boulders outlines the outer edge of debris proper. Immediately south of the void area is a distinct cluster of large partially buried boulders ranging in size from approximately 2,500 to 22,000 m^3. Some of these blocks have broken into several smaller blocks that lie in close proximity to each other. In fact, it is possible that most of these boulders may have had a common origin. To prove such a hypothesis a detailed stratigraphic reconstruction would be necessary.

Below the gorge area the stream branches and its floodplain widens. The thickness of the debris rapidly thins on the west side of the stream to probably less than a few metres. In some localities it appears to be virtually non-existent on the surface. For a distance of about 150 m in from the stream on the west side is a pattern of subparallel ridges and troughs (1-2 m in height) covered or mixed with rounded coarse river alluvium. This pattern of channels most probably originated from a time when there was a much higher water level and the streamload was considerably greater - conditions which might have been expected when the debris which blocked the stream drainage in the void area was breached.

An odd pattern of knolls and ridges mark the terminus of the grey to grey-brown coloured rock debris on the east side of the stream. Orange to red weathering, silty dolomite and dolomitic siltstone become more prevalent in this vicinity below the gorge.

Lateral Margins

Along the west margin of the debris stream, from below the ramp and extending as far as the gorge area are a series of parallel troughs and elongate hills of 1 to 2.5 m height with an average separation of 10 to 15 m (see Figure B.1) These ridges are oriented at between 55° and 60° to the principle movement direction and bear a striking resemblance to the pattern of chevron crevasses seen on glaciers. Nye (1952) attributed the presence of such a pattern in ice to the existence of tensile stresses. Similar features were observed on the surface of the Sherman Glacier rock avalanche by McSaveney (1978). He has shown that the crevasse features do not correspond with the orientation of crevasses known to be on the surface of the glacier prior to the avalanche.

The "red rim" as defined by the lateral margin of orange weathering debris (Eisbacher, 1979) is not a continuous feature around the periphery of the avalanche deposit. There appear to be certain areas, e.g., south and east of the void area, where there is a greater concentration of such orange-coloured debris. Thicknesses are varied but appear to be between 1 and 3 m deep near the lateral margins. Block size is conspicuously smaller in these areas as well. In some cases the orange weathering debris would appear to be scattered thinly at some distance away from the thicker, more distinct grey-coloured debris.

Distal "Red Rim" Area

The area beneath the gorge, on both sides of the stream and extending as far as the distal tip of the debris is thinly covered by distinctive orange weathering debris. Eisbacher (1979) has referred to this distal "red rim" area as a spray feature, analogous to the similar features observed at the Nozzle and Damocles avalanches.

There would appear to be a marked thinning of the debris lobe as one moves up valley from the most extreme tip of debris. In some places the debris is quite thin or non-existent. On the east side of the stream a series of lobate accumulations along a wide ridge mark the furthest extent of the debris. West of the stream the debris extends another 300 m on a relatively flat ground surface. A large lobate accumulation marks the distal end of the deposit, while thinner yet distinct patches of orange debris are found up valley from here.

The surface of the distal area is covered by metre size or less, orange to light brown weathering dolomite and silty dolomite. Sections through the debris exposed by the stream reveal about a 4 m thickness of coarse, angular to subangular boulders which appear to grade to finer gravel and cobbles with depth. It was not possible here to visually distinguish the presence of morainal or alluvial materials within the debris, but their presence cannot be ruled out.

One of the most remarkable features observed in the avalanche was the presence of a connectable string of blocks at the very end of the deposit. As initially discovered by Eisbacher (1979), this less than 1 m thick dilated slab of laminated carbonate, originally of about 5 m length, is stretched over a distance of 11.5 m with minor lateral offsets. As shown in Figure B.4c the angular blocks are connectable on the basis of a dark grey, crystalline marker bed located at the base of the cream-coloured limestone. Beneath this exposure there is no hint of a similar stratigraphic congruence, but up-valley from this location a number of connectable boulders of smaller dimensions are exposed in the stream cut. This unique feature is striking evidence to suggest, for at least this part of the avalanche, that turbulence was not prevalent through the entire thickness of the debris and most probably the dilated slab of rock was essentially rafted along into its position.

Debris Size, Sorting and Fabric

The range and distribution of boulder sizes within the debris do not show a distinct pattern; with the exception of the distal and lateral "red rim" areas the largest boulders appear to be scattered throughout the debris with only a slightly greater concentration in the ramp area. Detailed percent-by-area studies were not done as part of this investigation. However, some general observations on the topic as obtained from air photos and field observations may be made.

Beneath the ramp the distribution of large boulder sizes is concentrated on the east side of the debris stream. Some of the largest boulders with volumes in excess of 20,000 m^3 are found in that region between the ramp and the second "wave" (see Figure B.4d). The largest measured boulder in the deposit, which is probably only about 60%

exposed, had dimensions 41 m x 32 m x 33 m, which would give a total volume in excess of 70,000 m^3. Large shattered blocks and a well developed talus blanket on the flanks of this boulder would suggest that an even larger block of rock had originally arrived at this position.

A cluster of some of the largest blocks is found opposite the void area closer to the distal "red rim" part of the deposit. From this area onwards the maximum boulder size diminishes, although a faint arc of larger size fractions defines the terminus of the debris proper on the east side of the gorge. A similar rim does not exist on the west side. Within the distal and lateral margins of the debris the mean boulder size is much reduced, probably as a function of the different lithology.

A thorough examination of clast size and fabric was not conducted in this study, although a small sample of large boulders was measured for an initial evaluation of the fabric in the debris. Because of the almost cubic shape of the larger boulders it was found to be nearly impossible to determine an accurate major axis orientation. Initial examination of the surface debris suggests, at least in some areas, that the bedding attitudes may be preferentially oriented. This could be a direct result of the stratigraphic congruence which appears to be maintained within parts of the debris. To further investigate this postulate the bedding attitudes in some 41 large boulders were measured. The stations where measurements were made are shown on the map of the avalanche (Figure B.1) Figure B.5 is an equal area plot of the poles to bedding for this random selection. The mean bedding plane orientation in the failure block (SO) is also shown for comparison.

Only those boulders located within Station 1 or on the ramp can be seen to have a bedding fabric resembling the initial bedding plane attitude. For the most part ,the fabric within these large boulders is quite random. Futhermore, there does not appear to be a systematic change in bedding attitudes in boulders as one moves towards the distal end of the debris stream, although, the scatter in the cluster may increase slightly. The original postulate is therefore rejected, although this does not preclude the possibility of there being a preferred bedding attitude in clasts in one particular area.

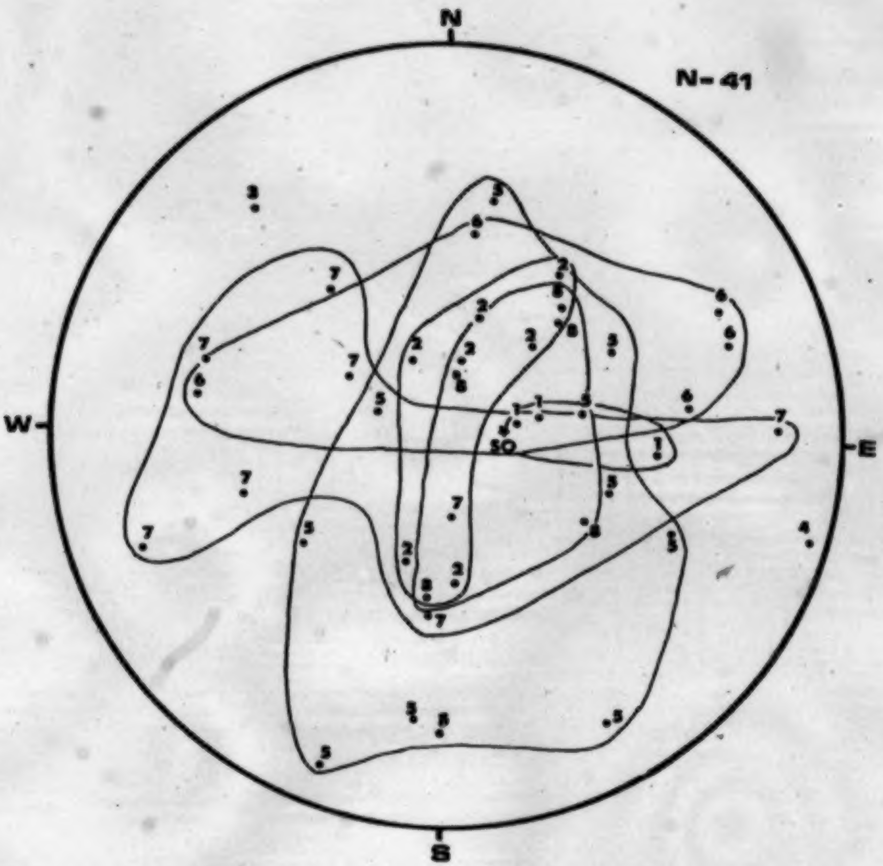

Figure B.5 Equal area plot of poles to bedding for scattered large boulders within the debris with numbered locations from Figure B.1.

APPENDIX C

VELOCITY PROFILES

The following velocitiy profiles were determined using the entire travel paths as found from 1:50,000 scale topographic maps and survey measurements and assuming these rock avalanches were single events. Refer to Chapter 5 for a discussion of the limitations of Koerner's (1976) analysis.

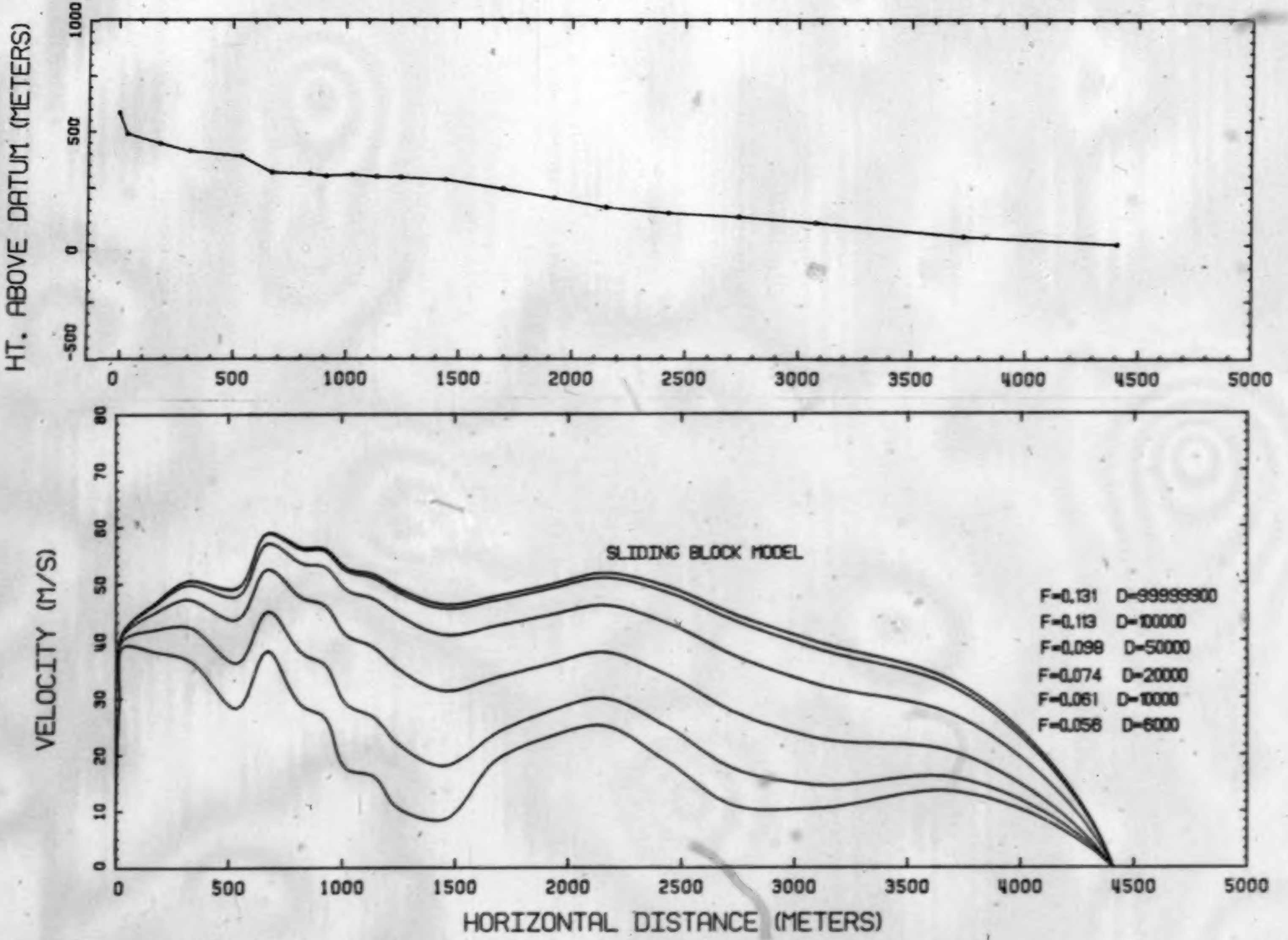

Figure C.1 Velocity profile, Damocles rock avalanche.

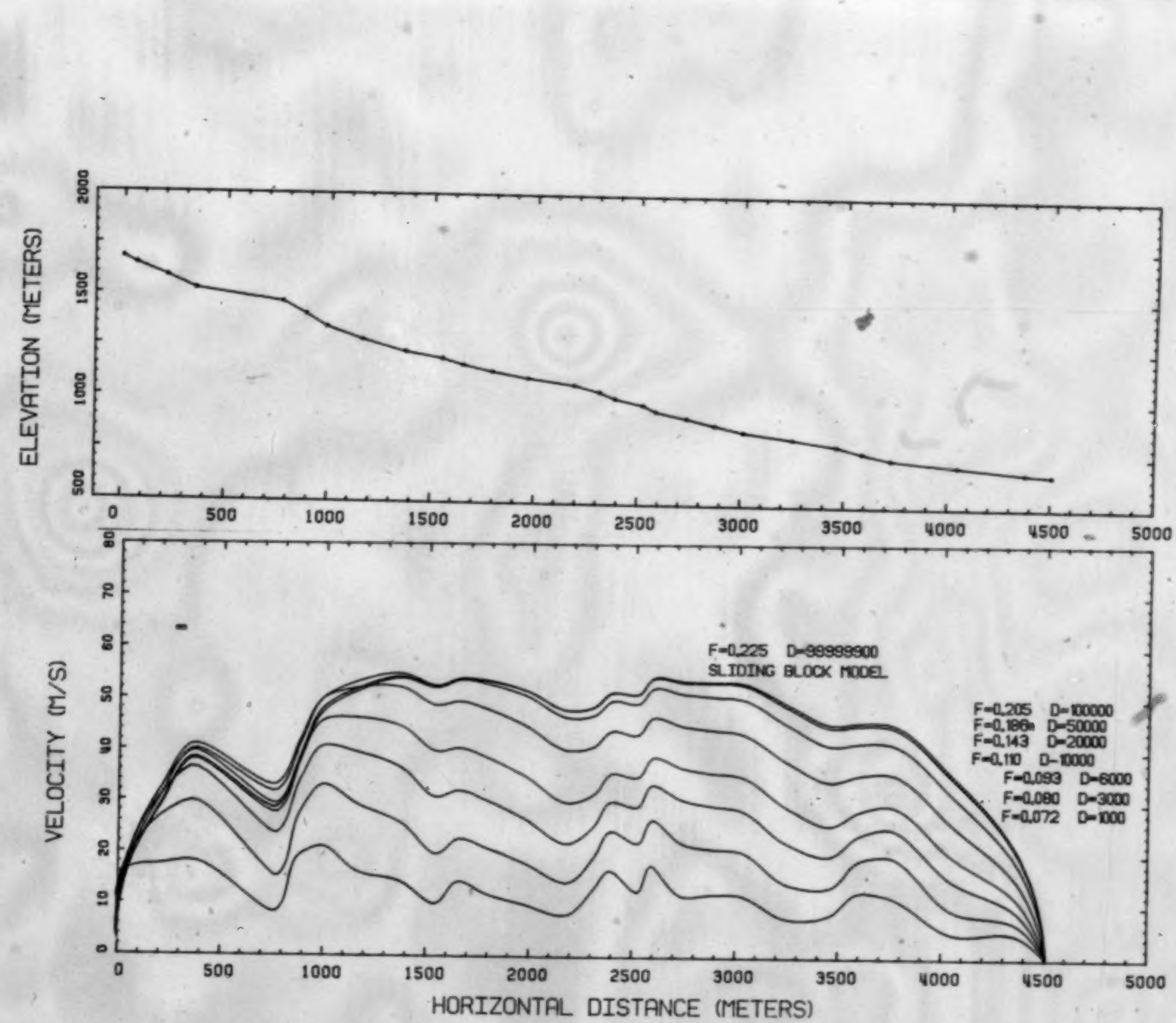

Figure C.2 Velocity profile, North Twin rock avalanche.

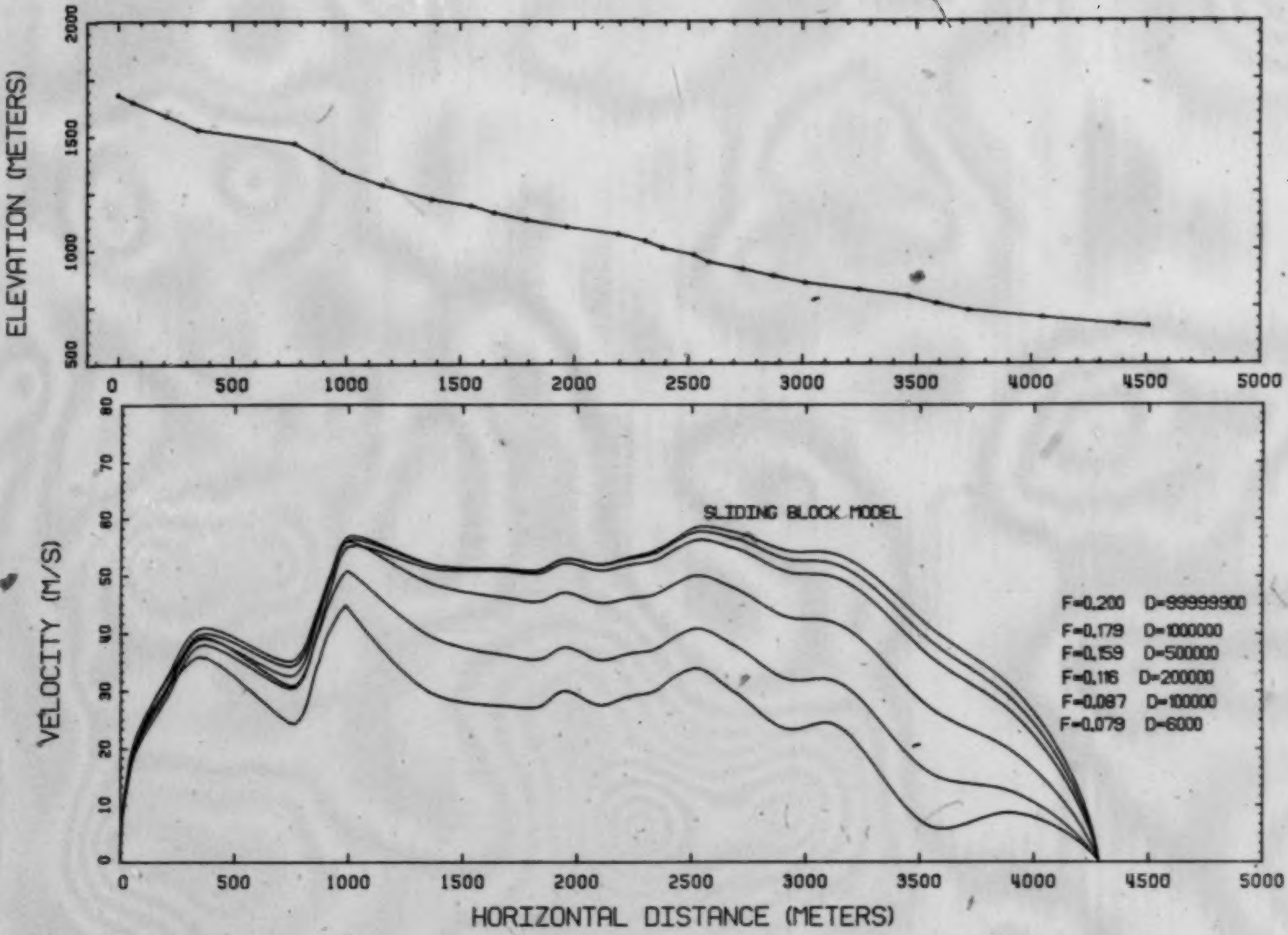

Figure C.3 Velocity profile, South Twin rock avalanche.

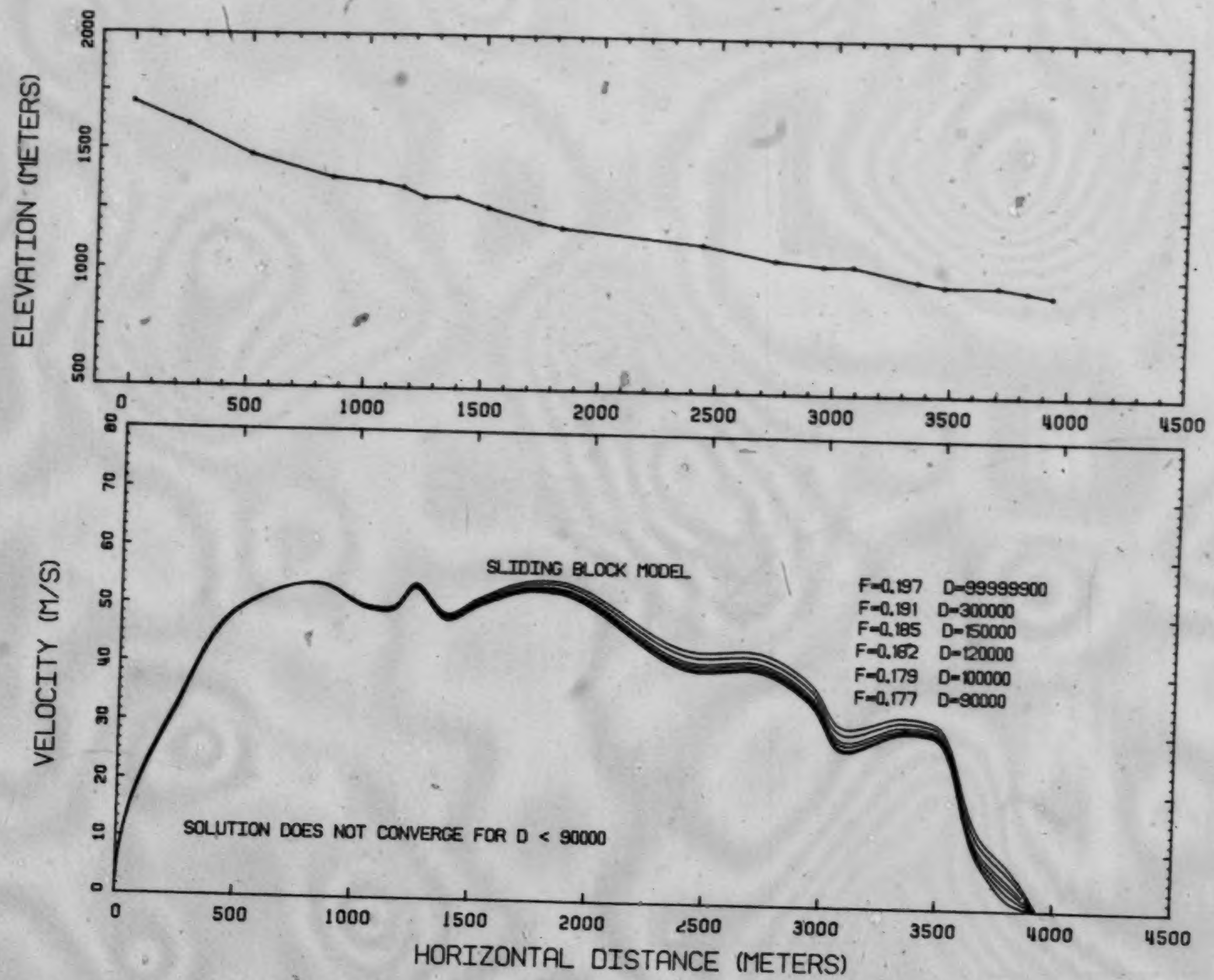

Figure C.4 Velocity profile, U-Turn rock avalanche.

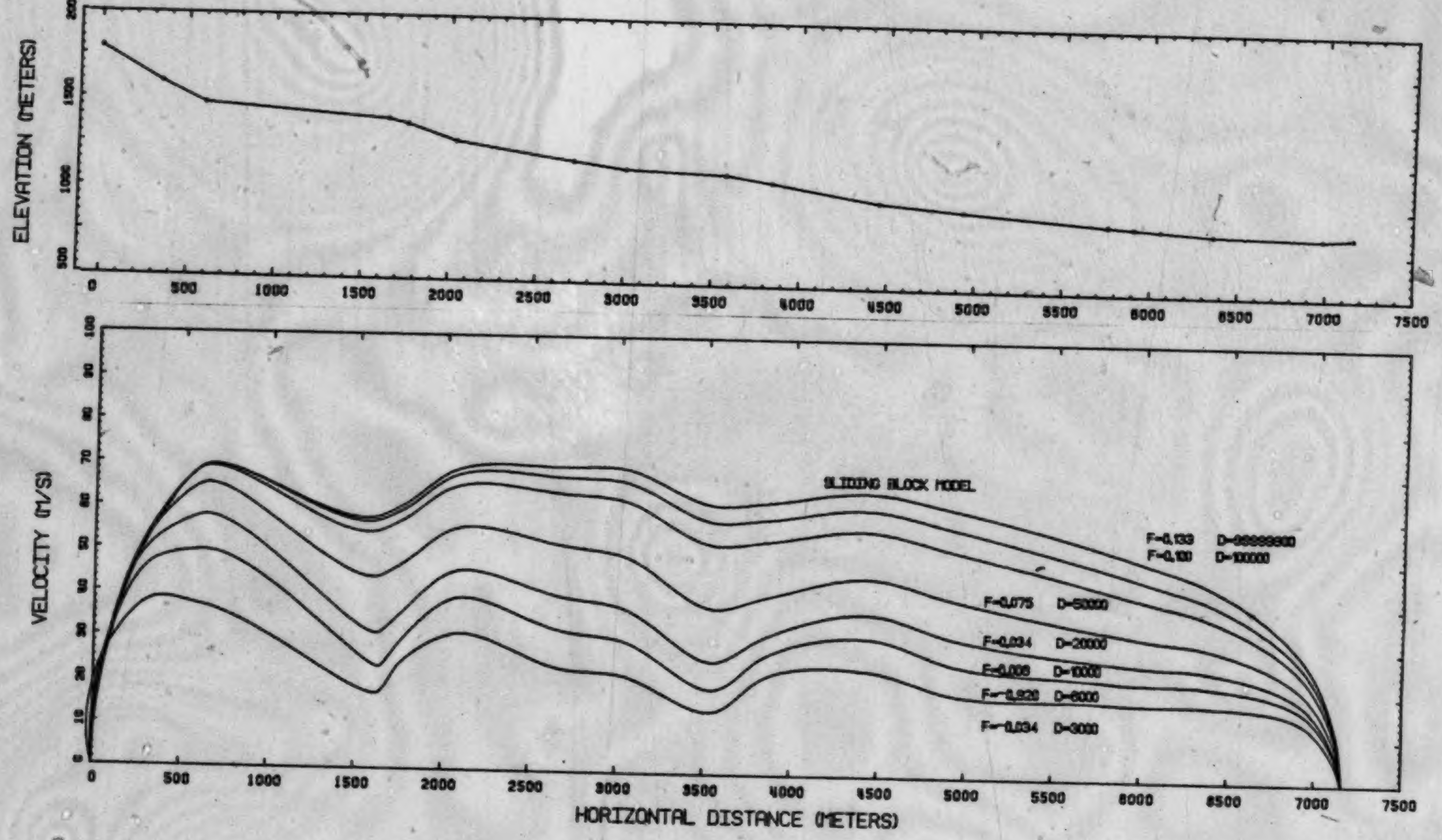

Figure C.5 Velocity profile, Nozzle rock avalanche.

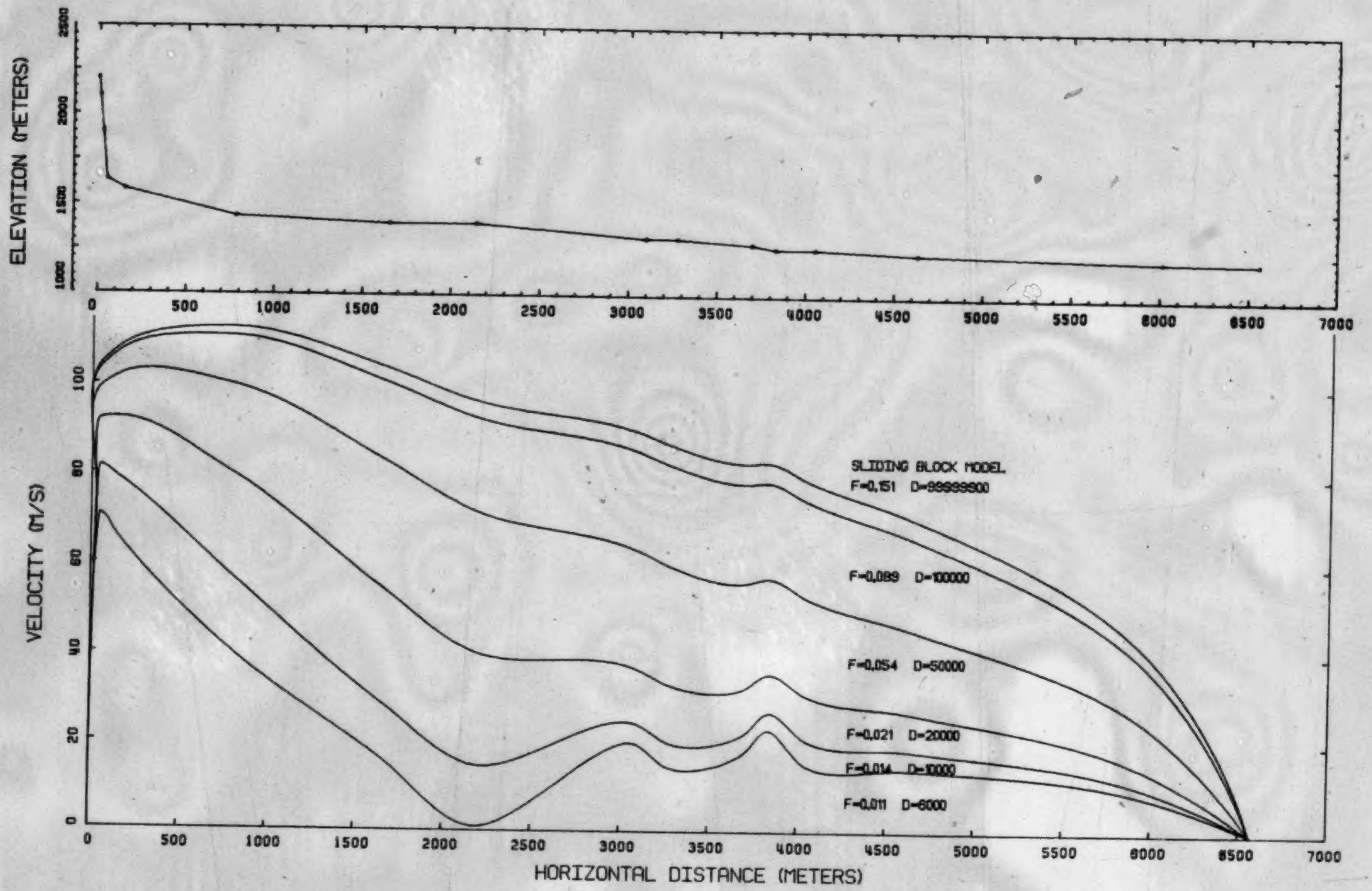

Figure C.6 Velocity profile, Rockslide Pass rock avalanche.